JSCSEN 87(12)1349–1466(2022)

ISSN 1820-7421(Online)

Journal of the Serbian Chemical Society

Electronic version

Serbian Chemical Society 125 ANNIVERSARY

Available on line at

CXII 1897

www.shd.org.rs/JSCS/

VOLUME 87

No 12

BELGRADE 2022

The full search of JSCS is available through

DOAJ DIRECTORY OF OPEN ACCESS JOURNALS

www.doaj.org

The **Journal of the Serbian Chemical Society** (formerly Glasnik Hemijskog društva Beograd), one volume (12 issues) per year, publishes articles from the fields of chemistry. The **Journal** is financially supported by the **Ministry of Education, Science and Technological Development of the Republic of Serbia.**

Articles published in the **Journal** are indexed in **Clarivate Analytics products: Science Citation Index-Expanded™** – accessed *via* **Web of Science®** and **Journal Citation Reports®**.

Impact Factor announced 2022: **1.100; 5-year Impact Factor**: **1.175**.

Articles appearing in the **Journal** are also abstracted by: **Scopus, Chemical Abstracts Plus (CAplus℠), Directory of Open Access Journals, Referativnii Zhurnal (VINITI), RSC Analytical Abstracts, EuroPub, Pro Quest** and **Asian Digital Library.**

Publisher:	**Serbian Chemical Society**, Karnegijeva 4/III, P. O. Box 36, 1120 Belgrade 35, Serbia tel./fax: +381–11–3370–467, E-mails: **Society** – shd@shd.org.rs; **Journal** – jscs@shd.org.rs Home Pages: **Society** – http://www.shd.org.rs/, **Journal** – http://www.shd.org.rs/JSCS/
Internet Service:	Contents, Abstracts and full papers (from Vol 64, No. 1, 1999) are available in the electronic form at the Web Site of the **Journal** (http://www.shd.org.rs/JSCS/).
Former Editors:	**Nikola A. Pušin** (1930–1947), **Aleksandar M. Leko** (1948–1954), **Panta S. Tutundžić** (1955–1961), **Miloš K. Mladenović** (1962–1964), **Đorđe M. Dimitrijević** (1965–1969), **Aleksandar R. Despić** (1969–1975), **Slobodan V. Ribnikar** (1975–1985), **Dragutin M. Dražić** (1986–2006).
Editor-in-Chief:	BRANISLAV Ž. **NIKOLIĆ**, Serbian Chemical Society (E-mail: jscs-ed@shd.org.rs)
Deputy Editor:	DUŠAN **SLADIĆ**, Faculty of Chemistry, University of Belgrade
Sub editors:	
Organic Chemistry	DEJAN **OPSENICA**, Institute of Chemistry, Technology and Metallurgy, University of Belgrade JÁNOS **CSANÁDI**, Faculty of Science, University of Novi Sad
Biochemistry and Biotechnology	OLGICA **NEDIĆ**, INEP – Institute for the Application of Nuclear Energy, University of Belgrade
Inorganic Chemistry	MILOŠ **ĐURAN**, Serbian Chemical Society
Theoretical Chemistry	IVAN **JURANIĆ**, Serbian Chemical Society
Physical Chemistry	LJILJANA **DAMJANOVIĆ-VASILIĆ**, Faculty of Physical Chemistry, University of Belgrade
Electrochemistry	SNEŽANA **GOJKOVIĆ**, Faculty of Technology and Metallurgy, University of Belgrade
Analytical Chemistry	SLAVICA **RAŽIĆ**, Faculty of Pharmacy, University of Belgrade
Polymers	BRANKO **DUNJIĆ**, Faculty of Technology and Metallurgy, University of Belgrade
Thermodynamics	MIRJANA **KIJEVČANIN**, Faculty of Technology and Metallurgy, University of Belgrade
Chemical Engineering	TATJANA **KALUĐEROVIĆ RADOIČIĆ**, Faculty of Technology and Metallurgy, University of Belgrade
Materials	RADA **PETROVIĆ**, Faculty of Technology and Metallurgy, University of Belgrade
Metallic Materials and Metallurgy	ANA **KOSTOV**, Mining and Metallurgy Institute Bor, University of Belgrade
Environmental and Geochemistry	VESNA **ANTIĆ**, Faculty of Agriculture, University of Belgrade
History of and Education in Chemistry	DRAGICA **TRIVIĆ**, Faculty of Chemistry, University of Belgrade
English Language Editors:	LYNNE **KATSIKAS**, Serbian Chemical Society VLATKA **VAJS**, Serbian Chemical Society JASMINA **NIKOLIĆ**, Faculty of Technology and Metallurgy, University of Belgrade
Technical Editors:	VLADIMIR **PANIĆ**, ALEKSANDAR **DEKANSKI**, VUK **FILIPOVIĆ**, Institute of Chemistry, Technology and Metallurgy, University of Belgrade
Journal Manager & Web Master:	ALEKSANDAR **DEKANSKI,** Institute of Chemistry, Technology and Metallurgy, University of Belgrade
Office:	VERA **ĆUŠIĆ**, Serbian Chemical Society

Editorial Board

From abroad: **R. Adžić**, Brookhaven National Laboratory (USA); **A. Casini**, University of Groningen (The Netherlands); **G. Cobb**, Baylor University (USA); **D. Douglas**, University of British Columbia (Canada); **G. Inzelt**, Etvos Lorand University (Hungary); **J. Kenny**, University of Perugia (Italy); **Ya. I. Korenman**, Voronezh Academy of Technology (Russian Federation); **M. D. Lechner**, University of Osnabrueck (Germany); **S. Macura**, Mayo Clinic (USA); **M. Spiteller**, INFU, Technical University Dortmund (Germany); **M. Stratakis**, University of Crete (Grecce); **M. Swart**, University de Girona (Cataluna, Spain); **G. Vunjak-Novaković**, Columbia University (USA); **P. Worsfold**, University of Plymouth (UK); **J. Zagal**, Universidad de Santiago de Chile (Chile).

From Serbia: **B. Abramović**, **V. Antić**, **V. Beškoski**, **J. Csanadi**, **Lj. Damjanović-Vasilić**, **A. Dekanski**, **V. Dondur**, **B. Dunjić**, **M. Đuran, S. Gojković**, **I. Gutman**, **B. Jovančićević**, **I. Juranić**, **T. Kaluđerović Radioičić**, **L. Katsikas**, **M. Kijevčanin**, **A. Kostov**, **V. Leovac**, **S. Milonjić**, **V.B. Mišković-Stanković**, **O. Nedić**, **B. Nikolić**, **J. Nikolić**, **D. Opsenica**, **V. Panić**, **M. Petkovska**, **R. Petrović**, **I. Popović**, **B. Radak**, **S. Ražić**, **D. Sladić**, **S. Sovilj**, **S. Šerbanović**, **B. Šolaja**, **Ž. Tešić**, **D. Trivić**, **V. Vajs**.

Subscription: The annual subscription rate is **150.00 €** including postage (surface mail) and handling. For Society members from abroad rate is **50.00 €**. For the proforma invoice with the instruction for bank payment contact the Society Office (E-mail: shd@shd.org.rs) or see JSCS Web Site: http://www.shd.org.rs/JSCS/, option Subscription.

Godišnja pretplata: Za članove SHD: **2.500,00 RSD**, za penzionere i studente: **1000,00 RSD**, a za ostale: **3.500,00 RSD**:za organizacije i ustanove: **16.000,00 RSD**. Uplate se vrše na tekući račun Društva: **205-13815-62**, poziv na broj **320**, sa naznakom "pretplata za JSCS".

Nota: Radovi čiji su svi autori članovi SHD prioritetno se publikuju.

Odlukom Odbora za hemiju Republičkog fonda za nauku Srbije, br. 66788/1 od 22.11.1990. godine, koja je kasnije potvrđena odlukom Saveta Fonda, časopis je uvršten u kategoriju međunarodnih časopisa (**M-23**). Takođe, aktom Ministarstva za nauku i tehnologiju Republike Srbije, 413-00-247/2000-01 od 15.06.2000. godine, ovaj časopis je proglašen za publikaciju od posebnog interesa za nauku. **Impact Factor** časopisa objavljen 2022. godini iznosi **1,100**, a petogodišnji **Impact Factor 1,175**.

INSTRUCTIONS FOR AUTHORS (2021)

GENERAL

The *Journal of the Serbian Chemical Society* (the *Journal* in further text) is an international journal publishing papers from all fields of chemistry and related disciplines. Twelve issues are published annually. The Editorial Board expects the editors, reviewers, and authors to respect the well-known standard of professional ethics.

Types of Contributions

Original scientific papers	(up to 15 typewritten pages, including Figures, Tables and References) report original research which must not have been previously published.
Short communications	(up to 8 pages) report unpublished preliminary results of sufficient importance to merit rapid publication.
Notes	(up to 5 pages) report unpublished results of short, but complete, original research
Authors' reviews	(up to 40 pages) present an overview of the author's current research with comparison to data of other scientists working in the field
Reviews[a]	(up to 40 pages) present a concise and critical survey of a specific research area. Generally, these are prepared at the invitation of the Editor
Surveys	(about 25 pages) communicate a short review of a specific research area.
Book and Web site reviews	(1 - 2 pages)
Extended abstracts	(about 4 pages) of Lectures given at meetings of the Serbian Chemical Society Divisions
Letters to the Editor	report miscellaneous topics directed directly to the Editor

[a]Generally, Authors' reviews, Reviews and Surveys are prepared at the invitation of the Editor.

Research Data Policy

The Journal of the Serbian Chemical Society (JSCS) encourages that all supporting data sets and the results, which were used for discussion and making conclusions in the presented paper, should be available to readers. We strongly support authors to deposits their datasets in free available repositories. Read more at https://www.shd-pub.org.rs/index.php/JSCS/DataPolicy.

PrePrint Policy

Authors are allowed to store a preprint version of their manuscript on a recognized preprint server such as ChemRxiv, arXiv, or on any repository that provides a public identifier (e.g. DOI) prior to submission. Read more at https://www.shd-pub.org.rs/index.php/JSCS/Preprint.

ORCID

The journal requires from corresponding authors to submit ORCID upon registration, while co-authors are forwarded an ORCID attribution request upon manuscript submission, and upon potential acceptance of the paper for publication. Read more at https://www.shd-pub.org.rs/index.php/JSCS/Orcid.

Submission of manuscripts

Manuscripts should be submitted using the **OnLine Submission Form**, available on the JSCS Web Site (**http://www.shd-pub.org.rs/index.php/JSCS**). The manuscript must be uploaded as a Word.doc or .rtf file, with tables and figures (including the corresponding captions – above Tables and below Figures), placed within the text to follow the paragraph in which they were mentioned for the first time.

Please note that **Full Names (**First Name, Last Name), **Full Affiliation** and **Country** (from drop down menu) of **ALL OF AUTHORS** (written in accordance with English spelling rules - the first letter capitalized) must be entered in the manuscript Submission Form (Step 3). Manuscript Title, authors' names and affiliations, as well as the Abstract, **WILL APPEAR** in the article listing, as well as in **BIBLIOGRAPHIC DATABASES (WoS, SCOPUS...)**, in the form and in the order entered in the author details

Graphical abstract

Graphical abstract is a one-image file containing the main depiction of the authors work and/or conclusion and must be supplied along with the manuscript. It must enable readers to quickly gain the main message of the paper and to encourage browsing, help readers identify which papers are most relevant to their research interests. Authors must provide an image that clearly represents the research described in the paper. The most relevant figure from the work, which summarizes the content, can also be submitted. The image should be submitted as a separate file in **Online Submission Form - Step 2**.

Specifications: The graphical abstract should have a clear start and end, reading from top to bottom or left to right. Please omit unnecessary distractions as much as possible.

- **Image size:** minimum of 500×800 pixels (W×H) and a minimum resolution of 300 dpi. If a larger image is sent, then please use the same ratio: 16 wide × 9 high. Please note that your image will be scaled proportionally to fit in the available window in TOC; a 150x240 pixel rectangle. Please be sure that the quality of an image cannot be increased by changing the resolution from lower to higher, but only by rescanning or exporting the image with a higher resolution, which can be set in usual "settings" option.
- **Font:** Please use Calibri and Symbol font with a large enough font size, so it is readable even from the image of a smaller size (150 × 240 px) in TOC.
- **File type:** JPG and PNG only.

No additional text, outline or synopsis should be included. Please do not use white space or any heading within the image.

Cover Letter

Manuscripts must be accompanied by a cover letter (strictly uploaded in **Online Submission Step 2**) in which the type of the submitted manuscript and a warranty as given below are given. The Author(s) has(have) to warranty that the manuscript submitted to the *Journal* for review is original, has been written by the stated author(s) and has not been published elsewhere; is currently not being considered for publication by any other journal and will not be submitted for such a review while under review by the *Journal*; the manuscript contains no libellous or other unlawful statements and does not contain any materials that violate any personal or proprietary rights of any other person or entity. All manuscripts will be acknowledged on receipt (by e-mail).

Illustrations

Illustrations (Figs, schemes, photos…) in TIF or EPS format (JPG format is acceptable for colour and greyscale photos, only), must be additionally uploaded (Online Submission Step 2) as a separate file or one archived (.zip, .rar or .arj) file. Figures and/or Schemes should be prepared according to the **Artwork Instructions -** http://www.shd.org.rs/JSCS/jscs-pdf/Artwork_Instructions.pdf!

For any difficulties and questions related to **OnLine Submission Form -** https://www.shd-pub.org.rs/index.php/JSCS/submission/wizard, please refer to **User Guide -** https://openjournal-systems.com/ojs-3-user-guide/ , Chapter **Submitting an Article -** https://openjournalsystems.com/ojs-3-user-guide/submitting-an-article/. If difficulties still persist, please contact JSCS Editorial Office at **JSCS@shd.org.rs**

A manuscript not prepared according to these instructions will be returned for resubmission without being assigned a reference number.

Conflict-of-Interest Statement*: Public trust in the peer review process and the credibility of published articles depend in part on how well a conflict of interest is handled during writing, peer review, and editorial decision making. A conflict of interest exists when an author (or the author's institution), reviewer, or editor has financial or personal relationships that inappropriately influence (bias) his or her actions (such relationships are also known as dual commitments, competing interests, or competing loyalties). These relationships vary from those with negligible potential to those with great potential to influence judgment, and not all relationships represent true conflict of interest. The potential for a conflict of interest can exist whether or not an individual believes that the relationship affects his or her scientific judgment. Financial relationships (such as employment, consultancies, stock ownership, honoraria, paid expert testimony) are the most easily identifiable conflicts of interest and the most likely to undermine the credibility of the journal, the authors, and of science itself. However, conflicts can occur for other reasons, such as personal relationships, academic competition, and intellectual passion.

Informed Consent Statement*: Patients have a right to privacy that should not be infringed without informed consent. Identifying information, including patients' names, initials, or hospital numbers, should not be published in written descriptions, photographs, and pedigrees unless the information is essential for

*International Committee of Medical Journal Editors ("Uniform Requirements for Manuscripts Submitted to Biomedical Journals"), February 2006

scientific purposes and the patient (or parent or guardian) gives written informed consent for publication. Informed consent for this purpose requires that a patient who is identifiable be shown the manuscript to be published. Authors should identify Individuals who provide writing assistance and disclose the funding source for this assistance. Identifying details should be omitted if they are not essential. Complete anonymity is difficult to achieve, however, and informed consent should be obtained if there is any doubt. For example, masking the eye region in photographs of patients is inadequate protection of anonymity. If identifying characteristics are altered to protect anonymity, such as in genetic pedigrees, authors should provide assurance that alterations do not distort scientific meaning and editors should so note. The requirement for informed consent should be included in the journal's instructions for authors. When informed consent has been obtained it should be indicated in the published article.

Human and Animal Rights Statement* When reporting experiments on human subjects, authors should indicate whether the procedures followed were in accordance with the ethical standards of the responsible committee on human experimentation (institutional and national) and with the Helsinki Declaration of 1975, as revised in 2000 (5). If doubt exists whether the research was conducted in accordance with the Helsinki Declaration, the authors must explain the rationale for their approach, and demonstrate that the institutional review body explicitly approved the doubtful aspects of the study. When reporting experiments on animals, authors should be asked to indicate whether the institutional and national guide for the care and use of laboratory animals was followed.

PROCEDURE

All contributions will be peer reviewed and only those deemed worthy and suitable will be accepted for publication. The Editor has the final decision. To facilitate the reviewing process, authors are encouraged to suggest up to three persons competent to review their manuscript. Such suggestions will be taken into consideration but not always accepted. If authors would prefer a specific person not be a reviewer, this should be announced. The Cover Letter must be accompanied by these suggestions. Manuscripts requiring revision should be returned according to the requirement of the Editor, within 60 days upon reception of the reviewing comments by e-mail.

The *Journal* maintains its policy and takes the liberty of correcting the English as well as false content of manuscripts **provisionally accepted** for publication in the first stage of reviewing process. In this second stage of manuscript preparation by JSCS Editorial Office, the author(s) may be required to supply some **additional clarifications and corrections**. This procedure will be executed during copyediting actions, with a demand to author(s) to perform corrections of unclear parts before the manuscript would be published OnLine as **finally accepted manuscript (OLF Section of the JSCS website)**. Please note that the manuscript can receive the status of **final rejection** if the author's corrections would not be satisfactory.

When finally accepted manuscript is ready for printing, the corresponding author will receive a request for proof reading, which should be performed within 2 days. Failure to do so will be taken as the authors agree with any alteration which may have occurred during the preparation of the manuscript for printing.

Accepted manuscripts of active members of the Serbian Chemical Society (all authors) have publishing priority.

MANUSCRIPT PRESENTATION

Manuscripts should be typed in English (either standard British or American English, but consistent throughout) with 1.5 spacing (12 points Times New Roman; Greek letters in the character font Symbol) in A4 format leaving 2.5 cm for margins. For Regional specific, non-standard characters that may appear in the text, save documents with Embed fonts Word option: *Save as -> (Tools) -> Save Options… -> Embed fonts in the text.*

The authors are requested to seek the assistance of competent English language expert, if necessary, to ensure their English is of a reasonable standard. The Serbian Chemical Society can provide this service in advance of submission of the manuscript. If this service is required, please contact the office of the Society by e-mail (jscs-info@shd.org.rs).

Tables, figures and/or schemes must be embedded in the main text of the manuscript and should follow the paragraph in which they are mentioned for the first time. **Tables** must be prepared with the aid of the **WORD table function**, without vertical lines. The minimum size of the font in the tables should be **10 pt**. Table columns must not be formatted using multiple spaces. Table rows must not be formatted using any returns (enter key; ↵ key) and are **limited to 12 cm width**. Tables should not be incorporated as graphical objects. **Footnotes to Tables** should follow them and are to be indicated consequently (in a single line) in superscript letters and separated by semi-column.

Table caption must be placed above corresponding Table, while **Captions of the Illustrations** (Figs. Schemes...) must follow the corresponding item. **The captions, either for Tables or Illustrations**, should make the items comprehensible without reading of the main text (but clearly referenced in), must follow numerical order (Roman for Tables, Arabic for Illustrations), and should not be provided on separate sheets or as separate files.

High resolution Illustrations (named as Fig. 1, Fig. 2… and/or Scheme 1, Scheme 2…) in **TIF or EPS format** (JPG format is acceptable for photos, only) **must be additionally uploaded as a separate files or one archived (.zip, .rar) file.**

Illustrations should be prepared according to the ARTWORK INSTRUCTIONS - http://www.shd.org.rs/JSCS/jscs-pdf/Artwork_Instructions.pdf. **!**

All pages of the manuscript must be numbered continuously.

DESIGNATION OF PHYSICAL QUANTITIES AND UNITS

IUPAC recommendations for the naming of compounds should be followed. SI units, or other permissible units, should be employed. The designation of physical quantities must be in italic throughout the text (including figures, tables and equations), whereas the units and indexes (except for indexes having the meaning of physical quantities) are in upright letters. They should be in Times New Roman font. In graphs and tables, a slash should be used to separate the designation of a physical quantity from the unit (example: p / kPa, j / mA cm^{-2}, t / °C, T_0 / K, τ / h, ln (j / mA cm^{-2})…). Designations such as: p (kPa), t [min]…, are not acceptable. However, if the full name of a physical quantity is unavoidable, it should be given in upright letters and separated from the unit by a comma (example: Pressure, kPa; Temperature, K; Current density, mA cm^{-2}…). Please do not use the axes of graphs for additional explanations; these should be mentioned in the figure captions and/or the manuscript (example: "pressure at the inlet of the system, kPa" should be avoided). The axis name should follow the direction of the axis (the name of y-axis should be rotated by 90°). Top and right axes should be avoided in diagrams, unless they are absolutely necessary.

Latin words, as well as the names of species, should be in *italic*, as for example: *i.e.*, *e.g.*, *in vivo*, *ibid*, *Calendula officinalis* L., *etc*. The branching of organic compound should also be indicated in *italic*, for example, *n*-butanol, *tert*-butanol, *etc*.

Decimal numbers must have decimal points and not commas in the text (except in the Serbian abstract), tables and axis labels in graphical presentations of results. Thousands are separated, if at all, by a comma and not a point.

Mathematical and chemical equations should be given in separate lines and must be numbered, Arabic numbers, consecutively in parenthesis at the end of the line. All equations should be embedded in the text Complex equations (fractions, integrals, matrix…) should be prepared with the aid of the **Microsoft Equation 3.0** (or higher) or **MathType** (Do not use them to create simple equations and labels). **Using the Insert -> Equation option, integrated in MS Office 2010 and MS Office 2013, as well as insertion of equation objects within paragraph text IS NOT ALLOWED.**

ARTICLE STRUCTURE

- TITLE PAGE
- MAIN TEXT – including Tables and Illustrations with corresponding captions
- SUPPLEMENTARY MATERIAL (optional**)**

Title page

- **Title** in bold letters, should be clear and concise, preferably 12 words or less. The use of non-standard abbreviations, symbols and formulae is discouraged.
- AUTHORS' NAMES in capital letters with the full first name, initials of further names separated by a space and surname. Commas should separate the author's names except for the last two names when 'and' is to be used. In multi-affiliation manuscripts, the author's affiliation should be indicated by an Arabic number placed in superscript after the name and before the affiliation. Use * to denote the corresponding author(s).
- *Affiliations* should be written in italic. The e-mail address of the corresponding author should be given after the affiliation(s).

- *Abstract:* A one-paragraph abstract written of 150 – 200 words in an impersonal form indicating the aims of the work, the main results and conclusions should be given and clearly set off from the text. Domestic authors should also submit, on a separate page, an Abstract - Izvod, the author's name(s) and affiliation(s) in Serbian (Cyrillic letters). (Домаћи аутори морају доставити Извод (укључујући имена аутора и афилијацију) на српском језику, исписане ћирилицом, иза Захвалнице, а пре списка референци.) For authors outside Serbia, the Editorial Board will provide a Serbian translation of their English abstract.
- *Keywords:* Up to 6 keywords should be given. Do not use words appearing in the manuscript title
- RUNNING TITLE: A one line (maximum five words) short title in capital letters should be provided.

Main text – should have the form:

- **INTRODUCTION,**
- **EXPERIMENTAL (RESULTS AND DISCUSSION),**
- **RESULTS AND DISCUSSION (EXPERIMENTAL),**
- **CONCLUSIONS,**
- **NOMENCLATURE (optional) and**
- ***Acknowledgements*: If any.**
- REFERENCES (Citation of recent papers published in chemistry journals that highlight the significance of work to the general readership is encouraged.)

The sections should be arranged in a sequence generally accepted for publication in the respective fields. They subtitles should be in capital letters, centred and NOT numbered.

- The INTRODUCTION should include the aim of the research and a concise description of background information and related studies directly connected to the paper.
- The EXPERIMENTAL section should give the purity and source of all employed materials, as well as details of the instruments used. The employed methods should be described in sufficient detail to enable experienced persons to repeat them. Standard procedures should be referenced and only modifications described in detail. On no account should results be included in the experimental section.

Chemistry

Detailed information about instruments and general experimental techniques should be given in all necessary details. If special treatment for solvents or chemical purification were applied that must be emphasized.

Example: Melting points were determined on a Boetius PMHK or a Mel-Temp apparatus and were not corrected. Optical rotations were measured on a Rudolph Research Analytical automatic polarimeter, Autopol IV in dichloromethane (DCM) or methanol (MeOH) as solvent. IR spectra were recorded on a Perkin-Elmer spectrophotometer FT-IR 1725X. ^{1}H and ^{13}C NMR spectra were recorded on a Varian Gemini-200 spectrometer (at 200 and 50 MHz, respectively), and on a Bruker Ultrashield Advance III spectrometer (at 500 and 125 MHz, respectively) employing indicated solvents (*vide infra*) using TMS as the internal standard. Chemical shifts are expressed in ppm (δ / ppm) values and coupling constants in Hz (J / Hz). ESI-MS spectra were recorded on Agilent Technologies 6210 Time-Of-Flight LC-MS instrument in positive ion mode with CH_3CN/H_2O 1/1 with 0.2 % HCOOH as the carrying solvent solution. Samples were dissolved in CH_3CN or MeOH (HPLC grade purity). The selected values were as follows: capillary voltage = 4 kV, gas temperature = 350 °C, drying gas flow 12 L min^{-1}, nebulizer pressure = 310 kPa, fragmentator voltage = 70 V.The elemental analysis was performed on the Vario EL III- C,H,N,S/O Elemental Analyzer (Elementar Analysensysteme GmbH, Hanau-Germany). Thin-layer chromatography (TLC) was performed on precoated Merck silica gel 60 F254 and RP-18 F254 plates. Column chromatography was performed on Lobar LichroPrep Si 60 (40-63 μm), RP-18 (40-63 µm) columns coupled to a Waters RI 401 detector, and on Biotage SP1 system with UV detector and FLASH 12+, FLASH 25+ or FLASH 40+ columns pre packed with KP-SIL [40-63 µm, pore diameter 6 nm (60 Å)], KP-C18-HS (40-63 µm, pore diameter 9 nm (90 Å) or KP-NH [40-63 µm, pore diameter 10 nm (100 Å)] as adsorbent. Compounds were analyzed for purity (HPLC) using a Waters 1525 HPLC dual pump system equipped with an Alltech, Select degasser system, and dual λ 2487 UV-VIS detector. For data processing, Empower software was used (methods A and B). Methods C and D: Agylent Technologies 1260 Liquid Chromatograph equipped with Quat Pump (G1311B), Injector (G1329B) 1260 ALS, TCC 1260 (G1316A) and Detector 1260 DAD VL+ (G1315C). For data processing, LC OpenLab CDS ChemStation software was used. For details, see Supporting Information.

1. Synthesis experiments

Each paragraph describing a synthesis experiment should begin with the name of the product and any structure number assigned to the compound in the Results and Discussions section. Thereafter, the compound should be identified by its structure number. Use of standard abbreviations or unambiguous molecular formulas for reagents and solvents, and of structure numbers rather than chemical names to identify starting materials and intermediates, is encouraged.

When a new or improved synthetic method is described, the yields reported in key experimental examples, and yields used for comparison with existing methods, should represent amounts of isolated and purified products, rather than chromategraphically or spectroscopically determined yields. Reactant quantities should be reported in weight and molar units and for product yields should be reported in weight units; percentage yields should only be reported for materials of demonstrated purity. When chromatography is used for product purification, both the support and solvent should be identified.

2. Microwave experiments

Reports of syntheses conducted in microwave reactors must clearly indicate whether sealed or open reaction vessels were used and must document the manufacturer and model of the reactor, the method of monitoring the reaction mixture temperature, and the temperature-time profile. Reporting a wattage rating or power setting is not an acceptable alternative to providing temperature data. Manuscripts describing work done with domestic (kitchen) microwave ovens will not be accepted except for studies where the unit is used for heating reaction mixtures at atmospheric pressure.

3. Compound characterization

The Journal upholds a high standard for compound characterization to ensure that substances being added to the chemical literature have been correctly identified and can be synthesized in known yield and purity by the reported preparation and isolation methods. For **all new** compounds, evidence adequate to establish both **identity** and **degree of purity** (homogeneity) must be provided.

Identity *- Melting point.* All homogeneous solid products (*e.g.* not mixtures of isomers) should be characterized by melting or decomposition points. The colors and morphologies of the products should also be noted.

Specific rotations. Specific rotations based on the equation $[\alpha]^{t};D = (100\ \alpha) / (l\ c)$ should be reported as unitless numbers as in the following example: $[\alpha]^{20}$; D = -25.4 (c 1.93, $CHCl_3$), where c / g mL^{-1} is concentration and l / dm is path length. The units of the specific rotation, (deg mL) / (g dm), are implicit and are not included with the reported value.

Spectra/*Spectral Data.* Important IR adsorptions should be given.

For all new diamagnetic substances, NMR data should be reported (^1H, ^{13}C, and relevant heteronuclei). ^1H NMR chemical shifts should be given with two digits after the decimal point. Include the number of protons represented by the signal, signal multiplicity, and coupling constants as needed (*J* italicized, reported with up to one digit after the decimal). The number of bonds through which the coupling is operative, ^{x}J, may be specified by the author if known with a high degree of certainty. ^{13}C NMR signal shifts should be rounded to the nearest 0.01 ppm unless greater precision is needed to distinguish closely spaced signals. Field strength should be noted for each spectrum, not as a comment in the general experimental section. Hydrogen multiplicity (C, CH, CH_2, CH_3) information obtained from routine DEPT spectra should be included. If detailed signal assignments are made, the type of NOESY or COSY methods used to establish atom connectivity and spatial relationships should be identified in the Supporting Information. Copies of spectra should also be included where structure assignments of complex molecules depend heavily on NMR interpretation. Numbering system used for assignments of signals should be given in the Supporting Information with corresponding general structural formula of named derivative.

HPLC/LCMS can be substituted for biochemistry papers where the main focus is not on compound synthesis.

HRMS/*elemental analysis.* To support the molecular formula assignment, HRMS data accurate within 5 ppm, or combustion elemental analysis [carbon and hydrogen (and nitrogen, if present)] data accurate within 0.5 %, should be reported for new compounds. HRMS data should be given in format as is usually given for combustion analysis: calculated mass for given formula following with observed mass: (+)ESI-HRMS *m*/*z*: [molecular formula + H]$^+$ calculated mass, observed mass. Example: (+)ESI-HRMS *m*/*z*: calculated for [$C_{13}H_8BrCl_2N$ + H^+] 327.92899, observed 327.92792.

NOTE: in certain cases, a crystal structure may be an acceptable substitute for HRMS/elemental analysis.

Biomacromolecules. The structures of biomacromolecules may be established by providing evidence about sequence and mass. Sequences may be inferred from the experimental order of amino acid, saccharide, or nucleotide coupling, from known sequences of templates in enzyme-mediated syntheses, or through standard sequencing techniques. Typically, a sequence will be accompanied by MS data that establish the molecular weight.

Example: Product was isolated upon column chromatography [dry flash (SiO_2, eluent EA, EA/MeOH gradient 95/5 → 9/1, EA/MeOH/NH_3 gradient 18/0.5/0.5 → 9/1/1, and flash chromatography (Biotage SP1, RP column, eluent MeOH/H_2O gradient 75/25 → 95/5, N-H column, eluent EA/Hex gradient 6/3 → EA). was obtained after flash column chromatography (Biotage SP NH column, eluent hexane/EA 4:6 → 2:6). Yield 968.4 mg (95 %). Colorless foam softens at 96-101 °C. $[\alpha]^{20}$; D = +0,163 (c =2.0×10^{-3} g/mL, CH_2Cl_2). IR (ATR): 3376w, 2949m, 2868w, 2802w, 1731s, 1611w, 1581s, 1528m, 1452m, 1374s, 1331w, 1246s, 1171m, 1063w, 1023m, 965w, 940w, 881w, 850w, 807w, cm^{-1}. ^{1}H NMR (500 MHz, $CDCl_3$, δ): 8.46 (*d*, 1H, J = 5.4, H-2'), 7.89 (*s*, 1H, J = 2.0, H-8'), 7.71 (*d*, 1H, J = 8.9, H-5'), 7.30 (*dd*, 1H, J_1 = 8.8, J_2 = 2.1, H-6'), 6.33 (*d*, 1H, J = 5.4, H-3'), 6.07 (*s*, HN-Boc, exchangeable with D_2O), 5.06 (*s*, 1H, H-12), 4.92-4.88 (*m*, 1H, H-7), 4.42 (*bs*, H-3), 3.45 (*s*,CH_3-N), 3.33 (*bs*, H-9'), 3.05-2.95 (*m*, 2H, H-11'), 2.70-2.43 (*m*, 2H, H-24) and HN, exchangeable with D_2O), 2.07 (*s*, CH_3COO), 2.04 (*s*, CH_3COO), 1.42 (*s*, 9H, $(CH_3)_3$C-N(Boc)), 0.88 (*s*, 3H, CH_3-10), 0.79 (*d*, 3H,J = 6.6, CH_3-20), 0.68 (*s*, 3H, CH_3-13). ^{13}C NMR (125 MHz, $CDCl_3$, δ): 170.34, 170.27, 151.80, 149.92, 148.87, 134.77, 128.36, 125.11, 121.43, 117.29, 99.98, 75.41, 70.82, 50.43, 49.66, 47.60, 47.33, 44.97, 43.30, 41.83, 41.48, 37.65, 36.35, 35.44, 34.89, 34.19, 33.23, 31.24, 28.79, 28.35, 27.25, 26.45, 25.45, 22.74, 22.63, 21.57, 21.31, 17.85, 12.15. (+)ESI-HRMS (*m*/*z*): calculated for $[C_{45}H_{67}ClN_4O_6 + H]^+$ 795.48219, observed 795.48185. Combustion analysis for $C_{45}H_{67}ClN_4O_6$: Calculated. C 67.94, H 8.49, N 7.04; found C 67.72, H 8.63, N 6.75. HPLC purity: method A: RT 1.994, area 99.12 %; method C: RT 9.936, area 98.20 %.

Purity - Evidence for documenting compound purity should include one or more of the following:

a) Well-resolved high field 1D ^{1}H NMR spectrum showing at most only trace peaks not attributable to the assigned structure and a standard 1D proton-decoupled ^{13}C NMR spectrum. Copies of the spectra should be included as figures in the Supporting Information.
b) Quantitative gas chromatographic analytical data for distilled or vacuum-transferred samples, or quantitative HPLC analytical data for materials isolated by column chromatography or separation from a solid support. HPLC analyses should be performed in two diverse systems. The stationary phase, solvents (HPLC), detector type, and percentage of total chromatogram integration should be reported; a copy of the chromatograms may be included as a figure in the Supporting Information.
c) Electrophoretic analytical data obtained under conditions that permit observing impurities present at the 5 % level.

HRMS data may be used to support a molecular formula assignment **but cannot be used as a criterion of purity**.

4. Biological Data

Quantitative biological data are required for all tested compounds. Biological test methods must be referenced or described in sufficient detail to permit the experiments to be repeated by others. Detailed descriptions of biological methods should be placed in the experimental section. Standard compounds or established drugs should be tested in the same system for comparison. Data may be presented as numerical expressions or in graphical form; biological data for extensive series of compounds should be presented in tabular form. Tables consisting primarily of negative data will not usually be accepted; however, for purposes of documentation they may be submitted as supporting information. Active compounds obtained from combinatorial syntheses should be resynthesized and retested to verify that the biology conforms to the initial observation.

Statistical limits (statistical significance) for the biological data are usually required. If statistical limits cannot be provided, the number of determinations and some indication of the variability and reliability of the results should be given. References to statistical methods of calculation should be included. Doses and concentrations should be expressed as molar quantities (*e.g.*, mol/kg, μmol/kg, M, mM). The routes of administration of test compounds and vehicles used should be indicated, and any salt forms used (hydrochlorides, sulfates, *etc.*) should be noted. The physical state of the compound dosed (crystalline, amorphous; solution, suspension) and the formulation for dosing (micronized, jet-milled, nanoparticles) should be indicated. For those compounds found to be inactive, the highest concentration (*in vitro*) or dose level (*in vivo*) tested should be indicated.

- The RESULTS AND DISCUSSION should include concisely presented results and there significance discussed and compared to relevant literature data. The results and discussion may be combined or kept separate.
- The inclusion of a CONCLUSION section, which briefly summarizes the principal conclusions, is recommended.
- NOMENCLATURE is optional but, if the authors wish, a list of employed symbols may be included.
- REFERENCES should be numbered sequentially as they appear in the text. Please note that any reference numbers appearing in the Illustrations and/or Tables and corresponding captions must follow the numbering sequence of the paragraph in which they appear for the first time. When cited, the reference number should be superscripted in Font 12, following any punctuation mark. In the reference list, they should be in normal position followed by a full stop. Reference entry must not be formatted using Carriage returns (enter key; ↵ key) or multiple space key. The formatting of references to published work should follow the *Journal*'s style as follows:

Journals[a]:	A. B. Surname1, C. D. Surname2, *J. Serb. Chem. Soc.* **Vol** (Year) first page Number (https://doi.org/doi)[b]
Books:	A. B. Surname1, C. D. Surname2, *Name of Book*, Publisher, City, Year, pp. 100-101 (https://doi.org/doi)[b]
Compilations:	A. B. Surname1, C. D. Surname2, in *Name of Compilation*, A. Editor1, C. Editor2, Ed(s)., Publisher, City, Year, p. 100 (https://doi.org/doi)[b]
Proceedings:	A. B. Surname1, C. D. Surname2, in *Proceedings of Name of the Conference or Symposium*, (Year), Place of the Conference, Country, *Title of the Proceeding*, Publisher, City, Year, p. or Abstract No. 100
Patents:	A. B. Inventor1, C. D. Inventor2, (Holder), Country Code and patent number (registration year)
Chemical Abstracts:	A. B. Surname1, C. D. Surname2, *Chem. Abstr*. CA 234 567a; For non-readily available literature, the Chemical Abstracts reference should be given in square brackets: [C.A. 139/2003 357348t] after the reference
Standards:	EN ISO 250: *Name of the Standard* (Year)
Websites:	Title of the website, URL in full (date accessed)

[a] When citing Journals, the International Library Journal abbreviation is required. Please consult, *e.g.*, https://images.webofknowledge.com/WOK46/help/WOS/A_abrvjt.html

[b] doi should be replaced by doi number of the Article, for example: http://dx.doi.org/10.2298/JSC161212085B (as active link). If doi do not exist, provide the link to the online version of the publication.

Only the last entry in the reference list should end with a full stop.

The names of all authors should be given in the list of references; the abbreviation *et al.* may only be used in the text. The original journal title is to be retained in the case of publications published in any language other than English (please denote the language in parenthesis after the reference). Titles of publications in non-Latin alphabets should be transliterated. Russian references are to be transliterated using the following transcriptions:

ж→zh, х→kh, ц→ts, ч→ch, ш→sh, щ→shch, ы→y, ю→yu, я→ya, э→e, й→i, ь→'.

Supplementary material

Authors are encouraged to presentthe information and results non-essential to the understanding of their paper as SUPPLEMENTARY MATERIAL (can be uploaded inStep 4 of Online Submission). This material may include as a rule, but is not limited to, the presentation of analytical and spectral data demonstrating the identity and purity of synthesized compounds, tables containing raw data on which calculations were based, series of figures where one example would remain in the main text, etc. The Editorial Board retain the right to assign such information and results to the Supplementary material when deemed fit. Supplementary material does not appear in printed form but can be downloaded from the web site of the JSCS.

Mathematical and chemical equations should be given in separate lines and must be numbered, Arabic numbers, consecutively in parenthesis at the end of the line. All equations should be embedded in the text Complex equations (fractions, integrals, matrix…) should be prepared with the aid of the

Microsoft Equation 3.0 (or higher) or MathType (Do not use them to create simple equations and labels). Using the Insert -> Equation option, integrated in MS Office 2010 and MS Office 2013, as well as insertion of equation objects within paragraph text IS NOT ALLOWED.

Deposition of crystallographic data

Prior to submission, the crystallographic data included in a manuscript presenting such data should be deposited at the appropriate database. Crystallographic data associated with organic and metal-organic structures should be deposited at the Cambridge Crystallographic Data Centre (CCDC) by e-mail to **deposit@ccdc.cam.ac.uk**

Crystallographic data associated with inorganic structures should be deposited with the Fachinformationszentrum Karlsruhe (FIZ) by e-mail to **crysdata@fiz-karlsruhe.de**. A deposition number will then be provided, which should be added to the reference section of the manuscript.

For detailed instructions please visit the JSCS website:
https://www.shd-pub.org.rs/index.php/JSCS/Instructions

ARTWORK INSTRUCTIONS

JSCS accepts only **TIFF** or **EPS** formats, as well as **JPEG** format (only for colour and greyscale photographs) for electronic artwork and graphic files. **MS files** (Word, PowerPoint, Excel, Visio) **NOT acceptable**. Generally, scanned instrument data sheets should be avoided. Authors are responsible for the quality of their submitted artwork. Every single Figure or Scheme, as well as any part of the Figure (A, B, C…) should be prepared according to following instructions (every part of the figure, A, B, C…, must be submitted as an independent single graphic file):

TIFF

Virtually all common artwork and graphic creation software is capable of saving files in TIFF format. This 'option' can normally be found under 'the 'Save As...' or 'Export...' commands in the 'File' menu.

TIFF (Tagged Image File Format) is the recommended file format for bitmap, greyscale and colour images.

- Colour images should be in the RGB mode
- When supplying TIFF files, please ensure that the files are supplied at the correct resolution:
    1. Line artwork: minimum of 1000 dpi
    2. RGB image: minimum of 300 dpi
    3. Greyscale image: minimum of 300 dpi
    4. Combination artwork (line/greyscale/RGB): minimum of 500 dpi
- Images should be tightly cropped, without frame and any caption.
- If applicable please re-label artwork with a font supported by JSCS (Arial, Helvetica, Times, Symbol) and ensure it is of an appropriate font size.
- Save an image in TIFF format with LZW compression applied.
- It is recommended to remove Alpha channels before submitting TIFF files.
- It is recommended to flatten layers before submitting TIFF files.

Please be sure that quality of an image cannot be increased by changing the resolution from lower to higher, but only by rescanning or exporting the image with higher resolution, which can be set in usual "settings" facilities.

EPS

Virtually all common artwork creation software, such as Canvas, ChemDraw, CorelDraw, SigmaPlot, Origin Lab…, are capable of saving files in EPS format. This 'option' can normally be found under the 'Save As...' or 'Export...' commands in the 'File' menu.

For vector graphics, EPS (Encapsulated PostScript) files are the preferred format as long as they are provided in accordance with the following conditions:

- when they contain bitmap images, the bitmaps should be of good resolution (see instructions for TIFF files)
- when colour is involved, it should be encoded as RGB
- an 8-bit preview/header at a resolution of 72 dpi should always be included
- embed fonts should always included and only the following fonts should be used in artwork: Arial, Helvetica, Times, Symbol
- the vertical space between the parts of an illustration should be limited to the bare necessity for visual clarity
- no data should be present outside the actual illustration area
- line weights should range from 0.35 pt to 1.5 pt
- when using layers, they should be reduced to one layer before saving the image (Flatten Artwork)

JPEG

Virtually all common artwork and graphic creation software is capable of saving files in JPEG format. This 'option' can normally be found under 'the 'Save As...' or 'Export...' commands in the 'File' menu.

JPEG (Joint Photographic Experts Group) is the acceptable file format **only for colour and greyscale photographs**. JPEG can be created with respect to photo quality (low, medium, high; from 1 to 10), ensuring file sizes are kept to a minimum to aid easy file transfer. Images should have a minimum resolution of 300 dpi. Image width: minimum 3.0 cm; maximum 12.0 cm.

Please be sure that quality of an image cannot be increased by changing the resolution from lower to higher, but only by rescanning or exporting the image with higher resolution, which can be set in usual "settings" facilities.

SIZING OF ARTWORK

- JSCS aspires to have a uniform look for all artwork contained in a single article. Hence, it is important to be aware of the style of the journal.
- Figures should be submitted in black and white or, if required, colour (charged). If coloured figures or photographs are required, this must be stated in the cover letter and arrangements made for payment through the office of the Serbian Chemical Society.
- As a general rule, the lettering on an artwork should have a finished, printed size of 11 pt for normal text and no smaller than 7 pt for subscript and superscript characters. Smaller lettering will yield a text that is barely legible. This is a rule-of-thumb rather than a strict rule. There are instances where other factors in the artwork, (for example, tints and shadings) dictate a finished size of perhaps 10 pt. Lines should be of at least 1 pt thickness.
- When deciding on the size of a line art graphic, in addition to the lettering, there are several other factors to address. These all have a bearing on the reproducibility/readability of the final artwork. Tints and shadings have to be printable at the finished size. All relevant detail in the illustration, the graph symbols (squares, triangles, circles, *etc*.) and a key to the diagram (to explain the explanation of the graph symbols used) must be discernible.
- The sizing of halftones (photographs, micrographs,...) normally causes more problems than line art. It is sometimes difficult to know what an author is trying to emphasize on a photograph, so you can help us by identifying the important parts of the image, perhaps by highlighting the relevant areas on a photocopy. The best advice that can be given to graphics suppliers is not to over-reduce halftones. Attention should also be paid to magnification factors or scale bars on the artwork and they should be compared with the details inside. If a set of artwork contains more than one halftone, again please ensure that there is consistency in size between similar diagrams.

General sizing of illustrations which can be used for the Journal of the Serbian Chemical Society:

- Minimum fig. size: 30 mm width
- Small fig. size - 60 mm width
- Large fig. size - 90 mm width
- Maximum fig. size - 120 mm width

Pixel requirements (width) per print size and resolution for bitmap images:

	Image width	A	B	C
Minimal size	30 mm	**354**	**591**	**1181**
Small size	60 mm	**709**	**1181**	**2362**
Large size	90 mm	**1063**	**1772**	**3543**
Maximal size	120 mm	**1417**	**2362**	**4724**

A: 300 dpi > RGB or Greyscale image
B: 500 dpi > Combination artwork (line/greyscale/RGB)
C: 1000 dpi> Line artwork

The designation of physical quantities and graphs formatting

The designation of physical quantities on figures must be in italic, whereas the units are in upright letters. They should be in Times New Roman font. In graphs a slash should be used to separate the designation of a physical quantity from the unit (example: p / kPa, t °C, T_0 / K, τ / h, ln (j / mA cm^{-2})…). Designations such as: p (kPa), t [min]…, are not acceptable. However, if the full name of a physical quantity is unavoiable, it should be given in upright letters and separated from the unit by a comma (example: Pressure, kPa, Temperature, K…). Please do not use the axes of graphs for additional explanations; these should be mentioned in the figure captions and/or the manuscript (example: "pressure at the inlet of the system, kPa" should be avoided). The axis name should follow the direction of the axis (the name of y-axis should be rotated by 90°). Top and right axes should be avoided in diagrams, unless they are absolutely necessary. Decimal numbers must have decimal points and not commas in the axis labels in graphical presentations of results. Thousands are separated, if at all, by a comma and not a point.

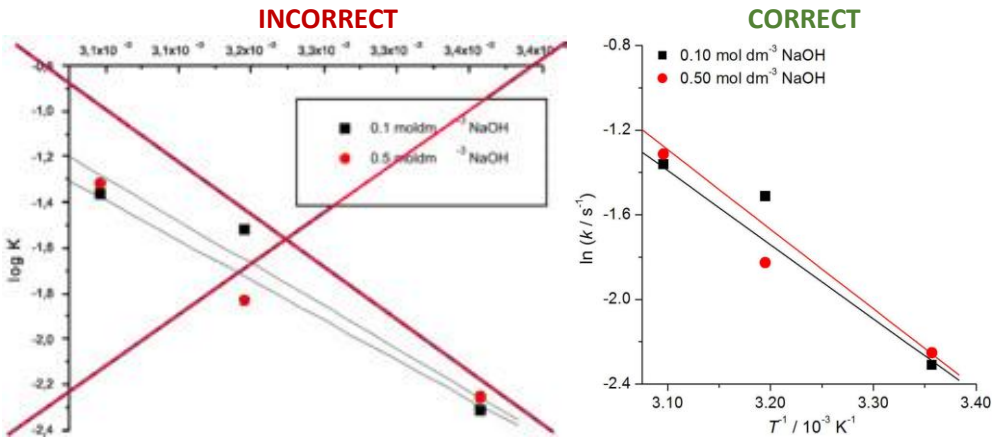

Journal of the Serbian Chemical Society
JSCS-info@shd.org.rs • www.shd.org.rs/JSCS

J. Serb. Chem. Soc. Vol. 87, No. 12 (2022)

CONTENTS*

Published by the Serbian Chemical Society
Karnegijeva 4/III, P. O. Box 36, 11120 Belgrade, Serbia
Printed by the Faculty of Technology and Metallurgy
Karnegijeva 4, P. O. Box 35-03, 11120 Belgrade, Serbia

* For colored figures in this issue please see electronic version at the Journal Home Page: http://www.shd.org.rs/JSCS/

Journal of the Serbian Chemical Society
JSCS@tmf.bg.ac.rs • www.shd.org.rs/JSCS
J. Serb. Chem. Soc. *87* (12) 1349–1358 (2022)
JSCS–5598
Original scientific paper
Published 1 August 2022

Synthesis and biological activity of novel zingerone–thiohydantoin hybrids

KATARINA D. VIRIJEVIĆ[1], PETAR B. STANIĆ[1], JOVANA M. MUŠKINJA[1], JELENA S. KATANIĆ STANKOVIĆ[1], NIKOLA SREĆKOVIĆ[2], MARKO N. ŽIVANOVIĆ[1] and BILJANA M. ŠMIT[1]*

[1]*University of Kragujevac, Institute for Information Technologies, Department of Science, Jovana Cvijića bb, 34000 Kragujevac, Serbia and* [2]*University of Kragujevac, Faculty of Science, Department of Chemistry, Radoja Domanovića 12, 34000 Kragujevac, Serbia*

(Received 4 April, revised 28 May, accepted 9 June 2022)

Abstract: A series of zingerone–thiohydantoin hybrids were synthesized from *O*-alkyl zingerone derivatives by cyclocondensation with thiosemicarbazide in a two-step reaction. The obtained new potentially bioactive compounds were structurally characterized by IR and NMR spectroscopy, as well as by elemental and HRMS analysis. In addition, their antimicrobial and *in vitro* anticancer activities were tested. The tested compounds showed low to moderate antimicrobial activity. Zingerone–thiohydantoin hybrid with an *O*-butyl substituent exerted the significant cytotoxic activity on colon HCT-116 cancer cells, without toxicity on healthy MRC-5 cells.

Keywords: molecular hybrids; antimicrobial activity; cytotoxic activity.

INTRODUCTION

The development of novel synthetic molecular hybrids is one of the main challenges in the drug discovery field. Hybrid drugs represent a combination of specific agents aimed to be more efficient than classic single synthesized compounds. In that way, the hybrid approach allows the connection of two distinct compounds in one molecule, increasing the biological potential of at least one of the compounds.[1] Many natural products play an important role in this field. For example, zingerone also called vanillylacetone, obtained from a ginger extract, is a natural compound that belongs to the methoxyphenol class, along with its derivatives. Both natural and synthetic zingerone derivatives exhibit different biological and pharmacological activities such as anti-inflammatory, anti-microbial, anti-cancer and hepatoprotective.[2] Furthermore, zingerone appears to be a potential agent for inhibiting colon cancer progression, as the number of

* Corresponding author. E-mail: biljana.smit@uni.kg.ac.rs
https://doi.org/10.2298/JSC220404047V

larger foci was found to be significantly lower after zingerone treatment, compared to dimethyl hydrazine-induced colon cancer cells.[2]

On the other hand, 2-thiohydantoin (2-thioxoimidazoline-4-one) is a non-aromatic five-membered heterocyclic compound with a cyclic ureide core.[3] Many synthesized thiohydantoin derivatives with various substituents attached to their nucleus exhibit a wide range of biological and pharmacological potentials, such as antimicrobial,[4] anti-convulsive,[5] anti-diabetes[6] and anti-HIV.[7] However, novel studies showed that thiohydantoins and their synthesized derivatives could be used as promising anti-proliferative and anti-metastatic agents.[8] Taking into account that colon cancer is one of the most prominent tumors in the world and less sensitive to cytostatics, the search for new effective therapeutic drugs is crucial.

In this study, different zingerone derivatives were prepared as starting materials for obtaining a short series of new zingerone-thiohydantoin hybrids for the evaluation of their potential biological activity.

EXPERIMENTAL

General methods

All reagents and chemicals were commercially available and used without additional purification. Solvents were distilled before use. Anhydrous methanol was prepared by standard drying methods. Zingerone, starting material for a preparation of *O*-alkyl zingerone derivatives, was obtained by condensation reaction of vanillin and acetone and subsequent reduction of yielded dehydrozingerone, according to well-known procedure.[9] IR spectra were recorded through KBr pellets on a Perkin–Elmer FT-IR spectrometer model Spectrum One in the 4000 to 450 cm^{-1} range. ^{1}H- and ^{13}C-NMR spectra were recorded on a Varian Gemini 2000 NMR spectrometer using $CDCl_3$ as the solvent and TMS as the internal standard. Elemental analysis was done on an Elemental Vario ELIII CHNSO analyzer. HRMS were measured on an Agilent 6550 iFunnel Q-TOF LC/MS system. For biological assays microtiter plates and Multiskan SkyHigh Microplate spectrophotometer by Thermo Scientific were used.

General procedure for the preparation of O-*alkyl zingerone derivatives* ***1a*** *and* ***b***

Zingerone derivatives **1a** and **b** were synthesized according to a procedure that uses dimethyl and diethyl sulfate, respectively.[10] A mixture of zingerone (0.971 g, 5 mmol) and 50 mL of boiling water is heated on a steam bath. A 2 mL portion of 20 % NaOH solution is heated to about 100 °C and added in one lot to the hot mixture of zingerone and water. Heating is continued and 6.25 mmol of methyl/ethyl sulphate is slowly added in portions. After the addition of all methyl/ethyl sulphate, which requires about 1.5 h, the reaction mixture is heated for 45 min longer and an additional portion of 1.1 mmol of methyl/ethyl sulphate is added at the same rate as the first portion. At the end of this addition the reaction mixture should show an acid reaction. The reaction mixture is rendered slightly alkaline with NaOH solution, and the addition of Me/Et sulfate and NaOH solution is done two more times until the total amount of Me/Et sulfate (11.25 mmol) is added. The mixture is then made strongly alkaline by the addition of 1 mL NaOH solution and is heated another 20 min. The reaction mixture is rapidly cooled at ambient temperature with continued stirring and the product is

extracted with diethyl ether (3×10 mL). The combined ether extracts are dried over anhydrous $MgSO_4$ and the ether is evaporated, giving yellow oil that soon solidifies.

General procedure for the preparation of O-*alkyl zingerone derivatives* ***1c*–*g***

Zingerone derivatives **1c**–**g** were synthesized according to a known procedure that uses alkyl halides with potassium carbonate in acetone.[11] The mixture of zingerone (0.971 g, 5 mmol), alkyl halide (12.5 mmol) and anhydrous K_2CO_3 (2.25 g, 16.3 mmol) in acetone (25 mL) were heated to reflux for 3 h. The mixture was cooled at ambient temperature and then poured into cold water. The products were extracted from the mixture with ethyl acetate (3×10 mL). Combined extracts were rinsed with water and then dried over anhydrous Na_2SO_4. The solvent was removed by vacuum distillation and the product was separated from the residue by column chromatography with hexane/EtOAc (from 3:1 to 6:1).

Zingerone derivatives **1a**, **1b** and **1f** are known and commercially available chemicals, while the others are novel. The structure and purity of all new products were confirmed by IR and NMR spectroscopy.

Synthesis of zingerone–thiohydantoin derivatives ***2a*–*g***

The zingerone–thiohydantoin derivatives were synthesized according to a previously published protocol for the synthesis of arylidene thiohydantoin derivatives.[12] A mixture of *O*-alkyl zingerone derivative **1a**–**g** (2 mmol) and thiosemicarbazide (0.182 g, 2 mmol) in 30 mL of methanol were heated to reflux for 3 h and then cooled to ambient temperature, resulting in the corresponding intermediate thiosemicarbazone without isolation. Ethyl chloroacetate (0.245 g, 2 mmol) and anhydrous sodium acetate (0.492 g, 6 mmol) were added *in situ* and the mixture was refluxed for another 6 h. The reaction mixture was cooled to room temperature at first and then poured into cold water. The resulting precipitate was filtered off, rinsed with hot water and re-crystallized from hot methanol, giving white amorphous powder in all cases. The structure of the synthesized compounds was confirmed by IR and NMR spectroscopy, as well as elemental analysis and HRMS (Supplementary material to this paper). All compounds are obtained as an inseparable mixture of *Z* and *E* stereoisomers, as can be seen through the duplication of most signals in the ^{1}H-NMR spectra. NMR spectral data are given for the major stereoisomer.

Antimicrobial activity determination

In this preliminary testing, five microbial strains were used, four of which were bacteria, *Salmonella enteritidis* ATCC 13076, *Pseudomonas aeruginosa* ATCC 10145, *Staphylococcus aureus* ATCC 25923, *Escherichia coli* ATCC 25922, and the yeast *Candida albicans* ATCC 10259. The microorganisms were acquired from the Institute of Public Health Kragujevac, University of Kragujevac, Serbia, kept at 4 °C with subcultivation once a month. The broth used for bacteria cultivation was nutrient agar and yeast was cultured on Sabouraud dextrose agar. For antimicrobial evaluation of synthesized compounds, a standard microdilution method by Sarker *et al*. was used.[13,14]

Cytotoxic activity determination

All synthesized derivatives were dissolved in dimethyl sulfoxide (DMSO) in order to obtain stock solutions of 5 mM concentration, followed by further dilution in Dulbecco's Modified Eagle Medium (DMEM) to obtain working concentrations (0.1, 1, 10, 50, 100 and 250 μM). At the highest applied concentration of derivatives, the concentration of DMSO in the solution was lower than 0.05 %, which was previously confirmed as non-toxic to cancer cells.[15]

The healthy human lung fibroblasts (MRC-5) and colorectal carcinoma cell lines (HCT--116) were obtained from the European Collection of Authenticated Cell Cultures. Cells were cultured in a complete medium in humidified conditions, at 37 °C and 5 % CO_2. When cells reached 70–80 % of confluence, the detachment was done using 0.25 % trypsin–EDTA, followed by seeding (1×10^4 cells/well) in 96-well flat-bottomed microtitre plates. The treatment with 100 μL of synthesized compounds solution was done 24 h after cell seeding.

The effects of synthesized compounds on the viability of tested cell lines were assessed after 24 and 72 h using MTT (3-(4,5-dimethylthiazol-2-yl)-2,5-diphenyltetrazolium bromide) assay according to the previously described protocol.[16] At the end of the incubation period, 25 μL of MTT solution (from a 5 mg mL^{-1} stock) was added to each well, followed by incubation at 37 °C for 2 h, after which 100 μL of DMSO was added. The evaluation of cytotoxic activity was done by measuring the absorbances at 550 nm wavelength. The obtained results are presented as mean ± standard error (*SE*), expressed as a percent of cell viability (%). IC_{50} values (minimal inhibitory treatment concentration that induces the death of 50 % of treated cells) were calculated from dose curves obtained by the MTT test. 5-Fluorouracil (5-FU) was used as positive control.

The magnitude of the correlation between variables was calculated using statistical software SPSS (SPSS for Windows, ver. 20, 2008, Chicago, IL, USA) whereat the ANOVA test was applied, and for all comparisons $p < 0.05$ was considered as a statistically significant difference between the control and the tested compounds. The IC_{50} values were calculated by using the CalcuSyn software program.

RESULTS AND DISCUSSION

Synthesis of the zingerone–thiohydanoin molecular hybrids

The zingerone–thiohydantoin derivatives **2a**–**g** were obtained through a condensation reaction with thiosemicarbazide, utilizing a previously published two--step protocol (Scheme 1).[12] In the first step, synthesized *O*-alkyl zingerone derivatives **1a**–**g** reacted with thiosemicarbazone, giving corresponding thiosemicarbazides. The thiosemicarbazides then undergo intramolecular cyclocondenzation with ethyl chloroacetate in the presence of anhydrous sodium acetate, yielding the final thiohydantoin products **2a**–**g**. The structure and purity of the novel zingerone–thiohydantoin derivatives were confirmed by IR and NMR spectroscopy, as well as by elemental and HRMS analysis. The compounds were obtained in medium to high yields, with the exception of **2d**, which was obtained in a modest yield. Naturally occurring zingerone itself did not react in this manner and the corresponding thiohydantoin derivative was not obtained. Similar to some Schiff--base derivatives,[17] all newly synthesized zingerone–thiohydantoin derivatives are obtained as a mixture of *Z* and *E* stereoisomers, which could be found in corresponding NMR spectra. Most signals in the ^{1}H-NMR spectra are duplicated, which indicates the presence of isomers. This is best seen through the singlets of CH_2-5, CH_3-6 and CH_3-16, which have the most pronounced difference of the chemical shifts and thus, less overlap. The ratios of *Z*/*E* isomers are obtained from relative integration of the most suitable and distinct pairs of singlets. Their ratios range from 1:1.06 to 1:9.82 (Scheme 1). In all cases the *E* isomer is favoured.

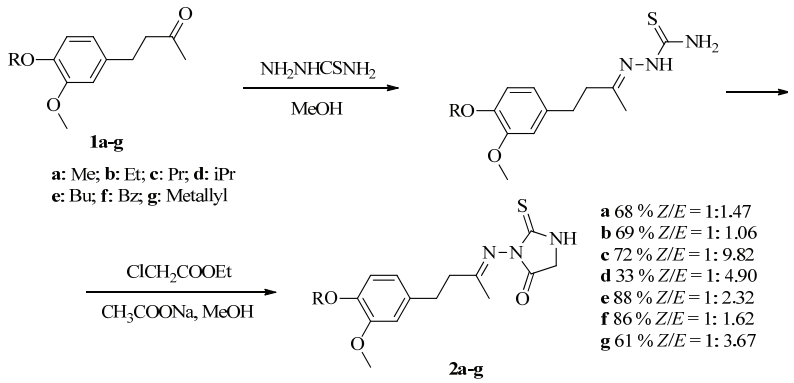

Scheme 1. Synthesis of the zingerone–thiohydantoin hybrids **2a**–**g**.

Furthermore, the computational data for both possible configurations of **2a** were also calculated using the DFT method in order to determine the more stable isomer as seen in Fig. 1. When any internal interconnection between molecules for both isomers is neglected the less internal steric repulsion factor plays an important role in fixing the *E* isomer over *Z* isomer, as it is with less internal repulsion. The gaseous state DFT calculations also showed that the energy difference value ΔE = 4.0 kJ mol^{-1} between *E* and *Z* isomer was very small.

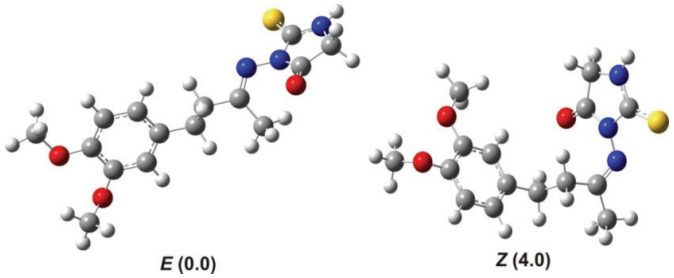

Fig. 1. The optimized geometries of *E* and *Z* isomers of **2a**, with relative free energy values indicated in kJ mol^{-1}.

Antimicrobial activity

The results of antimicrobial effects of the zingerone–thiohydantoin hybrids are presented in Table I. The compounds were tested against two Gram-negative (*S. enteritidis* and *P. aeruginosa*) and two Gram-positive (*S. aureus* and *E. coli*) bacterial species, as well as against the yeast *C. albicans*. *S. aureus* and *C. albicans* were the most resistant to the action of **2a**–**g**, wherein the compounds had not shown any activity even at the highest applied concentration (*MIC* > 4 mg mL^{-1}). Moreover, compound **2c** was completely inactive towards all used microorganisms at the same concentration, while in the cases of other compounds *MIC* values were quite high, mostly in range 2–4 mg mL^{-1}. **2b** was able to inhibit the

growth of *S. enteritidis* in moderate concentration (*MIC* 0.5 mg mL^{-1}). Only *E. coli* was more susceptible to the action of the compounds, particularly **2a** and **g** with *MIC* 0.25 mg mL^{-1}. Nevertheless, the quite high concentrations at which the compounds exhibit their activity cannot be easily compared with the activity of the reference standards, erythromycin and nystatin, where *MIC*s were expressed in mg/mL. This is the first study regarding the antimicrobial potential of zingerone–thiohydantoin hybrids. The literature data about similar compounds are scarce. There are some recently published results regarding the influence of some thiohydantoin derivatives on several bacterial species.[4] These compounds were the most active against Gram-positive bacteria such as *S. epidermidis*, *S. pyogenes*, *S. agalactiae*, *E. faecium* and *S. aureus* with *MIC*s below 1 mg mL^{-1}, but were less effective against Gram-negative bacteria like *K. pneumonia*, *P. mirabilis* and *E. coli*.

TABLE I. Antimicrobial activity (*MIC* / mg mL^{-1}) of the synthesized zingerone–thiohydantoin derivatives **2a**–**g**; –: not tested

Compound	Microorganism				
	S. enteritidis	*P. aeruginosa*	*S. aureus*	*E. coli*	*C. albicans*
2a	4	4	> 4	0.25	> 4
2b	0.5	4	> 4	2	> 4
2c	> 4	> 4	> 4	> 4	> 4
2d	–	–	–	–	–
2e	4	4	> 4	2	> 4
2f	> 4	4	> 4	4	> 4
2g	4	4	> 4	0.25	> 4
Erythromycin	20	20	1.25	2.5	–
Nystatin	–	–	–	–	1.25

Cytotoxic activity

Thiohydantoin analogs have been already confirmed as potent anti-tumor agents. Furthermore, apoptosis-inducing activity of some thiohydantoin derivatives has been demonstrated.[18] Previous research has identified zingerone as a potential anti-cancer agent, an inhibitor of colon cancer progression,[2,19] with significant cytotoxicity (IC_{50} = 11.49 mM) when applied to mesothelioma cells. Su *et al*. showed that the zingerone-induced cytotoxic effect on colon cancer cells (HCT-116) was achieved through the mechanism of ROS-mediated apoptosis.[20] Besides that, the cytotoxic potential of thiohydantoin derivatives on HCT-116 was noticed when applied to colon cancer cells (with IC_{50} > 50 μM).[21]

In this study, the cytotoxic activity of newly synthesized zingerone–thiohydantoin derivatives was evaluated on healthy lung (MRC-5) and human colorectal carcinoma (HCT-116) cell lines by MTT assay. As positive control, the commercial chemotherapeutic drug, 5-fluorouracil (5-FU) was used. 5-FU is widely used

in the treatment of different types of cancer, such as gastric, pancreatic, breast, and ovarian cancers.[22]

In regard to the influence on the viability of the healthy MRC-5 cells, a moderate cytotoxic effect was observed only for compound **2a** after an extended time of exposure with $IC_{50}^{72\ h}$ = 184.15 μM (Fig. S-44 of the Supplementary material) and control with $IC_{50}^{72\ h}$ = 181.71 μM (Fig. S-46 of the Supplementary material). The tested compounds manifest their cytotoxicity potentials in a time and dose-dependent manner. The reduction of HCT-116 cells viability was obtained mainly after 72 h and at the highest applied concentration of the investigated compounds (Fig. S-45 of the Supplementary material). The effects of the synthesized compounds were expressed by dose curves (Figs. S-44 and S-45) and IC_{50} values (Fig. 2). Based on the results, **2e** exhibited the most prominent antiproliferative activity on the HCT-116 cell line with an $IC_{50}^{24\ h}$ = 209.08 μM and $IC_{50}^{72\ h}$ = 160.93 μM. 5-FU exerted a weaker cytotoxic effect than **2e** on HCT--116 after 24 and 72 h with $IC_{50}^{24\ h}$ > 250 μM and $IC_{50}^{72\ h}$ = 181.71 μM, respectively. (Fig. 2).

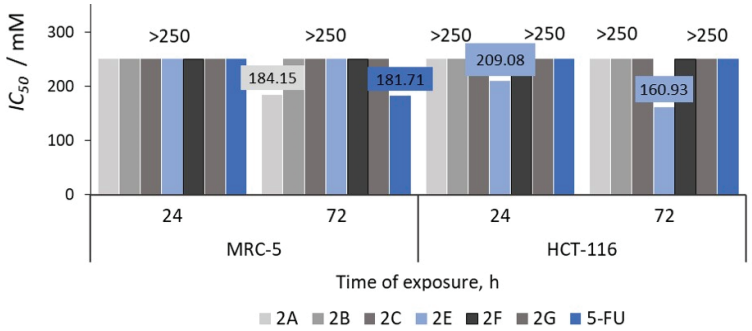

Fig. 2. The cytotoxic effects of zingerone-thiohydantoin derivatives and 5-FU after 24 and 72 h exposure, represented as IC_{50} values.

Unlike other tested compounds, **2e** contains a butyl group. The result of its activity is probably related to the lipophilicity of the substituents in the structure of the tested molecule. The lipophilicity of molecules plays a major role in the transport of molecules across biological membranes.[23] As the length of hydrocarbon chain increases, the polarity of compounds decreases resulting in increased molecule permeability. Cell membranes are relatively impermeable to hydrophilic compounds, hence the permeability of molecules depends on the hydrophobic characteristics, *i.e.*, lipophilicity of the compound.[24] In addition, a previous study reported that the lipophilicity of the substituents (Ph > Allyl > Me) had a significant impact on the cytotoxic effect.[25]

Compound **2f**, with a benzyl group, did not exhibit a cytotoxic effect (IC_{50} > 250 μM). However, based on the obtained dose curves, it can be concluded that

the wider range of concentrations could provide promising effects. Increasing the concentration range of the tested compounds would probably lead to a rise of the cytotoxic activity of some of them, and also would allow the determination of the selectivity index on tested cell lines.

The presented results indicate the potential of tested compounds as anticancer agents with no significant toxicity on healthy cell lines. Compound **2e** exhibited the most promising bioactivity and is the leading candidate in the synthesized series. The increased cytotoxicity of **2e**, compared to zingerone itself, could be attributed to the introduction of thiohydantoin moiety.

CONCLUSION

This study presents the synthesis, characterization, and biological evaluation of new zingerone–thiohydantoin molecular hybrids as potential anticancer agents. In addition to the zingerone-induced cytotoxic effect, it is known that the biological activity of thiohydantoin compounds depends largely on the nature of the substitution of the thiohydantoin ring. The difference in the cytotoxic activity of the tested compounds depends on the nature of the *O*-alkyl substituent of the benzene ring. Among the tested compounds, **2e** exerted significant cytotoxic potential without toxicity to healthy MRC-5 cells. However, all tested compounds showed low to moderate antimicrobial activity. Further toxicological testing is required to assess its therapeutic potential.

SUPPLEMENTARY MATERIAL

Additional data and information are available electronically at the pages of journal website: https://www.shd-pub.org.rs/index.php/JSCS/article/view/11747, or from the corresponding author on request.

Acknowledgement. The authors are grateful for financial support from the Ministry of Education, Science and Technological Development of the Republic of Serbia (Agreements No. 451-03-68/2022-14/200378 and 451-03-68/2022-14/200122).

ИЗВОД

СИНТЕЗА И БИОЛОШКА АКТИВНОСТ НОВИХ ЗИНГЕРОН–ТИОХИДАНТОИНСКИХ ХИБРИДА

КАТАРИНА Д. ВИРИЈЕВИЋ[1], ПЕТАР Б. СТАНИЋ[1], ЈОВАНА М. МУШКИЊА[1], ЈЕЛЕНА С. КАТАНИЋ СТАНКОВИЋ[1], НИКОЛА СРЕЋКОВИЋ[2], МАРКО Н. ЖИВАНОВИЋ[1] и БИЉАНА М. ШМИТ[1]

[1]Универзитет у Крагујевцу, Институт за информационе технологије, Сектор за природно–математичке науке, Јована Цвијића бб, 34000 Крагујевац и [2]Универзитет у Крагујевцу, Природно–математички факултет, Институт за хемију, Радоја Домановића 12, 34000 Крагујевац

Серија зингерон–тиохидантоинских хибрида је синтетисана из деривата *O*-алкил зингерона циклокондензацијом са тиосемикарбазидом у двостепеној реакцији. Добијена нова потенцијално биоактивна једињења структурно су окарактерисана IC и NMR спектроскопијом, као и елементалном анализом. Поред тога, тестиране су њихове антимикробне и *in vitro* антиканцерогене активности. Испитана једињења су показала ниску до умерену антимикробну активност. Зингерон–тиохидантоински хибрид са *O*-бутил суп-

ституентом је показао значајну цитотоксичну активност на ћелије рака дебелог црева HCT-116 без токсичности на здраве ћелије MRC-5.

(Примљено 4. априла, ревидирано 28. маја, прихваћено 9.јуна 2022)

REFERENCES

1. G. Bérubé, *Expert Opin. Drug Discov.* **11** (2016) 281 (https://www.doi.org/10.1517/17460441.2016.1135125)
2. V. A. S. Jesudoss, S. Victor Antony Santiago, K. Venkatachalam, P. Subramanian, in *Gastrointestinal Tissue: Oxidative Stress and Dietary Antioxidants*, J. Gracia-Sancho, J. Salvadó, Eds., Academic Press, Cambridge, MA, 2017, p. 289 (https://www.doi.org/10.1016/B978-0-12-805377-5.00021-7)
3. M. A. Metwally, E. Abdel-Latif, *J. Sulfur Chem.* **33** (2012) 229 (https://www.doi.org/10.1080/17415993.2011.643550)
4. P. G. C. de Carvalho, J. M. Ribeiro, R. P. B. Garbin, G. Nakazato, S. F. Yamada Ogatta, Â. de Fátima, M. de Lima Ferreira Bispo, F. Macedo, *Lett. Drug Des. Discov.* **17** (2020) 94 (https://www.doi.org/10.2174/1570180816666181212153011)
5. R. M. Gesler, C. E. Lints, E. A. Swinyard, *Toxicol. Appl. Pharmacol.* **3** (1961) 107 (https://doi.org/10.1016/0041-008X(61)90014-X)
6. L. Somsák, L. Kovács, M. Tóth, E. Ösz, L. Szilágyi, Z. Györgydeák, Z. Dinya, T. Docsa, B. Tóth, P. Gergely, *J. Med. Chem.* **44** (2001) 2843 (https://www.doi.org/10.1021/jm010892t)
7. S. Rajamaki, A. Innitzer, C. Falciani, C. Tintori, F. Christ, M. Witvrouw, Z. Debyser, S. Massa, M. Botta, *Bioorganic Med. Chem. Lett.* **19** (2009) 3615 (https://www.doi.org/10.1016/j.bmcl.2009.04.132)
8. M. Zuo, X. Xu, Z. Xie, R. Ge, Z. Zhang, Z. Li, J. Bian, *Eur. J. Med. Chem.* **125** (2017) 1002 (https://www.doi.org/10.1016/j.ejmech.2016.10.049)
9. L. R. Smith, *Chem. Educ.* **1** (1996) 1 (https://doi.org/10.1007/s00897960034a)
10. J. S. Buck, *Org. Synth.* **13** (1933) 102 (https://www.doi.org/10.15227/orgsyn.013.0102)
11. R. Katritzky, Q. Long, H. Y. He, G. Qiua, A. L. Wilcox, *Arkivoc* **2000** (2000) 868 (https://www.doi.org/10.3998/ark.5550190.0001.603)
12. Šmit, R. Z. Pavlović, A. Radosavljević-Mihailović, A. Došen, M. G. Ćurčić, D. S. Šeklić, M. N. Živanović, *J. Serb. Chem. Soc.***78** (2013) 217 (https://www.doi.org/10.2298/JSC120725154S)
13. S. D. Sarker, L. Nahar, Y. Kumarasamy, *Methods* **42** (2007) 321 (https://www.doi.org/10.1016/j.ymeth.2007.01.006)
14. Halilagić, E. Selimović, J. S. K. Stanković, N. Srećković, K. Virijević, M. N. Živanović, B. Šmit, T. V. Soldatović, *J. Coord. Chem.* (2022) 1 (https://www.doi.org/10.1080/00958972.2022.2048376)
15. K. Hostanska, G. Jürgenliemk, G. Abel, A. Nahrstedt, R. Saller, *Cancer Detect. Prev.* **31** (2007) 129 (https://www.doi.org/10.1016/j.cdp.2007.03.001)
16. T. Mosmann, *J. Immunol. Methods* **65** (1983) 55 (https://www.doi.org/10.1016/0022-1759(83)90303-4)
17. R. A. Mekheimer, A. M. A. Hameed, K. U. Sadek, *Molecules* **13** (2008) 195 (https://doi.org/10.3390/molecules13010195)
18. G. Sprengler, J. Handzlik, I. Ocsovszki, M. Viveiros, K. Kiec-Kononowicz, J. Molnar, L. Amaral, *Anticancer Res.* **31** (2011) 3285 (https://ar.iiarjournals.org/content/31/10/3285)
19. R. Vinothkumar, R. Vinothkumar, M. Sudha, N. Nalini, *Eur. J. Cancer Prev.* **23** (2014) 361 (https://www.doi.org/10.1097/CEJ.0b013e32836473ac)

20. P. Su, V. P. Veeraraghavan, S. Krishna Mohan, W. Lu, *J. Biochem. Mol. Toxicol.* **33** (2019) e22403 (https://doi.org/10.1002/jbt.22403)
21. H. A. Elhady, H. F. Al-Shareef, *Mini-Rev. Med. Chem.* **20** (2020) 1929 (https://www.doi.org/10.2174/1389557520666200611093510)
22. Kurasaka, Y. Ogino, A. Sato, *Int. J. Mol. Sci.* **22** (2021) 2916 (https://www.doi.org/10.3390/ijms22062916)
23. J. M. Mayer, H. Van De Waterbeemd, *Environ. Health Perspect.* **61** (1985) 295 (https://www.doi.org/10.1289/ehp.8561295)
24. M. R. Naylor, A. M. Ly, M. J. Handford, D. P. Ramos, C. R. Pye, A. Furukawa, V. G. Klein, R. P. Noland, Q. Edmondson, A. C. Turmon, W. M. Hewitt, J. Schwochert, C. E. Townsend, C. N. Kelly, M. J. Blanco, R. S. Lokey, *J. Med. Chem.* **61** (2018) 11169 (https://www.doi.org/10.1021/acs.jmedchem.8b01259)
25. O. O. Krasnovskaya, Y. V. Fedorov, V. M. Gerasimov, D. A. Skvortsov, A. A. Moiseeva, A. V. Mironov, E. K. Beloglazkina, N. V. Zyk, A. G. Majouga, *Arab. J. Chem.* **12** (2019) 835 (https://www.doi.org/10.1016/j.arabjc.2016.04.013).

Journal of the Serbian Chemical Society
JSCS@tmf.bg.ac.rs • www.shd.org.rs/JSCS
J. Serb. Chem. Soc. 87 (12) S450–S479 (2022) *Supplementary material*

SUPPLEMENTARY MATERIAL TO

Synthesis and biological activity of novel zingerone–thiohydantoin hybrids

KATARINA D. VIRIJEVIĆ[1], PETAR B. STANIĆ[1], JOVANA M. MUŠKINJA[1], JELENA S. KATANIĆ STANKOVIĆ[1], NIKOLA SREĆKOVIĆ[2], MARKO N. ŽIVANOVIĆ[1] and BILJANA M. ŠMIT[1]*

[1]*University of Kragujevac, Institute for Information Technologies, Department of Science, Jovana Cvijića bb, 34000 Kragujevac, Serbia and* [2]*University of Kragujevac, Faculty of Science, Department of Chemistry, Radoja Domanovića 12, 34000 Kragujevac, Serbia*

J. Serb. Chem. Soc. 87 (12) (2022) 1349–1358

SPECTRAL AND ANALYTICAL DATA

*4-(3-methoxy-4-propoxyphenyl)butan-2-one (**1c**)*

Yield: 0.947 g (80 %). IR (KBr): 2963m, 2877m, 1714s, 1589w, 1514s, 1465m, 1419m, 1363m, 1258s, 1231s, 1158m, 1138s, 1036m, 978m, 800m cm^{-1}. ^{1}H NMR (200 MHz, $CDCl_3$, δ / ppm): 6.74 (d, 1H, J = 8.0, H-9), 6.71 (s, 1H, H-6), 6.69 (d, 1H, J = 8.2 Hz, H-10), 3.94 (t, 2H, J = 6.8 Hz, CH_2-12), 3.84 (s, 3H, CH_3-11), 2.68-2.88 (m, 4H, CH_2-3, CH_2-4), 2.13 (s, 3H, CH_3-1), 1.84 (sext, 2H, J = 7.2 Hz, CH_2-13), 1.02 (t, 3H, J = 7.5 Hz, CH_3-14). ^{13}C NMR (50 MHz, $CDCl_3$, δ / ppm): 208.01 (C2), 149.14 (C7), 146.71 (C8), 133.44 (C5), 119.94 (C10), 112.99 (C9), 112.02 (C6), 70.42 (C12), 55.78 (C11), 45.24 (C4), 29.94 (C3), 29.20 (C1), 22.34 (C13), 10.28 (C14).

*4-(4-isopropoxy-3-methoxyphenyl)butan-2-one (**1d**)*

Yield: 0.926 g (78 %). IR (KBr): 2975m, 2933m, 1714s, 1587w, 1510s, 1465m, 1451m, 1419m, 1369m, 1259s, 1229m, 1157m, 1138m, 1110m, 1035m, 955w, 806w cm^{-1}. ^{1}H NMR (200 MHz, $CDCl_3$, δ / ppm): 6.65-6.83 (m, 3H, H-6, H-9, H-10), 4.46 (sept, 1H, J = 6.0 Hz, CH-12), 3.83 (s, 3H, CH_3-11), 2.68-2.90 (m, 4H, CH_2-3, CH_2-4), 2.14 (s, 3H, CH_3-1), 1.33 (d, 6H, J = 6.2 Hz, CH_3-13, CH_3-14). ^{13}C NMR (50 MHz, $CDCl_3$, δ / ppm): 208.24 (C2), 150.24 (C7), 145.44 (C8), 134.02 (C5), 119.98 (C10), 116.01 (C9), 112.28 (C6), 71.45 (C12), 55.8 (C11), 45.31 (C4), 30.04 (C3), 29.30 (C1), 22.02 (C13, C14).

*4-(4-butoxy-3-methoxyphenyl)butan-2-one (**1e**)*

Yield: 1.088 g (87 %). IR (KBr): 2957m, 2935m, 2872w, 1715s, 1589m, 1514s, 1465m, 1419m, 1362m, 1257s, 1233s, 1158s, 1139s, 1034s, 972, 800m cm^{-1}. ^{1}H NMR (200 MHz, $CDCl_3$, δ / ppm): 6.79 (d, 1H, J = 7.8 Hz, H-9), 6.71 (s, 1H, H-6), 6.69 (d, 1H, J = 8.0 Hz, H-10), 3.98 (t, 2H, J = 6.8 Hz, CH_2-12), 3.84 (s, 3H, CH_3-11), 2.68-2.88 (m, 4H, CH_2-3, CH_2-4), 2.13 (s, 3H, CH_3-1), 1.81 (quint, 2H, J = 3.6 Hz, CH_2-13), 1.48 (sext, 2H, J = 3.7 Hz, CH_2-14), 0.96 (t, 3H, J = 7.3 Hz, CH_3-15). ^{13}C NMR (50 MHz, $CDCl_3$, δ / ppm): 208.03 (C2),

* Corresponding author. E-mail: biljana.smit@uni.kg.ac.rs

149.17 (C7), 146.78 (C8), 133.44 (C5), 119.96 (C10), 112.97 (C9), 112.04 (C6), 68.65 (C12), 55.81 (C11), 45.28 (C4), 31.14 (C3), 29.98 (C1), 29.24 (C13), 19.07 (C14), 13.74 (C15).

*4-(3-methoxy-4-((2-methylallyl)oxy)phenyl)butan-2-one (**1g**)*

Yield: 0.942 g (76 %). IR (KBr): 2938w, 1714s, 1603w, 1515s, 1452m, 1430m, 1364m, 1268s, 1235m, 1158m, 1140m, 1035m, 906w, 860w, 809w, 630w cm^{-1}.^{1}H NMR (200 MHz, $CDCl_3$, δ / ppm): 6,83 (d, 1H, J = 7.8 Hz, H-9) 6.77 (s, 1H, H-6) 6.67 (d, 1H, J = 7.2 Hz, H-10), 5.07 (m, 1H, H-14), 4.96 (m, 1H, H-14), 3.86 (s, 3H, CH_3-11), 2.67-2.90 (m, 4H, CH_2-3, CH_2-4), 2.14 (s, 3H, CH_3-1), 1.82 (s, 3H, CH_3-15). ^{13}C NMR (50 MHz, $CDCl_3$, δ / ppm): 207.85 (C2), 148.99 (C7), 146.63 (C8), 143.89 (C13), 133.99 (C5), 120.03 (C10), 114.02 (C9), 112.46 (C14), 111.04 (C6), 72.95 (C12), 56.04 (C11), 45.52 (C4), 30.08 (C3), 29.44 (C1), 19.32 (C15).

*3-((4-(3,4-dimethoxyphenyl)butan-2-ylidene)amino)-2-thioxoimidazolidin-4-one (**2a**)*

Yield: 0.439 g (68 %). IR (KBr): 3152w, 3079w, 2935m, 1722s, 1638s, 1604s, 1515s, 1452m, 1418m, 1346m, 1257s, 1158m, 1138m, 1035m, 897w, 844w, 799w, 702w, 632w, 516w cm^{-1}. ^{1}H NMR (200 MHz, $CDCl_3$, δ / ppm): 9.98 (bs, NH, exchangeable with D_2O), 6.95 (d, 1H, J = 11.6 Hz, H-14), 6.86 (d, 1H, J = 8.4 Hz, H-15), 6.79 (s, 1H, H-11), 3.88 (s, 3H, OCH_3), 3.86 (s, 3H, OCH_3), 3.75 (s, 2H, CH_2-5), 2.57-2.96 (m, 4H, CH_2-8, CH_2-9), 2.03 (s, 3H, CH_3-6). ^{13}C NMR (50 MHz, $CDCl_3$, δ / ppm): 173.02 (C2), 167.29 (C4), 160.76 (C7), 149.26 (C12), 148.90 (C13), 135.70 (C10), 127.11 (C15), 120.16 (C14), 111.49 (C11), 55.96 (C16, C17), 40.55 (C9), 33.04 (C5), 31.91 (C8), 13.34 (C6). (+)LC-HRMS (*m*/*z*): calculated for $[C_{15}H_{19}O_3N_3S + H]^+$ 320.1074, observed 320.1220. Combustion analysis for $C_{15}H_{19}O_3N_3S$: Calculated. C 56.06, H 5.96, N 13.07; found C 56.10, H 5.98, N 13.04.

*3-((4-(4-ethoxy-3-methoxyphenyl)butan-2-ylidene)amino)-2-thioxoimidazolidin-4-one (**2b**)*

Yield: 0.465 g (69 %). IR (KBr): 3148m, 2983m, 1724s, 1694s, 1636s, 1602s, 1515s, 1449w, 1418w, 1344m, 1255m, 1233m, 1197m, 1154m, 1137m, 1032m, 896w, 792w, 701w, 516w cm^{-1}. ^{1}H NMR (200 MHz, $CDCl_3$, δ / ppm): 9.68 (bs, NH, exchangeable with D_2O), 6.70-6.86 (m, 3H, H-11, H-14, H-15), 3.87 (s, 3H, CH_3-16), 3.75 (s, 2H, CH_2-5), 2.55-2.93 (m, 4H, CH_2-8, CH_2-9), 2.02 (s, 3H, CH_3-6), 1.45 (t, 3H, J = 7.0 Hz, CH_3-18). ^{13}C NMR (50 MHz, $CDCl_3$, δ / ppm): 172.95 (C2), 167.35 (C4), 160.40 (C7), 149.32 (C12), 143.84 (C13), 134.17 (C10), 120.94 (C15), 114.30 (C14), 111.11 (C11), 64.55 (C17), 56.01 (C16), 40.58 (C9), 32.99 (C5), 32.00 (C8), 17.86 (C6), 14.94 (C18). (+)LC-HRMS (*m*/*z*): calculated for $[C_{16}H_{21}O_3N_3S + H]^+$ 336.1376, observed 336.1378. Combustion analysis for $C_{16}H_{21}O_3N_3S$: Calculated. C 57.29, H 6.31, N 12.53; found C 57.33, H 6.33, N 14.49.

*3-((4-(3-methoxy-4-propoxyphenyl)butan-2-ylidene)amino)-2-thioxoimidazolidin-4-one (**2c**)*

Yield: 0.504 g (72 %). IR (KBr): 3142m, 2965m, 2933m, 2876m, 1709s, 1633s, 1598s, 1516s, 1470m, 1454m, 1418m, 1347m, 1256s, 1230s, 1160m, 1135m, 1034m, 1019m, 978w, 897w, 796m, 702w, 516w, 500w cm^{-1}. ^{1}H NMR (200 MHz, $CDCl_3$, δ / ppm): 9.33 (bs, NH, exchangeable with D_2O), 6.65-6.85 (m, 3H, H-11, H-14, H-15), 3.95 (t, 2H, J = 6.8 Hz, CH_2-17), 3.86 (s, 3H, CH_3-16), 3.75 (s, 2H, CH_2-5), 2.56-2.94 (m, 4H, CH_2-8, CH_2-9), 2.02 (s, 3H, CH_3-6), 1.86 (sext, 2H, J = 7.2 Hz, CH_2-18), 1.03 (t, 3H, J = 7.4 Hz, CH_3-19). ^{13}C NMR (50 MHz, $CDCl_3$, δ / ppm): 172.66 (C2), 167.40 (C4), 159.90 (C7), 149.44 (C12), 146.94 (C13), 134.17 (C10), 120.28 (C15), 113.53 (C14), 112.59 (C11), 70.85 (C17), 56.13 (C16), 40.52 (C9), 32.93 (C5), 31.67 (C8), 22.64 (C18), 17.83 (C6), 10.48 (C19). (+)LC-HRMS (*m*/*z*): calculated for $[C_{17}H_{23}O_3N_3S + H]^+$ 350.1533, observed 350.1532. Combustion

analysis for $C_{17}H_{23}O_3N_3S$: Calculated. C 58.43, H 6.63, N 12.02; found C 58.40, H 6.30, N 12.06.

3-((4-(4-isopropoxy-3-methoxyphenyl)butan-2-ylidene)amino)-2-thioxoimidazolidin-4-one ***(2d)***

Yield: 0.228 g (33 %). IR (KBr): 2973m, 2931m, 2857w, 1717s, 1639s, 1610s, 1511s, 1465m, 1334m, 1262s, 1157w, 1139m, 1111m, 1037w, 956w, 850w, 809w, 736w, 710w, 514w cm^{-1}. ^1H NMR (200 MHz, $CDCl_3$, δ / ppm): 9.39 (bs, NH, exchangeable with D_2O), 6.66-6.87 (m, 3H, H-11, H-14, H-15), 4.47 (sept, 1H, J = 6.2 Hz, CH-17), 3.85 (s, 3H, CH_3-16), 3.75 (s, 2H, CH_2-5), 2.56-2.94 (m, 4H, CH_2-8, CH_2-9), 2.02 (s, 3H, CH_3-6), 1.35 (d, 6H, J = 6.0 Hz, CH_3-18, CH_3-19). ^{13}C NMR (50 MHz, $CDCl_3$, δ / ppm): 172.82 (C2), 167.33 (C4), 160.97 (C7), 150.54 (C12), 145.63 (C13), 134.76 (C10), 120.28 (C15), 116.75 (C14), 112.81 (C11), 71.83 (C17), 56.08 (C16), 40.49 (C9), 32.97 (C5), 32.02 (C8), 22.24 (C18, C19), 17.84 (C6). (+)LC-HRMS (m/z): calculated for $[C_{17}H_{23}O_3N_3S + H]^+$ 350.1533, observed 350.1533. Combustion analysis for $C_{17}H_{23}O_3N_3S$: Calculated. C 58.43, H 6.63, N 12.02; found C 58.45, H 6.36, N 11.98.

3-((4-(4-butoxy-3-methoxyphenyl)butan-2-ylidene)amino)-2-thioxoimidazolidin-4-one ***(2e)***

Yield: 0.637 g (88 %). IR (KBr): 3145m, 2958m, 2935m, 2871m, 1709s, 1636s, 1604s, 1517s, 1467m, 1419m, 1346m, 1257s, 1234s, 1161m, 1138m, 1034m, 1009w, 972w, 897w, 844w, 795w, 701w, 516w cm^{-1}. ^1H NMR (200 MHz, $CDCl_3$, δ / ppm): 9.27 (bs, NH, exchangeable with D_2O), 6.65-6.85 (m, 3H, H-11, H-14, H-15), 3.99 (t, 2H, J = 6.8 Hz, CH_2-17), 3.86 (s, 3H, CH_3-16), 3.75 (s, 2H, CH_2-5), 2.56-2.94 (m, 4H, CH_2-8, CH_2-9), 2.02 (s, 3H, CH_3-6), 1.82 (quint, 2H, J = 7.3 Hz, CH_2-18), 1.48 (sext, 2H, J = 7.4 Hz, CH_2-19), 0.97 (t, 3H, J = 7.2 Hz, CH_3-20). ^{13}C NMR (50 MHz, $CDCl_3$, δ / ppm): 172.73 (C2), 167.37 (C4), 159.97 (C7), 149.46 (C12), 147.00 (C13), 134.15 (C10), 120.28 (C15), 113.50 (C14), 112.60 (C11), 69.03 (C17), 56.13 (C16), 40.51 (C9), 32.94 (C5), 31.96 (C8), 31.41 (C18), 19.27 (C19), 17.82 (C6), 13.88 (C20). (+)LC-HRMS (m/z): calculated for $[C_{18}H_{25}O_3N_3S + H]^+$ 364.1689, observed 364.1689. Combustion analysis for $C_{18}H_{25}O_3N_3S$: Calculated. C 59.48, H 6.93, N 11.56; found C 59.44, H 6.95, N 11.51.

3-((4-(4-(benzyloxy)-3-methoxyphenyl)butan-2-ylidene)amino)-2-thioxoimidazolidin-4-one ***(2f)***

Yield: 0.686 g (86 %). IR (KBr): 3152w, 3035w, 3954w, 2870w, 1710s, 1639s, 1605s, 1515s, 1455w, 1418w, 1345m, 1256s, 1227s, 1161m, 1136m, 1034w, 1011w, 857w 806w, 745m, 698m, 515w cm^{-1}. ^1H NMR (200 MHz, $CDCl_3$, δ / ppm): 8.97 (bs, NH, exchangeable with D_2O), 7.25-7.50 (m, 5H, H-19, H-20, H-21, H22, H-23), 6.65-6.85 (m, 3H, H-11, H-14, H-15), 5.13 (s, 2H, CH_2-17), 3.88 (s, 3H, CH_3-16), 3.74 (s, 2H, CH_2-5), 2.55-2.93 (m, 4H, CH_2-8, CH_2-9), 2.00 (s, 3H, CH_3-6). ^{13}C NMR (50 MHz, $CDCl_3$, δ / ppm): 172.52 (C2), 167.34 (C4), 160.12 (C7), 149.71 (C12), 146.58 (C13), 137.46 (C18), 134.86 (C10), 128.43 (C19, C23), 127.69 (C21), 127.26 (C20, C22), 120.28 (C15), 114.65 (C14), 112.65 (C11), 71.41 (C17), 56.13 (C16), 40.45 (C9), 32.90 (C5), 31.97 (C8), 17.83 (C6). (+)LC-HRMS (m/z): calculated for $[C_{21}H_{23}O_3N_3S + H]^+$ 398.1533, observed 398.1532. Combustion analysis for $C_{21}H_{23}O_3N_3S$: Calculated. C 63.45, H 5.83, N 10.57; found C 63.50, H 5.81, N 10.62.

*3-((4-(3-methoxy-4-((2-methylallyl)oxy)phenyl)butan-2-ylidene)amino)-2-thioxoimidazolidin-4-one (**2g**)*

Yield: 0.441 g (61 %). IR (KBr): 3150m, 3079m, 2934m, 2852w, 1709s, 1634s, 1601s, 1514s, 1452m, 1418m, 1346m, 1256s, 1158m, 1137m, 1034m, 896w, 834w, 798w, 701w, 516w cm^{-1}. ^1H NMR (200 MHz, $CDCl_3$, δ / ppm): 9.79 (bs, NH, exchangeable with D_2O), 6.65-6.85 (m, 3H, H-11, H-14, H-15), 5.08 (m, 1H, H-19), 4.97 (m, 1H, H-19), 4.49 (s, 2H, CH_2-17), 3.87 (s, 3H, CH_3-16), 3.75 (s, 2H, CH_2-5), 2.55-2.94 (m, 4H, CH_2-8, CH_2-9), 2.02 (s, 3H, CH_3-6), 1.82 (s, 3H, CH_3-20). ^{13}C NMR (50 MHz, $CDCl_3$, δ / ppm): 173.02 (C2), 167.27 (C4), 160.53 (C7), 149.50 (C12), 146.63 (C13), 141.06 (C18), 134.54 (C10), 120.21 (C15), 114.13 (C14), 112.64 (C11), 112.42 (C19), 73.05 (C17), 56.11 (C16), 40.47 (C9), 32.99 (C5), 31.94 (C8), 19.34 (C20), 17.84 (C6). (+)LC-HRMS (*m*/*z*): calculated for $[C_{18}H_{23}O_3N_3S + H]^+$ 362.1533, observed 362.1533. Combustion analysis for $C_{18}H_{23}O_3N_3S$: Calculated. C 59.81, H 6.41, N 11.63; found C 59.86, H 6.44, N 11.58.

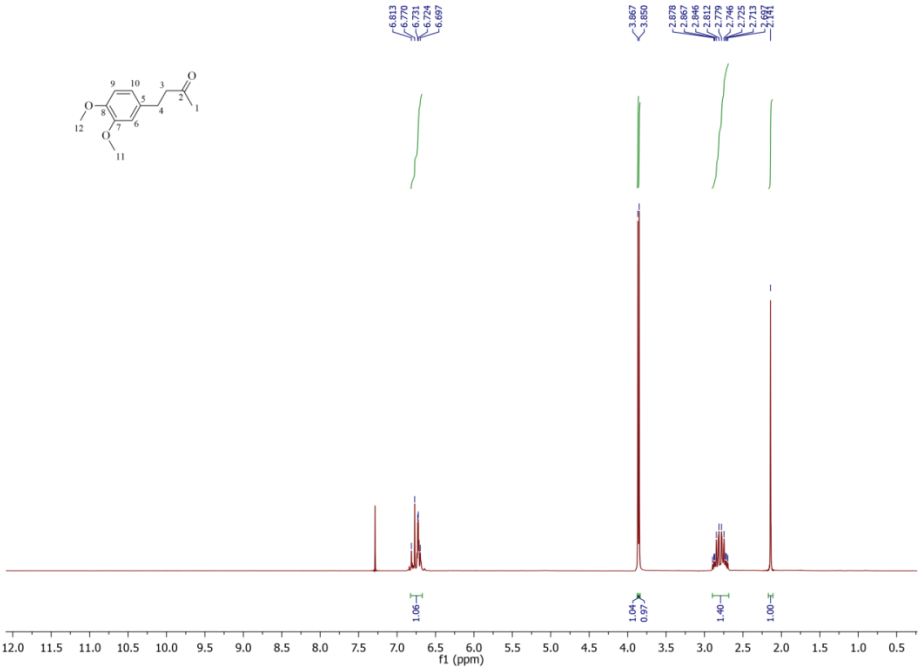

Fig. S-1. ^1H-NMR spectra of 4-(3,4-dimethoxyphenyl)butan-2-one (**1a**)

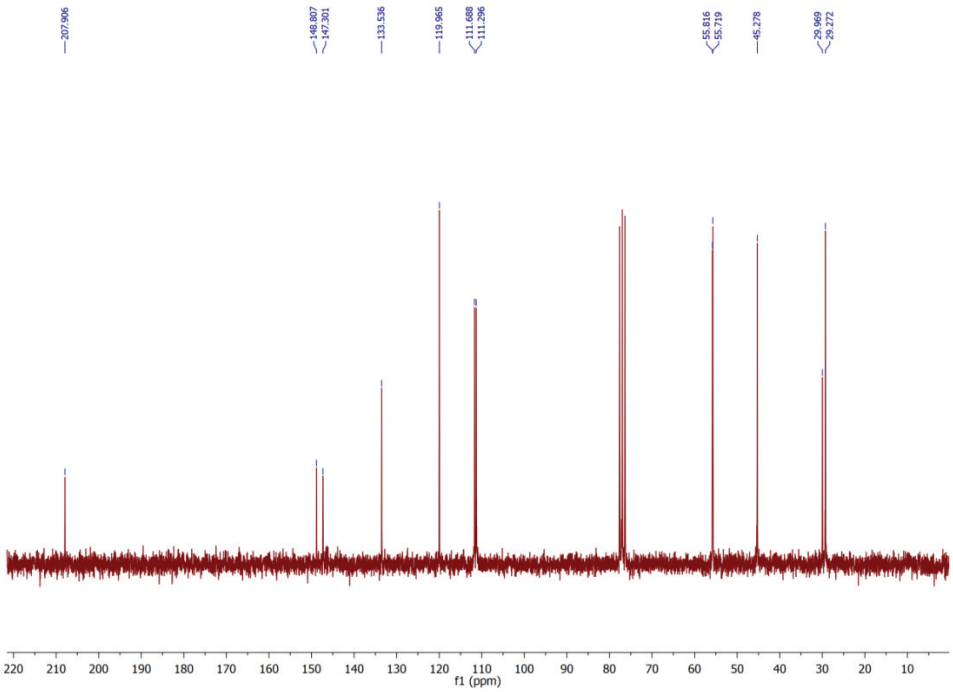

Fig. S-2. ^{13}C-NMR spectra of4-(3,4-dimethoxyphenyl)butan-2-one (**1a**)

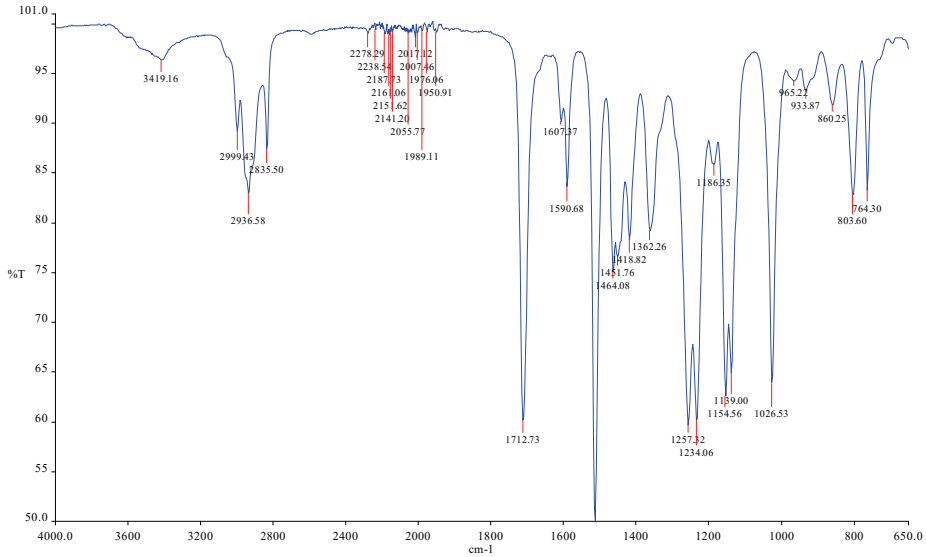

Fig. S-3. IR spectra of4-(3,4-dimethoxyphenyl)butan-2-one (**1a**)

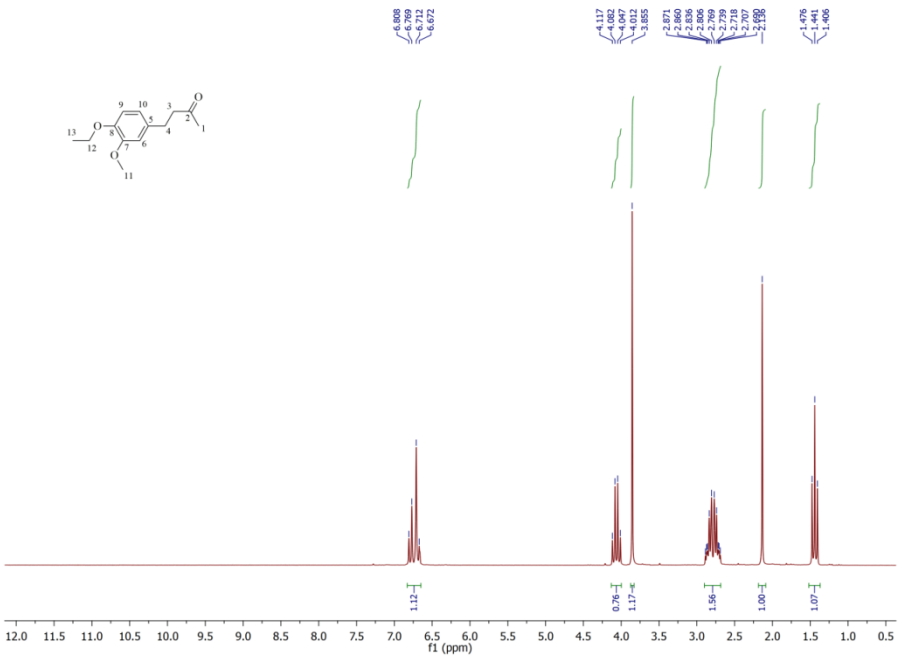

Fig. S-4. ^{1}H-NMR spectra of4-(4-ethoxy-3-methoxyphenyl)butan-2-one (**1b**)

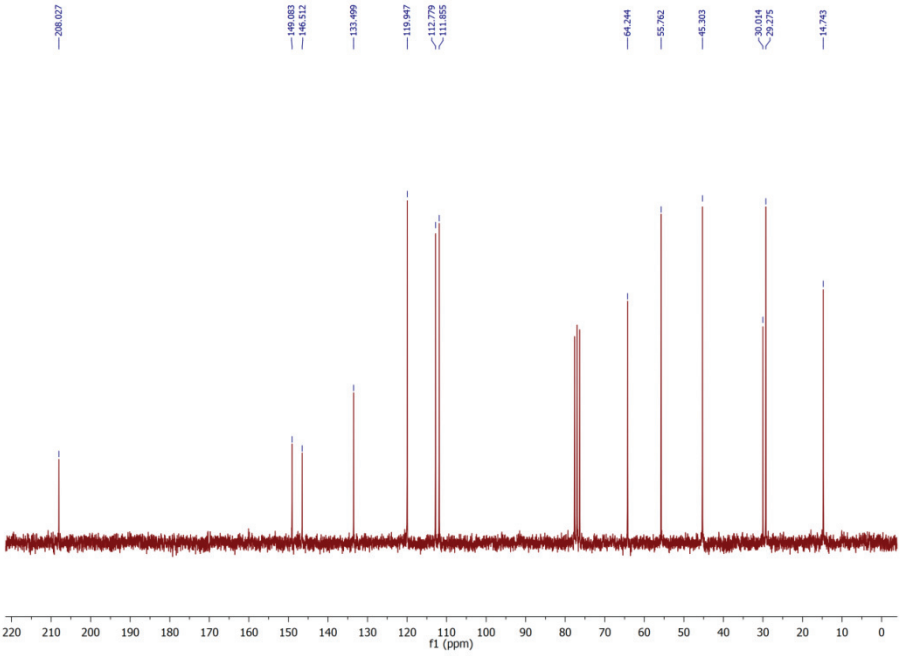

Fig. S-5. ^{13}C-NMR spectra of4-(4-ethoxy-3-methoxyphenyl)butan-2-one (**1b**)

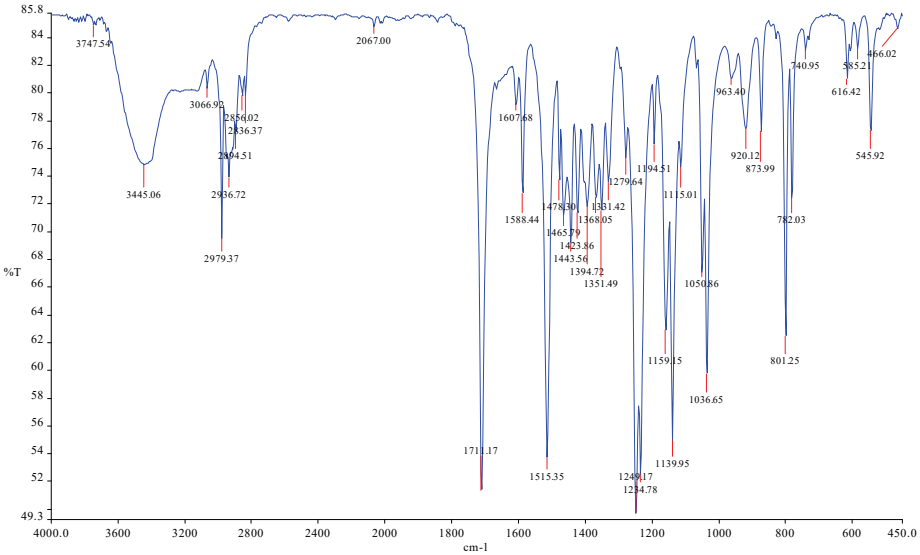

Fig. S-6. IR spectra of4-(4-ethoxy-3-methoxyphenyl)butan-2-one (**1b**)

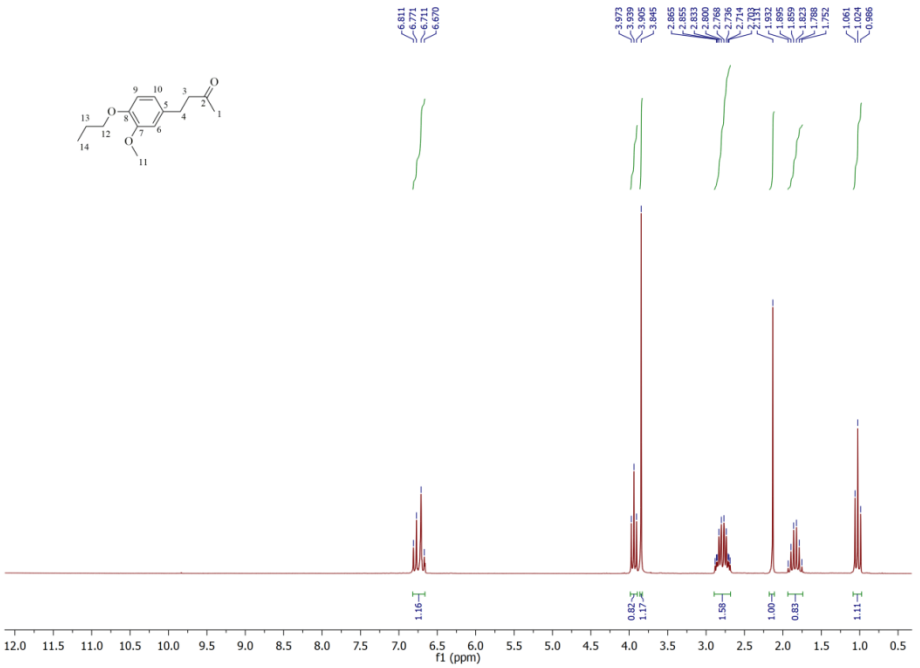

Fig. S-7. ^{1}H-NMR spectra of 4-(3-methoxy-4-propoxyphenyl)butan-2-one (**1c**)

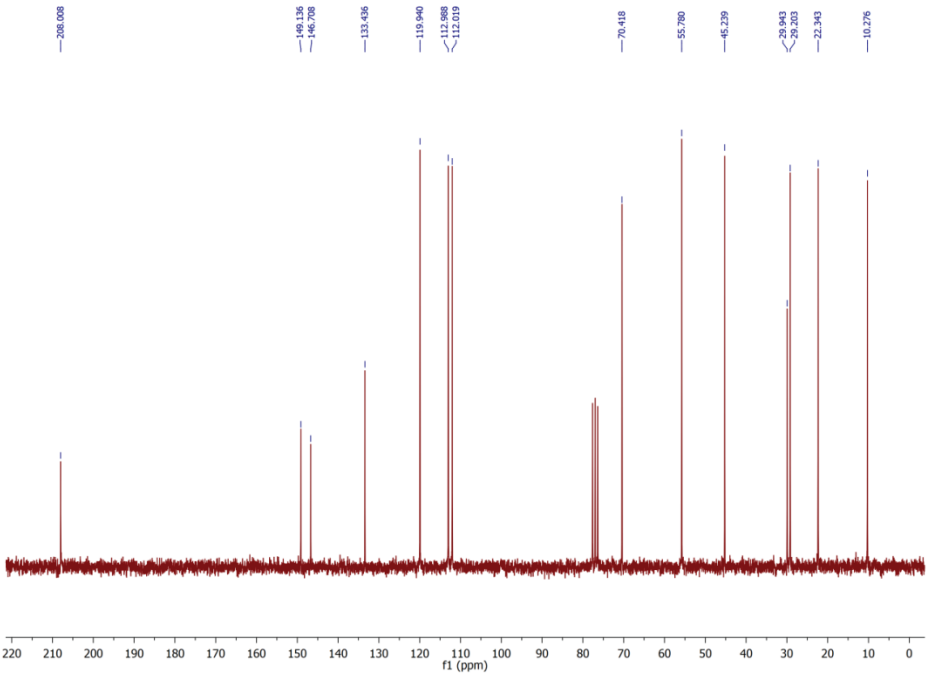

Fig. S-8. ^{13}C-NMR spectra of4-(3-methoxy-4-propoxyphenyl)butan-2-one (**1c**)

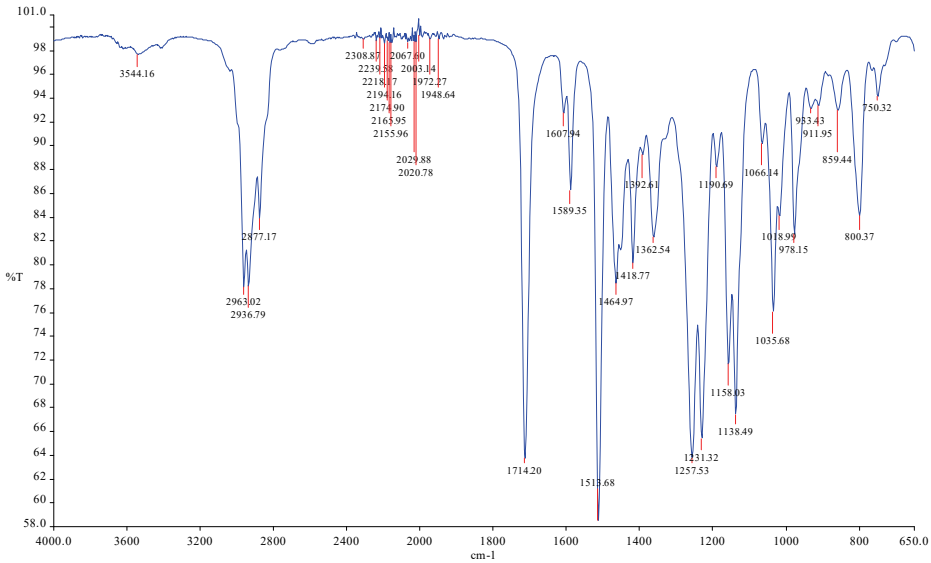

Fig. S-9. IR spectra of4-(3-methoxy-4-propoxyphenyl)butan-2-one (**1c**)

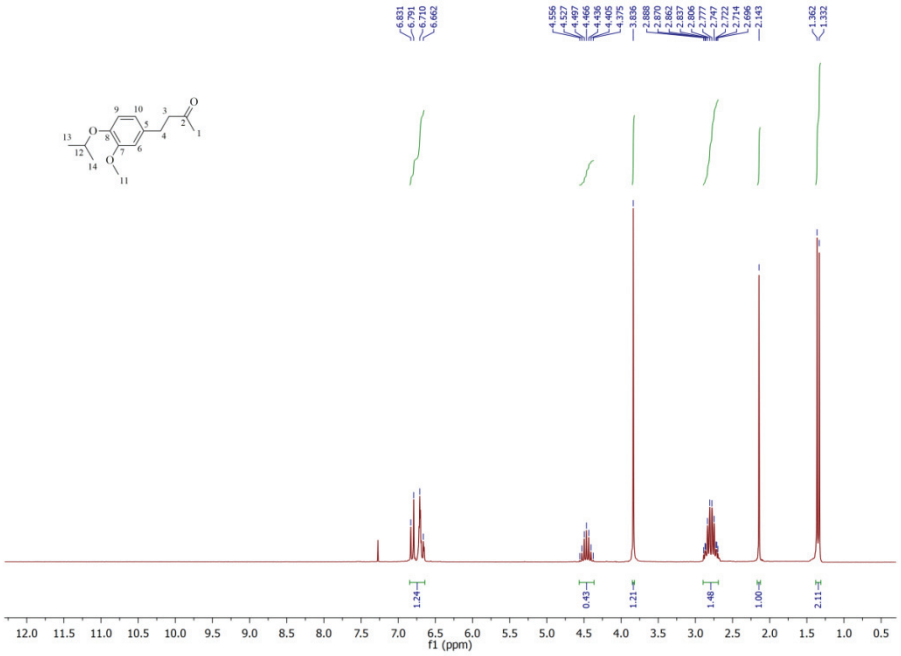

Fig. S-10. ^{1}H-NMR spectra of 4-(4-isopropoxy-3-methoxyphenyl)butan-2-one (**1d**)

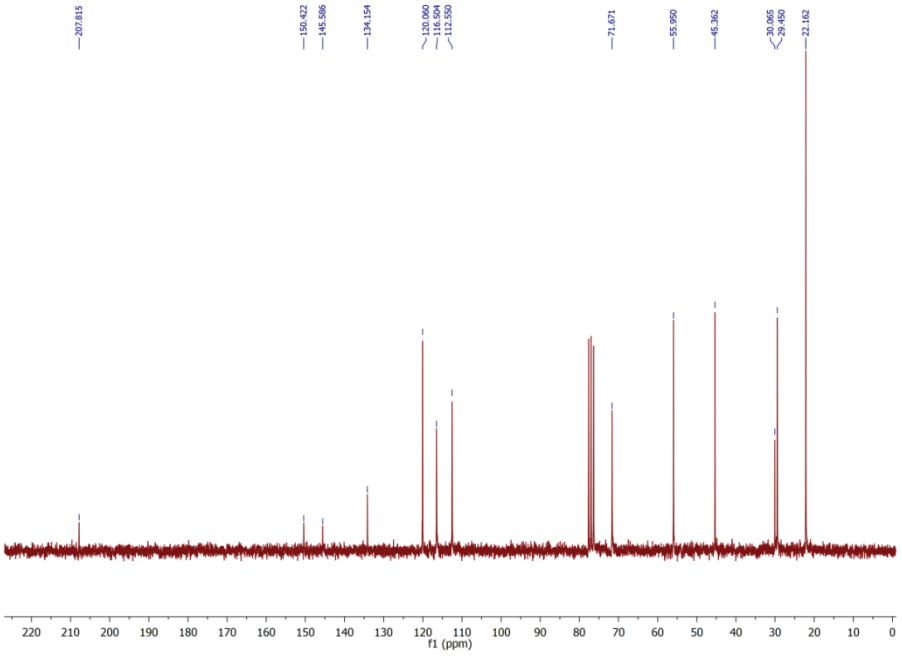

Fig. S-11. ^{13}C-NMR spectra of4-(4-isopropoxy-3-methoxyphenyl)butan-2-one (**1d**)

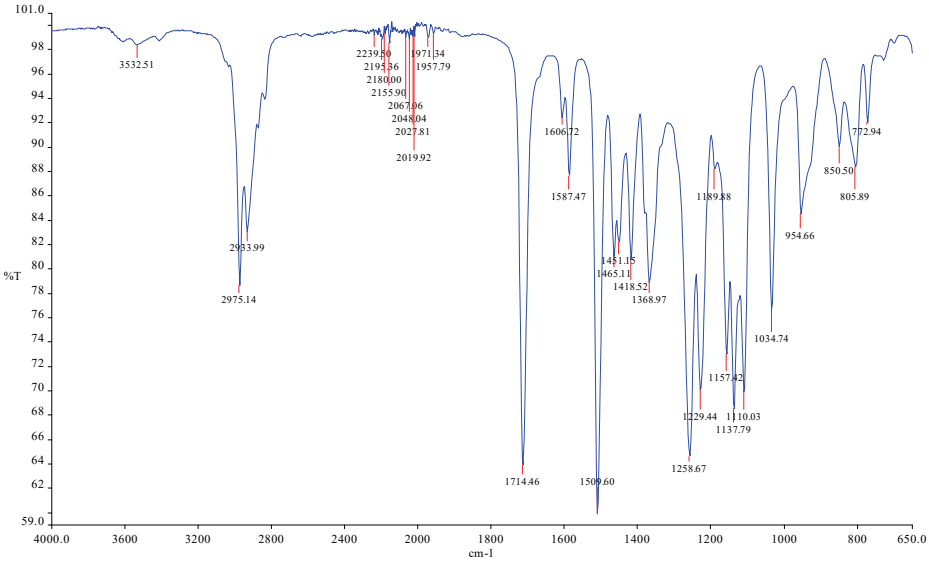

Fig. S-12. IR spectra of4-(4-isopropoxy-3-methoxyphenyl)butan-2-one (**1d**)

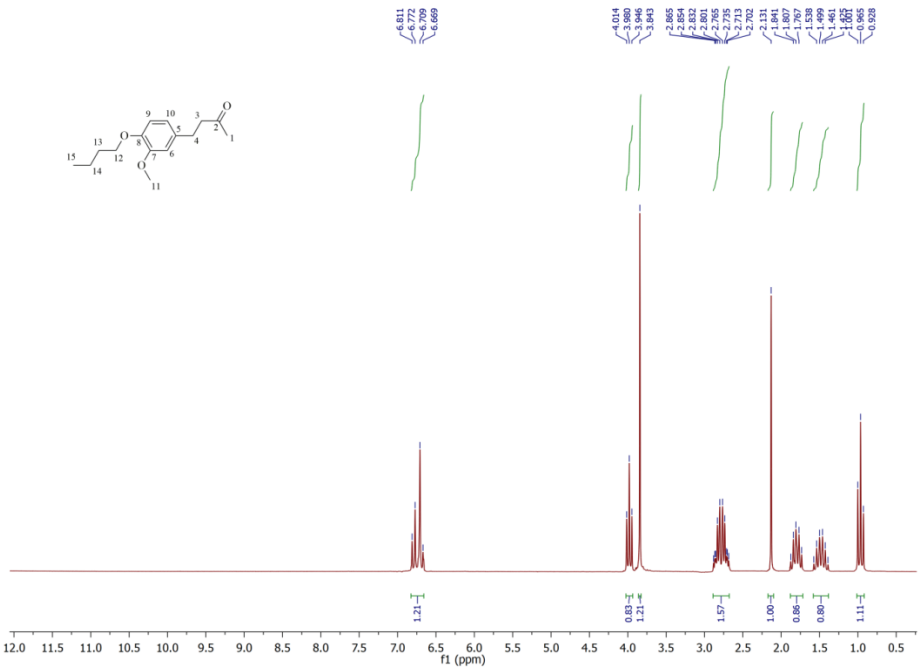

Fig. S-13. ^{1}H-NMR spectra of 4-(4-butoxy-3-methoxyphenyl)butan-2-one (**1e**)

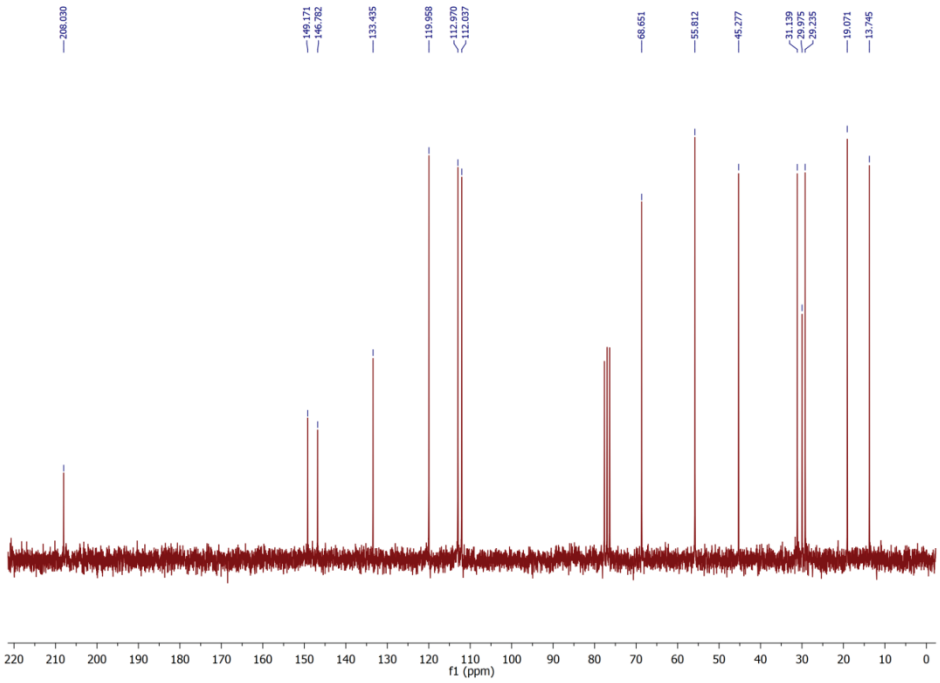

Fig. S-14. ^{13}C-NMR spectra of4-(4-butoxy-3-methoxyphenyl)butan-2-one (**1e**)

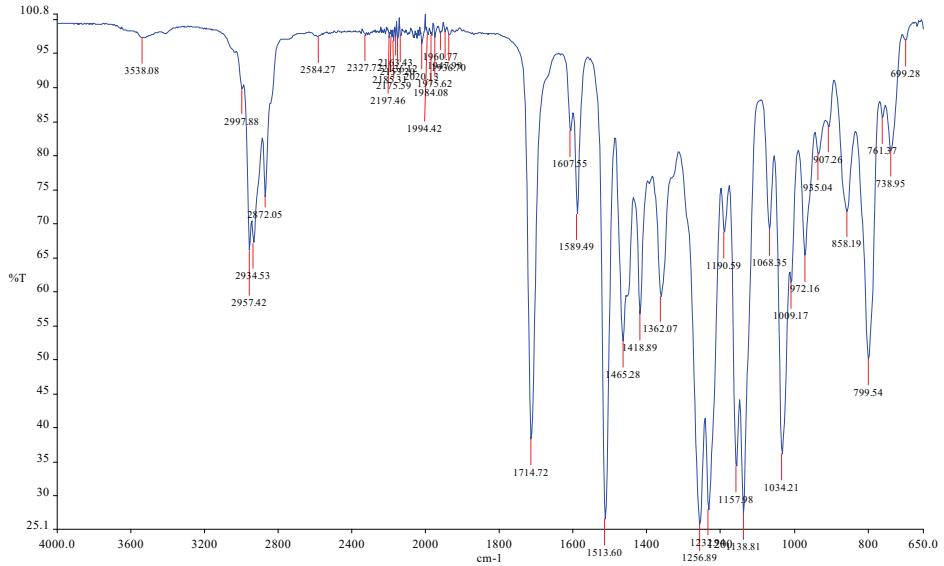

Fig. S-15. IR spectra of4-(4-butoxy-3-methoxyphenyl)butan-2-one (**1e**)

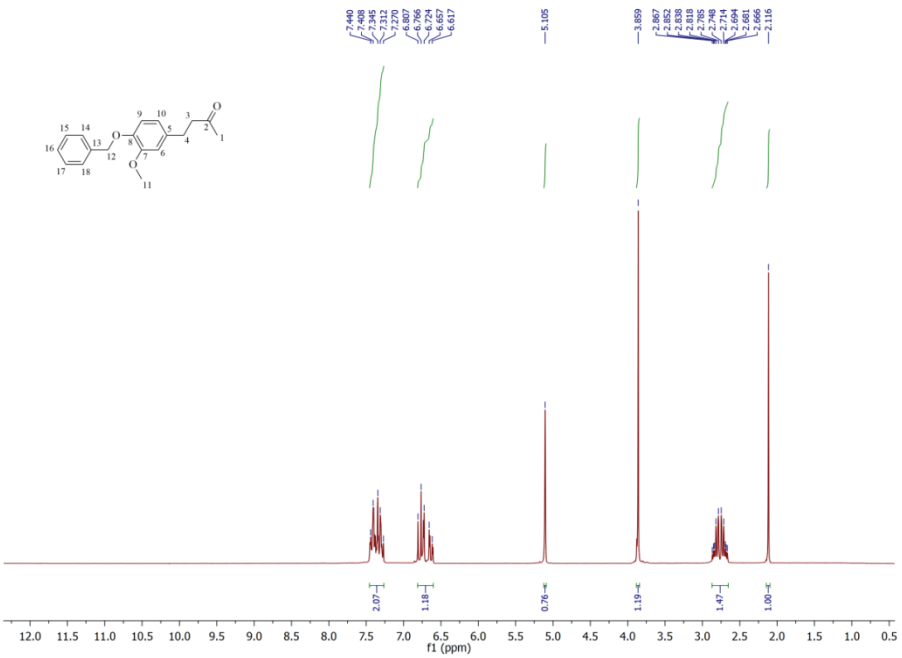

Fig. S-16. ^{1}H-NMR spectra of 4-(4-(benzyloxy)-3-methoxyphenyl)butan-2-one (**1f**)

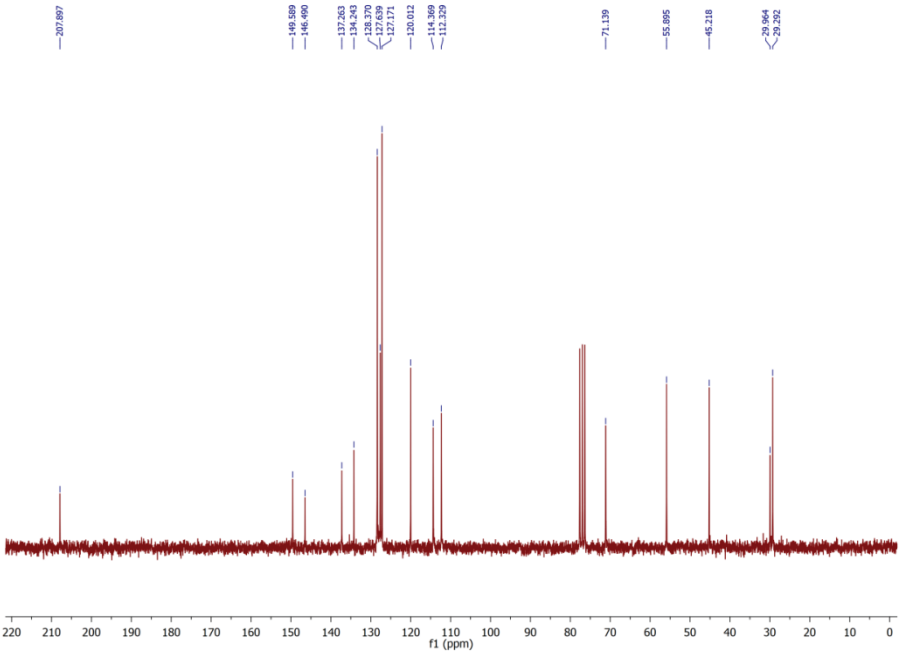

Fig. S-17. ^{13}C-NMR spectra of4-(4-(benzyloxy)-3-methoxyphenyl)butan-2-one (**1f**)

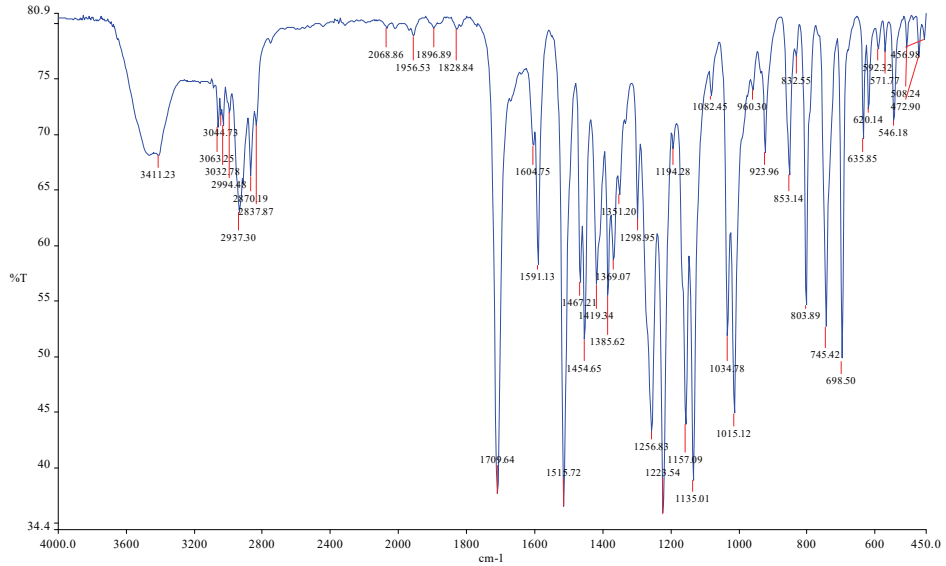

Fig. S-18. IR spectra of4-(4-(benzyloxy)-3-methoxyphenyl)butan-2-one (**1f**)

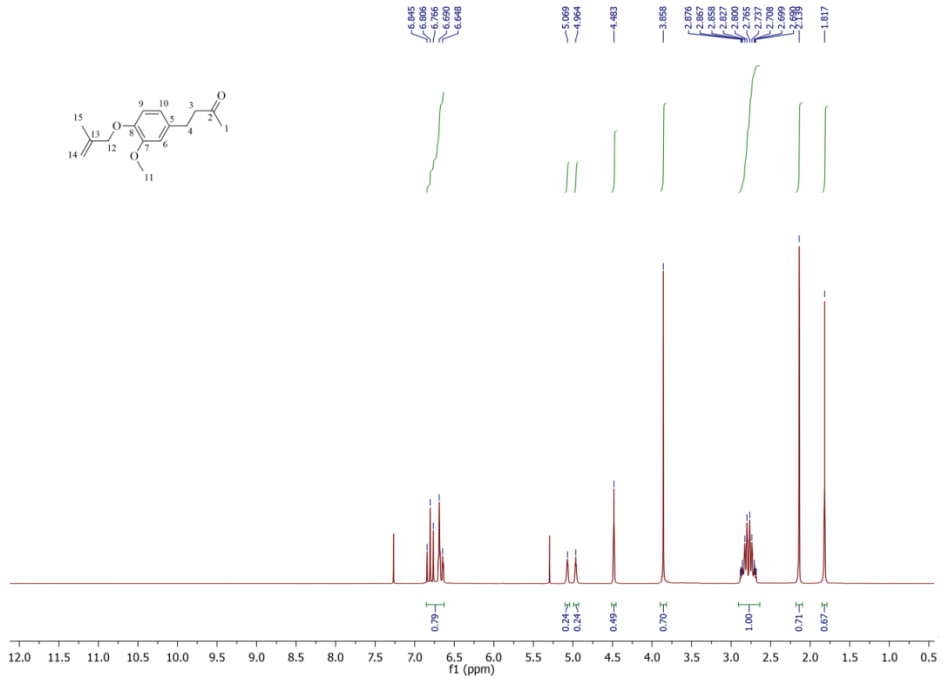

Fig. S-19. ^{1}H-NMR spectra of 4-(3-methoxy-4-((2-methylallyl)oxy)phenyl)butan-2-one (**1g**)

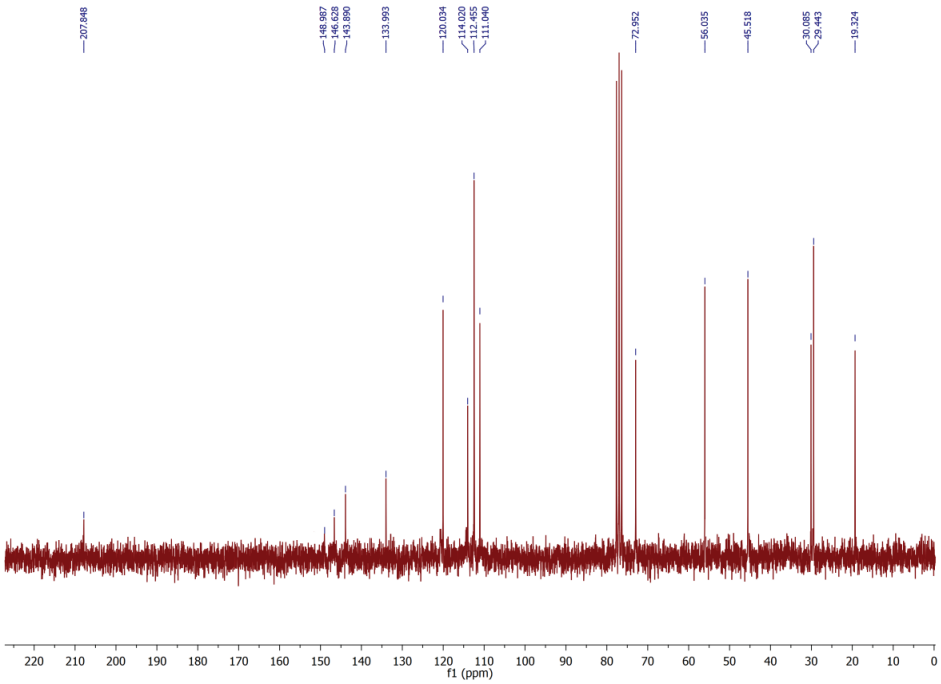

Fig. S-20. ^{13}C-NMR spectra of4-(3-methoxy-4-((2-methylallyl)oxy)phenyl)butan-2-one (**1g**)

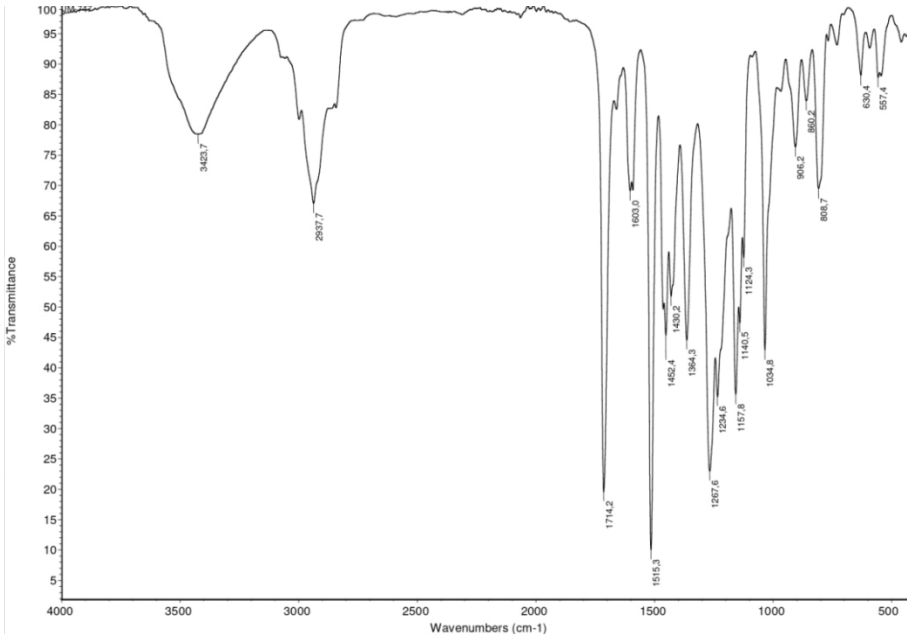

Fig. S-21. IR spectra of4-(3-methoxy-4-((2-methylallyl)oxy)phenyl)butan-2-one (**1g**)

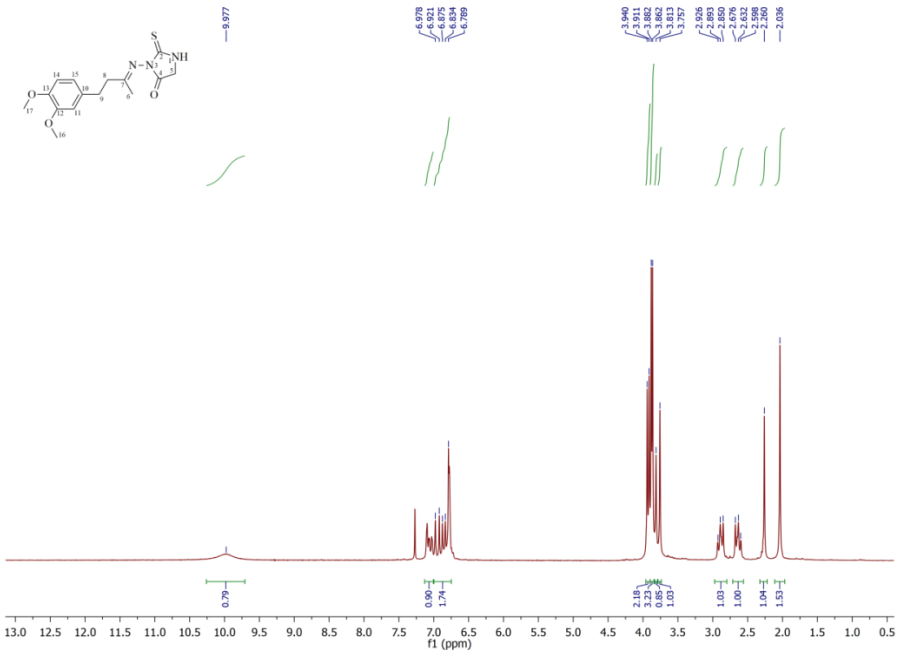

Fig. S-22. ^{1}H-NMR spectra of 3-((4-(3,4-dimethoxyphenyl)butan-2-ylidene)amino)-2-thioxoimidazolidin-4-one (**2a**)

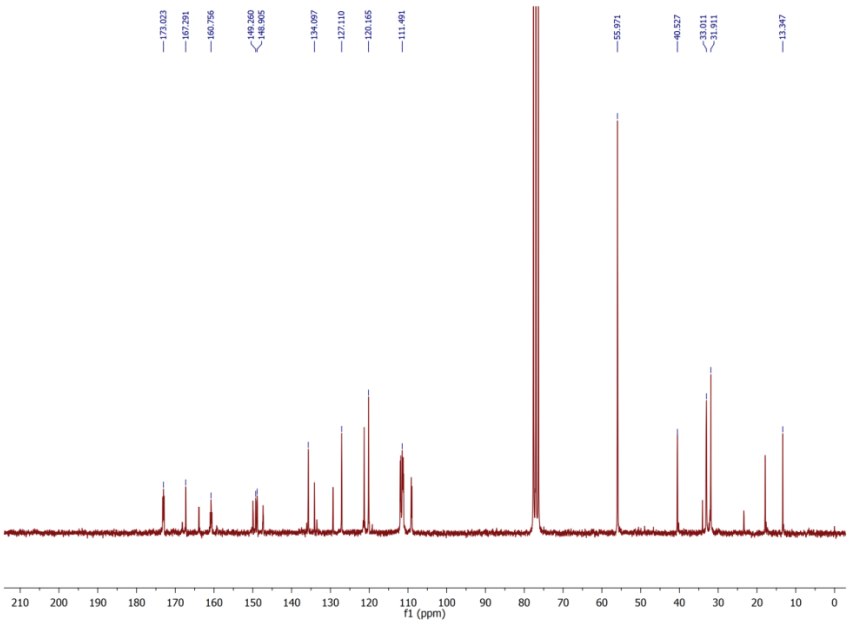

Fig. S-23. ^{13}C-NMR spectra of 3-((4-(3,4-dimethoxyphenyl)butan-2-ylidene)amino)-2-thioxoimidazolidin-4-one (**2a**)

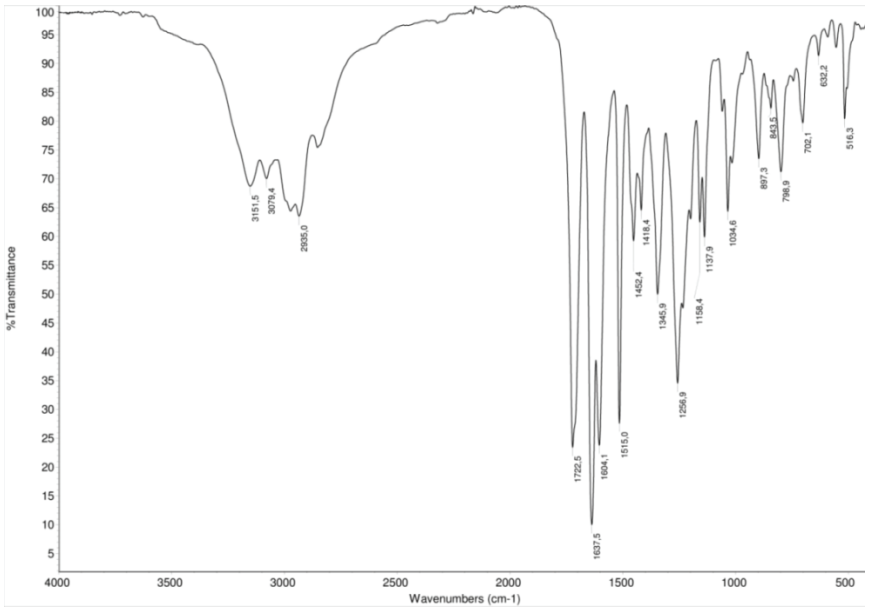

Fig. S-24. IR spectra of3-((4-(3,4-dimethoxyphenyl)butan-2-ylidene)amino)-2-thioxoimidazolidin-4-one (**2a**)

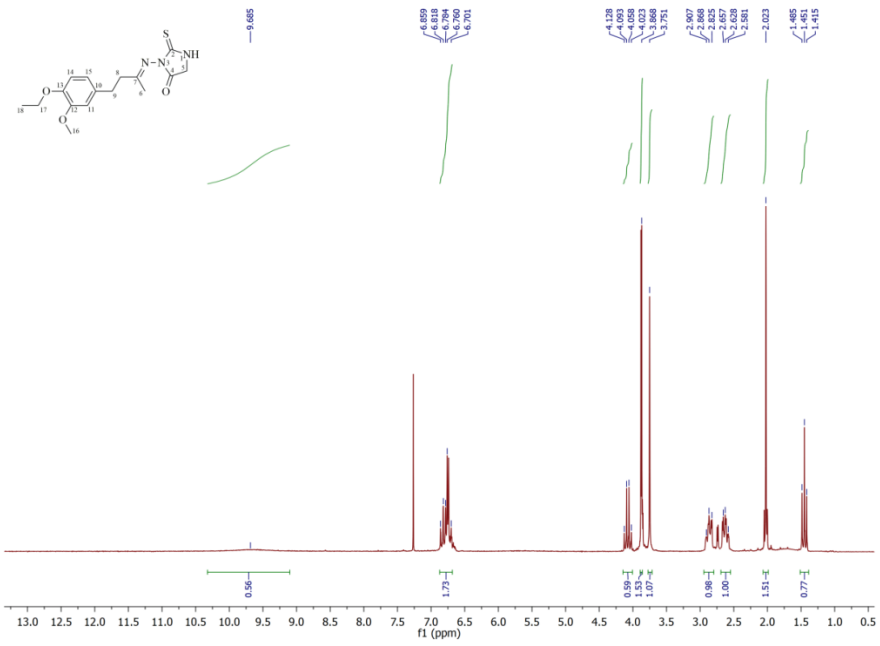

Fig. S-25. ^{1}H-NMR spectra of *3*-((4-(4-ethoxy-3-methoxyphenyl)butan-2-ylidene)amino)-2-thioxoimidazolidin-4-one (**2b**)

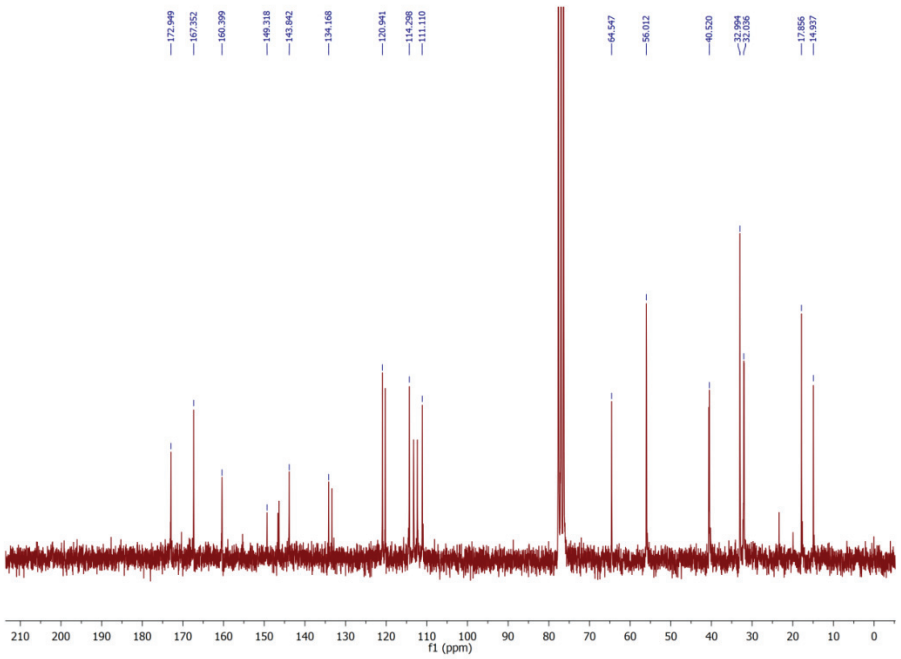

Fig. S-26. ^{13}C-NMR spectra of *3*-((4-(4-ethoxy-3-methoxyphenyl)butan-2-ylidene)amino)-2-thioxoimidazolidin-4-one (**2b**)

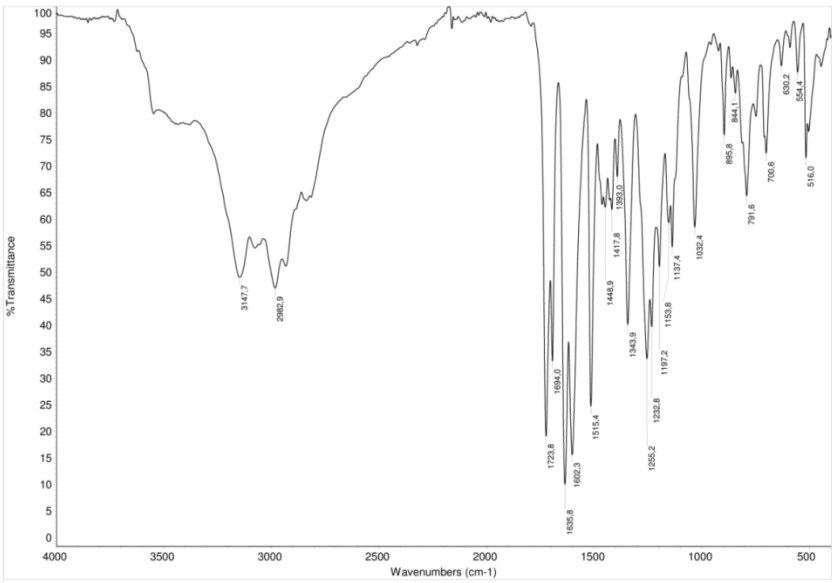

Fig. S-27. IR spectra of *3*-((4-(4-ethoxy-3-methoxyphenyl)butan-2-ylidene)amino)-2-thioxoimidazolidin-4-one (**2b**)

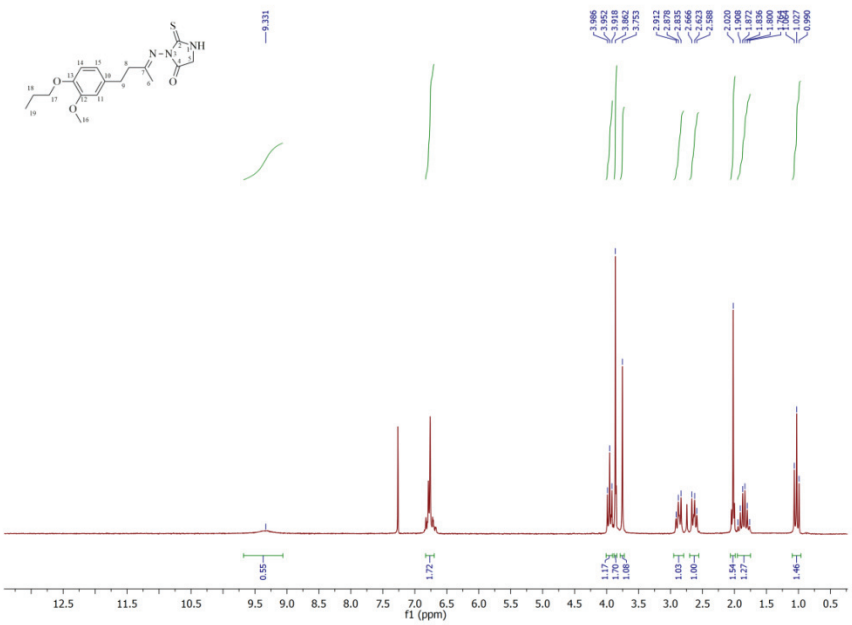

Fig. S-28. ^{1}H-NMR spectra of
3-((4-(3-methoxy-4-propoxyphenyl)butan-2-ylidene)amino)-2-thioxoimidazolidin-4-one (**2c**)

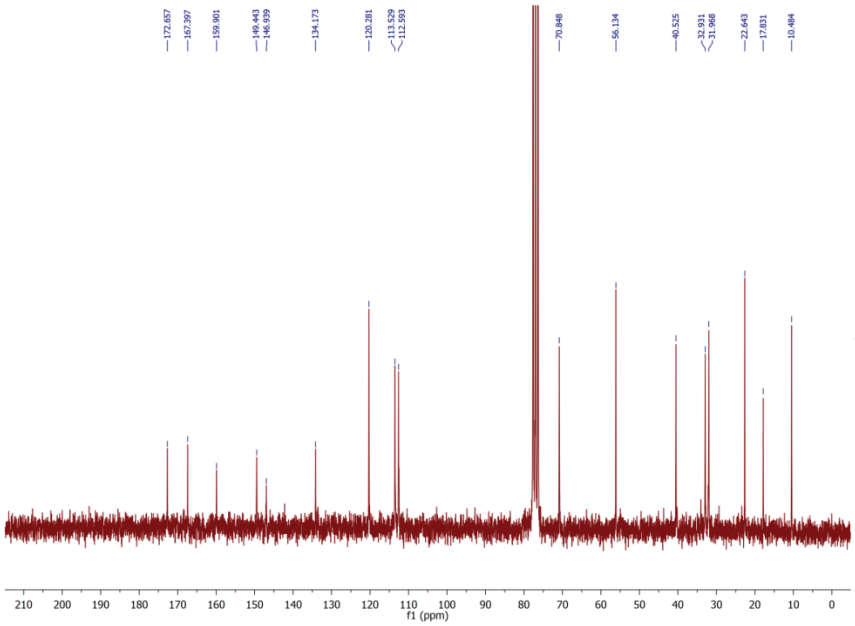

Fig. S-29. ^{13}C -NMR spectra of
3-((4-(3-methoxy-4-propoxyphenyl)butan-2-ylidene)amino)-2-thioxoimidazolidin-4-one (**2c**)

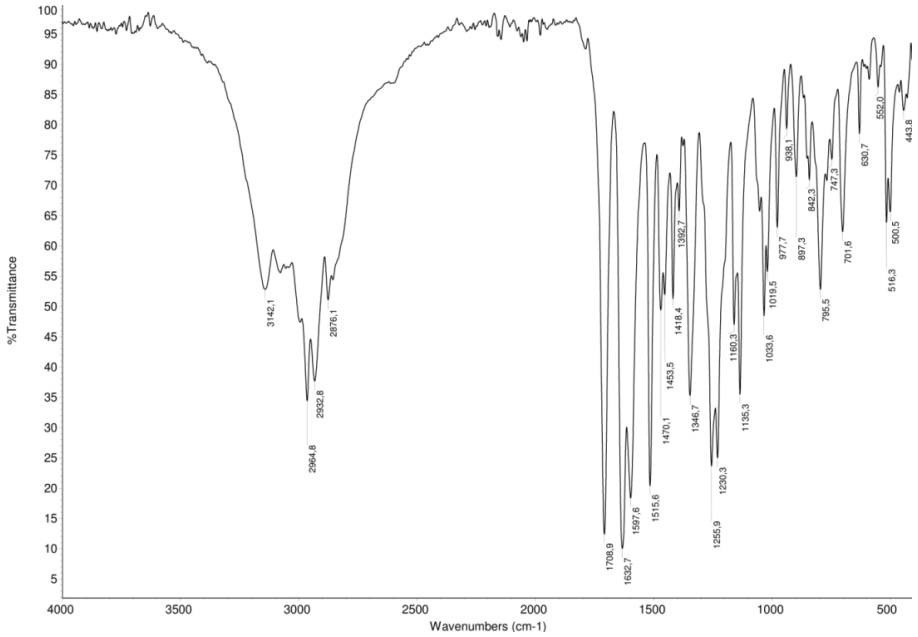

Fig. S-30. IR spectra of 3-((4-(3-methoxy-4-propoxyphenyl)butan-2-ylidene)amino)-2-thioxoimidazolidin-4-one (**2c**)

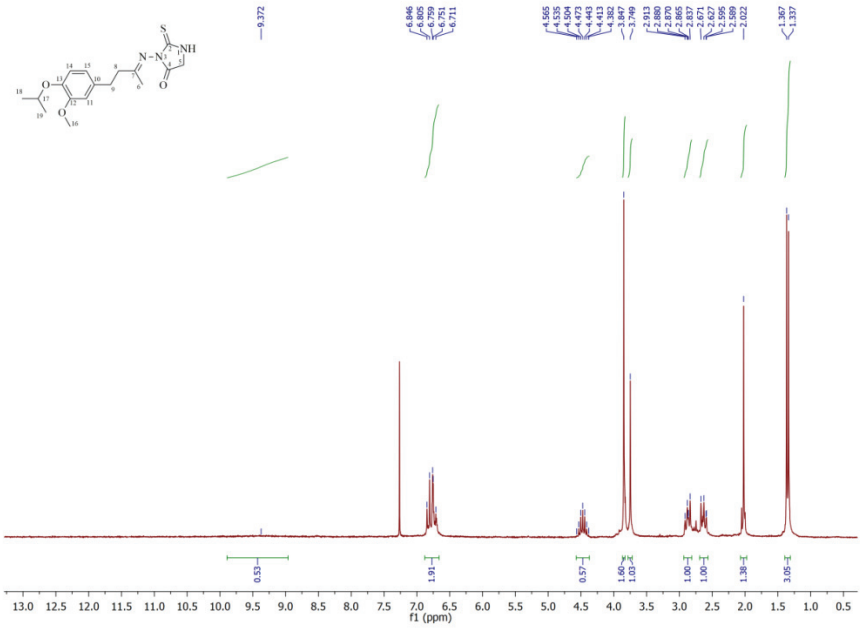

Fig. S-31. ^{1}H-NMR spectra of3-((4-(4-isopropoxy-3-methoxyphenyl)butan-2-ylidene)amino)-2-thioxoimidazolidin-4-one (**2d**)

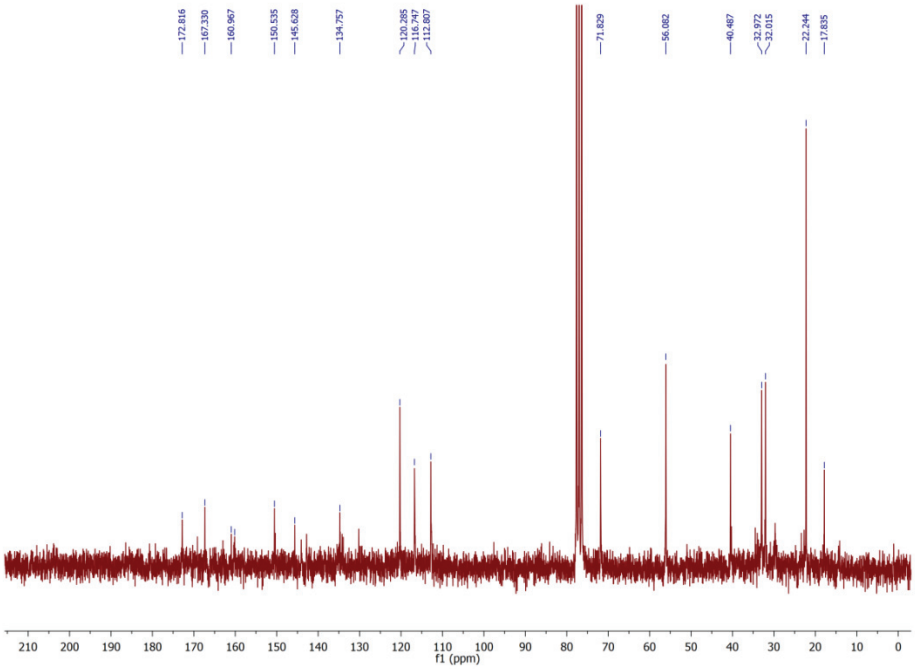

Fig. S-32. ^{13}C -NMR spectra of3-((4-(4-isopropoxy-3-methoxyphenyl)butan-2-ylidene)amino)-2-thioxoimidazolidin-4-one (**2d**)

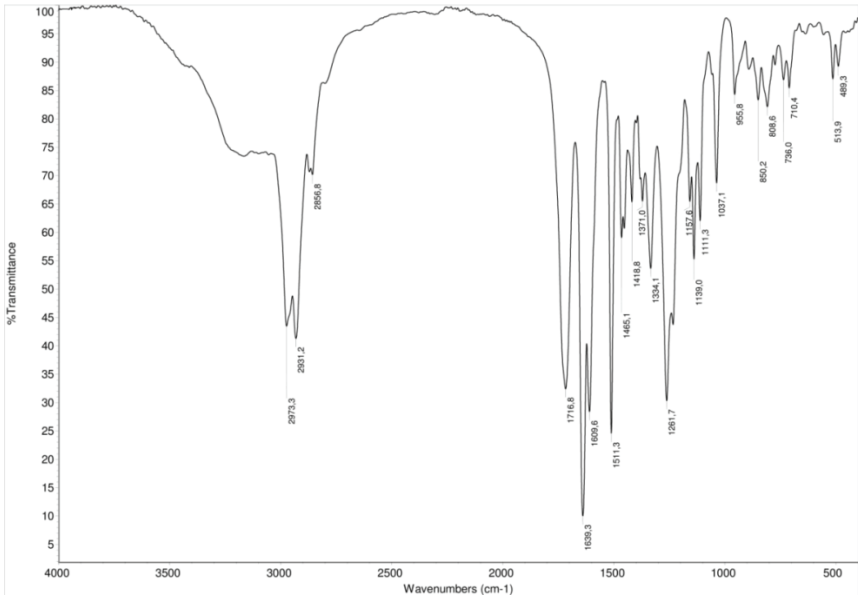

Fig. S-33. IR spectra of3-((4-(4-isopropoxy-3-methoxyphenyl)butan-2-ylidene)amino)-2-thioxoimidazolidin-4-one (**2d**)

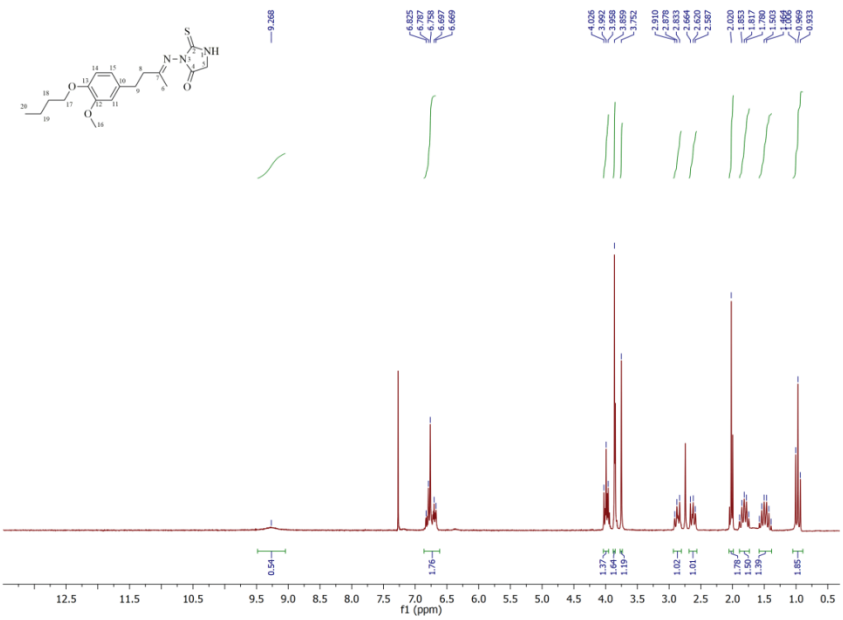

Fig. S-34. ^{1}H-NMR spectra of 3-((4-(4-butoxy-3-methoxyphenyl)butan-2-ylidene)amino)-2-thioxoimidazolidin-4-one (**2e**)

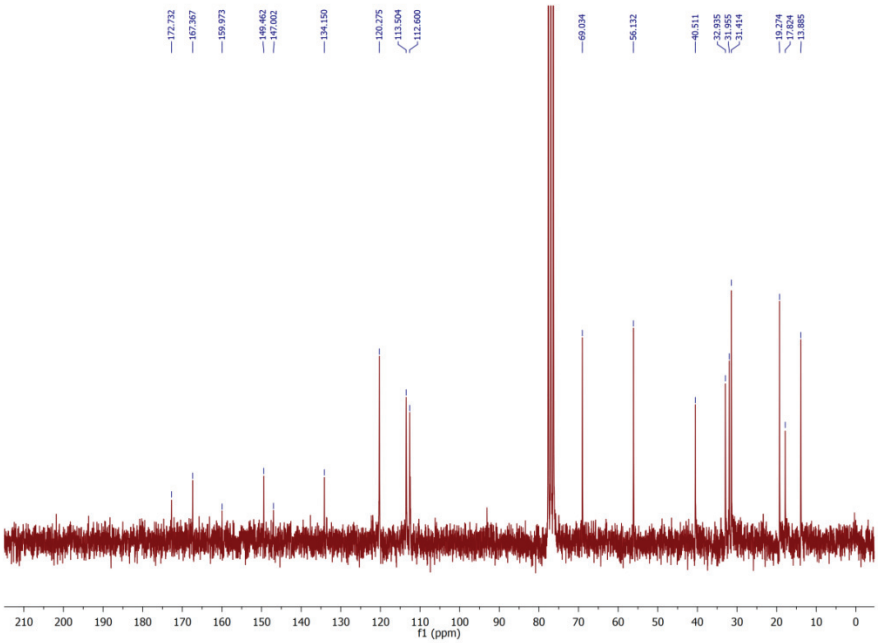

Fig. S-35. ^{13}C -NMR spectra of 3-((4-(4-butoxy-3-methoxyphenyl)butan-2-ylidene)amino)-2-thioxoimidazolidin-4-one (**2e**)

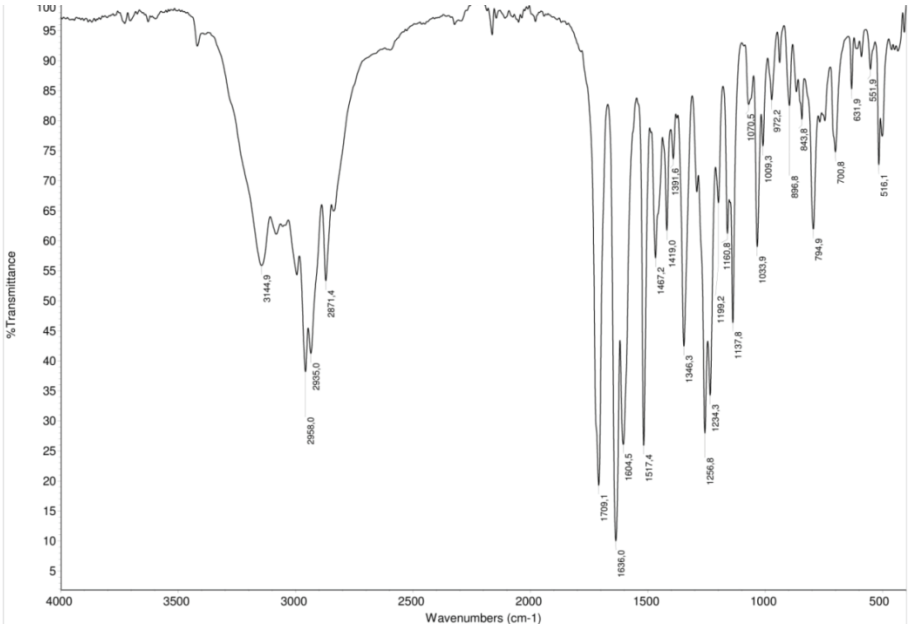

Fig. S-36. IR spectra of 3-((4-(4-butoxy-3-methoxyphenyl)butan-2-ylidene)amino)-2-thioxoimidazolidin-4-one (**2e**)

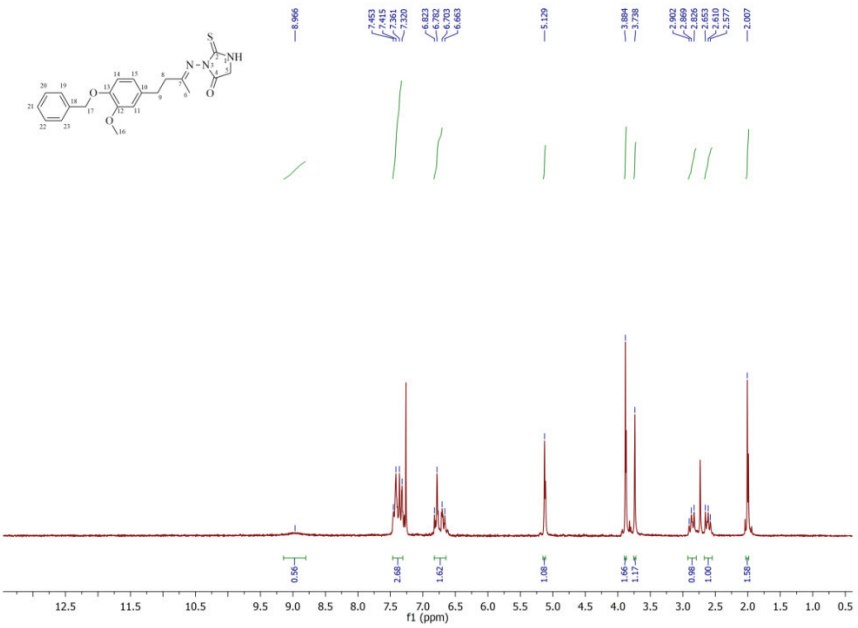

Fig. S-37. ^{1}H-NMR spectra of3-((4-(4-(benzyloxy)-3-methoxyphenyl)butan-2-ylidene)amino)-2-thioxoimidazolidin-4-one (**2f**)

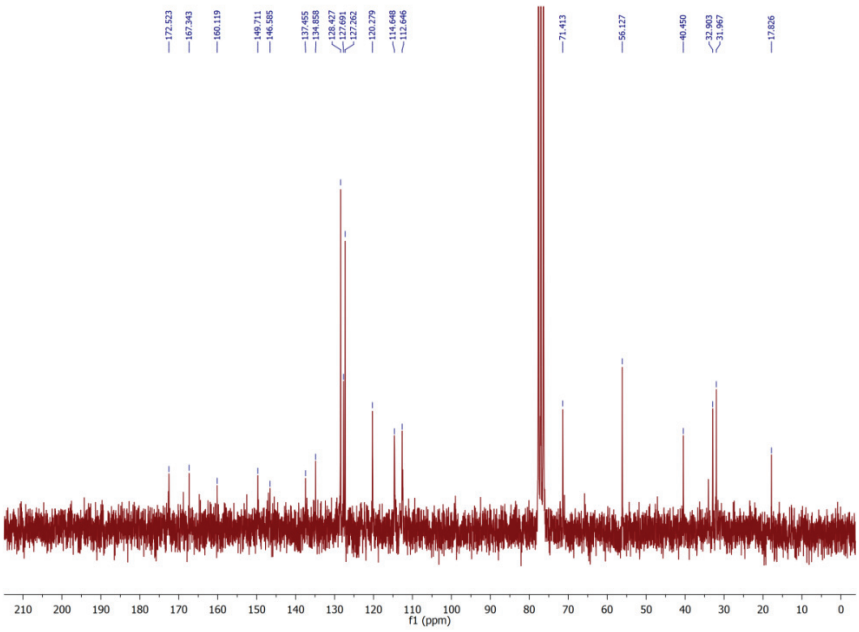

Fig. S-38. ^{13}C -NMR spectra of3-((4-(4-(benzyloxy)-3-methoxyphenyl)butan-2-ylidene)amino)-2-thioxoimidazolidin-4-one (**2f**)

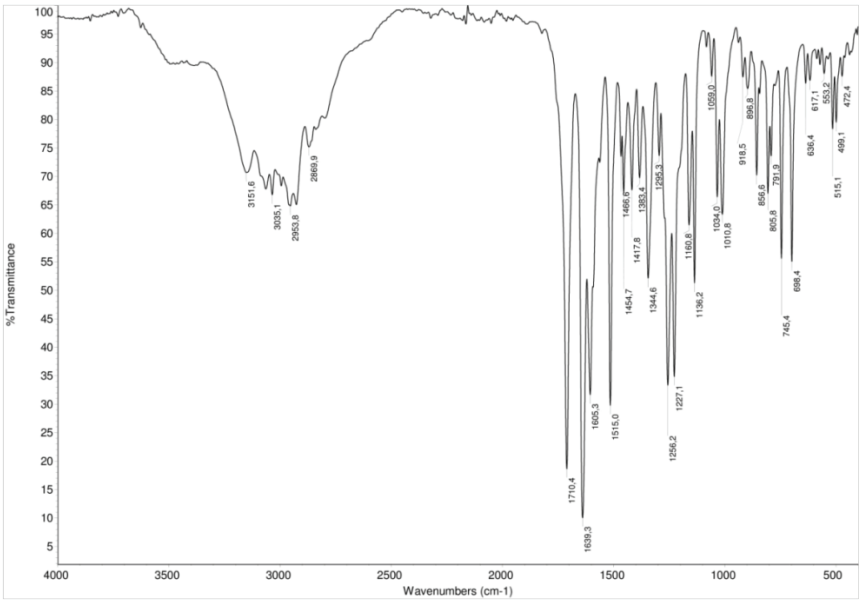

Fig. S-39. IR spectra of3-((4-(4-(benzyloxy)-3-methoxyphenyl)butan-2-ylidene)amino)-2-thioxoimidazolidin-4-one (**2f**)

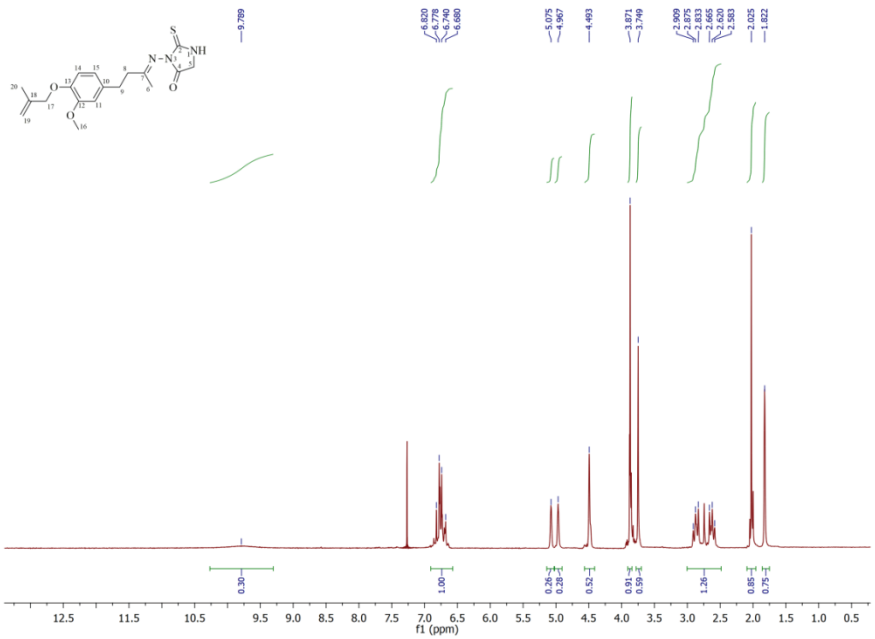

Fig. S-40. ^{1}H-NMR spectra of3-((4-(3-methoxy-4-((2-methylallyl)oxy)phenyl)butan-2-ylidene)amino)-2-thioxoimidazolidin-4-one (**2g**)

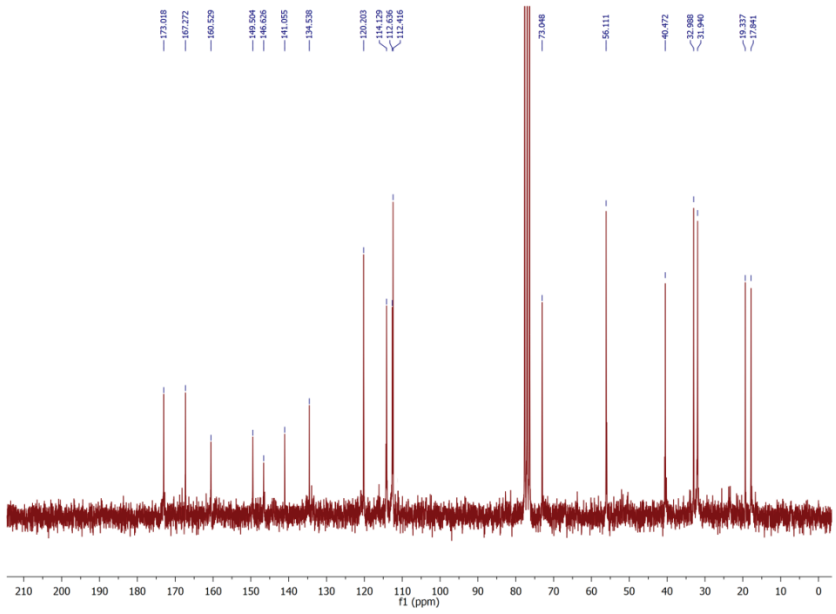

Fig. S-41. ^{13}C-NMR spectra of3-((4-(3-methoxy-4-((2-methylallyl)oxy)phenyl)butan-2-ylidene)amino)-2-thioxoimidazolidin-4-one (**2g**)

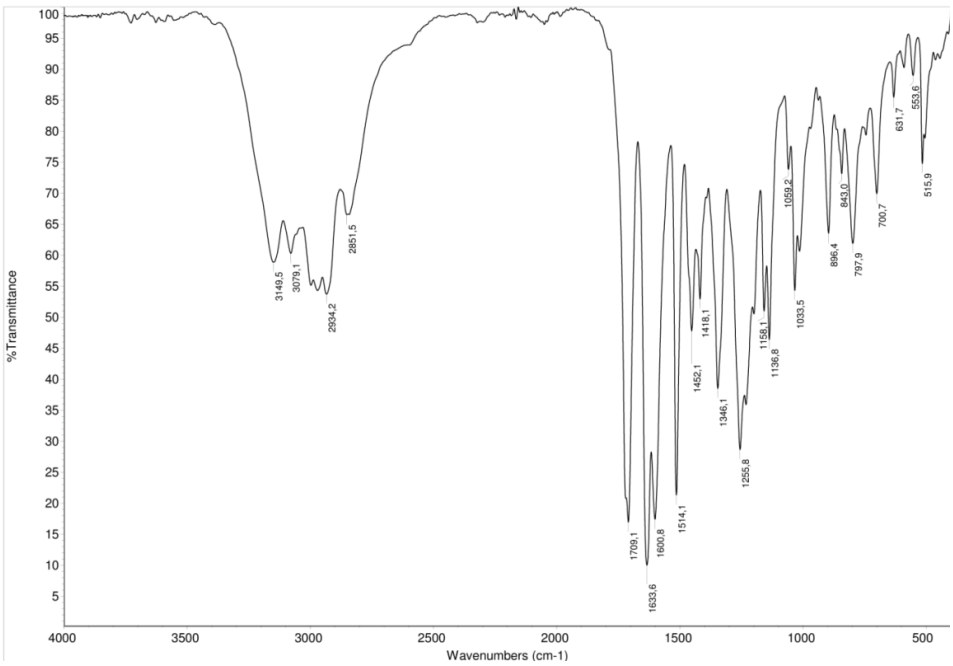

Fig. S-42. IR spectra of3-((4-(3-methoxy-4-((2-methylallyl)oxy)phenyl)butan-2-ylidene)amino)-2-thioxoimidazolidin-4-one (**2g**)

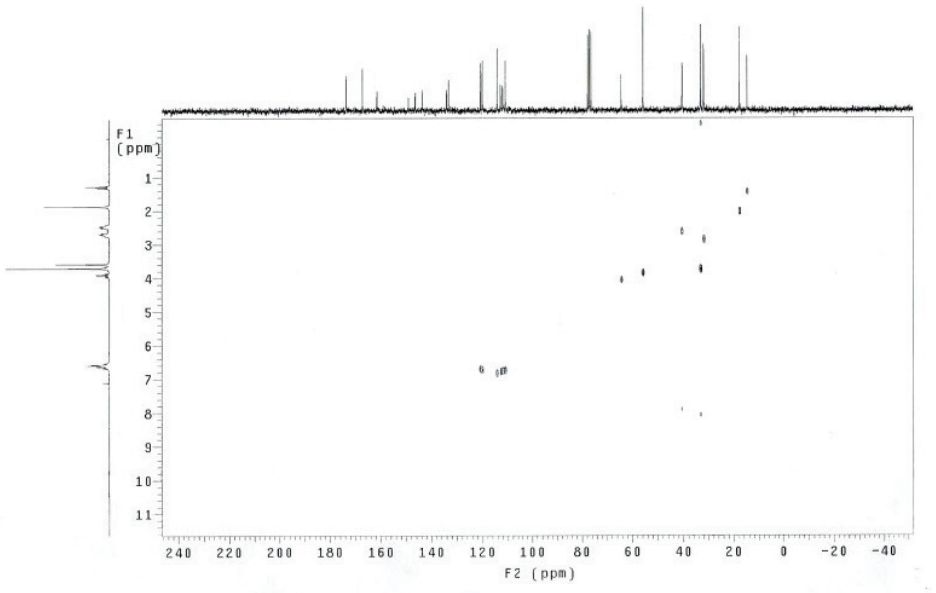

Fig. S-43. 2D HETCOR spectra of *3*-((4-(4-ethoxy-3-methoxyphenyl)butan-2-ylidene)amino)-2-thioxoimidazolidin-4-one (**2b**)

DFT calculation

All calculations were conducted using Gaussian 09[1] with the B3LYP functional[2,3] and the split-valence triple-zeta basis set 6-311+G.[4,5] To attain better description of the delocalization effects which are crucial for the geometry and electronic structure of the investigated molecules, diffuse functions were added to the heavy atoms. The p and d polarization functions were also used. Full geometry optimizations, without any symmetry constraints, and frequency calculations were performed for all species in gas phase. The frequency calculations were performed to confirm that the optimized structures are energetic minima (no imaginary frequencies).

LC-HRMS analysis

Samples dissolved in the methanol (c @ 0.1 mg mL^{-1}) were directly, without separation, injected into analysing system including liquid chromatograph (1290 Infinity LC system; Agilent Technologies, Waldbronn, Germany) with a quarternary pump, a column oven, and an autosampler, connected to the Quadrupole Time-of-Flight mass detector (6550 iFunnel QTOF MS, Agilent Technologies; Santa Clara, CA, USA) equipped with a dual spray Agilent Jet Stream (AJS) electrospray ion source. Mobile phase was composed of a solvents A (water containing both 0.1 % formic acid and 5 mM ammonium formate) and B (ACN containing 0.1 % formic acid), 1:1 (v/v). The mobile phase flow rate was 0.20 mL min^{-1}, the column oven temperature was 25 °C and the injection volumes of samples were 0.2 μL. The compounds were analysed using a mass detector. Positive ion mode was recorded, and the instrument was operated in accurate TOF/MS scanning mode in the *m/z* range of 100 – 1,500, under following conditions: capillary voltage, 3,500 V, fragmentor voltage, 70 V, nozzle voltage, 1,000 V, skimmer 1, 65 V, octupole RF peak, 750 V, desolvation gas (nitrogen) temperature, 200 °C, desolvation gas (nitrogen) flow, 14 L min^{-1}, nebulizer, 241.32 kPa, sheath gas (nitrogen) temperature, 350 °C, sheat gas (nitrogen) flow, 11 L min^{-1}. Ions *m/z* 121.05087300 and 922.00979800 were used as a lock mass for accurate mass measurements. A personal computer system running Agilent MassHunter software (revisions B.06.01 and B.07.00) was used for data acquisition and processing, respectively.

Table S-I. LC-HRMS analysis of **2a-g**

Sample code	Molecular formula	Molecular mass calculated	Molecular mass measured	$[M+H]^+$ *m/z* calculated	$[M+H]^+$ *m/z* measured	Difference (ppm)
2a	$C_{15}H_{19}N_3O_3S$	321.1147	321.1138	320.1074	322.1220	-0.04
		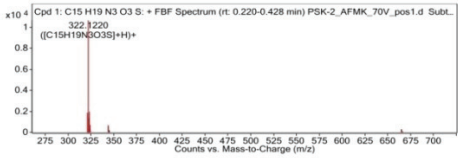				
2b	$C_{16}H_{21}N_3O_3S$	335.1304	335.1305	336.1376	336.1378	-0.48
		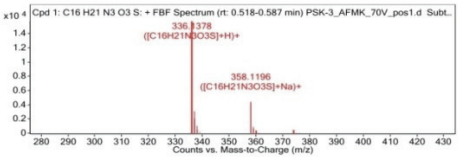				
2c	$C_{17}H_{23}N_3O_3S$	349.1460	349.1459	350.1533	350.1532	+0.25
		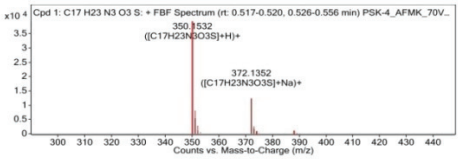				
2d	$C_{17}H_{23}N_3O_3S$	349.1460	349.1459	350.1533	350.1533	-0.03
		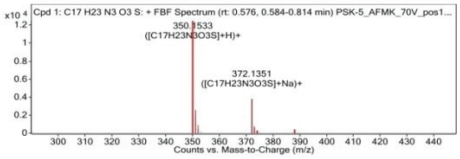				
2e	$C_{18}H_{25}N_3O_3S$	363.1617	363.1616	364.1689	364.1689	+0.11
		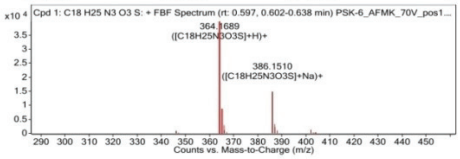				
2f	$C_{21}H_{23}N_3O_3S$	397.1460	397.1459	398.1533	398.1532	-0.03
		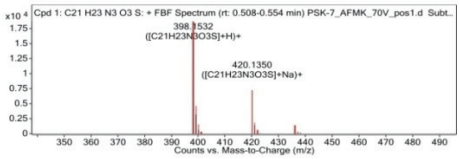				
2g	$C_{18}H_{23}N_3O_3S$	361.1460	361.1460	362.1533	362.1533	-0.03
		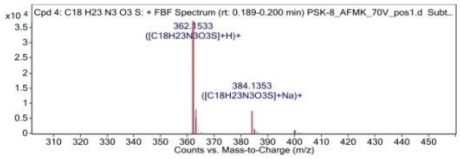				

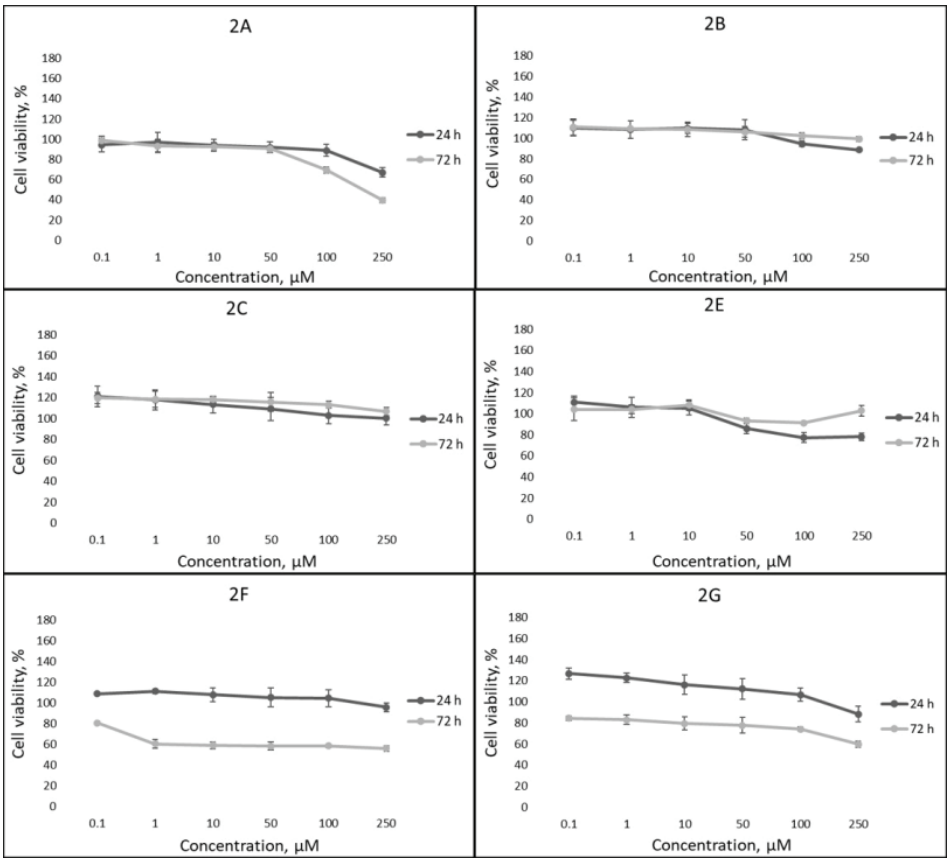

Fig. S-44. The effects of zingerone-thiohydantoin derivatives on MRC-5 cell viability

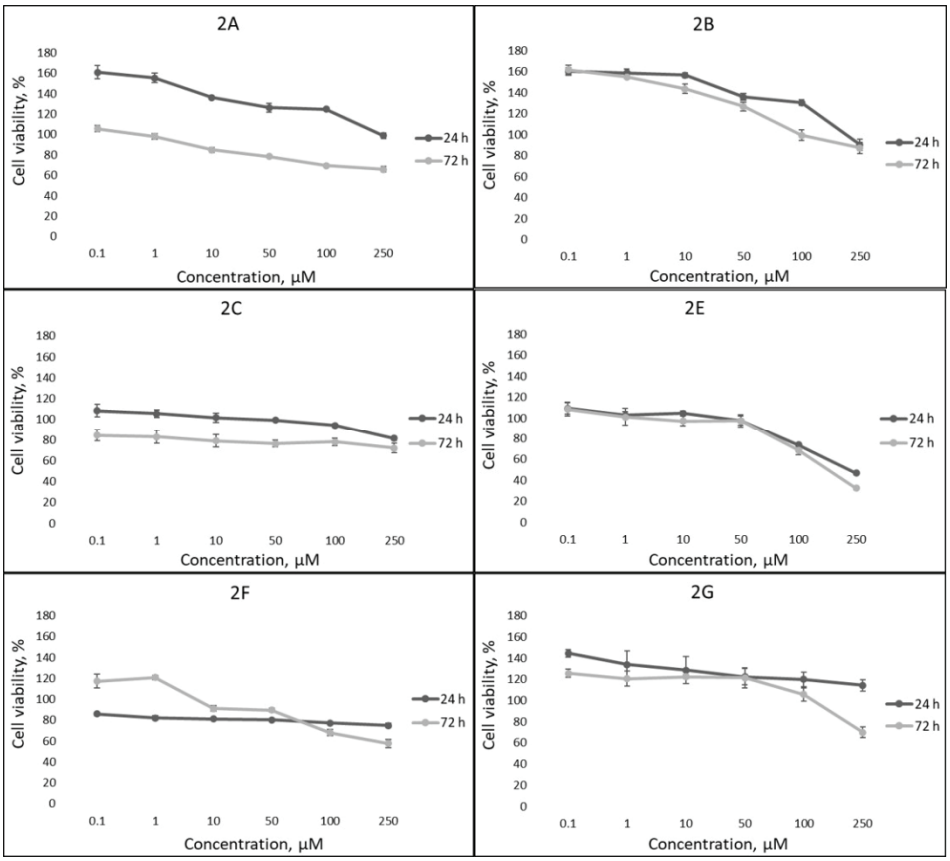

Fig. S-45. The effects of zingerone-thiohydantoin derivatives on HCT-116 cell viability

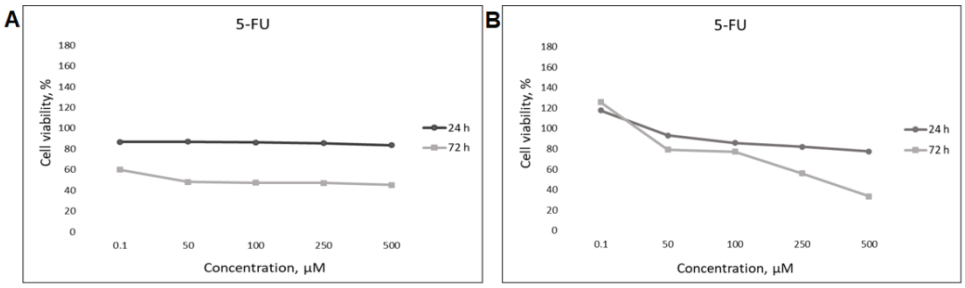

Fig. S-46. The effects of reference control 5-FU on MRC-5 (A) and HCT-116 (B) cell viability

REFERECES

1. Gaussian 09, Revision C.01; Gaussian, Inc.: Wallingford, CT (2009)
2. C. Lee, W. Yang, R. G. Parr, *Phys. Rev. B* **37** (1988) 785 (https://doi.org/10.1103/PhysRevB.37.785)

3. D. J.Becke, *Chem. Phys.* **98** (1993) 5648 (https://doi.org/10.1063/1.464913)
4. J. H. J. Wachters, *Chem. Phys.* **52** (1970) 1033 (https://doi.org/10.1063/1.1673095)
5. P. J. J. Hay, *Chem. Phys.* **66** (1977) 4377 (https://doi.org/10.1063/1.433731).

Journal of the Serbian Chemical Society
JSCS-info@shd.org.rs • www.shd.org.rs/JSCS
J. Serb. Chem. Soc. *87* (12) 1359–1365 (2022)
JSCS–5599
Short communication
Published 1 August 2022

SHORT COMMUNICATION

Modern green approaches for obtaining *Satureja kitaibelii* Wierzb. ex Heuff extracts with enhanced biological activity

VANJA ŠEREGELJ[1], OLJA ŠOVLJANSKI[1]*, JAROSLAVA ŠVARC-GAJIĆ[1], TEODORA CVANIĆ[1], ALEKSANDRA RANITOVIĆ[1], JELENA VULIĆ[1] and MILICA AĆIMOVIĆ[2#]

[1]Faculty of Technology Novi Sad, University of Novi Sad, Bulevar cara Lazara 1, 21000 Novi Sad, Serbia and [2]Institute of Field and Vegetable Crops Novi Sad, Maksima Gorkog 30, 21000 Novi Sad, Serbia

(Received 14 March, revised 14 May, accepted 16 May 2022)

Abstract: Modern trends in phytochemical extraction from alternative crops support the use of alternative technologies, such as ultrasound- and microwave--assisted extractions. Considering the reduction of toxic solvents, rapid and effective extraction process, the above-mentioned technologies have become the foundation of green chemistry approaches in a wide range of applications. These extractions have not been studied on *Satureja kitaibelii* Wierzb. ex Heuff, which is a highly potent plant when considering its aromatic and medicinal properties. This preliminary study presents an *in vitro* evaluation of biological activities of ultrasound- and microwave-assisted extracts of *S. kitaibelii*, for the first time. Furthermore, it offers a totally green, modern, fast and reproducible method for extraction of phytochemicals from *S. kitaibelii* herba (Rtanj Mountain, Serbia). This short communication suggests that the applied microwave-assisted extraction, using only water as the solvent, can be a promising approach for obtaining green products with commercial potential.

Keywords: ultrasound-assisted extraction; microwave-assisted extraction; *in vitro* antioxidant analysis; in vitro antimicrobial analysis; Lamiaceae.

INTRODUCTION

Satureja kitaibelii Wierzb. ex Heuff. or Rtanj tea is an endemic Lamiaceae species, mainly spread across the Balkan Peninsula.[1] *Satureja kitaibelii* is well known for its aromatic and medicinal properties; hence it is used as a culinary herb in Mediterranean dishes, in aromatherapy, or in traditional medicine to treat various ailments.[2] The extraction process is a crucial step in the valorisation of

* Corresponding author. E-mail: vanjaseregelj@tf.uns.ac.rs
# Serbian Chemical Society member.
https://doi.org/10.2298/JSC220314043S

the plant sources; different extraction techniques and extracting solvents can influence the final phytochemical composition and bioactive potential of the obtained extracts. After reviewing scientific-relevant literature it was found that the articles regarding *S. kittaibelii* usually include conventional extraction approaches, essential oil, and with two non-conventional method (subcritical water extraction and ultrasound-assisted extraction).[1,3–5] Conventional extraction techniques have disadvantages like thermal degradation of bioactive compounds, or the use of a large quantity of organic solvents with toxic impact on the environment or on human health. Recent trends in phytochemical extraction from plants recommend exploring the use of modern technologies; ultrasound-assisted (UA) and microwave-assisted extractions (MA) which become popular due to the fact that these techniques reduce the consumption of toxic solvents, increase the speed and extraction efficiency, thus being compliant to the principles of green chemistry.[6]

UA extracts (UAE) and MA extracts (MAE) of *S. kittaibelii* have not been studied until now. Thus, the aim of this study was to investigate the effects of UAE and MAE on the extraction of phytochemicals from this plant, in order to obtain valuable information regarding possible application in food and pharmaceutical industries. The impact of these modern extraction technologies on the phytochemical composition and biological activity (antioxidant and antimicrobial) was evaluated by varying different green extraction solvents.

EXPERIMENTAL

Plant material

The *Satureja kitaibelii* herb was collected on the Rtanj Mountain, Serbia (43◦46′34″ N; 21◦53′36″ E) in July 2020. Voucher specimens (BUNS 2-1373) were used for the identification of species. The collected aboveground flowering parts were dried naturally in shade at ambient temperature. Constant weight was gained after one week of drying. Dry plant material was placed in a soft paper bag until further analysis.

Ultrasound-assisted extraction

Ultrasound-assisted (UA) extraction was carried out in an ultrasonic bath (Iskra, Slovenia) by placing samples in the proximity of the ultrasound source. Ground sample (5 g) was extracted at room temperature with 100 ml of solvent (70% methanol or distilled water) for 30 min. The extracts were filtered (Whatman paper No. 1) and stored at 4 °C until further analysis.

Microwave-assisted extraction

Microwave-assisted (MA) extraction was carried out in an adapted microwave oven described previously by Švarc-Gajić *et al.*[7] Ground sample was extracted maintaining the same sample-to-solvent ratio, extraction time, and solvent type as in the case of UA extraction, for comparison reasons. The extraction was carried for 30 min applying magnetron power of 450 W. After completing the extraction process, the extracts were filtered (Whatman paper No. 1) and stored at 4 °C until further analysis.

Phytochemical analysis

Phenolic quantification was performed using Shimadzu Prominence HPLC, connected to an SPD-20AV UV/Vis detector (Shimadzu, Kyoto, Japan). Separation was performed on a Luna C-18 RP column, 5 μm, 250 mm×4.6 mm (Phenomenex, Torrance, CA, USA) with a C18 guard column, 4 mm×9 mm×30 mm (Phenomenex, Torrance, CA, USA). The filtered extracts were examined by HPLC reverse phase analysis as described by Aćimović *et al.*[4]

In vitro *antioxidant analysis*

Antioxidant activity of extracts was investigated using four *in vitro* assays, as outlined by Aćimović *et al.*:[4] 2,2-diphenyl-1-picrylhydrazyl (DPPH), 2,2′-azino-bis-3-ethylbenzothiazoline-6-sulphonic acid (ABTS), superoxide anion (SOA) and reducing power (RP). The antioxidant activities were expressed as μmol of Trolox equivalents per g of dry plant material.

In vitro *antimicrobial analysis*

Antimicrobial activity of *S. kitaibelii* extracts was determined against the following ATTC referent strains: *Escherichia coli*, *Pseudomonas aeruginosa*, *Salmonella typhimurium*, *Bacillus cereus*, *Staphylococcus aureus*, *Enterococcus faecalis* and *Listeria monocytogenes* (bacteria), *Saccharomyces cerevisiae*, *Candida albicans* (yeasts), and *Aspergillus brasiliensis* (fungi). Disk diffusion and microdilution methods for *in vitro* evaluation of antimicrobial activity as well as for testing minimal inhibitory concentration were performed by methods defined by Mićić *et al.*[8]

Statistical analysis

Statistical analyses were carried out using Origin v. 8.0 SRO software. Significant differences were calculated by ANOVA ($p < 0.05$). Results are presented as mean value ± standard deviation ($n = 3$).

RESULTS AND DISCUSSION

The phenolics profiles of the analyzed extracts are presented in Table I. They possess obviously different phenolics contents depending on the applied technique and solvent, which could be related to different extraction mechanisms and polarity of the presented compounds. The highest concentration of phenolic compounds was found in the extracts prepared by MAE; in terms of used solvent, significantly higher phenolic content was noted in water extract. In extracts prepared by UAE, the concentration of phenolic compounds was lower, but not their number. In this case, 70 % methanol exhibited better efficiency for phenolic extraction. The obtained results were in correlation with the literature data; Mašković *et al.*[6] reported that MAE ethanol extract of summer savory (*Satureja hortensis* L.) was richer in phenolic compounds than UAE. In general, microwaves induce a sudden increase in temperature inside the cellular structure, which leads to rupturing of cell walls and fast release of phytochemicals into extracting medium. The efficiency of microwave-assisted extraction lies in the fact that the energy of microwaves is directly converted to heat, by instantaneous absorption, *i.e.*, by rapid alignment of sample dipoles with the frequency of microwaves, thus generating heat inside the matrix.[10] Consequently, an induced sudden increase in temperature inside cells causes rupture of cell walls and fast release of phyto-

chemicals into the extracting medium. Apart from solvent selectivity towards the analyte, the dielectric constant is a significant factor for obtaining high-quality extracts as well. According to Vladić *et al.*,[9] the chosen solvent should possess a high dielectric constant and strongly absorb the microwave energy; water has the highest dielectric constant, followed by methanol and ethanol. Conversely, in the case of the UAE, the cavitation phenomenon and free-radical formation can cause degradation of phytochemicals.[10]

TABLE I. HPLC analysis of phenolic compounds in extracts (c / mg g^{-1}) obtained by ultrasound-assisted (UAE) and microwave-assisted extraction (MAE); values in rows with different superscripts are significantly different at $p < 0.05$

Compound	UAE 70 % methanol	UAE water	MAE 70 % methanol	MAE water
Vanilic acid	3.15±0.01^{b}	–	1.13±0.00^{a}	–
Epicatechin gallate	7.94±0.01^{d}	0.15±0.01^{a}	0.40±0.00^{b}	7.31±0.05^{c}
Syringic acid	31.03±0.03^{b}	5.17±0.04^{a}	58.62±0.07^{c}	59.76±0.02^{d}
Coumarin acid	1.65±0.00^{c}	0.36±0.01^{a}	0.81±0.00^{b}	2.50±0.02^{d}
Caffeic acid	4.26±0.03^{d}	0.55±0.00^{a}	0.96±0.00^{b}	2.45±0.01^{c}
Gentisic acid	–	1.61±0.01^{a}	2.95±0.03^{b}	–
Sinapic acid	4.01±0.02^{c}	1.14±0.02^{a}	1.45±0.01^{b}	4.65±0.02^{d}
Rosmarinic acid	4.44±0.03^{c}	1.45±0.00^{a}	2.23±0.06^{b}	8.63±0.03^{d}
Ferulic acid	4.01±0.01^{b}	3.12±0.02^{a}	7.97±0.03^{c}	17.96±0.1^{d}
Rutin	0.04±0.00^{a}	0.45±0.00^{b}	0.95±0.00^{c}	4.25±0.02^{d}
Luteolin	–	–	0.05±0.00^{a}	–
Total phenolic compounds	60.53±0.14^{b}	14.00±0.11^{a}	77.52±0.20^{c}	107.51±0.28^{d}

HPLC analysis showed that the dominant compound in all extracts was syringic acid, which ranged from 5.17 m/g (UAE water extract) to 59.76 mg/g (MAE water extract). The highest content of syringic acid was earlier confirmed in *S. kitaibelii* subcritical water extract.[4] Ćetković *et al.*[3] have also classified syringic acid among the most main phenolic compounds in *S. kitaibelii* extracts obtained by a conventional extraction technique and different organic solvents.

In general, a single assay method is not sufficient for *in vitro* assessment of antioxidant activity of endogenous phytochemicals. Antioxidant molecules differ in polarities, thus they can act by different mechanisms. Antioxidant activity of *S. kitaibelii* extracts was challenged by four methods (Table II); significant antioxidant potential was found in water and 70 % methanol extracts, obtained by MAE. More precisely, the antioxidant potential of tested samples decreased respectively: MAE water > MAE 70 %methanol > UAE 70 % methanol > UAE water.

There were considerable differences noted in antimicrobial effects against tested microorganisms between UAE and MAE extracts (Table III). The UAE extracts did not show antimicrobial effect, with the exception of water extract which showed low inhibition potential against *A. brasiliensis*. Consequently, the

defined minimal inhibitory concentration is above the initial concentration of extract, and further antimicrobial potential of the concentrated extracts is required. However, the antimicrobial effect was observed in the case of MAE extract, especially in the one prepared by using water as a solvent.

TABLE II. *In vitro* antioxidant activity (μmol TE/g) of *Satureja kitaibelii* extracts obtained by ultrasound (UAE)- and microwave-assisted extraction (MAE); values in rows with different superscripts are significantly different at $p < 0.05$

Antioxidant	UAE 70 % methanol	UAE water	MAE 70 % methanol	MAE water
DPPH	78.99±14.33^b	33.64±2.07^a	225.63±11.45^c	385.38±16.56^d
ABTS	744.66±9.74^b	685.30±17.73^a	1757.86±82.45^c	2571.12±76.58^d
RP	153.20±2.99^b	133.50±1.64^a	336.71±5.68^c	414.93±20.07^d
SOA	3730.81±20.57^b	1993.66±45.94^a	4417.17±15.30^c	4506.69±0.53^d

TABLE III. *In vitro* antimicrobial activity of *Satureja kitaibelii* extracts obtained by ultrasound (UAE)- and microwave-assisted extraction (MAE)

Test organism	UAE 70 % methanol	UAE water	MAE 70 % methanol	MAE water
Inhibition zone, mm[a]				
E. coli ATCC 25922	nd	nd	13.33± 0.57	40.00±0.00
P. aeruginosa ATCC 27853	nd	nd	nd	29.00±0.00
S. Typhimurium ATCC 13311	nd	nd	nd	nd
B. cereus ATCC 11778	nd	nd	nd	28.00±0.00
S. aureus ATCC 25923	nd	nd	27.33±0.57	27.00±1.00
E. faecalis ATCC 19433	nd	nd	nd	nd
L. monocytogenes ATCC 35152	nd	nd	24.00±1.00	17.33±0.57
S. cerevisiae ATCC 9763	nd	nd	nd	nd
C. albicans ATCC 10231	nd	nd	nd	18.33±0.57
A. brasiliensis ATCC 16404	nd	11.00±0.0	nd	nd
Minimal inhibitory concentration, mg/mL[b]				
E. coli ATCC 25922	> 50	> 50	> 50	0.78
P. aeruginosa ATCC 27853	> 50	> 50	> 50	1.56
S. Typhimurium ATCC 13311	> 50	> 50	> 50	> 50
B. cereus ATCC 11778	> 50	> 50	> 50	0.78
S. aureus ATCC 25923	> 50	> 50	12.5	0.78
E. faecalis ATCC 19433	> 50	> 50	> 50	> 50
L. monocytogenes ATCC 35152	> 50	> 50	25	> 50
S. cerevisiae ATCC 9763	> 50	> 50	> 50	> 50
C. albicans ATCC 10231	> 50	> 50	> 50	> 50
A. brasiliensis ATCC 16404	> 50	> 50	> 50	> 50

[a]< 22 mm – low; 22–26 mm – intramedier; >26 mm – high antimicrobial activity, nd – not detected; [b]according to the initial concentration of the extracts

Both MAE extracts showed the antimicrobial effect against *E. coli*, *S. aureus* and *L. monocytogenes*, while water extract expressed a similar effect against *P.*

aeruginosa, *B. cereus* and *C. albicans*. These differences can be explained by the phenolic compounds profile of the tested samples. Unlike the UAE samples, the methanolic MAE sample contains syringic acid, while the water MAE sample contains syringic acid, ferulic acid and rutin. All three mentioned phenolic compounds have previously been reported as antimicrobial agents; ferulic acid is an inhibition factor for *P. aeruginosa*, *S. aureus, E. coli* and *L. monocytogenes* growth,[11] syringic acid inhibits the growth of *S. aureus*, while *E. coli*, *P. aeruginosa*, *B. cereus* and *C. albicans* are sensitive to the presence of rutin.[12] The minimal inhibitory concentrations of the *S. kitaibelii* extracts varied according to strain level in the range of 0.78 to 25 mg/mL (Table III). The lower *MIC* values were obtained for the water extract compared with methanolic, which also lead to differences in chemical compositions.

CONCLUSION

In summary, this preliminary study indicates that the extract prepared with MAE and water as solvent exhibited the highest biological activity. Special significance of the presented approach is reflected in a totally green, modern, fast and reproducible process technology. According to the bioactivity screening, this research suggests that the MAE water extract of *S. kitaibelii* could be used as a natural source of antioxidants for developing a wide range of safe and functional products which will be investigated further.

Acknowledgement. This work was supported by the Ministry of Education, Science and Technological Development of the Republic of Serbia, Contract No. 451-03-68/2022-14/ /200134 and 451-03-68/2022-14/200032.

ИЗВОД

МОДЕРНИ „ЗЕЛЕНИ“ НАЧИНИ ЗА ДОБИЈАЊЕ *Satureja kitaibelii* WIERZB. EX HEUFF ЕКСТРАКТА СА ИЗРАЖЕНОМ БИОЛОШКОМ АКТИВНОШЋУ

ВАЊА ШЕРЕГЕЉ[1], ОЉА ШОВЉАНСКИ[1], ЈАРОСЛАВА ШВАРЦ-ГАЈИЋ[1], ТЕОДОРА ЦВАНИЋ[1], АЛЕКСАНДРА РАНИТОВИЋ[1], ЈЕЛЕНА ВУЛИЋ[1] и МИЛИЦА АЋИМОВИЋ[2]

[1]*Технолошки факултет Нови Сад, Универзитет у Новом Саду, Бул. цара Лазара 1, 21000 Нови Сад и* [2]*Институт за ратарство и повртарство Нови Сад, Максима Горког 20, 21 000 Нови Сад*

Савремени трендови у фитохемијској екстракцији из алтернативних усева подржавају истраживање употребе алтернативних технологија као што су екстракције уз помоћ ултразвука и микроталаса. С обзиром на редукцију токсичних растварача и брз и ефикасан процес екстракције, поменуте технологије су постале темељ приступа “зеленој” хемији у широком спектру примена. С друге стране, ове екстракције нису проучаване на *Satureja kitaibelii* Wierzb. ex Heuff, која је веома значајна ендемична биљка с обзиром на ароматична и лековита својства. Ова прелиминарна студија је по први пут представила *in vitro* процену биолошке активности ултразвучних и микроталасних екстраката *S. kitaibelii*. Нудећи апсолутно “зелену”, модерну, брзу и поновљиву методу за екстракцију фитокемикалија из *S. kitaibelii* (планина Ртањ), ово истраживање сугерише да примењена екстракција уз помоћ микроталаса, користећи само воду као растварач, може бити

перспективан приступ за добијање "зелених" производа са комерцијалним потенцијалом.

(Примљено 14. марта, ревидирано 14. маја, прихваћено 16. маја 2022)

REFERENCES

1. M. Aćimović, L. Pezo, V. Tešević, I. Čabarkapa, M. Todosijević, *Ind. Crops Prod.* **154** (2020) 112752 (https://dx.doi.org/10.1016/j.indcrop.2020.112752)
2. A. Đorđević, I. Palić, G. Stojanović, N. Ristić, R. Palić, *Int. J. Food Properties* **17** (2014) 2157 (https://doi.org/10.1080/10942912.2013.784333)
3. G. Ćetković, J. Čanadanović-Brunet, S. Djilas, V.Tumbas, S. Markov, D. Cvetković, *Int. J. Mol. Sci.* **8** (2007) 1013 (https://www.ncbi.nlm.nih.gov/pmc/articles/PMC3871840/)
4. M. Aćimović, V. Šeregelj, O. Šovljanski, V. Tumbas Šaponjac, J. Švarc-Gajić, T. Brezo-Borjan, L. Pezo, *Ind. Crops Prod.* **169** (2021) 113672 (https://doi.org/10.1016/j.indcrop.2021.113672)
5. K. Gopčević, S. Grujić, J. Arsenijević, I. Karadžić, L. Izrael-Živković, Z. Maksimović. *Plant Foods Hum. Nutr.* **74** (2019) 179 (https://doi.org/10.1007/s11130-019-0716-3)
6. P. Mašković, V. Veličković, M. Mitić, S. Đurović, Z. Zeković, M. Radojković, A. Cvetanović, J. Švarc-Gajić, J. Vujić, *Ind. Crops Prod.* **109** (2017) 875 (https://doi.org/10.1016/j.indcrop.2017.09.063)
7. J. Švarc-Gajić, Z. Stojanović, A. Segura Carretero, D. Arráez Román, I. Borrás, I. Vasiljević, *J. Food Eng.* **19** (2013) 525 (https://doi.org/10.1016/j.jfoodeng.2013.06.030)
8. D. Micić, S. Đurović, P. Riabov, A. Tomić, O. Šovljanski, S. Filip, T. Tosti, B. Dojčinović, R. Božović, D. Jovanović, S. Blagojević, *Foods* **10** (2021) 2734 (https://doi.org/10.3390/foods10112734)
9. J. Vladić, T. Janković, J. Živković, M. Tomić, G. Zdunić, K. Šavikin, S. Vidović, S. *Plant Foods Hum. Nutr.* **75** (2020) 553 (https://doi.org/10.1007/s11130-020-00848-6)
10. J. Švarc-Gajić, *Samples and Sample Preparation in Analytical Chemistry*, Nova publishers, New York. 2011, pp. 47–49 (https://books.google.rs/books?id=VTkhYAAACAAJ&dq=jaroslava+svarc+gajic&hl=en&sa=X&redir_esc=y)
11. A. Pernin, V. Bosc, M. Maillard, F. Dubois-Brissonnet, *Front. Microbiol*. **10** (2019) 137 (https://doi.org/10.3389/fmicb.2019.00137)
12. S. Dubey, A. Ganeshpurkar, D. Bansal, N. Dubey, *Chron. Young Sci.* **4** (2013) 153 (https://doi.org/10.4103/2229-5186.115556).

Journal of the Serbian Chemical Society
JSCS-info@shd.org.rs • www.shd.org.rs/JSCS
J. Serb. Chem. Soc. *87* (12) 1367–1380 (2022)
JSCS–5600
Original scientific paper
Published 18 November 2022

Transformation of fluorite δ-Bi_2O_3 into a new tetragonal phase

VLADIMIR V. ZYRYANOV* and SERGEY A. PETROV

Institute of Solid State Chemistry and Mechanochemistry, Siberian Branch of Russian Academy of Sciences, Novosibirsk, Kutateladze 18, 630090 Russian Federation

(Received 22 June, revised 12 August, accepted 21 September 2022)

Abstract: Bismuth oxide kinetically stabilized by doping with a metastable structure of disordered fluorite δ-Bi_2O_3 has a unique conductivity. Oxygen selective membranes at intermediate temperatures ~550 °C, on the base of cermet δ-Bi_2O_3/Ag, have the highest potential for air separation and can be used to produce oxygen for distributed multigeneration by burning fossil carbon fuels. When searching for the optimal composition of δ-Bi_2O_3, the degradation of fluorite into a new tetragonal phase was discovered in ceramics synthesized using mechanical activation. The tetragonal phase is formed and exists in a topotaxial composite with the fluorite structure. For a relatively stable over a wide temperature range tetragonal phase with a = 0.3854, c = 0.88905 nm, S.G. *P*-4, crystal structure and atomic coordinates have been proposed. In samples of fluorite and topotaxial composite, the Raman and Mössbauer spectra were recorded and discussed. The discovery of a new tetragonal phase of doped bismuth oxide and its existence area makes it possible to optimize the composition and the synthesis of a more stable solid electrolyte δ-Bi_2O_3 with high conductivity.

Keywords: Bi_2O_3 polymorphs; mechanical activation; solid state synthesis; powder XRD; Mössbauer spectroscopy; Raman spectroscopy.

INTRODUCTION

Bismuth oxide and Bi_2O_3-rich solid solutions exist in the form of several polymorphic modifications. All of them find applications in medicine, catalysis, materials science, *etc.*[1–5] However, great interest in this compound is associated primarily with the superionic properties of the high-temperature phase with the structure of disordered fluorite δ-Bi_2O_3.[1–4] Practical use of the unique oxygen conductivity of pure bismuth oxide is impossible due to its high reactivity and stability at t > 730 °C. Doping with cations of a smaller ionic radius makes it possible to kinetically stabilize the fluorite structure at lower temperatures with a

* Corresponding author. E-mail: vladinetta@academ.org
https://doi.org/10.2298/JSC220622075Z

partial deterioration of conductivity. The search for a composition and synthesis method of δ-Bi_2O_3 with optimal properties has been going on for a long time, but the results achieved so far do not provide practical implementation. Along with the experimental search, the theoretical studies are also carried out by first-principles calculations based on the density-functional theory DFT.[5] The generally accepted Bi_2O_3 polymorphs are listed in literature[6] and they are α-Bi_2O_3 with a monoclinic structure (stable at room temperature, S.G. $P2_1/c$, No. 14) and δ-Bi_2O_3 with a cubic structure (stable above 730 °C up to a melting point of 817 °C, S.G. *Fm*-3*m*, No. 225). When δ-Bi_2O_3 is cooled below 647 °C, a metastable β modification of the tetragonal structure is formed (S.G. $P\text{-}42_1c$, No. 114) and below 635 °C in an oxygen atmosphere γ modification of the cubic structure (sillenite, S.G. *I*23, No. 197) is formed. In addition to them, ε-Bi_2O_3 is also known, which is obtained by hydrothermal synthesis (S.G. *Pcnn*, No. 56, irreversibly transforms into the α-form at 400 °C), and ω-Bi_2O_3, which is formed on the BeO substrate. Theoretical studies were carried out on the basis of disordered fluorite with the ordering of oxygen vacancies along the <100>, <110>, and <111> directions, and combined superlattices.[6] The found polymorphic modifications with respect to the minimum energy relative to α-Bi_2O_3 were tested for stability. The approach used is supported by the fact that founded structure is very close to the experimentally observed phase ε-Bi_2O_3, called by the authors ε'-Bi_2O_3 (S.G. *Pbcn*, No. 60).[6] The existence of modifications with lining up of vacancies in the unit cell of fluorite is predicted to be tetragonal structures (S.G. $P4_2/mcm$, No. 132, and *P*-4*m*2, No. 115) and a cubic structure (S.G. *Pn*-3*m*, No. 224). In the model of vacancy superstructure 2×2×2, theoretically possible modifications were found: bixbyite observed for Y_2O_3, In_2O_3, Mn_2O_3 (S.G. *Ia*-3, No. 206), cubic (S.G. *Fd*-3*m*, No. 227) and trigonal (S.G. *R*3*m*, No. 160).

Optimization of the composition of δ-Bi_2O_3 fluorite is very important for practical applications because these materials exhibit the highest oxygen–ion conductivity of any material known to date. Doped with rare earth cations, δ-Bi_2O_3 retains disordered fluorite structure upon cooling down to room temperature. However, all known materials at about 600 °C undergo phase transformations with deterioration of their conductive properties.[7–11] The process of degradation of the fluorite structure (S.G. *Fm*-3*m*) begins with the ordering of oxygen vacancies along the <111> axis.[10] This change leads to an elongation of the lattice along the <111> axis and the transformation of fluorite into a rhombohedral phase (S.G. *R*-3) with the appearance of mechanical stresses that promote the segregation of dopants with the gradual formation of a rhombohedral phase (S.G. *R*-3*m*) or sillenite (S.G. *I*23).[11]

A relative failure of the theoretical method can be attributed to the discrepancy between the calculated and experimentally observed lattice parameters for known phases, which limits the reliability of the scientific forecasts. The prin-

ciple of searching for possible structures using the minimum energy is necessary but insufficient condition for the existence of phases, since under experimental conditions, the formation of a particular structure requires nucleation with subsequent growth. This stage is determined by kinetic factors. In this regard, it is *a priori* interesting to use mechanochemical synthesis or mechanical activation (MA), when the formation of products arranged in order at the contact of solid particles proceeds through the formation of mechanical loading above the threshold, so-called dynamic state, (D)*, in the form of growing rollers from an atomic mixture and then through its relaxation under quenching conditions.[12,13] As a result, the arranged products of certain structural types are formed, which have a high tolerance to changes in composition and a huge free volume of up to 9 % (vacancy defects).[11–13] The process of cumulative mass transfer, even at ambient temperature, is many orders of magnitude higher than the diffusion process at relatively high temperatures. This feature of the mechanochemical method makes it possible to detect crystal structures that were not observed due to kinetic limitations. Ultimately, the use of MA makes it possible to considerably accelerate the search for compositions of δ-Bi_2O_3 with an optimal combination of high oxygen conductivity and phase stability.

EXPERIMENTAL

For the synthesis of ceramic powders, the reagents from Russia and China were used in the form of oxides – Bi_2O_3 (purity >99.99 %) and Ta_2O_5 (>99.99 %), Dy_2O_3 and Er_2O_3 (>99.9 %), WO_3 (>99.9 %). Nitrates $Dy(NO_3)_3{\cdot}6H_2O$ and $Er(NO_3)_3{\cdot}6H_2O$ (>99.9 %), and $HfOCl_2$ (>99 %) were used as well. In the synthesis of some samples, a mixture of salts of highly charged cations (Hf, Ta, W, denoted as M^{5+} for brevity) was used to produce high-entropy ceramics. To introduce the Mössbauer isotope ^{57}Fe, Fe_2O_3 oxide was used with an isotope content of ~85 %, which was dissolved in a mixture of nitric and hydrochloric acid, followed by neutralization with ammonia to pH~3 and impregnation of MA powders, followed by drying.

The synthesis of ceramic powders was carried out in 3 cycles of grinding and firing at 800 to 950 °C. Dopants in the case of nitrates were introduced into MA bismuth oxide nanopowder by preliminary mixing in an agate mortar, followed by drying the resulting paste with gradual heating up to 600 °C until complete removal of water and nitrates. Mechanical processing of dry powders was carried out with steel balls of 4 mm in diameter in an AGO-2 planetary mill, Russia, with water-cooled steel jars (volume 2×150 ml) using a well-known technique.[8] Such method with pre-coating of the steel surface with ground ceramics and periodic mixing of material with balls provides a prominent reduction of iron contamination to <0.01 wt. % and an improvement in homogeneity. The treatment was carried out at the ratio of the mass of material and inox steel balls of 10–25 g/200 in an intensive mode of 60*g* (speed of rotation 750 rpm) in which the phenomenon of MA is accomplished. The supplied mechanical energy was 15–50 MJ/kg. Dense ceramics were obtained by pressing nanopowders at a pressure of 200 MPa and sintering at 950 °C for 1 min, cooling in furnace and air quenching from 820 °C to avoid cracking of a ceramic disk.

XRD studies (CuK_α radiation) were carried out on a diffractometer Bruker D8 Advance, Germany, using high-temperature (HT) camera HTK 1200N Anton Paar, Austria. Full-profile

Rietveld analysis of diffraction patterns was performed using the PowderCell 2.4 and Topas V4.2 software. The structure was visualized using Diamond-3 program. Mössbauer spectra were recorded at room temperature on an NZ-640 setup, Hungary, a γ-radiation source – ^{57}Co/Rh, a chemical shift relative to α-Fe. The spectra were processed using an original program developed in ISSCM SB RAS. Some powders and ceramics with fluorite and tetragonal phase were studied by Raman spectroscopy, using Bruker RFS100/s with NdYAl-laser, wavelength 1064 nm. To avoid possible errors, SEM studies of sintered ceramics and powders with EDS to control the composition were carried out on a TM-1000 microscope, Hitachi, Japan. Since the accuracy of weighing in the synthesis of compounds is much higher than the measurement error by the EDS method, the data on the estimated composition are not given. The EDS data obtained did not show the appearance of impurities and, within the experimental error, corresponded to the composition of the samples.

RESULTS AND DISCUSSION

XRD and structure

The diffraction patterns of $Bi_{0.76}Dy_{0.12}Er_{0.1}Hf_{0.02}O_{1.51}$ (DEH2) ceramics prepared from different precursors are shown in Figs. 1 and 2. The ceramics from oxide precursors are a composite of fluorite and a new tetragonal phase. According to the Rietveld full profile analysis, the crystallite sizes in ceramics fired at 850 °C are d = 116 for fluorite and 100 nm for tetragonal phase, with its fraction 35, 19, 18 and 27 % after heating to 400, 600, 700 and 950 °C, respectively. Fluorite lattice parameter was a_F = 0.54934(7) nm in single phase ceramics DEH2 with good homogenization of dopants and annealed free volume (Fig. 2), and in composite it was a_F = 0.5460(1) nm (Fig. 1, 950 °C), which means the segregation of dopants and the enrichment in tetragonal phase with Hf^{4+}.

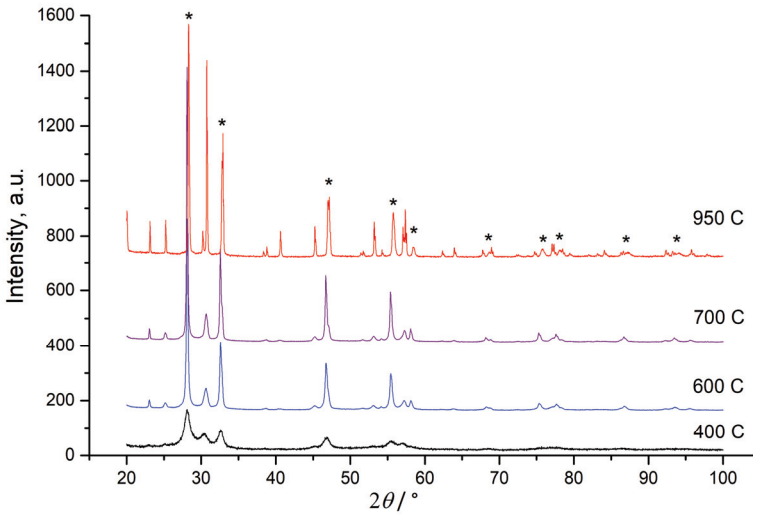

Fig. 1. Diffraction patterns of $Bi_{0.76}Dy_{0.12}Er_{0.1}Hf_{0.02}O_{1.51}$ ceramics after heating MA powders to different temperatures, asterisks indicate the peaks of fluorite.

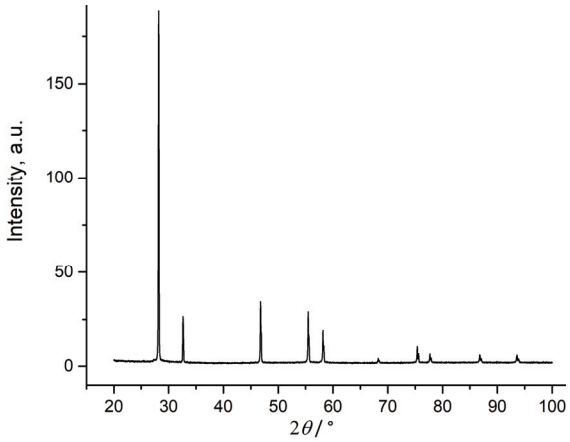

Fig. 2. Diffraction pattern of single-phase $Bi_{0.76}Dy_{0.12}Er_{0.1}Hf_{0.02}O_{1.51}$ fluorite, a = 0.54934(7) nm, synthesized from rare earth nitrates, sintered at 950 °C and air quenching.

The results of the Rietveld full profile analysis of DEH2 ceramics sample are shown in Fig. 3. All observed peaks of new phase are indicated in the tetragonal symmetry unit cell model (S.G. *P*-4, No. 81), Tables I and II, and the structure is shown in Fig. 4.

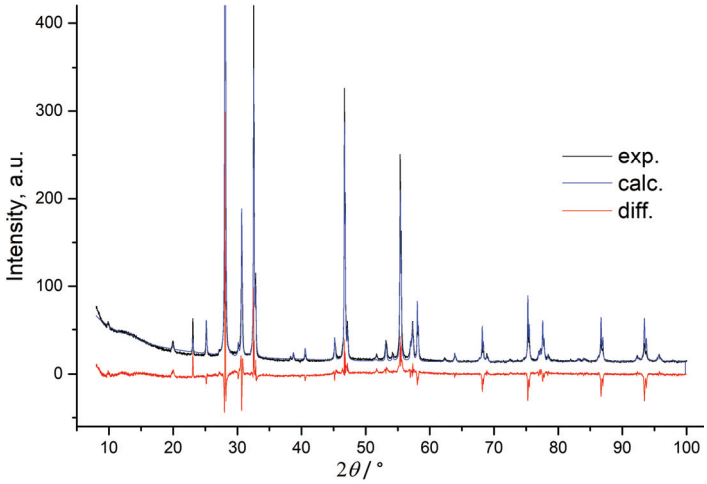

Fig. 3. Full-profile Rietveld analysis of diffraction pattern in topotaxial composite $Bi_{0.76}Dy_{0.12}Er_{0.1}Hf_{0.02}O_{1.51}$ after firing at 850 °C for 24 h. *R*-values for tetragonal phase: R_{wp} = 14.64, R_p = 10.91, *R*-Bragg = 7.568.

The structure of the tetragonal phase consists of fluorite-like layers separated by partially occupied polyhedron HfO_4 (FeO_4). The lattice parameters a_F = = 0.54982(1) nm, $\sqrt{2}a_t$ = 0.54341 nm, and the structures themselves are very

close. Therefore, there are grounds for asserting a topotaxial composite of fluorite and tetragonal phase. The formation of a tetragonal phase in contact with fluorite is similar to the formation ω-Bi_2O_3 on the BeO substrate.[6]

TABLE I. Atomic coordinates and occupation for the tetragonal phase in ceramics $Bi_{0.76}Dy_{0.12}Er_{0.1}Hf_{0.02}O_{1.51}$ after firing at 850 °C for 24 h (27 % of tetra phase, main phase fluorite with a = 0.54983 nm); space group, P-4, No 81; lattice parameters, a = 0.385405(24), c = 0.889047(98) nm; number of formula units, Z = 3.2; density, 8.7899(15)

Atom	Site	x	y	z	Occupation
Bi	2f	½	½	0.719	1
Bi(Dy,Er)	1a	0	0	0	0.799
Hf	1b	0	0	½	0.20
O1	2g	0	½	0.132	0.75
O2	2g	0	½	0.835	0.75
O3	2g	0	½	0.43	0.95

TABLE II. Interatomic distances

Atom 1	Atom 2	Distance, nm
Bi	O1	0.234
Bi	O2	0.219
Bi	O3	0.234
Bi(Dy,Er)	O1	0.226
Bi(Dy,Er)	O2	0.242
Hf	O3	0.203
O1	O2	0.274
O1	O3	0.265

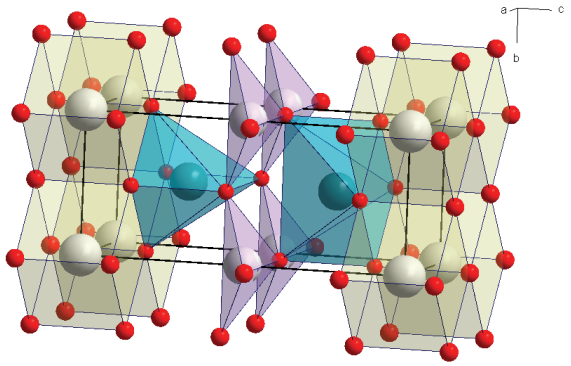

Fig. 4. Structure of tetragonal phase. Small dark balls – oxygen, big light balls – Bi, medium light balls – Hf, medium dark balls – Bi(Dy,Er).

The structure of the tetragonal phase suggests many variants of possible superlattices due to the low occupation of the position 1b by hafnium or other small cations, including iron. This circumstance is one of the possible reasons for the discrepancies in the observed and calculated peak intensities. This is con-

firmed by the presence of a halo in XRD patterns in the range of angles of 10 to 20°. In addition, the texturing of the samples adds discrepancy.

Existence area of the tetragonal phase

The combination of peaks at 19.9, 23.1, 25.2 and 30.7° is a good marker for the new tetragonal phase, which was observed as an impurity in many samples of stabilized δ-Bi_2O_3 obtained by high energy ball milling (MA) and doping with highly charged cations or small cations like Fe^{3+}, especially after prolonged annealing as a result of phase degradation of fluorite, Figs. 5 and 6. It can be assumed that the admixture of the tetragonal phase, due to the low intensity of the peaks, was incorrectly attributed to known phases in many works.

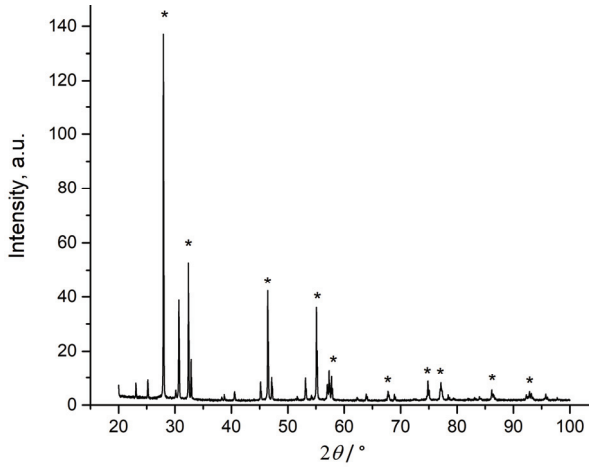

Fig. 5. XRD pattern of ceramics $Bi_{0.76}Dy_{0.12}Er_{0.09}(M^{5+})_{0.02}Fe_{0.01}O_{1.52}$ after heating to 950 °C and air quenching, asterisks indicate the peaks of fluorite. Topotaxial composite of fluorite 76 % and tetragonal phase 24 %; a_F = 0.55256(3) nm, d = 338(5) nm; a_t = 0.3854 ($\sqrt{2}a_t$ = 0.5449 nm), c = 0.88895(6) nm, d = 306(10) nm.

Diffraction patterns of powders and ceramics with different compositions and prehistories make it possible to reveal the existence area of tetragonal phase. Doping with highly charged cations Hf^{4+} at a level of 1 % gives a little effect on conductivity.[15]

When doping 3 % or more, non-conductive clusters are inevitably formed. Therefore, the minor doping in the development of a solid electrolyte was limited to 2 %. With the introduction of 2 % Ta^{5+} and W^{6+}, the tetragonal phase is not formed or is observed in trace amounts, due to the inhomogeneity of the samples, Fig. 6. This indicates the importance of the oxygen content for the formation of the tetragonal phase. At an oxygen content of ~1.50, the annealing of fluorite δ-Bi_2O_3 at t < 730 °C leads to the formation of sillenite, β-Bi_2O_3 or a rhombohedral phase. At an oxygen content >1.52, the structure of fluorite with a usual

coordination number of 8 for cations is stabilized much more efficiently. Therefore, the reasons for the degradation of metastable fluorite can be free volume, inhomogeneity, small cations, cationic diffusion and segregation, the outer and inner surfaces of ceramics in the form of pores. The tetragonal phase in topotaxial composites with fluorite is observed mainly at an oxygen content of 1.51––1.52. The formation of tetragonal phase during MA indicates stability in a wide temperature range, Figs. 1 and 5–7.

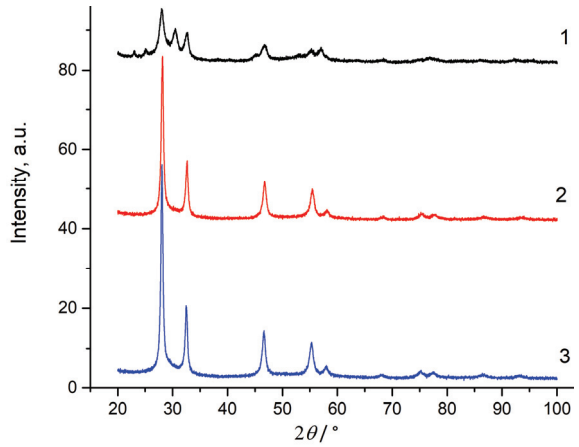

Fig. 6. Diffraction patterns of MA powders: 1 – topotaxial nanocomposite of fluorite and tetragonal phase $Bi_{0.765}Dy_{0.12}Er_{0.09}(M^{5+})_{0.02}Fe_{0.005}O_{1.52}$, 2 – fluorite $Bi_{0.76}Dy_{0.12}Er_{0.1}Ta_{0.02}O_{1.52}$, 3 – fluorite $Bi_{0.76}Dy_{0.12}Er_{0.1}W_{0.02}O_{1.53}$.

The diffraction patterns of Hf^{4+}-doped samples (EH2). after MA of powders and annealing at 400 °C are shown in Fig. 7. All powders are topotaxial composites of fluorite and tetragonal phase. A similar phenomenon of equilibrium of two phases during MA, the so-called mechanochemical equilibrium, was found in the $PbO–2WO_3$ and $PbO–2MoO_3$ systems.[13] The essence of this phenomenon is related to the formation and relaxation of (*D*)*.

According to the structure of the tetragonal phase, an increase in the content of Hf^{4+} should lead to an increase in the probability of its formation. However, $Bi_{0.7}Er_{0.2}Hf_{0.1}O_{1.55}$ ceramics with ideal homogenization obtained from nitrate precursors and a long three-stage firing at 800 °C without MA turned out to be a mixture of two fluorites with different hafnium content, Fig. 8. Nevertheless, the traces of the tetragonal phase appear in the diffraction patterns after annealing at 600 °C, as a result of degradation of metastable fluorite structure.

$Bi_{0.79}Er_{0.2}Hf_{0.01}O_{1.505}$ and $Bi_{0.77}Er_{0.2}Hf_{0.03}O_{1.515}$ ceramics (like EH2, 3 in Fig. 7) are positioned in the literature as the best solid electrolytes, which possess the conductivity of $Bi_{0.8}Er_{0.2}O_{1.50}$ ceramics while maintaining the structure of disordered fluorite and conductive properties after 1000 h of annealing at 600 °C,

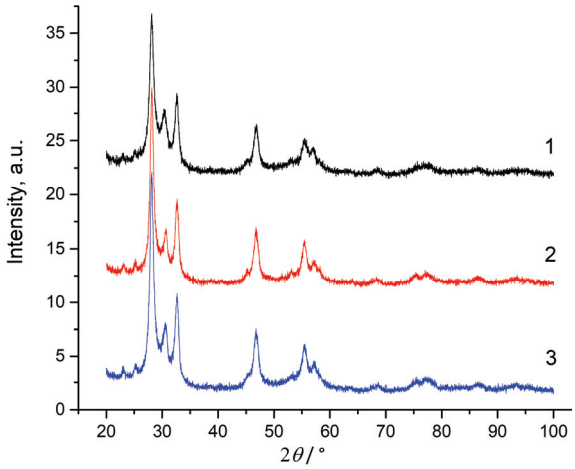

Fig. 7. Diffraction patterns of MA powders doped with Hf^{4+}, after annealing at 400 °C, topotaxial nanocomposites of fluorite and tetragonal phase: 1,2 – DEH2 from oxides and nitrates, respectively, 3 – EH2 from oxide.

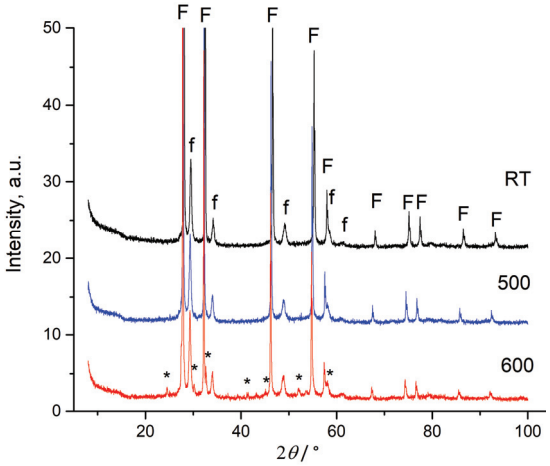

Fig. 8. HT XRD patterns of $Bi_{0.7}Er_{0.2}Hf_{0.1}O_{1.55}$ ceramics after sintering for 24 h at 850 °C at different temperatures, F and f – peaks of fluorites with a = 0.55072 and 0.52451 nm, asterisks indicate peaks of tetragonal phase.

due to hafnium doping.[15] For the fluorite structure degradation, only nuclei of the tetragonal phase are needed, which did not appear in dense homogenized ceramics, due to prolonged firing during synthesis and sintering (16 h at 890 °C).[16] When creating oxygen membranes based on δ-Bi_2O_3, such sintering conditions cannot be realized. Hafnium cations indeed stabilizes the fluorite structure due to slow diffusion.[14] However, the relatively small radius and charge of Hf^{4+} can lead to the appearance of nuclei of the tetragonal phase. The additional doping

with highly charged cations with a relatively large ionic radius can more effectively inhibit the formation of tetragonal phase nuclei.[11] The development of a solid electrolyte based on metastable fluorite ceramics by complex doping is within the framework of the concept of high-entropy ceramics (HEC).[11,14,16]

Mössbauer spectroscopy

The lowered doping of the ceramics with the ^{57}Fe isotope under the same conditions of synthesis yielded fluorite with a 3 % impurity of the tetragonal phase, which is insignificant for studies by γ-resonance spectroscopy, Fig. 9.

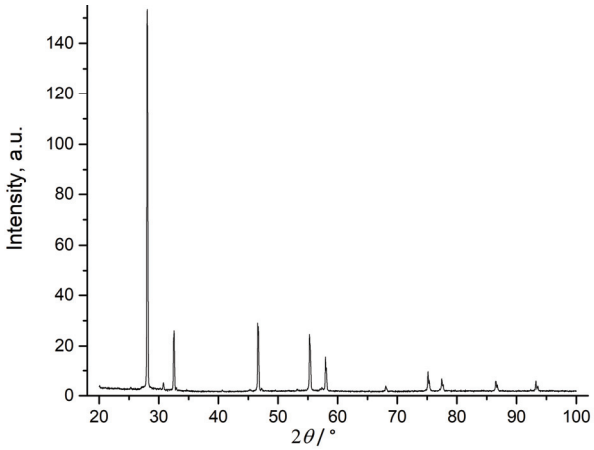

Fig. 9. Diffraction pattern of $Bi_{0.765}Dy_{0.12}Er_{0.09}(M^{5+})_{0.02}Fe_{0.005}O_{1.52}$ ceramics, synthesized from nitrates, sintered at 950 °C and air quenching. Fluorite, a = 0.55080(4) nm, tetragonal phase.

Mössbauer spectra of $Bi_{0.765}Dy_{0.12}Er_{0.09}(M^{5+})_{0.02}Fe_{0.005}O_{1.52}$ fluorite ceramics after heating to 950 °C and air quenching, and topotaxial composite of fluorite and tetragonal phase after synthesis and 8 min MA (Fig. 6, 1), are shown in Fig. 10, 1 and 2, respectively. The spectra are represented by doublets differing in parameters (Table III), which correlates with different structures. In a fluorite sample with a lattice parameter a_F = 0.55080(4) nm, a relatively small chemical shift, δ = 0.25 mm s^{-1} and quadrupole splitting, ε = 0.77 mm s^{-1} indicates low Fe^{3+} coordination or large distances to oxygen atoms, Fig. 10 (1). In a cerium dioxide nanopowder with a fluorite structure (a_F = 0.5401 nm) doped with 10 % molar Fe^{3+}, a similar doublet with δ = 0.24 mm s^{-1} and ε = 0.95 mm s^{-1} was observed.[17] It is most likely that Fe^{3+} has an octahedral environment. In fluorite $CeZrO_4$ (a_F = 0.526 nm) with the occupied oxygen positions, the spectrum parameters δ = 0.33 mm s^{-1} and ε = 1.09 mm s^{-1} are significantly different.[18] The authors believe that iron ions locally deform the lattice.[17] Taking

into account all the results, it is most likely that small Fe^{3+} ions in the fluorite lattice occupy cation positions with the distortion of the local environment.

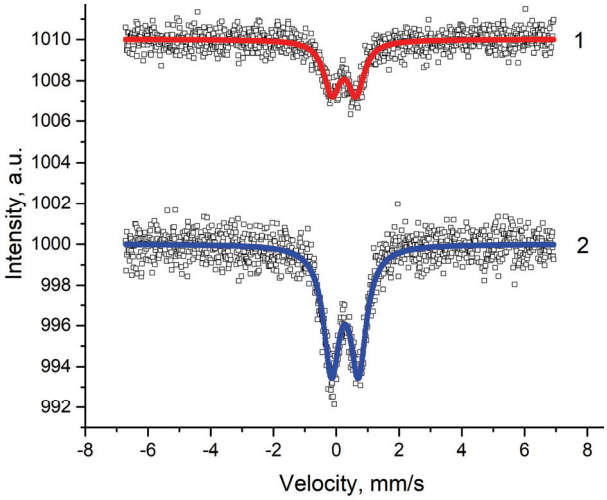

Fig. 10. Mössbauer spectra of ^{57}Fe in $Bi_{0.765}Dy_{0.12}Er_{0.09}(M^{5+})_{0.02}Fe_{0.005}O_{1.52}$ sample after firing at 950 °C and air quenching with fluorite structure (1) and after synthesis and 8 min MA, topotaxial nanocomposite of fluorite and tetragonal phase (2).

TABLE III. Parameters of $^{57}Fe^{3+}$ Mössbauer spectra at room temperature of samples with composition $Bi_{0.765}Dy_{0.12}Er_{0.09}(M^{5+})_{0.02}Fe_{0.005}O_{1.51}$

Structure	Conditions of preparation	Line width, mm s^{-1}	δ / mm s^{-1}	ε / mm s^{-1}
Fluorite	950 °C, air quenching	0.62(1)	0.25(1)	0.77(2)
Tetra-phase	950 °C , MA 8 min	0.61(1)	0.28(1)	0.86(2)

In the topotaxial composite of fluorite and tetragonal phase, like ω-Bi_2O_3 on the BeO substrate, the main part of the introduced iron is segregated in the tetragonal phase, as evidenced by its formation when even a small impurity of 0.5 % molar Fe^{3+} is introduced into a relatively stable fluorite. In the tetragonal phase, the chemical shift is slightly larger (δ = 0.28 mm s^{-1}) than in fluorite, Fig. 10 (2), but it is still noticeably smaller than the usual chemical shift for $Fe^{3+}O_6$. In the tetragonal phase, Fe^{3+} is uniquely located in the centre of the tetrahedron with a distance of ~0.203 nm to oxygen ions, Fig. 4. The parameters of doublet δ = 0.28 mm s^{-1} and ε = 0.86 mm s^{-1} are close to those of 5-coordinated Fe^{3+} in MA perovskites (δ = 0.29 and ε = 1.19).[14] For comparison, parameters of doublet of the $Fe^{3+}O_6$ states in perovskites were δ = 0.34 to 0.35 mm s^{-1}, ε = 0.57 to 0.66 mm s^{-1}, and a distance Fe-O 0.193 nm.[14] Parameters of doublet of $Fe^{3+}O_4$ in mullite-like structure $Bi_2Fe_4O_9$ were δ = 0.231 mm s^{-1} and ε = 0.95 mm s^{-1} (0.352 and ~0.95 mm s^{-1} for $Fe^{3+}O_6$).[19]

Raman spectroscopy

The Raman spectra of fluorite and topotaxial composite are shown in Fig. 11.

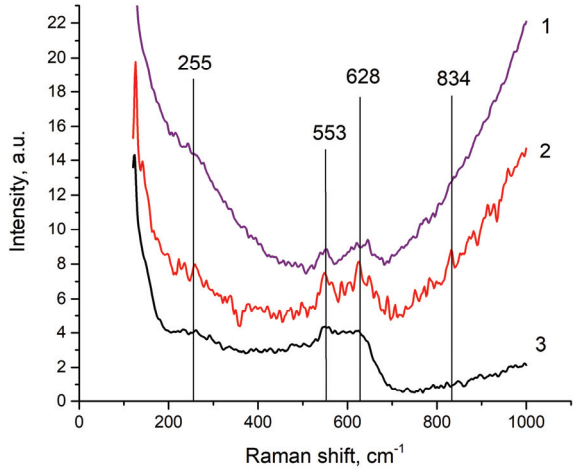

Fig. 11. Raman spectra with accumulation time 60, 10 and 10 min respectively: 1) MA powder DEH2 after heating up to 700 °C (topotaxial nanocomposite of fluorite with tetragonal phase, Fig. 1), 2) EH2 ceramics with fluorite structure, after synthesis at 900 and sintering at 700 °C, 3) the same EH2 sample after MA 8 min, nanopowder with fluorite structure.

Spectra exhibit broad bands at 255, 553, 628 and a very weak sharp band at 834 cm^{-1} at the noise level and only in EH2 ceramics. In fluorite δ-Bi_2O_3, stabilized with 20 mol. % Nb^{5+} or Ta^{5+}, two broad bands are observed at 550 and 320 cm^{-1},[20] which are attributed to Bi–O stretches with interatomic distances of 0.226 and 0.204 nm in 5-fold coordination, and a sharp band at 821 cm^{-1}. A similar band was found in sillenite and is attributed to the $Bi^{5+}O_4$ tetrahedron.[20] In stabilized EH2 fluorite, a greater number of bands is related to high content of oxygen vacancies relative to $Bi_{0.8}Ta_{0.2}O_{1.7}$, which leads to different states. On the whole, no new bands were found in the topotaxial composite of fluorite and the tetragonal phase, and the bands common to fluorite have a very weak intensity. The absence of bands that could be attributed to the tetragonal phase can be associated with a large number of possible states with low symmetry, in addition to being in the field of mechanical stress due to topotaxial bonding with fluorite.

CONCLUSION

A new tetragonal phase of doped bismuth oxide as a degradation product of the disordered fluorite structure δ-Bi_2O_3 was found in a topotaxial composite with fluorite. The tetragonal phase is stable over a wide temperature range. The free volume arising during MA and inhomogeneous doping promote the form-

ation of nuclei of the tetragonal phase. The area of existence of the tetragonal phase in doped bismuth oxide is determined by the oxygen content of approximately 1.51 to 1.52 and the content of minor dopants ~0.01 to 0.05 with a small ionic radius, including Hf^{4+} and Fe^{3+}. The structure of the tetragonal phase is proposed on the basis of powder XRD data, which can form superlattices when arranged. The Mössbauer and Raman spectra are in agreement with the proposed structure. The data obtained make it possible to optimize the composition of the solid electrolyte and the conditions for its synthesis for the kinetic stabilization of the fluorite structure. Possible contamination of the solid electrolyte with iron, hafnia (or zirconia) during MA and grinding, as well as other cations upon contact with certain components of oxygen membranes, promotes phase degradation of metastable fluorite δ-Bi_2O_3.

Acknowledgements. This work was supported by the Russian Foundation for Basic Research, Grant 20-03-00349, and within the framework of the state assignment of the Institute of Solid State Chemistry and Mechanochemistry, SB RAS (project 0301-2019-0002).

ИЗВОД

ТРАНСФОРМАЦИЈА ФЛУОРИТА δ-BI_2O_3 У НОВЕ ТЕТРАГОНАЛНЕ ФАЗЕ

VLADIMIR V. ZYRYANOV и SERGEY A. PETROV

Institute of Solid State Chemistry and Mechanochemistry, Siberian Branch of Russian Academy of Sciences, Novosibirsk, Kutateladze 18, 630090 Russian Federation

Бизмут(III)-оксид, кинтетички стабилизаван додатком неуређене метастабилне структуре флуорита, има изузетно велику проводљивост. Селективне кисеоничне мембране, применом кермет (cermet) Bi_2O_3/Ag композитног материјала на температури од око 550 °C, имају највећи потенцијал за сепарацију ваздуха и могу се употребити за мултифункционалну производњу кисеоника на бази сагоревања фосилних угљеничних горива. Приликом истраживања оптималног састава δ-Bi_2O_3, нађено је да у керамици која је синтетисана механичком активацијом долази до деградације флуорита у нове тетрагоналне фазе. Тетрагонална фаза постоји у топотаксијалном композиту структуре флуорита. За тетрагоналну фазу са a = 3,854 nm, c = 0,88905 nm и S.G. P-4, која је релативно стабилну у широком температурском опсегу, предложена је кристална структура и атомске координате. За узорке флуорита и топотаксијалне композите дискутовани су њихови Raman и Mössbauer спектри. Откриће нове тетрагоналне фазе допираног бизмут(III)-оксида и подручја његове оптималне стабилности омогућава оптимизацију састава и синтезу стабилнијег чврстог електролита δ-Bi_2O_3 са великом проводљивости.

(Примљено 22. јуна, ревидирано 12. августа, прихваћено 21. септембра 2022)

REFERENCES

1. H. A. Harwig, A.G. Gerards, *J. Solid State Chem*. **26** (1978) 265 (https://dx.doi.org/10.1016/0022-4596(78)90161-5)
2. P. Shuk, H. D. Wiemhofer, U. Guth, W. Gopel, M. Greenblatt, *Solid State Ionics* **89** (1996) 179 (https://dx.doi.org/10.1016/0167-2738(96)00348-7)

3. V. V. Kharton, F. M. B. Marques, A. Atkinson, *Solid State Ionics* **174** (2004) 135 (https://dx.doi.org/10.1016/j.ssi.2004.06.015)
4. B. Singh, S. Ghosh, S. Aich, B. Roy, *J. Power Sources* **339** (2017) 103 (https://dx.doi.org/10.1016/j.jpowsour.2016.11.019)
5. A. Dapčević, D. Poleti, L. Karanović, J. Miladinović, *J. Serb. Chem. Soc*. **82** (2017) 1433 (https://doi.org/10.2298/JSC170711111D)
6. A. Matsumoto, Y. Koyama, I. Tanaka, *Phys. Rev., B* **81** (2010) 094117 (https://dx.doi.org/10.1103/PhysRevB.81.094117)
7. N. Jiang, R. M. Buchanan, F. E. G. Henn, A. F. Marshall, D. A. Stevenson, E. D. Wachsman, *Mater. Res. Bull*. **29** (1994) 247 (https://doi.org/10.1016/0025-5408(94)90020-5)
8. S. Boyapati, E. D. Wachsman, N. Jiang, *Solid State Ionics* **140** (2001) 149 (https://doi.org/10.1016/S0167-2738(01)00698-1)
9. S. Boyapati, E. D. Wachsman, B. C. Chakoumakos, *Solid State Ionics* **138** (2001) 293 (https://doi.org/10.1016/s0167-2738(00)00792-x)
10. E. D. Wachsman, *J. Eur. Ceram. Soc*. **24** (2004) 1281 (http://dx.doi.org/10.1016/s0955-2219(03)00509-0)
11. V. V. Zyryanov, A. S. Ulihin, *Ceram. Int*. **48** (2022) 16877 (https://doi.org/10.1016/j.ceramint.2022.02.242)
12. V. V. Zyryanov, *Inorg. Mater*. **41** (2005) 378 (http://dx.doi.org/10.1007/s10789-005-0140-y)
13. V. V. Zyryanov, *Russ. Chem. Rev*. **77** (2008) 105 (https://doi.org/10.1070/RC2008v077n02ABEH003709)
14. V. V. Zyryanov, S. A. Petrov, A. S. Ulihin, *Ceram. Int*. **47** (2021) 29499 (https://doi.org/10.1016/j.ceramint.2021.07.118)
15. B.-H. Yun, C.-W. Lee, I. Jeong, K. T. Lee, *Chem. Mater*. **29** (2017) 10289 (https://doi.org/10.1021/acs.chemmater.7b03894)
16. A. J. Wright, J. Luo, *J. Mater. Sci*. **1000** (2020) 9812 (https://doi.org/10.1007/s10853-020-04583-w)
17. F. F. H. Aragon, J. C. R. Aquino, J. E. Ramos, J. A. H. Coaquira, I. Gonzalez, W. A. A. Macedo, S. W. da Silva, P. C. Morais, *J. Appl. Phys*. **122** (2017) 204302 (https://doi.org/10.1063/1.4999457)
18. R. Nedyalkova, D. Niznansky, A-C. Roger, *Catal. Comm*. **10** (2009) 1875 (http://dx.doi.org/10.1016/j.catcom.2009.06.017)
19. A. Kirsch, M. M. Murshed, F. J. Litterst, T. M. Gesing, *J. Phys. Chem., C* **123** (2019) 3161 (http://dx.doi.org/10.1021/acs.jpcc.8b09698)
20. F. D. Hardcastle, I. E. Wachs, *J. Solid State Chem*. **97** (199) 319 (https://doi.org/10.1016/0022-4596(92)90040-3).

Journal of the Serbian Chemical Society
JSCS-info@shd.org.rs • www.shd.org.rs/JSCS
J. Serb. Chem. Soc. *87* (12) 1381–1393 (2022)
JSCS–5601
Original scientific paper
Published 14 December 2022

3D-QSAR and molecular docking studies of aminothiazole derivatives as Lim kinase 1 inhibitors

JING-XUAN HOU, QING-SHAN GU, MEI-QI SHI, HUI GAO, LU ZHENG* and QING-KUN WU**

School of Pharmacy, Jiangsu Ocean University, Jiangsu, 320000, P.R. China

(Received 10 May, revised 14 July, accepted 23 September 2022)

Abstract: Lim kinase (Limk), as an important cytoskeletal regulator, plays an important role in cancer manifestations and neuronal diseases. Limk1 is a member of the Limk family, which is mainly involved in the invasion and metastasis of tumor cells and is abnormally expressed in a variety of cell carcinoma tissues. In this paper, a series of Limk1 inhibitors with aminothiazole skeleton were used to design potent and efficient Limk1 inhibitors by computational approaches. Firstly, the 3D-QSAR model was constructed, and both CoMFA and CoMSIA models have good correlation and prediction ability. The binding requirements between ligand and receptor protein were then further explored through molecular docking, including the critical forces between Limk1 inhibitors and active site residues. Finally, based on the 3D-QSAR model and molecular docking results analysis, three new compounds with theoretically better activity were designed and their ADME properties were predicted.

Keywords: cancer; CoMFA; CoMSIA; computational drug design.

INTRODUCTION

Invasiveness and metastasis are essential features of malignant tumours and two of the most important causes of death in cancer patients.[1] Limk is known to regulate the conversion of filamentous actin (F-actin) into globular actin (G--actin) by phosphorylation of cofilin substrates and control microtubule dynamics during cell cycle interphase.[2] Due to its associated activity, Limk is involved in many cellular physiological functions, and its dysregulation may lead to cancers and viral infections.[1,3,4] Numerous studies have confirmed that Limk is highly expressed in a variety of human tumours, particularly in highly aggressive tumours.

Members of the Limk family include Limk1 and Limk2, which are characterized by their dual serine/threonine and tyrosine kinase activities. They show

* Corresponding authors. E-mail: (*)zhel-123@163.com; (**)qingkunwuchem@163.com
https://doi.org/10.2298/JSC220510076H

significant similarity in primary amino acid sequences (55 %) and more similarity (72 %) at the level of their kinase structural domains and ATP binding sites.[5] However, the subcellular localization of the two is different, suggesting that they have different roles in tumor cells. Limk1 is mainly involved in the invasion and metastasis of tumor cells,[6] and its phosphorylation can induce cytoskeletal actin dynamics and microtubule depolymerization,[7] so it has abnormal expression in many kinds of tumors.[8,9] Therefore, Limk1 is considered as a therapeutic target to interfere with tumor proliferation, invasion and metastasis.

In 2008, Bristol Myers Squibb disclosed a (BMS-3, Fig. 1) and b (BMS-5) as the first class of Limk1 inhibitors, however their mechanism of action is not yet known.[10] In 2011, Sleebs *et al.* identified c from a series of 5,6-substituted 4-aminothieno[2,3-*d*]pyrimidines, and it had potential for drug-like properties optimization.[11] In 2015, Yin *et al.* identified bisarylurea compounds d and e (SR--11124 and SR-11157), however their application in indications has not been reported.[12] In the same year, starting from a series of aminothiazole skeletons, Charles *et al.* reported Limk1 inhibitors f and g (CRT0105446 and CRT0105950) and follow-up investigation found that rhabdomyosarcoma, neuroblastoma and kidney cancer cells were all significantly sensitive to both of them.[13,14] In 2020, Zhang *et al*. discovered the second generation tyrosine kinase inhibitor h (Dasatinib), which also had a strong inhibitory effect on Limk1.[15] Although a large number of compounds that bind to the ATP pocket of Limk1 have been designed and tested in recent years for their ability to affect Limk1 mediated cofilin phosphorylation and microtubule stability, the clinical achievement of such drugs is limited. Therefore, more Limk1 inhibitors with less side effects and higher efficiency need to be developed to meet the unmet clinical needs.

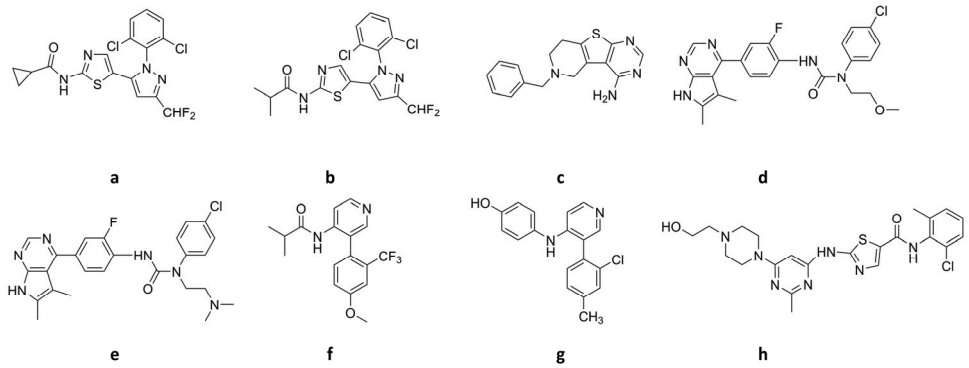

Fig. 1. Structures of some Limk1 inhibitors.

In this study, to design more Limk1 inhibitors, a 3D-QSAR model was firstly constructed based on aminothiazole Limk1 inhibitors reported by Charles *et al.*[16] Then, the binding requirements between ligand and receptor protein were

further explored through molecular docking study. Finally, based on the results, three theoretically superior compounds were designed and their ADME properties were predicted.

MATERIALS AND EXPERIMENTS

Software

In this paper, ChemDraw 19.0 was used to draw compounds, SYBYL X-2.0 was used to conduct 3D-QSAR models and Discovery Studio 2019 (DS) was used to do molecular docking.

Compounds source

The data used for quantitative structure-activity relationship study were reported by Charles *et al.*,[16] including 20 aminothiazole compounds. The given IC_{50} values were converted to pIC_{50} (pIC_{50} = –log IC_{50}) as the dependent variable. The structure and antagonistic activity of the compounds were listed in Table I. 16 inhibitors were selected as the training set for model building and 4 inhibitors (marked as *) were used as the test set for model evaluation in a random screening manner.

TABLE I. The studied Limk1 inhibitors and the corresponding experimental and predicted activity; * – inhibitors used as the test set for model evaluation in a random screening manner

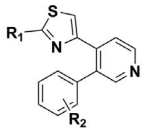

No.	R_1	R_2	pIC_{50}		
			Observed	Predicted	
				CoMFA	CoMSIA
1*	–NHPr	*o*-Cl	7.824	7.731	7.702
2		*m*-Cl	6.301	6.295	6.206
3		*p*-Cl	6.208	6.678	6.536
4		H	6.071	6.121	6.105
5		*o*-Me	7.086	6.979	6.840
6		*o*-*i*-Pr	5.481	5.429	5.597
7		*o*-CF_3	7.432	7.588	7.483
8		*o*-CF_3, *p*-OMe	7.886	7.603	7.719
9*	–NMePr	*o*-Cl	5.509	5.875	5.714
10	–NHEt	*o*-Cl	6.921	6.554	6.833
11	–NH-*i*-Bu	*o*-Cl	8.301	7.767	8.054
12	–NHCHMe(*S*)Ph	*o*-Cl	7.398	7.833	7.476
13	–NHCHMe(*R*)Ph	*o*-Cl	8.398	8.339	8.365
14	–NHPh	*o*-Cl	8.523	8.828	8.654
15	–NH-4-PhOH	*o*-Cl, *p*-Me	9.523	9.273	9.663
16	–NH_2	*o*-Cl	6.569	6.749	6.566
17*	–NHCOMe	*o*-Cl	7.699	7.517	7.137
18	–NHCO-*i*-Pr	*o*-Cl	8.523	8.919	8.732
19		*o*-Cl, *p*-Me	9.000	8.666	8.794
20*		*o*-CF_3, *p*-OMe	8.097	7.680	7.819

Molecular conformations generation

The drawn structures were put into the SYBYL X-2.0 form, the Tripos force field was chosen for energy optimization and Gasteiger-Hückel charges were imparted to the molecules. To get the lowest energy conformation, multi-search was used for conformation search. The search yielded 200 conformations for each molecule, which were saved in different databases, and the conformation with lowest energy from each database was selected for follow-up research.[16]

Molecular alignment

In order to clarify the structure-activity relationship, the most active compound **15** was selected as the template molecule. The "align database" function was then applied to align the train/test compounds with the common substructure respectively, as shown in Fig. 2.

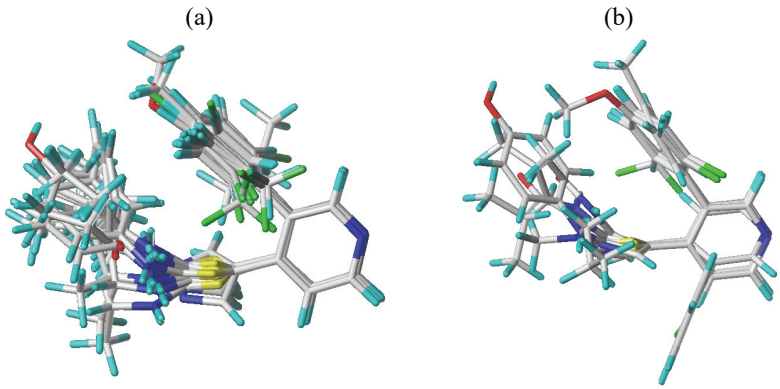

Fig. 2. a) The alignment of the training set. b) The alignment of the test set.

CoMFA and CoMSIA models construction

The CoMFA model describes two features: the steric and the electrostatic field; while the CoMSIA analysis has more exploratory capability: steric, electrostatic, hydrophobic, hydrogen bond donor and acceptor.

The lowest energy conformation of each compound in the previously saved database was selected. The pIC_{50} of each compound was used as the dependent variable, while the eigenvalues of CoMFA and CoMSIA were used as independent variables. Then the partial least-square (PLS) analysis was applied to establish the CoMFA and CoMSIA models. Firstly, the leave-one-out (LOO) cross-validation in PLS was used to obtain the maximum principal component value and cross-validation coefficient. After a reasonable maximum principal component value was obtained, a series of statistical parameters (Table I) were calculated through non-cross-validation under the condition of the maximum principal component value. Finally, the test set was used to validate the prediction ability of CoMFA and CoMSIA models from the external.

Molecular docking

The structure of the recently reported Limk1-staurosporine complex (PDB 3S95) was used and a series of very critical preparations of this protein, such as hydrogenation, charge addition and ligands deletion, were carried out in DS software using the Prepare Protein protocol.[17] The ATP pocket where the staurosporine is located was chosen as the docking pocket

with coordinates X = 45.2308, Y = 21.0287, Z = 68.0594, and a radius of 7.195037. Finally, the LibDock module was used in the docking process, while other parameters were kept as default.

ADME prediction

ADME prediction was performed using the online server http://www.swissadme.ch/,[18] a web-based ADME screening tool that predicts the drug-likeness of newly designed compounds to reduce waste of money and time in later drug development process.

RESULTS AND DISCUSSION

3D-QSAR model parameters

The reliability of the model was evaluated by the LOO cross-validated correlation coefficient, q^2, the non-validated correlation coefficient, r^2, the standard error of the estimated *SEE* and the F statistic. The predicted correlation coefficient, r^2_{pred}, was applied to validate the model's predictive power. The relevant values were listed in Table II.

TABLE II. Statistical parameters of 3D-QSAR models

Parameter						Contribution, %				
q^2	r^2	*ONC*	*F*	*SEE*	r^2_{pred}	*S*	*E*	*H*	*D*	*A*
CoMFA										
0.517	0.932	3	54.532	0.343	0.876	52.7	47.3	–	–	–
CoMSIA										
0.772	0.980	4	132.088	0.196	0.896	6.3	17.4	21.4	14.0	40.9

A model with $q^2 > 0.5$ is generally considered to be reliable and has good predictive power. The CoMFA model has 52.7 and 47.3 % of the steric and electrostatic fields, respectively, with optimal number of components (*ONC*) = 3, r^2 = = 0.932, q^2 = 0.517, *SEE* = 0.343 and r^2_{pred} = 0.876. The CoMSIA model has 6.3, 17.4, 21.4, 14 and 40.9 % of the steric, electrostatic, hydrophobic, hydrogen bond donor and hydrogen bond acceptor fields respectively. Its *ONC* = 4, r^2 = = 0.980, q^2 = 0.772, *SEE* = 0.196 and r^2_{pred} = 0.896. The training and test sets were regressed linearly on the values of the experimental pIC_{50} and the predicted pIC_{50} using a scatter plot. The resulting fitted curves were shown in Fig. 3, indicating that the CoMFA and CoMSIA models are stable and reliable.

Contour map analysis

CoMFA contour maps. The steric field contour map was shown in Fig. 4. As shown in Fig. 4a, the green and yellow contours distribute evenly in the R_1 region, which indicates that the substituted group with appropriate size in R_1 is beneficial to the activity (IC_{50} = 5 nM for **11** *vs.* 120 nM for **10** *vs.* IC_{50} = 270 nM for **16**). It is also observed that the benzene ring in the R_1 region is preferred to the alkyl substitution (IC_{50} = 3 nM for **14** *vs.* 120 nM for **10**). There are three big yellow contours in the R_2 region, which indicates that bulky groups are dis-

favored for Limk1 inhibition in this region. As shown in Fig. 4b, the activity of the compound decreases when there is a bulky group in the R_2 region (IC_{50} = 3300 nM for **6** *vs.* 850 nM for **4**). In general, groups with appropriate size in the R_1 region (where aromatic groups would be preferred over alkyl substitutions) can improve the activity, and when there are bulky groups in the R_2 region, the activity of the compound would decrease.

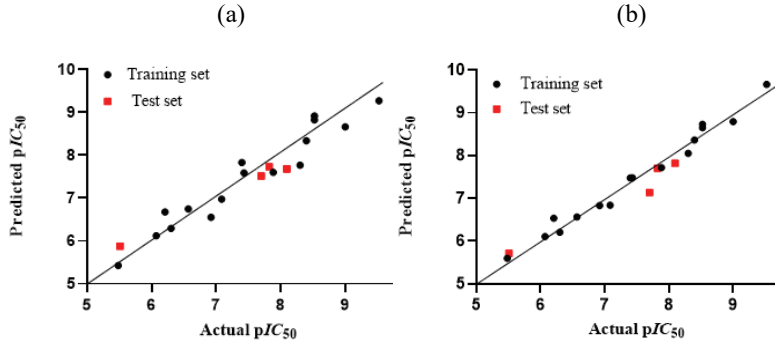

Fig. 3. Plots of actual versus predicted values. a) CoMFA model. b) CoMSIA model.

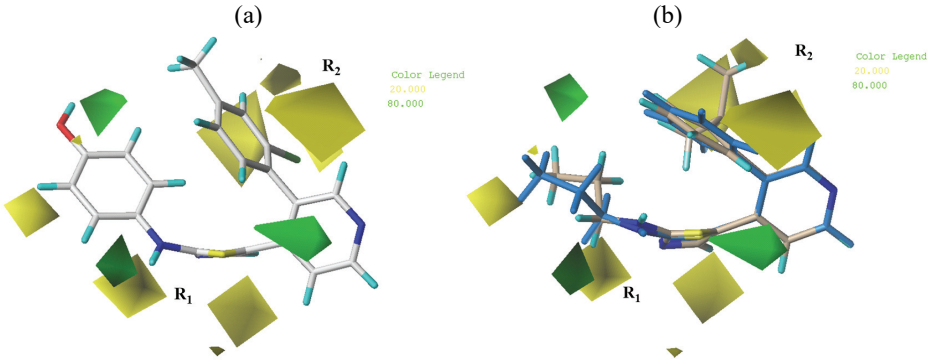

Fig. 4. Contour maps of CoMFA steric field (bulky groups are favored in the green regions and disfavored in the yellow regions). a) Compound **15** in steric field. b) Compound **4** (blue) and **6** (gray) in steric field.

The electrostatic field contour map was shown in Fig. 5.

As shown in Fig. 5a, there are both blue and red contours in the R_1 region, suggesting that groups with appropriate charge are favorable for Limk1 inhibition. For example, –NHCHMe(*R*)Ph (**13**), –NH-4-PhOH (**15**) and –NHCO-*i*-Pr (**19**) are all good for Limk1 inhibitory activity (IC_{50} = 4 nM for **13** *vs.* 0.3 nM for **15** *vs.* 1 nM for **19**). According to Fig. 5b, there is a blue contour in the R_2 region, which indicates that electropositive groups, such as $–CH_3$, are beneficial to inhibiting Limk1 (IC_{50} = 1 nM for **19** *vs.* 2 nM for **18**).

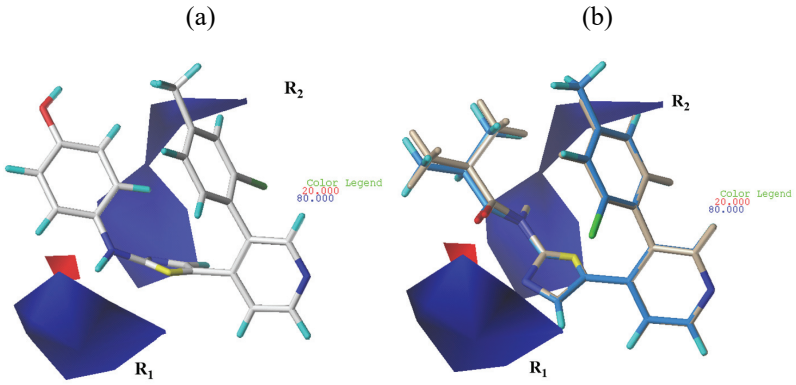

Fig. 5. Contour maps of CoMFA electrostatic field (electropositive groups are favored in the blue regions, and electronegative groups are favored in the red regions). a) Compound **15** in electrostatic field. b) Compound **19** (blue) and **18** (gray) in electrostatic field.

CoMSIA contour maps. As shown in Fig. 6, compound **15** was put into contour maps of CoMSIA model. Since the steric field accounts for only 6.3 %, the effect is negligible. In Fig. 6a, the R_2 region is surrounded by the blue contours, same as the CoMFA electrostatic field. But unlike CoMFA, the R_1 region has a small red contour, indicating that the introduction of $–NO_2$, –F, –Cl, *etc*. may contribute to the activity increase.

In Fig. 6b, no contours appear in the R_1 region, indicating that the substituent groups in this region are not sensitive to hydrophilic and hydrophobic interactions. The R_2 region is surrounded by a white contour, which means that the introduction of hydrophilic groups can enhance the inhibitory activity, such as –OH and $–NH_2$. In Fig. 6c, the N atom in the R_1 region attached to the aminothiazole ring is surrounded by a cyan contour, suggesting that the alkylated N atom is less active than the unsubstituted –NH (IC_{50} = 3100 nM for **9** *vs.* 270 nM for **16**). As shown in Fig. 6d, the addition of groups with a hydrogen bond donor or acceptor in the R_2 region has no effect on the activity. However, the magenta and red contours uniformly wrap the N atom in the R_1 region, indicating that groups with a hydrogen bond donor and acceptor, such as –OH and $–NH_2$, can both enhance the activity.

Molecular docking

3D-QSAR models can not directly show the interactions between ligands and the receptors. To further investigate the effect of the substituted groups in the R_1 and R_2 regions on the activity, the molecular docking was conducted.

In order to test the reliability of the molecular docking method, the original ligand was extracted and re-docked. The conformation with the highest score was selected to overlap with the original conformation. The original and the experi-

mental conformations are superimposed well, and the *RMSD* value is 0.07614 nm (< 0.2 nm), indicating that the docking method used is reliable.[19]

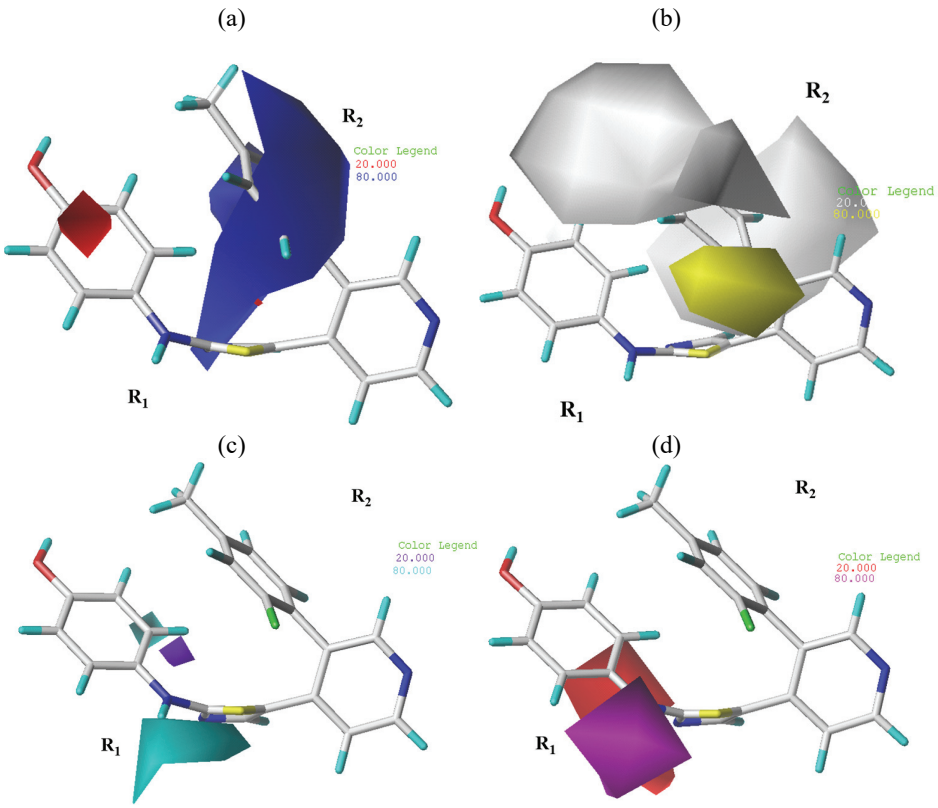

Fig. 6. Contour maps of the CoMSIA model (hydrophobic groups are favored in the yellow regions and disfavored in the white regions. H-bond donor groups are favored the cyan regions and disfavored in the purple regions. H-bond acceptor groups are favored in the magenta regions and disfavored in red regions). a) Electrostatic field. b) Hydrophobic field. c) Hydrogen bond donor field. d) Hydrogen bond acceptor field.

Twenty aminothiazole Limk1 inhibitors were docked to the protein ATP binding site. The top six scoring compounds were listed in Table III. It can be noticed that the compounds generally scored higher when there was a benzene ring in the R_1 region, which may be due to the hydrophobic interaction between the benzene ring and the surrounding amino acid residues. The active pocket in the R_1 region remains unfilled, suggesting that substituents with appropriate size could improve the interactions. These are consistent with the results of the 3D--QSAR model analysis. In addition, more than half of the inhibitors interacted with amino acids Leu345, Ala353, Val366, Lys368, Leu397, Tyr415, Ile416, Leu467 and Ala477, suggesting that these nine amino acids may be the primary

amino acids for protein-ligand interaction. 3D and 2D plots of the docking results for the highest scoring compound **12** and the most active compound **15** were shown in Fig. 7. Amino acid Ile416 formed hydrogen bond at distances of 0.183 nm (–N···H–) and 0.248 nm (–H···O–) with compounds **12** and **15**, respectively, and this hydrogen bond was considered to be essential for the inhibitory activity.[17] It can also be observed that compound **12** formed a hydrogen bond with Ile416 by the "N" in the pyridine ring on its common skeleton, while **15** formed a hydrogen bond with Ile416 by a substituted hydroxyl group in the R_1 region. When modifying the substituents in the R_1 and R_2 regions, the effect on the conformation of the compound should be considered.

TABLE III. Results of docking fraction study on the interaction of compounds and Limk1 protein

No.	Docking score	Mode of action			
		Hydrogen bonds	Hydrophobic	Pi-Anion	Pi-Alkyl
12	99.7584	Ile416	Glu384, Phe411, Asp478, Leu397, Thr413	–	Lys368, Ala477, Ala353
13	98.9368	–	Glu414, Gly419, Tyr415, Thr413, Phe411, Asn465	–	Leu345, Leu467, Ala477, Ala353, Leu397, LYS368
8	93.7566	Asp478	Ile416, Glu414	–	Ala353, Ala477, Leu397, Leu345, Leu467
7	92.0749	Asp478, Lys368	Glu414	–	Leu467, Leu345, Val366
20	91.7253	Asp478	Val366, Met367, Gly419	Asp478	Leu467, Ile416, LEU345
15	90.8909	Ile416	Lys368, Thr413, Phe411	Asp478	Val366, Leu467, Ala353, Leu397, Ala477

New compounds design

As shown in Fig. 8, three theoretically active Limk1 inhibitors were designed using compound **12** as the template based on the results analyses of contour maps and molecular docking. The results of activity prediction and molecular docking were shown in Table IV. The conformation of the new compound was overlapped with that of compound **12**, respectively, and the *RMSD* values showed that the conformation of the newly designed compound had little change compared with that of compound **12**. All of them scored better than **12**, forming hydrogen bonds with Ile416 (bond length = 0.203 nm for **N1**, 0.213 nm for **N2** and 0.201 nm for **N3**). Compound **N3** scored highest, probably due to the additional hydrogen bonding with Glu384. Overall, the newly designed compounds have high predicted activity and scores, indicating successful compound design.

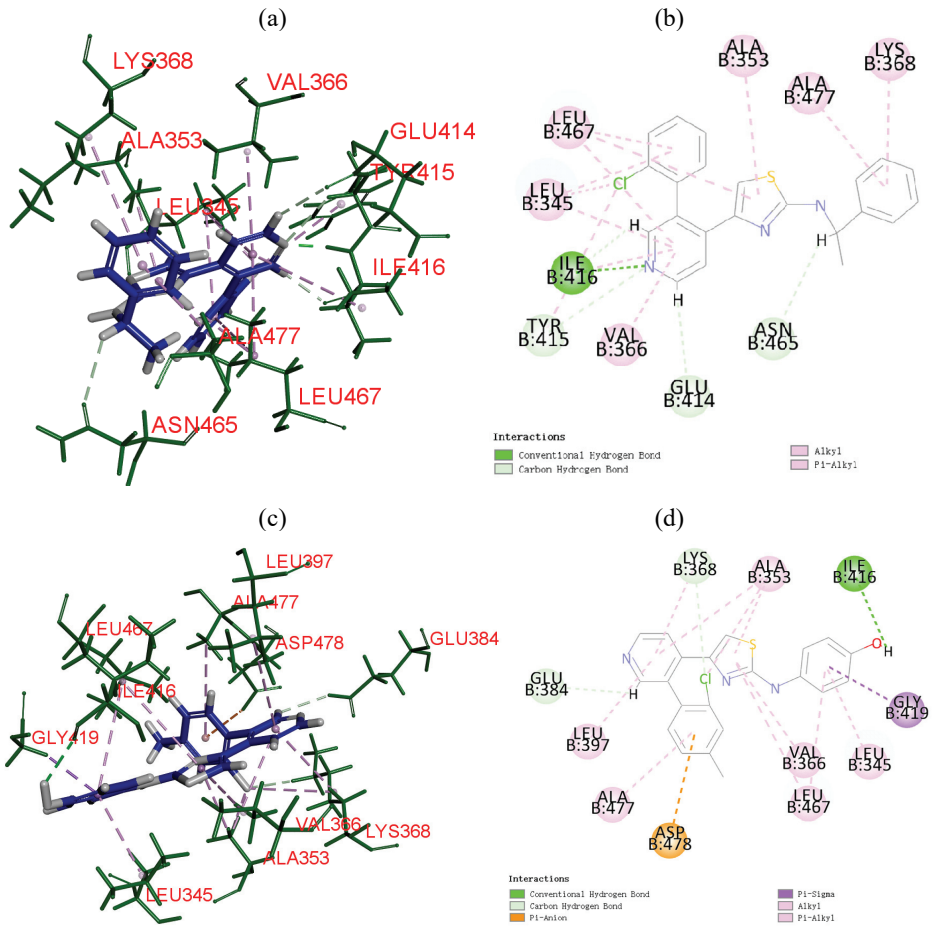

Fig. 7. a) 3D interaction map of compound **12**; b) 2D interaction map of compound **12**; c) 3D interaction map of compound **15**; d) 2D interaction map of compound **15**.

TABLE IV. The results of activity prediction and molecular docking

Compd.	Pred. IC_{50} / nM		Docking score	Critical amino acid residues	*RMSD* / nm
	CoMFA	CoMSIA			
N1	16.2	18.5	104.469	Ile416	0.1459
N2	23.4	32.6	104.290	Ile416	0.3144
N3	25.6	34.2	109.319	Ile416, Glu384	0.2092

ADME forecast results and analysis

The ADME projections were listed in Table V. The newly designed compounds have better lipid-water partition coefficient and solubility compared to compound **12**. They all have superior Human intestinal absorption, which indicates that the compounds have good absorption property. **N1** and **N2** are both meta-

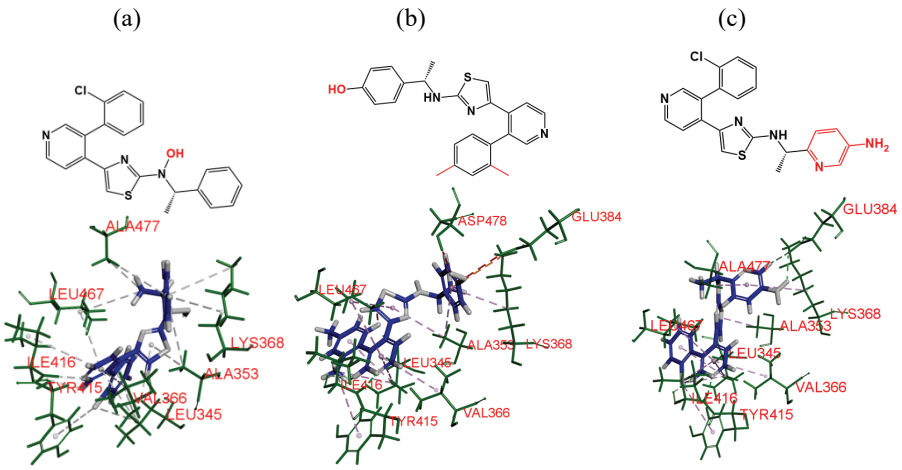

Fig. 8. a) 3D interaction map and structure of **N1**; b) 3D interaction map and structure of **N2**; c) 3D interaction map and structure of **N3**.

TABLE V. The results of predicted ADME; log *S* scale: insoluble < –10 < poorly < –6 < moderately < –4 < soluble < –2 very < 0 < highly; HIA: human intestinal absorption; BBB: blood brain barrier penetration; CYP450 inhibitor subtypes: CYP4501A2, CYP4502C19, CYP4502C9, CYP4502D6, CYP4503A4

No	MW	log $P_{o/w}$ (<5)	log *S*	Pharmacokinetics			Drug likeness
				HIA	BBB	CYP450 inhibitor	
12	391.92	5.25	-6.36	High	No	Yes	Yes
N1	407.92	4.96	-6.21	High	No	Yes	Yes
N2	401.52	4,94	-6.22	High	No	Yes	Yes
N3	407.92	3.94	-5.36	High	No	No	Yes

bolized by inhibitors of CYP450 subtypes 1A2, 2C19, 2C9, 2D6 and 3A4, while **N3** is not metabolized by 1A2. The drug-like properties were evaluated using Lipinski's rule and the results were all "Yes" which indicates that they all have good drug-like properties. From these results, it is clear that the newly designed compounds have good bioavailability and drug-like properties and are expected to be novel Limk1 inhibitors.

CONCLUSIONS

Limk1 is a target of great concern, but until now there has been no marketed drug for this target. In this paper, the reliable CoMFA and CoMSIA models were established based on a series of aminothiazole Limk1 inhibitors. The contour maps of the CoMFA and CoMSIA models demonstrate the key groups that influence the activity of Limk1 inhibitors. Molecular docking further indicates that Ala477, Glu384, Leu397, Lys368, Ala353, Leu467, Val366, Ile416 and Leu345 are the main amino acids for aminothiazole inhibitors to interact with Limk1 pro-

tein and hydrophobic interactions may increase the affinity. Based on these analyses, three novel aminothiazoles with potential Limk1 inhibitory activity with good feasibility and ADME evaluation results were designed.

Acknowledgements. The authors are grateful for Jiangsu Education Department (JSSCBS20211302), Jiangsu Institute of Marine Resources Development (JSIMR202015) and Jiangsu Ocean University for financial and technical support.

ИЗВОД

3D-QSAR И СТУДИЈЕ МОЛЕКУСКИМ ДОКИНГОМ ИНХИБИТОРА АМИНОТИАЗОЛ Lim КИНАЗЕ 1

JING-XUAN HOU, QING-SHAN GU, MEI-QI SHI, HUI GAO, LU ZHENG и QING-KUN WU

School of Pharmacy, Jiangsu Ocean University, Jiangsu, 320000, P.R. China

Lim киназа (Limk), као значајан цитоскелетни регулатор, има значајну улогу у испољавању канцера и нервним болестима. Limk1 је члан Limk породице, која је углавном укључена у инвазији и метастази туморских ћелија и ненормално је испољена у ћелијама различних ткива канцера. У овом раду је употребљена серија Limk1 инхибитора са аминотиазолским скелетом да би се рачунарским приступом дизајнирали моћни и ефикасни Limk1 инхибитори. Прво је конструисан 3D-QSAR модел, и CoMFA и CoMSIA су имали велику способност корелисања и претсказивања. Онда су путем молекулског докинга анализиране интеракције између лиганда и рецептора. На крају, сагласно 3D-QSAR анализи и резултатима молекулског докинга, дизајнирана су три једињења са теоретски бољом активношћу.

(Примљено 10. маја, ревидирано 14. јула, прихваћено 23. септембра 2022)

REFERENCES

1. K. Yoshioka, V. Foletta, O. Bernard, K. Itoh, *Proc. Natl. Acad. Sci.* **100** (2003) 7247 (https://doi.org/10.1073/pnas.1232344100)
2. C. Prunier, R. Prudent, R. Kapur, K. Sadoul, L. Lafanechère, *Oncotarget* **8** (2017) 41749 (https://doi.org/10.18632/oncotarget.16978)
3. F. Yi, J. Guo, D. Dabbagh, M. Spear, S. He, K. Kehn-Hall, J. Fontenot, Y. Yin, M. Bibian, C. M. Park, *J. Virol.* **91** (2017) e02418-16 (https://doi.org/10.1128/JVI.02418-16)
4. F. Manetti, *Drug Discov. Today* **17** (2012) 81 (https://doi.org/10.1016/j.drudis.2011.08.004)
5. A. Jayo, M. Parsons, J. C. Adams, *BMC Biol.* **10** (2012) 1 (https://doi.org/10.1186/1741-7007-10-72)
6. D. H. Vlecken, C. P. Bagowski, *Zebrafish* **6** (2009) 433 (https://doi.org/10.1089/zeb.2009.0602)
7. O. Bernard, *Int. J. Biochem. Cell Biol.* **39** (2007) 1071 (https://doi.org/10.1016/j.biocel.2006.11.011)
8. P. Chen, M. Zeng, Y. Zhao, X. Fang, *Oncol. Rep.* **32** (2014) 2070 (https://doi.org/10.3892/or.2014.3461)
9. J. Zhou, R. Liu, C. Luo, X. Zhou, K. Xia, X. Chen, M. Zhou, Q. Zou, P. Cao, K. Cao, *Cancer Biol. Ther.* **15** (2014) 1340 (https://doi.org/10.4161/cbt.29821)

10. P. Ross-Macdonald, H. de Silva, Q. Guo, H. Xiao, C.-Y. Hung, B. Penhallow, J. Markwalder, L. He, R. M. Attar, T. Lin, *Mol. Cancer Ther.* **7** (2008) 3490 (https://doi.org/10.1158/1535-7163.MCT-08-0826)
11. B. E. Sleebs, G. Nikolakopoulos, I. P. Street, H. Falk, J. B. Baell, *Bioorg. Med. Chem. Lett.* **21** (2011) 5992 (https://doi.org/10.1016/j.bmcl.2011.07.050)
12. Y. Yin, K. Zheng, N. Eid, S. Howard, J.-H. Jeong, F. Yi, J. Guo, C. M. Park, M. Bibian, W. Wu, *J. Med. Chem.* **58** (2015) 1846 (https://doi.org/10.1021/jm501680m)
13. M. D. Charles, J. L. Brookfield, T. C. Ekwuru, M. Stockley, J. Dunn, M. Riddick, T. Hammonds, E. Trivier, G. Greenland, A. C. Wong, *J. Med. Chem.* **58** (2015) 8309 (https://doi.org/10.1021/acs.jmedchem.5b01242)
14. K. Mardilovich, M. Baugh, D. Crighton, D. Kowalczyk, M. Gabrielsen, J. Munro, D. R. Croft, F. Lourenco, D. James, G. Kalna, *Oncotarget* **6** (2015) 38469 (https://doi.org/10.18632/oncotarget.6288)
15. M. Zhang, J. Tian, R. Wang, M. Song, R. Zhao, H. Chen, K. Liu, J.-H. Shim, F. Zhu, Z. Dong, *Front. Cell Dev. Biol.* (2020) 1361 (https://doi.org/10.3389/fcell.2020.556532)
16. X. Xu, B. Xu, X. Wang, & J. Li, *J. Mol. Struct.* **1201** (2020) 127128 (https://doi.org/10.1016/j.molstruc.2019.127128)
17. M. Sari-Hassoun, M.-J. Clement, I. Hamdi, G. Bollot, C. Bauvais, V. Joshi, F. Toma, A. Burgo, M. Cailleret, M. C. Rosales-Hernández, *Biochem. Pharmacol.* **102** (2016) 45 (https://doi.org/10.1016/j.bcp.2015.12.013)
18. A. Daina, O. Michielin, V. Zoete, *Sci. Rep.* **7** (2017) 1 (https://doi.org/10.1038/srep42717)
19. W. J. Egan, K. M. Merz, J. J. Baldwin, *J. Med. Chem.* **43** (2000) 3867 (https://doi.org/10.1021/jm000292e).

Journal of the Serbian Chemical Society
JSCS-info@shd.org.rs • www.shd.org.rs/JSCS
J. Serb. Chem. Soc. *87* (12) 1395–1407 (2022)
JSCS–5602
Original scientific paper
Published 18 November 2022

Ammonia removal by natural and modified clinoptilolite

AYTAÇ GÜNAL[1] and BURCU ERDOĞAN[2]*

[1]*Eskisehir Technical University, Graduate School of Sciences, Yunusemre Campus, 26470 Tepebasi, Eskisehir, Turkey and* [2]*Eskisehir Technical University, Faculty of Science, Department of Physics, Yunusemre Campus, 26470 Tepebasi, Eskisehir, Turkey*

(Received 10 November 2021, revised 30 May, accepted 11 June 2022)

Abstract: In this study, cation exchange and acid activation processes were applied to determine the effects of different cationic compositions of clinoptilolite on ammonia adsorption properties. Thermogravimetric (TG), differential thermal analysis (DTA), X-ray diffraction (XRD), X-ray fluorescence (XRF) and nitrogen adsorption techniques were used for the characterization of the clinoptilolite samples. As a result of ion exchange and acid activation, the amount, type and location of exchangeable cations in the structure significantly affected the thermal properties, as well as NH_3 removal efficiency. Ammonia adsorption isotherms were obtained at 298 K up to 100 kPa volumetrically. In addition, NH_3 adsorption capacities of the clinoptilolite samples within this study (3.823 to 5.372 mmol g^{-1}) were compared with those of the other materials (1.77 to 12.2 mmol g^{-1}) in terms of their textural and structural differences.

Keywords: activation; adsorption;zeolite; DTA; TG; XRF; XRD.

INTRODUCTION

Ammonia is a colorless, corrosive and pungent gas and is the most abundant alkaline component in the atmosphere. It is estimated that about 60 % of global ammonia emissions come from anthropogenic sources such as metabolic, agricultural and industrial processes. On the other hand, oceans, crops and biomass burning are also important.[1] Ammonia gas is irritating to throat, the skin, the eyes, nose and lungs. At high concentrations (1700 ppm) the gas causes extensive injuries and <30 min exposure may be fatal.[1,2] Studies related to experimental animals similarly show that exposure to high levels may adversely affect the respiratory system, the liver and spleen.[3] In addition, ammonia, one of the major environmental pollutants in water, is highly poisonous to fish and the toxicity is associated with the concentration of unionized ammonia (NH_3) which is dependent on the water pH value.[4]

* Corresponding author. E-mail: burcuerdogan@eskisehir.edu.tr
https://doi.org/10.2298/JSC211110051G

Atmospheric ammonia is a major aerial pollutant of poultry houses.[5] It has been reported that NH_3 concentrations are 5–20 ppm in the ventilation air of poultry and cattle houses and can reach up to 200 ppm during periods of low ventilation.[6] NH_3 should be removed from the environment as it can be hazardous to bird development and worker health.[7,8] There are many techniques such as catalytic decomposition and staged combustion processes in order to eliminate the ammonia emissions. In addition to these methods, NH_3 removal using natural zeolite is an alternative method due to its low cost, abundance and gas adsorption properties, which can be adjusted by cation exchange.

Zeolites are porous, crystalline, hydrated aluminosilicates containing alkali and alkaline earth cations. The zeolite framework has channels and interconnected voids and cavities occupied by the cations and water molecules.[9,10] Clinoptilolite is one of the most widely used natural zeolites. It contains three different channels. Channels A (10-membered ring, 0.44 nm×0.72 nm) and B (8-membered ring, 0.41 nm×0.47 nm) are parallel to each other and the c-axis, while the channels C (8-membered ring, 0.40 nm×0.55 nm) lies along *a*-axis, intersecting both channels A and B.[11] Within the clinoptilolite structure, Na^+ and Ca^{2+} are most efficient channel blockers and may occupy sites which are at the intersections of channels A/B with channel C, whilst the K^+ and Mg^{2+} have little effect on intersecting channels and reside in the centers of the C and A channels, respectively.[12–14] The high thermal and chemical stability and high internal surface area of this zeolite make it advantageous in removing hazardous gases.

Most of the studies on NH_3 removal have focused on 4A, 5A, 13X, faujasite, pentasil, ordered mesoporous carbon, activated alumina, alumina 1597, Cu-MOF-74, activated carbon and natural mordenite type materials.[15–22] Although studies on adsorption of ammonia by the natural clinoptilolite can be found in literature,[21,23–25] comparative studies on the effect of cation exchange and hydrochloric acid activation methods on thermal behavior and removal of ammonia gas by clinoptilolite have not been extensively performed. The novelty of this study is the detailed comparison of ammonia adsorption properties of both cation-exchanged and acid-modified forms of clinoptilolite type natural zeolite. Because the natural zeolites generally show low selectivity for NH_3, different methods should be used to increase this selectivity. The difference in the cation content of the mineral is one of the important factors that significantly affect the thermal properties of clinoptilolite and its affinity for polar gases, and thus its adsorption capacity. Therefore, the aim of this study is to examine natural and modified clinoptilolite samples in terms of chemical composition, thermal, structural and NH_3 adsorption properties.

EXPERIMENTAL

After grinding and sieving, the fraction below 63 μm of the natural clinoptilolite (CLN) from Gördes was used. The CLN label identifies a natural sample that has been free from any

chemical treatment. Five grams of each zeolite were exchanged by refluxing with 100 mL of 1.0 M $Ca(NO_3)_2$, $Mg(NO_3)_2$, $NaNO_3$ and KNO_3 solutions at 90 °C for 5 h. Prepared zeolites were labeled as X-CLN, which the X indicate the type of exchanged cation. Acid activations were carried out using a 0.1 M and 1.0 M HCl solutions at the same experimental condition. The samples were named as 01H-CLN and 1H-CLN, respectively. Then, the suspensions were filtered, washed several times with de-ionized water at approximately boiling point and then the samples were dried in an oven at 110 °C for 20 h. The dried clinoptilolites were stored in a desiccator. All chemicals were supplied by Merck Company.

Chemical compositions were evaluated on powdered samples fused with lithium tetraborate using XRF analysis (Rigaku ZSX Primus instrument). Loss on ignition (*LOI*) was determined from the mass loss after heating samples to 1000 °C for 2 h. The crystal structure of the original and modified forms was determined by powder XRD technique using a D8 Advance Bruker instrument, with CuK_α radiation at 40 kV and 30 mA, in the range of 2θ values 5–40° and step range of 0.02° at room temperature. DTA and TG measurements were performed in the Setsys Evolution Setaram device at heating rate 10 °C min^{-1} in the temperature range of 30–1000 °C. In each run, *ca*. 35 mg of sample was loaded into the alumina pan. N_2 adsorption isotherm measured at 77 K using Autosorb 1, Quantachrome. Specific surface areas were determined by BET equation using the adsorption branch of the isotherms using the 0.05 to 0.35 P/P_0 range and the micropore data were calculated by applying the *t*-plot method. Ammonia adsorption isotherms of these zeolites were obtained at 298 K using the 3Flex-Micromeritics instrument. In each run, *ca*. 250 mg of clinoptilolite sample was loaded into the sample cell. The gases (N_2 and NH_3) used were highly pure (>99 %). Prior to gas adsorption measurements, all zeolite samples were degassed at 300 °C for 10 h.

RESULTS AND DISCUSSION

Chemical composition

The chemical compositions of the clinoptilolite samples are given in Table I. The water content of samples was estimated by the loss on ignition technique. Table I shows that the main cations found in CLN sample are potassium and calcium. In addition, iron is also present as an impurity. It was found that there was an increase in the amount of the exchangeable cations depending on the chosen salt solution compared to the raw sample, as expected.

TABLE I. Chemical composition of the clinoptilolite samples (wt. %)

Sample	Component							*LOI*
	SiO_2	Al_2O_3	Fe_2O_3	MgO	CaO	Na_2O	K_2O	%
CLN	70.823	12.850	1.249	0.619	2.241	0.561	5.171	6.332
Na-CLN	71.178	12.809	1.178	0.383	0.471	3.490	3.686	6.430
K-CLN	70.465	12.740	1.118	0.393	0.176	0.185	9.855	5.078
01H-CLN	73.501	12.138	1.375	0.560	1.466	–	4.770	6.192
1H-CLN	81.284	8.219	1.175	0.351	0.378	–	2.314	6.150
Ca-CLN	70.836	12.631	1.271	0.506	3.762	–	3.316	7.595
Mg-CLN	70.641	12.641	1.285	2.012	1.433	0.281	3.638	8.070

After the clinoptilolite activated with hydrochloric acid solutions, aluminum and the exchangeable cations were removed from the material. On the other

hand, it was determined that the SiO_2 content increased with increasing acid molarity due to its insolubility. SiO_2/Al_2O_3 ratio for CLN sample increased from 5.5 to 6.0 and 9.9 in the 01H-CLN and 1H-CLN, respectively, indicating the gradual removal of aluminum from the structure (Table I).

X-Ray analysis

Powder XRD patterns of all the clinoptilolite samples are shown in Fig. 1. In addition to the main clinoptilolite (characteristic peaks at 2θ 9.83, 15.90, 22.4 and 30°) phase, minor amounts of illite, feldspar and opal CT were also identified.

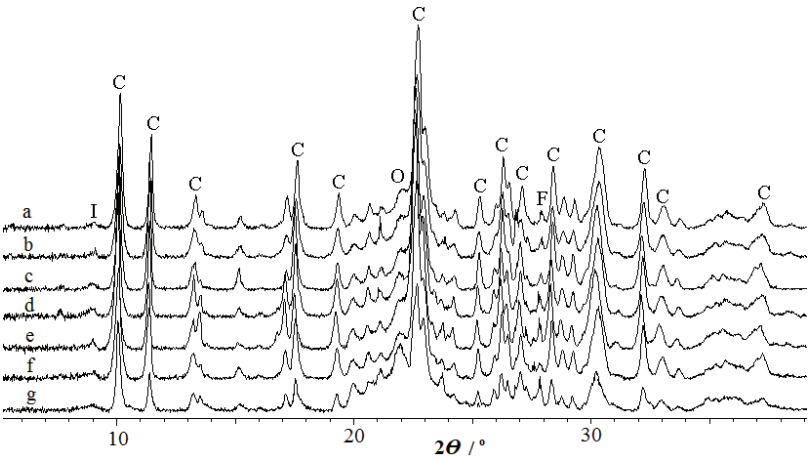

Fig. 1. X-ray powder diffraction patterns of the CLN (a), Na-CLN (b), K-CLN (c), Ca-CLN (d), Mg-CLN (e), 01H-CLN (f) and 1H-CLN (g) samples (C: clinoptilolite, I: illite, O: opal-CT, F: feldspar).

The quantitative XRD analysis demonstrated that the major component of the natural sample (CLN) is clinoptilolite (80 %), with minor amounts of opal A (4–5 %), opal-CT (4–5 %), smectite (1–2 %), mica-illite (1–2 %) and feldspar (6–7 %). The method given by Esenli and Sirkecioğlu[26] was used to determine the mineral ratio. It was determined that there was no significant change in the intensity of major clinoptilolite peaks in the clinoptilolite samples modified with different salt solutions. As a result of the dealumination (Table I) and partial destruction of the crystal structure, the intensity of the main clinoptilolite peaks for 1H-CLN decreased gradually. In addition, as the acid concentration increased, the crystallinity of the sample decreased and there is a broad hump in between 20–30° (2θ) on the patterns of the acid activated samples (Fig. 1g). Similar changes were obtained in previous studies on the activation of clinoptilolite with acid solutions.[27,28]

Nitrogen adsorption

N_2 adsorption isotherms of the samples are presented in Figs. 2 and 3 (relative pressure P/P_0 *vs*. adsorbed volume in cm^3 STP per g of clinoptilolite). All clinoptilolite samples show type-II isotherms.[29] The values of the specific surface areas and, micropore data of the samples are presented in Table II. It was determined that the specific surface areas of cation exchanged clinoptilolite samples increased slightly. Whilst it was found that 1.0 M HCl treatment (203 m^2 g^{-1}) caused about 5 times increase in specific surface area of CLN (42 m^2 g^{-1}). This result agrees well with the X-ray diffraction data (Fig. 1). As seen from Table I, the increase in the micropore areas and micropore volumes for acid activated (01H-CLN and 1H-CLN) samples is obviously due to the unblocking of the channels of the clinoptilolite through decationation and dealumination and the formation of secondary porosity owing to the dissolution of the free linkages.

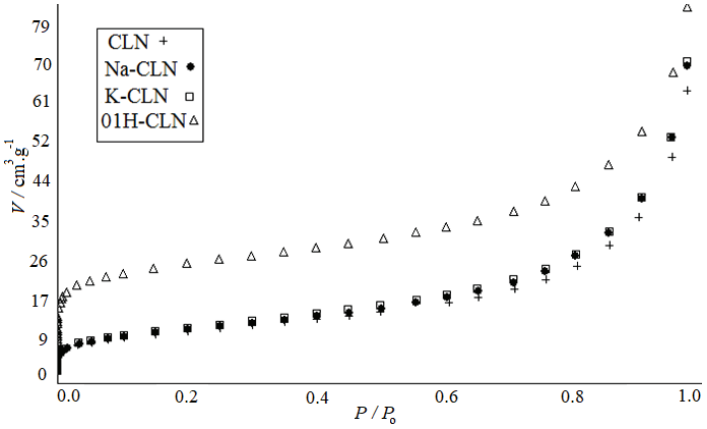

Fig. 2. Nitrogen adsorption isotherms of CLN, Na-CLN, K-CLN and 01H-CLN samples.

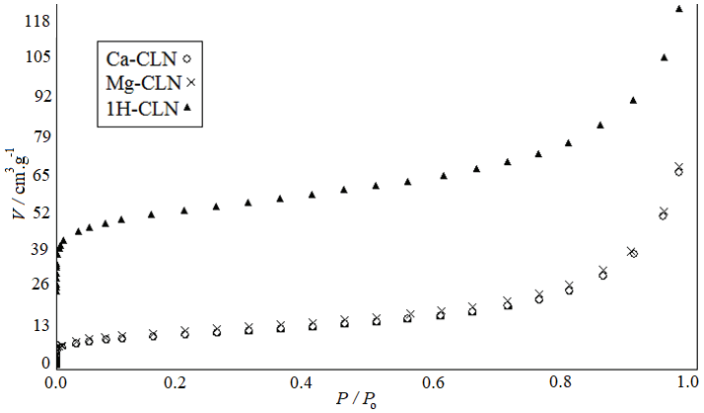

Fig. 3. Nitrogen adsorption isotherms of Ca-CLN, Mg-CLN and 1H-CLN samples.

TABLE II. Nitrogen adsorption data of the natural and modified clinoptilolite samples

Sample	Surface area, $m^2 g^{-1}$		Volume, $cm^3 g^{-1}$	
	BET	Micropore	Micropore	Total pore
CLN	42	10.0	0.004	0.100
Na-CLN	43	8.5	0.003	0.109
K-CLN	44	6.5	0.003	0.110
01H-CLN	97	54.6	0.023	0.129
1H-CLN	203	135.1	0.056	0.193
Ca-CLN	44	12.1	0.005	0.105
Mg-CLN	48	11.5	0.006	0.109

Thermal analysis (TG-DTA)

The DTA and TG curves of the clinoptilolite samples over the temperature range 30–1000 °C are shown in Fig. 4. DTA curves of clinoptilolite samples

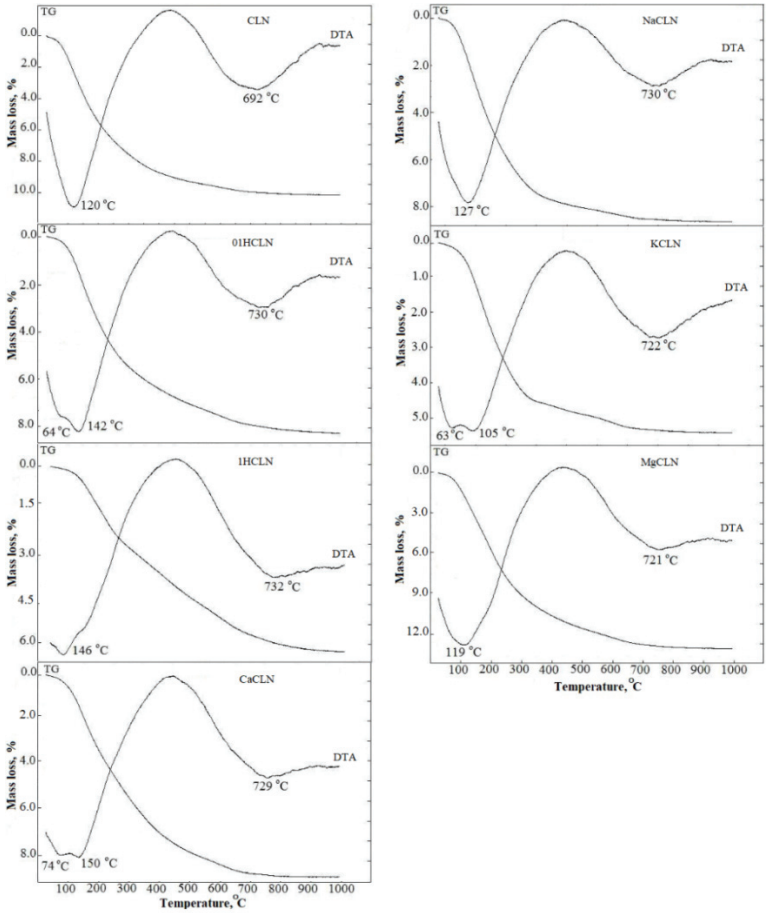

Fig. 4. TG-DTA curves of all clinoptilolite samples.

show the endotherms at temperature ranging from 63–74 °C and 120–150 °C between 30 and 200 °C as a result of the dehydration process. Third endothermic peaks at 692 to 732 °C in the temperature interval from 600 to 800 °C are due to the dehydroxylation. TG curves display the major mass losses (1.61 to 5.55 %) owing to the loss of the water located in the cavities and bound to the nonframework cations. In the temperature range between 200 and 600 °C more strongly associated water (2.79 to 6.46 %) is eliminated. In the temperature range from 600 to 800 °C, the rest of the water (0.28 to 0.70 %) is gradually removed. As seen in Fig. 4, clinoptilolite samples showed continuous mass loss curves and the mass losses are constant at temperatures above 800 °C.

For the cation exchanged samples, the mass losses recorded by TG analysis increased in the order of K-CLN < Na-CLN < Ca-CLN < Mg-CLN (Table III). The thermal behaviour of the clinoptilolite depends on many parameters such as the type of the exchangeable cations, their coordination to water molecules and their hydration energies.[30] It was found that the mass loss values were higher in clinoptilolites exchanged with divalent cations (Mg^{2+} and Ca^{2+}) with the high-hydration energies than those of exchanged with monovalent cations (K^+ and Na^+) with low-hydration energies. Moreover, for monovalent and divalent cations, less zeolite water loss of samples exchanged with larger sized cations can be attributed to the smaller space remaining in the zeolite structure.

TABLE III. Mass loss (%) of the natural and modified clinoptilolite samples at different temperature ranges

Sample	Temperature range, °C					Total
	30–200	200–400	400–600	600–800	800–1000	
CLN	5.50	3.23	0.92	0.42	0.09	10.17
Na-CLN	4.66	3.22	0.58	0.31	0.05	8.82
K-CLN	2.53	2.29	0.50	0.28	0.03	5.63
01H-CLN	3.64	2.75	1.08	0.54	0.13	8.14
1H-CLN	1.61	2.11	1.50	0.85	0.21	6.28
Ca-CLN	4.66	3.22	0.59	0.31	0.05	8.83
Mg-CLN	5.55	4.85	1.61	0.70	0.11	12.82

In the case of acid activated forms, the mass losses for the acid-treated clinoptilolites (6.28 and 8.14 %) are lower than that for the CLN (10.17 %). This can be explained by the elimination of the exchangeable cations and the dealumination (Table I).

Adsorption of NH_3

The ammonia adsorption isotherms of the raw, cation exchanged and acid activated variants were measured at 298 K (Figs. 5 and 6). All the isotherms are of type I.[29] The adsorption rate of ammonia on all samples decreased in the

order: Mg-CLN > Ca-CLN > Na-CLN > 01H-CLN > CLN > 1H-CLN > K-CLN (Table IV).

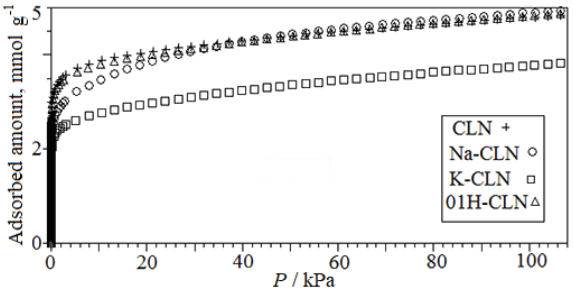

Fig. 5. Ammonia adsorption isotherms of CLN, Na-CLN, K-CLN and 01H-CLN samples at 298 K.

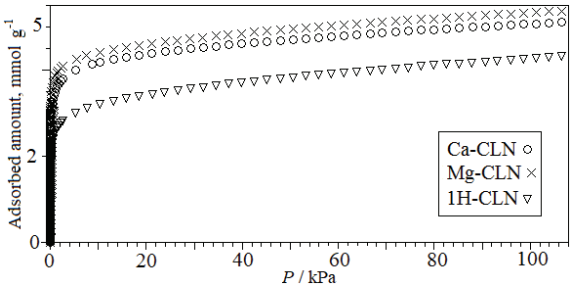

Fig. 6. Ammonia adsorption isotherms of Ca-CLN, Mg-CLN and 1H-CLN samples at 298 K.

TABLE IV. Ammonia uptake for various materials

Sample	Temperature, K	Adsorption capacity, mmol g^{-1}	Reference
CLN	298	4.840	Present work
Na-CLN	298	4.947	Present work
K-CLN	298	3.823	Present work
01H-CLN	298	4.875	Present work
1H-CLN	298	4.312	Present work
Ca-CLN	298	5.159	Present work
Mg-CLN	298	5.372	Present work
Alumina 1597	298	3.008	15
Silica gel 40	298	6.250	15
Clinoptilolite	298	5.904	15
13X	298	9.326	15
Pentasil dealuminated	298	2.34	15
Faujasite dealuminated	298	1.77	15
Activated carbon	298	4.19	15
Zs	295	6.30 mg g^{-1}	23
Mesoporous carbon	298	6.39	17
Activated alumina	298	2.53	18

TABLE IV. Continued

Sample	Temperature, K	Adsorption capacity, mmol g^{-1}	Reference
Natural clinoptilolite from Nizny Hrabovec	298	0.705	25
Natural clinoptilolite from Nizny Hrabovec	293	0.634	33
Natural clinoptilolite from Nizny Hrabovec	293	1.268	33
Natural clinoptilolite from Nizny Hrabovec treated with 30 % H_2SO_4	293	1.174	33
Natural clinoptilolite from Nizny Hrabovec treated with 30 % H_3PO_4	293	1.121	33
Natural clinoptilolite from Nizny Hrabovec treated with 30 % HNO_3	293	1.121	33
Cu-MOF-74	298	3.4	32
4A zeolite	298	8.71	15
In-PMOF	298	9.41	31
MOF-177	298	12.2	19

Due to the fact that the kinetic diameter of the ammonia molecule is 0.26 nm, it can penetrate into the zeolite channels of clinoptilolite. As can be seen from Figs. 5 and 6, the maximal sorption capacity of ammonia is exhibited by Mg-CLN sample (5.372 mmol g^{-1}) and minimal by K-CLN (3.823 mmol g^{-1}). Obviously, the gas adsorption on zeolites depends on many parameters such as their structure, size and distribution of the exchangeable cations within their channels, and features of the adsorbate (size, geometry and polarity, etc.). Na^+ and Ca^{2+} located at the intersections of the A/B channels with the C channel in the clinoptilolite structure are the most effective channel blockers, while the K^+ and Mg^{2+} cations have little effect on intersecting channels and they are located in the centers of the C and A channels, respectively.[12–14]

Hence, limited access to channels and consequent lower ammonia uptake of Na-CLN and Ca-CLN samples compared to Mg-CLN sample are due to the increased amount of Na^+ and Ca^{2+} in the channel A and B, respectively and continued presence of K^+ (Table I). In the Mg-CLN sample with the highest ammonia adsorption capacity, the location of this small cation in channel A caused more space between channels and increased NH_3 gas uptake. The lowest ammonia adsorption capacity for K-CLN can be attributed to its size (largest) and the location of the K^+ in the channel C. For this reason, it appears that the location of the exchangeable cations has a greater influence on adsorption capacity than the amount or size of the cations.

The wide variation in the adsorption capacity of ammonia gas for the cation exchanged clinoptilolites indicates that both electrostatic forces and dispersion forces played an active role in the adsorption dynamics of the adsorbents studied.

In addition, the high affinity for NH_3 can be attributed to the specific interactions of the permanent dipole moment (1.47 D*) of NH_3 molecule with the electric field created by the cations in the zeolite structure. 01-HCLN sample (4.875 mmol g^{-1}) exhibited a lower adsorption capacity than the Mg-CLN sample due to the removal of the cations from the structure and thus a decrease in the local electric field. Although 1H-CLN had the highest specific surface area (203 m^2 g^{-1}), its NH_3 uptake (4.312 mmol g^{-1}) was lower than those of CLN (4.840 mmol g^{-1}) and 01-HCLN (4.875 mmol g^{-1}) owing to the partial destruction of the crystal structure as presented by XRD data (Fig. 1) and XRF analysis (Table I).

When the ammonia adsorption capacities of all samples were compared, the adsorption capacity of raw clinoptilolite (CLN) was somewhere in between. This can be attributed to the mixed cationic (*i.e.*, Na^+, K^+ and Ca^{2+}) content of the CLN sample and partial blockages in the channel structure that allow less passage of the NH_3 molecule through the channels. CLN sample (4.840 mmol g^{-1}) adsorbed less ammonia gas than clinoptilolite from Mud Hills, USA (5.904 mmol g^{-1})[15] due to its different origin and mineral content. As seen from Table IV, retention of ammonia gas by Mg-CLN sample (5.372 mmol g^{-1}) were smaller than MOF-177 (12.2 mmol g^{-1}),[19] In-PMOF (9.41 mmol g^{-1}),[31] silica gel 40 (6.250 mmol g^{-1}),[15] 13X (9.326 mmol g^{-1}),[15] mesoporous carbon (6.39 mmol g^{-1})[17], 4A zeolite (8.71 mmol g^{-1})[15] but were higher than those of alumina 1597 (3.008 mmol g^{-1}),[15] faujasite dealuminated (1.77 mmol g^{-1})[15], pentasil dealuminated (2.34 mmol g^{-1}),[15] activated carbon (4.19 mmol g^{-1}),[15] Cu-MOF-74 (3.4 mmol g^{-1})[32] and natural clinoptilolite (from Nizny, Hrabovec) treated with 30 % H_2SO_4 (1.268 mmol g^{-1})[33]. It should be noted here that the structural and textural properties of all these synthetic materials are different from the sample of the present article. Although natural zeolites contain high levels of major mineral components, they often contain impurities in their structure. In addition, due to their uniform and tunable nature, synthetic zeolites generally show higher gas adsorption capacities than natural zeolites, but have the disadvantage of being more expensive than natural ones.

The abundance and high sorption capacity of the clinoptilolite-type natural zeolite provide low-cost and eco-friendly solutions. For this reason, the Mg-CLN sample with the highest capacity can be proposed as an effective adsorbent in environments where ammonia gas needs to be removed, such as poultry houses.

CONCLUSION

Our paper presents a novel view of discussion on the effect of cation content on the thermal and ammonia adsorption properties of clinoptilolite-rich tuff. The following conclusions can be drawn from the obtained results of this study.

* 1 D = 3.34×10^{-30} C m

1. XRF data show that significant changes occurred in the cation content of the clinoptilolite following both cation exchange and acid treatment. In addition, the thermal behavior of the clinoptilolite was affected by the dominant cation in the structure.

2. The powder XRD analysis demonstrated that treatment of clinoptilolite with 1.0 M HCl solutions at 90 °C for 5 h caused a partial destruction in structure and a significant decrease in ammonia adsorption capacity.

3. When using different cations for modification, the amount, size and location of the exchangeable cations in the zeolite structure were found to be more efficient than the extent of exchange in NH_3 adsorption. For the cation exchanged clinoptilolites, ammonia adsorption capacity decreased with the increasing cation radii.

4. Our study shows that Mg-CLN material exhibited the maximal ammonia adsorption capacity among all the clinoptilolite samples and thus this sample might be a good candidate for removing ammonia pollution from the environment.

Acknowledgements. This research was supported by the Anadolu University Commission of Scientific Research Project No. 1602F072. Special thanks to Prof. Dr. Matthias Thommes for his valuable insights and recommendations.

ИЗВОД

УКЛАЊАЊЕ NH_3 ПРИРОДНИМ И МОДИФИКОВАНИМ КЛИНОПТИЛОЛИТОМ

AYTAÇ GÜNAL[1] и BURCU ERDOĞAN[2]

[1]*Eskisehir Technical University, Graduate School of Sciences, Yunusemre Campus, 26470 Tepebasi, Eskisehir, Turkey и* [2]*Eskisehir Technical University, Faculty of Science, Department of Physics, Yunusemre Campus, 26470 Tepebasi, Eskisehir, Turkey*

Процеси катјонске измене и киселинске активације су коришћени да би се испитали ефекти различитих катјона у саставу клиноптилолита на адсорпцију амонијака. Термогравиметрија (TG), диференцијална термијска анализа (DTA), дифракција X-зрачења (XRD), флуоресценција X-зрачења (XRF) и адсорпција азота су технике коришћене за карактеризацију узорака клиноптилолита. Као резултат јонске измене и киселинске активације, количина, тип и положај измењених катјона у структури је значајно утицао на термалне особине као и на ефикасност уклањања NH_3. Адсорпционе изотерме за амонијак су добијене на 298 K и до 100 kPa волуметријски. Додатно, адсорпциони капацитети узорака клиноптилолита за NH_3 (3,823–5,372 mmol g^{-1}) су упоређени са адсорпционим капацитетима других материјала (1,77–12,2 mmol g^{-1}) ради утврђивања њихових текстуралних и стуктурних разлика.

(Примљено 10. новембра 2021, ревидирано 30. маја, прихваћено 11. јуна 2022)

REFERENCES

1. P. Carson, C. Mumford, *Hazardous Chemicals Handbook*. Butterworth-Heinemann, Oxford, 2002, pp. 276–279 (https://www.elsevier.com/books/hazardous-chemicals handbook/carson/978-0-7506-4888-2)

2. N. I. Sax, *Dangerous Properties of Industrial Materials*, Van Nostrand Reinhold, New York, 1984, p. 1251 (https://aiche.onlinelibrary.wiley.com/doi/abs/10.1002/aic.690260134)
3. *Toxicological Review of Ammonia Noncancer Inhalation: Executive Summary*, 2020 (https://cfpub.epa.gov/ncea/iris/iris_documents/documents/subst/0422_summary.pdf, Accessed 26 August 2021)
4. F. B. Eddy, in *Water/Air Transitions in Biology*, A. K. Mittal, F. B. Eddy, J. S. Datta Munshi, Eds., Science Publishers Inc, Enfield, NH, 1999, p. 281 (https://www.amazon.com/Water-Air-Transition-Biology-Mittal/dp/1578080592)
5. H. H. Kristensen, C. Wathes, *Worlds Poult. Sci. J.* **56** (2000) 235 (https://doi.org/10.1079/WPS20000018)
6. E. F. Wheeler, K. D. Casey, R. S. Gates, H. Xin, J. L. Zajaczkowski, P. A. Topper, Y. Liang, A. J. Pescatore, *Trans. ASABE* **49** (2006) 1495 (https://doi.org/10.13031/2013.22042)
7. D. M. Miles, S. L. Branton, B. D. Lott, *Poultry Sci.* **83** (2004) 1650 (https://doi.org/10.1093/ps/83.10.1650)
8. K. J. Donham, D. Cumro, S. Reynolds, *J. Agromed.* **8** (2002) 57 (https://doi.org/10.1300/J096v08n02_09)
9. D. W. Breck, *Zeolite Molecular Sieves*, Wiley, New York 1984 (https://books.google.com.tr/books/about/Zeolite_Molecular_Sieves.html?id=aY0vAQAAIAAJ&redir_esc=y)
10. G. Gottardi, E. Galli, *Natural zeolites*, Springer, Berlin, 1985 (https://link.springer.com/book/10.1007/978-3-642-46518-5)
11. M. W. Ackley, R. F. Giese, R. T. Yang, *Zeolites* **12** (1992) 780 (https://doi.org/10.1016/0144-2449(92)90050-Y)
12. K. Koyama, Y. Takeuchi, *Z. Krist.* **145** (1977) 216 (https://doi.org/10.1524/zkri.1977.145.3-4.216)
13. T. Armbruster, M. E. Gunter, in *Reviews in Mineralogy and Geochemistry, Natural Zeolites: Occurrences, Properties, Applications*, D. L. Bish, D. W. Ming, Eds. Mineralogical Society of America, Washington DC, 2001, p. 1 (https://pubs.geoscienceworld.org/msa/rimg/article-abstract/45/1/1/140719/Crystal-Structures-of-Natural-Zeolites?redirectedFrom=fulltext)
14. E. Kouvelos, K. Kesore, T. Steriotis, H. Grigoropoulou, D. Bouloubasi, N. Theophilou, S. Tzintzos, N. Kanelopoulos, *Micropor. Mesopor. Mater.* **99** (2007) 106 (https://doi.org/10.1016/j.micromeso.2006.07.036)
15. J. Helminen, J. Helenius, E. Paatero, I. Turunen, *J. Chem. Eng. Data* **46** (2001) 391 (https://doi.org/10.1021/je000273+)
16. L. Benco, D. Tunega, *Phys. Chem. Miner.* **36** (2009) 281 (https://doi.org/10.1007/s00269-008-0276-9)
17. D. Saha, S. Deng, *J. Colloid Interface Sci.* **345** (2010) 402 (https://doi.org/10.1016/j.jcis.2010.01.076)
18. D. Saha, S. Deng, *J. Chem. Eng. Data* **55** (2010) 5587 (https://doi.org/10.1021/je100405k)
19. D. Saha, S. Deng, *J. Colloid Interface Sci.* **348** (2010) 615 (https://doi.org/10.1016/j.jcis.2010.04.078)

20. D.T. Hayhurst, *Chem. Eng. Commun.* **4** (1980) 729 (https://doi.org/10.1080/0098644-8008935944)
21. D. Kallo, J. Papp, J. Valyon, *Zeolites* **2** (1982) 13 (https://doi.org/10.1016/S0144-2449(82)80034-1)
22. C. C. Huang, H. S. Li, C. H. Chen, *J. Hazar. Mater*. **159** (2008) 523 (https://doi.org/10.1016/j.jhazmat.2008.02.051)
23. H. Asilian, S. B. Mortazav, H. Kazemian, S. Phaghihzadeh, Sj. Shahtaheri, M. Salem, *Iran J. Public Health* **33** (2004) 45 (https://ijph.tums.ac.ir/index.php/ijph/article/view/1929)
24. D. Caputo, B. De Gennaro, B. Liguori, M. Pansini, C. Colella, *Stud. Surf. Sci. Catal*. **140** (2001) 121 (https://doi.org/10.1016/S0167-2991(01)80142-7)
25. K. Ciahotny, L. Melenova, H. Jirglova, O. Pachtova, M. Kocirık, M. Eic, *Adsorption* **12** (2006) 219 (https:// doi.org/ 10.1007/s10450-006-0148-x)
26. F. Esenli, A. Sirkecioğlu, *Clay Miner.* **40** (2005) 557 (https://doi.org/10.1180/0009855054040192)
27. G. E. Christidis, D. Moraeti, E. Keheyan, L. Akhalbedashvili, N. Kekelidze, R. Gevorkyan, H. Yeritsyan, H. Sargsyan, *Appl. Clay Sci*. **24** (2003) 79 (https://doi.org/10.1016/S0169-1317(03)00150-9)
28. Radosavljević-Mihajlović, V. Dondur, A. Daković, J. Lemic, M. Tomašević-Čanović, *J. Serb. Chem. Soc.* **69** (2004) 273 (https://doi.org/10.2298/JSC0404273R)
29. S. Lowell, J.E. Shields, M.A. Thomas, M. Thommes, *Characterization of porous solids and powders: surface area, pore size and density*, Springer, Amsterdam, 2006 (https://link.springer.com/book/10.1007/978-1-4020-2303-3)
30. D. L. Bish, in *Occurrence, properties and utilization of natural zeolites*, D. Kallo, H. S. Sherry, Eds., Akademiai Kiado, Budapest, 1988, p. 565 (https://books.google.com.tr/books/about/Occurrence_Properties_and_Utilization_of.html?id=e1LwAAAAMAAJ&redir_esc=y)
31. S. Moribe, Z. Chen, S. Alayoglu, Z. H. Syed, T. Islamoglu, O. K. Farha, *ACS Mater. Lett.* **1** (2019) 476 (https://doi.org/10.1021/acsmaterialslett.9b00307)
32. M. J. Katz, A.J. Howarth, P.Z. Moghadam, J.B. DeCoste, R.Q. Snurr, J. T. Hupp, O. K. Farha, *Dalton Trans.* **45** (2016) 4150 (https://doi.org/10.1039/C5DT03436A)
33. K. Ciahotny, L. Melenova, H. Jirglova, M. Boldis, M. Kocirik, in *Studies in Surface Science and Catalysis,* Vol. 142, R. Aiello, G. Giordano, F. Testa, Eds., Elsevier Science, Amsterdam, 2002, p. 1713 (https://doi.org/10.1016/S0167-2991(02)80344-5).

Journal of the Serbian Chemical Society
JSCS@tmf.bg.ac.rs • www.shd.org.rs/JSCS
J. Serb. Chem. Soc. *87* (12) 1409–1423 (2022)
JSCS–5603
Original scientific paper
Published 14 December 2022

Anticorrosion activity of 2-thiohydantoin–Shiff base derivatives for mild steel in 0.5 M HCl

PETAR B. STANIĆ[1], NATAŠA M. VUKIĆEVIĆ[2#], VESNA S. CVETKOVIĆ[2#], MIROSLAV M. PAVLOVIĆ[2#], SILVANA B. DIMITRIJEVIĆ[3], BILJANA ŠMIT[1*#] and MARIJA D. ŽIVKOVIĆ[4**#]

[1]*Institute for Information Technologies Kragujevac, University of Kragujevac, Jovana Cvijića bb, 34000 Kragujevac, Serbia,* [2]*Institute of Chemistry, Technology and Metallurgy, University of Belgrade, Njegoševa 12, 11000 Belgrade, Serbia,* [3]*Mining and Metallurgy Institute Bor, Zeleni bulevar 35, 19210 Bor, Serbia and* [4]*Faculty of Medical Sciences, University of Kragujevac, Svetozara Markovića 69, 34000 Kragujevac, Serbia*

(Received 12 April, revised 12 July, accepted 24 August 2022)

Abstract: Several 2-thiohydantoin–Shiff base derivatives were prepared as eco-friendly corrosion inhibitors for mild steel in acid environment. Their anticorrosion properties were studied on mild steel in 0.5 M HCl solution as corrosion electrolyte by using usual gravimetric and different electrochemical techniques (weight loss measurement, potentiodynamic polarization and potentiostatic electrochemical impedance spectroscopy). Mild steel surface was characterized using two analytical techniques, scanning electron microscopy for surface morphology and elemental composition and atomic force microscopy. The study has shown that the inhibiting action of these environmentally benign inhibitors synthesized from inexpensive commercially available starting materials could be attributed to adsorption on the metal surface.

Keywords: inhibitiors; electrochemistry; surface; potentiodynamic polarization.

INTRODUCTION

As corrosion scourges the production of most industries globally, rising financial costs take their toll. According to a report from 2016, the cost of mitigating the effects of corrosion is estimated to US$ 2.5 trillion, which amounts to about 3.4 % of the global gross domestic product.[1] Mild steel (MS) is a widely used construction material employed in many industries due to its exemplary mechanical properties and substantially low cost. Despite of its attractive properties and uses, low corrosion resistance of mild steel in acidic solutions notably limits its applications.[2] Aggressive mineral acid solutions are often used in ind-

* Corresponding authors. E-mail: (*)biljana.smit@uni.kg.ac.rs; (**)mzivkovic@kg.ac.rs
# Serbian Chemical Society member.
https://doi.org/10.2298/JSC220412071S

ustrial processes which apply mild steel, most notably HCl for acidifying, pickling and industrial cleaning. Corrosion inhibitors are the most practical and profitable way of abating corrosion of metals in aqueous media.[3–7] Molecules with conjugated multiple bonds, aromatic groups and various atoms like oxygen, sulfur and nitrogen display good corrosion inhibiting activities since they are readily adsorbed on metal surfaces.[8] But, due to adverse effects on the environment, many of these compounds cannot be used.[9] Environmental awareness, as well as the ever-rising demand of industry necessitates the use of new, safe, environmentally friendly corrosion inhibitors.[10–16]

2-Thiohydantoins are derivatives of hydantoins in which a carbonyl group has been replaced with a thiocarbonyl group.[17] They are a class of mostly non-toxic, biologically active drug-based compounds with many applications in medicine and industry.[18] Hydantoin, 2-thiohydantoin and some of their derivatives have displayed some anticorrosion properties.[19–22] Schiff base molecules that contain the azomethine group have also been shown to exhibit anticorrosion activities.[23–26] Keeping this in mind, the aim of this study is to explore the corrosion behaviour of four 2-thiohydantoin–Schiff base derivatives, synthesized from inexpensive and commercially available substrates as budget- and eco-friendly corrosion inhibitors, using gravimetric, electrochemical and microscopic methods.

EXPERIMENTAL

Materials and methods

All substrates and reagents were obtained commercially and used without further purification. Solvents were refined by distillation and standard drying procedure before use. IR spectra were recorded on a Perkin-Elmer FT-IR spectrometer model Spectrum One. NMR spectra were recorded on a Varian Gemini 2000 NMR spectrometer in DMSO as the solvent.

*Synthesis of inhibitor compounds **1–4***

A mixture of aldehyde (0.01 mol) and thiosemicarbazide (0.01 mol) in methanol (30 ml) was refluxed for 3 h and then cooled. The formed precipitate was filtered off, dried, and purified by re-crystallization with hot methanol, yielding thiosemicarbazone. A mixture of thiosemicarbazone (0.01 mol), ethyl chloroacetate (0.01 mol) and anhydrous sodium acetate (0.03 mol) in methanol (50 mL) was refluxed for 6 h. The mixture was cooled and poured into cold water. The resulting precipitate was filtered off, washed with hot water, dried and re-crystallized with hot methanol. The 2-thiohydantoin derivatives are fully characterized by NMR and IR spectroscopy. Spectral data is given in the Supplementary material to this paper.

Preparation of corrosion solutions

The corrosive electrolyte used for electrochemical experiments was 0.5 M HCl, prepared from a 37 % HCl solution diluted with Milli-Q water. Four synthesized 2-thiohydantoin derivatives, compounds **1**–**4**, used in five different concentrations (0.05, 0.1; 0.5, 1.0 and 10 mM) were tested as corrosion inhibitors for MS. Fresh test solutions were prepared by dissolving compounds **1**–**4** in 0.5 M HCl prior to each experiment.

Electrochemical measurements

The electrochemical measurements were carried out in a three-electrode Pyrex glass cell, where a saturated calomel electrode (SCE), with a Luggin capillary placed close to the working electrode (WE) to compensate the ohmic drop, was used as a reference electrode. All reported potentials were referred to the SCE. The counter electrode was a Pt plate. Mild steel (MS), of chemical composition (mass %) expressed as: Fe with C (max. 0.17 %), P (0.045 %), S (0.045 %), N (0.009 %) was used as the WEs. The MS cylinders were embedded in epoxy resin, leaving a surface area of 1.3 cm^2 exposed to the corrosive acidic solution. Before each experiment WEs was mechanically abraded using silicon carbide paper (grade 600–1200), followed by washing with Milli-Q water in an ultrasonic bath for 5 min, whereupon it was thoroughly rinsed with absolute ethanol and deionized water and finally dried. All experiments were performed at room temperature and without stirring.

Before any electrochemical measurement, the WEs were immersed into the prepared electrolyte for 30 min until a relatively stable open circuit potential (E_{OCP}) was achieved. The typical OCP *vs.* time diagram is shown in Fig. 1; it can be observed that after 30 min of immersion, only negligible changes in the E_{OCP} are measured, showing that the steady-state is achieved after 30 min.

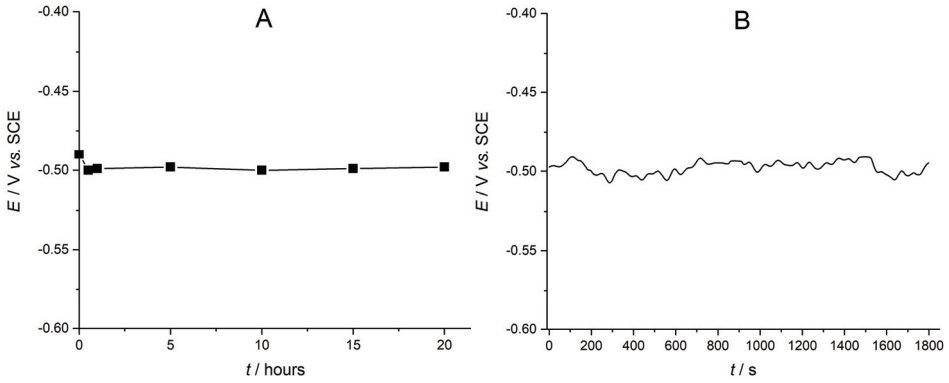

Fig. 1. Open circuit potential curves for MS corrosion in 0.5 M hydrochloric acid solution after 20 h (A) and 30 min (B) of immersion.

Potentiostat/galvanostat EG&G PAR 2631A, controlled by Power Suite software, was used for potentiodynamic polarization (PP) measurements. The PP curves were obtained by changing the potential between – 0.250 V and 0.250 V relative to the E_{OCP} with a scan rate of 1 mV s^{-1}.

Potentiostatic electrochemical impendance spectroscopy (PEIS) measurements were performed on potentiostat/galvanostat station BioLogic SAS SP-240 equipped with software for corrosion and physical electrochemistry. PEIS studies were carried out in the frequency range of 10^{-2}–10^6 Hz by using a 10 mV root mean square sinusoidal potential amplitude around open circuit readings (being in the range from –0.430 to –0.476 V) for all the samples. Randle's equivalent circuit was employed for fitting and analysis of the PEIS data using Zview® software.

Gravimetric measurements

MS weight loss test was performed in a 200 mL beaker with 100 mL of the test solution in the absence and the presence of different inhibitor concentrations. Before testing, MS cylinder samples were polished, thoroughly rinsed with absolute ethanol and deionized water, dried and weighted. Then, the samples were inserted in the test solutions for 24 h. All experiments were triplicated in order to reach a good reliability. Average weight loss in the absence and in the presence of inhibitor was reported.

Microscopic methods

The surface morphology characterization of the MS samples was performed using a scanning electron microscope (SEM) instrument (JOEL JSM-IT300LV operated at 20 keV) after 24 h of immersion in 0.5 M HCl solution in the absence and the presence of inhibitor. Chemical composition of the samples was determined using energy dispersive X-ray spectroscopy (EDS). The EDS spectra were recorded on the X-ray spectrometer (Oxford Instruments) attached to the SEM using Aztec software. Surface characteristics of the MS samples were performed using atomic force microscopy AFM NT-MDT Solver Pro instrument in contact mode.

RESULTS AND DISCUSSION

Synthesis of inhibitors

The inhibitors were synthesized according to a previously published procedure involving thiosemicarbazide.[27] The first part of the synthesis is the condensation of aromatic aldehydes and thiosemicarbazide into thiosemicarbazones, which then undergo cyclization with ethyl chloroacetate in the presence of anhydrous ethyl acetate to corresponding 2-thiohydantoin derivatives in good to excellent yields (Scheme 1).

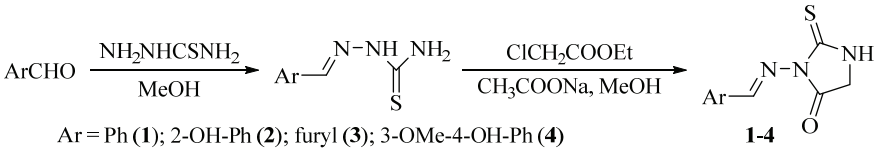

Ar = Ph (**1**); 2-OH-Ph (**2**); furyl (**3**); 3-OMe-4-OH-Ph (**4**) **1-4**

Scheme 1. Synthesis of 2-thiohydantoin–Schiff base derivatives.

Potentiodynamic polarization measurments

Potentiodynamic palarization (PP) curves for the electrochemical corrosion of MS in 0.5 M HCl without and with the inhibitors present in different concentrations are given in Fig. 2. As it can be seen from the Tafel plots, Fig. 2, the type of the polarization curves is almost the same in uninhibited and inhibited solutions. Anodic and cathodic Tafel slops have only slight change in their values, implying that the corrosion reaction of MS is kinetics-controlled and that the adsorbed inhibitor does not affect the primary mechanism.[28] According to the polarization measurements, the presence of the inhibitors does not cause any significant shift in E_{corr}, but the Tafel curves were moved towards lower current densities, indicating that inhibitors can reduce the MS anodic dissolution and slow

down the hydrogen ions reduction. It can be deduced that the corrosion rate of MS in 0.5 M HCl is decreased in the presence of inhibitors in the corrosive medium. The observed decrease in corrosion current density may be ascribed to the adsorption of an inhibitor onto the MS surface. The MS surface protection from acid dissolution can be explained by the adsorption of 2-thiohydantion derivative molecules (with high negative charge density at the hetero atom) which occupy the active sites on the metal surface, mainly composed of iron atoms with incomplete d shells.[19,21,29]

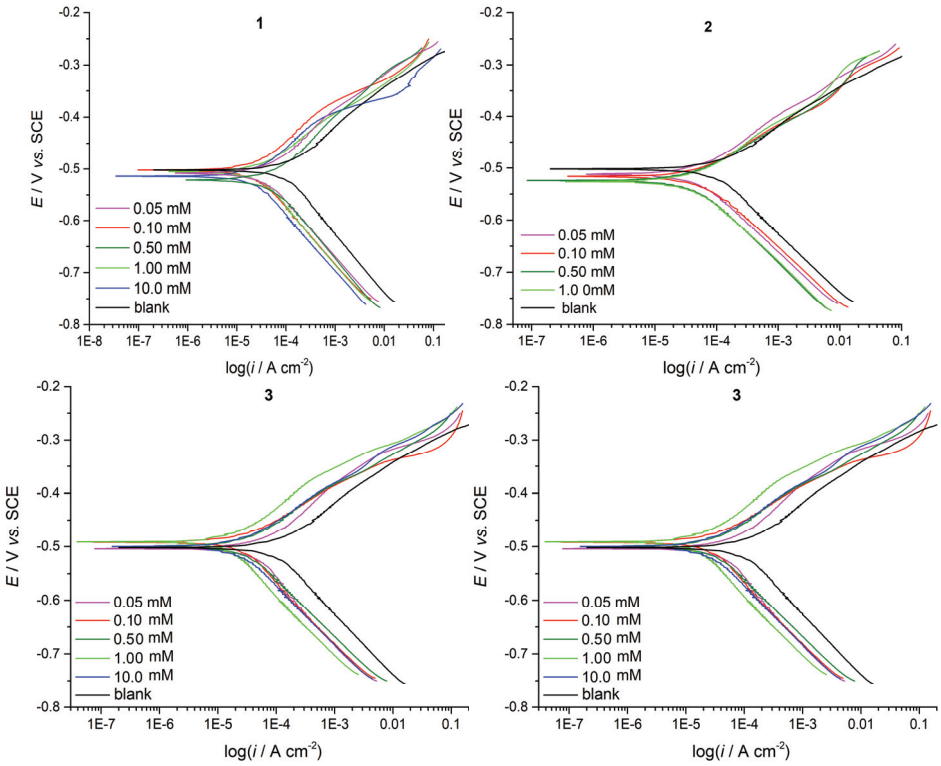

Fig. 2. The potentiodynamic polarization curves for MS in 0.5 M HCl solution in the absence and presence of inhibitor compounds **1**–**4**; v = 1 mV s^{-1}.

Tafel extrapolations of the linear section of the anodic and cathodic curves recorded were derived and the values of the electrochemical parameters, corrosion potential (E_{corr}), corrosion current densities (i_{corr}), anodic and cathodic Tafel slopes (β_a and β_c, respectively), are listed in Table I. The corrosion potential (E_{corr}) of MS exposed to the 0.5 M HCl is about –504 mV, while in the presence of the inhibitors, E_{corr} changes from –488 to –526 mV. Determination of the inhibitor type for any of the examined compounds depends on a difference

TABLE I. Electrochemical parameters derived from the potentiodynamic polarization curves obtained for MS in 0.5 M HCl solution without and with compounds **1**–**4** present in various concentrations

Medium	c_{inh} / mM	E_{corr} / mV *vs.* SCE	i_{corr} / μA cm^{-2}	β_a / mV dec^{-1}	β_c / mV dec^{-1}	η / %
Blank	–	–504	92	81	120	–
Compound **1**	0.05	–512	38	92	110	59
	0.1	–500	23	84	112	75
	0.5	–497	26	64	113	72
	1.0	–504	26	75	117	71
	10. 0	–515	21	82	105	77
Compound **2**	0.05	–515	45	92	107	51
	0.1	–514	46	74	102	50
	0.5	–521	39	74	111	58
	1.0	–526	39	84	107	58
Compound **3**	0.05	–505	45	95	141	51
	0.1	–488	23	65	113	75
	0.5	–500	23	104	73	74
	1.0	–494	17	80	115	82
	10. 0	–500	24	69	113	74
Compound **4**	0.05	–510	45	111	128	51
	0.1	–490	35	67	114	62
	0.5	–511	23	88	68	75
	1.0	–510	41	82	105	55
	10. 0	–513	47	76	102	49

recorded between E_{corr} (ΔE_{corr}) in the uninhibited and the inhibited solution.[21,29,30] If the difference ΔE_{corr} is greater than 85 mV, the inhibitor can be recognized as anodic or cathodic type, but if difference in ΔE_{corr} is lower than 85 mV, the inhibitors can be categorized as mixed type inhibitors. In our study, the shift ΔE_{corr} is less than 85 mV, indicating that the inhibition effect can be cathodic as well as anodic (mixed type inhibitors). This suggests that the presence of inhibitors in acid solutions used prevents the anodic metal dissolution reaction and controls the mechanism of cathodic hydrogen evolution at the same time. According to the PP curves recorded it can be assumed that compound **2** behaves as cathodic inhibitor reflected by decrease in the current density of the cathodic branch, and no significant effect in the anodic domain. Based on the PP curves obtained, the inhibition efficiency (η / %) was calculated by the equation:

$$\eta = 100\left(\frac{i^{0}_{corr} - i^{i}_{corr}}{i^{0}_{corr}}\right) \quad (1)$$

where: i^0_{corr} and i^i_{corr} are corrosion current density values recorded without and with the inhibitor present, respectively, and the results are presented in Table I. All inhibitors showed a substantial corrosion potential. The corrosion inhibition efficiency increases with increasing concentration of the 2-thiohydantoin deri-

vatives up to 1.0 mM, implying that the corrosion inhibition ability may be associated with the molecular structure of the inhibitor.

However, the additional increase in concentration up to 10.0 mM for compounds **3** and **4** resulted in the reduction of the inhibition efficiency. Recently, Alhaffar *et al.*[31] and Pavithra *et al.*[32] reported analogous behaviour of inhibitors in 1.0 M HCl and 0.5 M H_2SO_4. They assumed that after specific inhibitor quantity increments in solution, when optimum inhibitor concentration is achieved, no active sites remained for adsorption, because maximum surface coverage is accomplished, and the inhibitor molecules could not adsorb on the substrate. However, the corrosion still occurs, probably because the interactions among adsorbed and unadsorbed inhibitor molecules generate the desorption of molecules which results in reduced inhibition efficiency, with the additional increasing in concentration of inhibitors. For all studied inhibitors, the recorded corrosion inhibition is relatively stable at concentration around 0.5 mM, with the corrosion inhibition rate of ≈75 %. The mechanism of inhibition depends on the interaction between the inhibitor and the metal surface. It is known that organic corrosion inhibitors have at least one polar unit with heteroatoms (nitrogen, sulfur, oxygen and sometimes phosphorus) which is considered as the reaction centre for chemisorption processes. Additionally, the size, orientation, shape and electric charge on the inhibitor molecule determine the degree of adsorption and the inhibition effectiveness. Moreover, iron possesses great coordination affinity to heteroatom containing ligands. All these factors could explain the difference in the inhibiting action of the thiohydantoin-Schiff base derivatives. All compounds have four chelating sites (−NH, C=S, C=N and aromatic ring). The obtained results indicate that all compounds adhere to the chemisorption process through the adsorption on the MS surface established on the donor−acceptor interactions between the π electrons of donor atoms of the inhibitors and the vacant d orbitals of the ferric ion in the oxidized MS surface.[21,23] However, compound **3** exhibited the best performances with the inhibition rate of 82 %. This higher inhibitions efficiency might be attributed to the presence of an additional oxygen atom in the heteroaromatic ring, which contributed to better adsorbing.[20]

Potentiostatic electrochemical impendance spectroscopy

Potentiostatic electrochemical impendance spectroscopy (PEIS) was used for the estimation of the performance ability rate, characterization of the various corrosion processes and the study of the reaction mechanisms at the electrochemical interface. After PP studies, the best performing concentrations of all 2-thiohydantoin derivatives were used for further PEIS evaluation. Fig. 3 illustrates the Nyquist plots of the MS electrode in a 0.5 M HCl solution in the absence and the presence of different inhibitor (compounds **1**–**4**) concentrations. Since the potentiodynamic measurements showed that compound **2** has the smallest corrosion inhi-

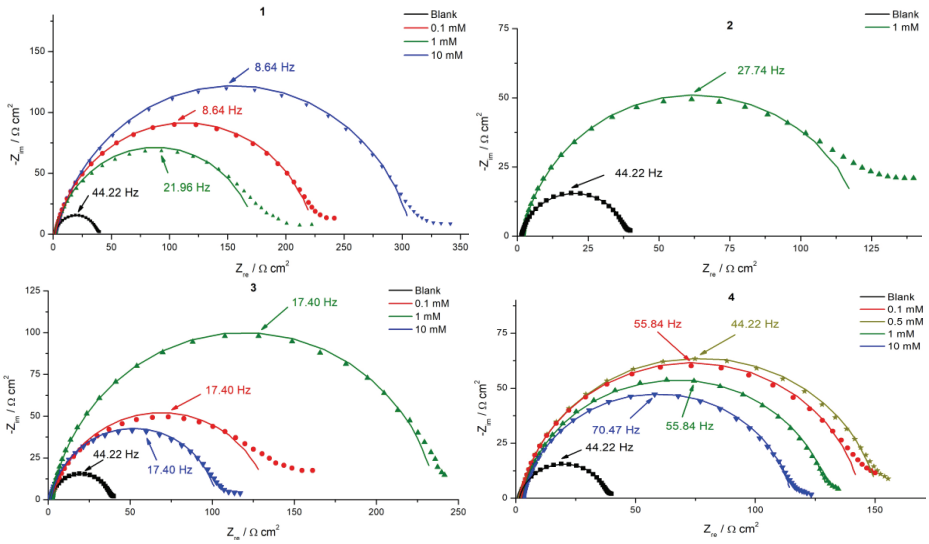

Fig. 3. Nyquist plots for MS electrode and different inhibitors compounds **1**–**4** at various concentrations with respect to blank 0.5 M HCl. Scattered dots represent experimental data, while solid lines represent calculated and fitted results.

bition efficiency among all tested, only the best performing concentration (1.0 mM, η = 58 %, Table I) was used for further PEIS evaluation. The presence of different inhibitors causes an increase in the capacitive loops, compared to the reference solution. Taking into consideration the shape of the impedance diagram, it can be said that their size depends on both structure and concentration of the inhibitor and that the Nyquist representations spectra consist of one single slightly depressed capacitive loop, showing that the charge transfer controls the corrosion reaction on an inhomogeneous and rough electrode surface.[33] Analysis of Nyquist plots reveals that the capacitive loops are depressed semicircles and not perfect semicircles, as expected from theory of PEIS, that accounts for frequency dispersion effect of a rough and inhomogeneous electrode surface, where the inhibitor molecular film is not acting as a perfect double layer capacitor. The results can be interpreted in terms of an equivalent circuit of the electrical double layer shown in Fig. 4. This equivalent circuit has been used to model the interface between iron and acid.[34] The double layer capacitance, C_{dl} was calculated using the following equation:[35,36]

$$C_{dl} = \left(\frac{1}{2\pi f \left(-Z''_{max} \right) R_{ct}} \right) \tag{2}$$

where: C_{dl} / F cm^{-2} is the double layer capacitance, $-Z''_{max}$ is the maximum imaginary component of the impedance, R_s / Ω cm^2 is the uncompensated solution resistance and R_{ct} / Ω cm^2 is the charge transfer resistance.

Fig. 4. Randle's equivalent circuit used for fitting of the PEIS curves.

The electrochemical data was evaluated using a Randle's equivalent circuit (Fig. 4) where R_s is the solution resistance, C_{dl} is the double layer capacitance and R_{ct} is the charge transfer resistance.[36,37]

The proposed equivalent circuit and the fitted results represent a good match, which is proved by very small chi-square values that are in the order of 10^{-3} for all the experimental data. All electrochemical impedance parameters are presented in Table II. As corrosion current (i_{corr}) is inversely related to R_{ct}, the inhibition efficiency, performance ability (η / %) can be determined by the following expression:[28,29]

$$\eta = 100\left(1 - \frac{R_{ct}^{0}}{R_{ct}}\right) \quad (3)$$

where: R_{ct}^0 and R_{ct} are the charge transfer resistances of uninhibited and inhibited solutions.

Data clearly shows that R_{ct} has an ascending trend, whereas C_{dl} has a descending trend at the whole concentration range. The decrease in C_{dl} values can be attributed to a decrease in local dielectric constant and, more likely, to an increase in the thickness of electrical double layer. This suggests that the inhibitor molecules inhibit the corrosion rate by adsorption at metal/solution interface.[38] The concentration of the inhibitor plays a crucial role, but it cannot be stated that for all the inhibitors there is a positive shift in the R_{ct} values with the increasing concentration. This shift in R_{ct} clearly shows the increasing inhibition efficiency and it may be attributed to the blocking of active sites of the metal surface by surface adsorption. The capacitance values showed a reduction due to decrease in the electric double layer, which is probably due to the replacement of water molecules, which have a higher dielectric constant, with inhibitor molecules possessing a lower dielectric constant, hence supporting the idea of surface adsorption of inhibitor molecules.[37] R_s refers to the solution resistance and its values increase noticeably only when compound **4** was used as an inhibitor.

The inhibitors were also analysed by Bode diagrams (Supplementary material, Fig. S-13). Bode diagrams of all inhibitor concentrations, as well as untreated MS electrode show phase shift that corresponds to the maximum of the

semi-circle presented in Nyquist diagram. This is typical behaviour for the process that is represented by Randle's equivalent circuit shown in Fig. 4. There is slight, but not significant, shift in the frequency for maximum phase shift, which could be due to different types of inhibitors, and not due to different mechanisms. The mechanism of corrosion inhibition is based on the adsorption of inhibitor on the MS electrode surface.

TABLE II. Electrochemical impedance parameters in absence and in the presence of inhibitors

Medium	c_{inh} / mM	R_s / Ω cm^2	R_{ct} / Ω cm^2	C_{dl} / μF cm^{-2}	η / %
Blank	–	2.86	82.3	987.2	–
Compound **1**	0.05	–	–	–	–
	0.1	2.31	433	38.2	81
	0.5	–	–	–	–
	1.0	2.64	343	49.4	76
	10. 0	2.19	748	31.4	89
Compound **2**	0.05	–	–	–	–
	0.1	–	–	–	–
	0.5	–	–	–	–
	1.0	3.01	187	118.4	56
	10. 0	–	–	–	–
Compound **3**	0.05	–	–	–	–
	0.1	2.75	329	47.6	75
	0.5	–	–	–	–
	1.0	2.87	633	34.8	87
	10. 0	3.14	211	98.1	61
Compound **4**	0.05	–	–	–	–
	0.1	2.56	294	55.8	72
	0.5	3.26	317	51.2	74
	1.0	3.55	257	66.9	68
	10. 0	2.98	305	76.5	63

Gravimetric measurements

Immersion test followed by the weight loss method is one of the cheapest, easiest, and most widely recognized strategies to explore and calculate the corrosion rate. The influence of varying concentrations of compound **3** on corrosion of MS in aggressive test solutions was studied by the weight loss method, and the obtained results of inhibition efficiencies and corrosion rates are presented in Table III. The inhibition efficiencies of compound **3** increase with its concentration, which may be ascribed to greater coverage of the metal surface with inhibitor molecules. From the weight loss, the corrosion rate (*CR*) and the inhibition efficiency (η / %) were estimated as:[33,39]

$$CR = \frac{w_I - w_F}{St} \quad (4)$$

where, w_I and w_F are the initial and the final weights (mg) of MS, S / cm^2 is the surface of the MS sample exposed to the test solution, and t / h is the immersion time.

$$\eta = 100\left(\frac{CR_0 - CR}{CR_0}\right) \quad (5)$$

where CR and CR_0 are the corrosion rates in the presence and the absence of compound **3**, respectively.

TABLE III. Corrosion parameters for MS sample after immersion for 24 h in 0.5 M HCl solution in the absence and presence of compound **3** at different concentrations.

Medium	c_{inh} / mM	CR / mg cm^{-2} h^{-1}	η / %
Blank	–	0.659	–
Compound **3**	0.1	0.268	59
	1.0	0.075	89
	10. 0	0.066	90

Surface study

Corrosion of the MS surface was characterized after immersion in 0.5 M HCl solution with and without inhibitor compound **3** using SEM/EDS technique. SEM was used for surface morphology while EDS provided data about the elemental composition. Fig. 5 illustrates SEM images of the uninhibited and the inhibited MS surfaces after immersion for 24 h in 0.5 M HCl solution. Surface of the MS sample directly exposed to free acid without the presence of inhibitors is severely damaged and rough with deep corrosion cracks and pits (Fig. 5A), while the surface of the sample submersed in the acid solution with the compound **3** at 1 mM was uniform, smoother and less corroded and cracked (Fig. 5B). The SEM surface analysis are in good agreement with corrosion metal evaluation and showed that the compound **3** has good inhibition properties and protects the MS surface from the effects of acid by the formation of the protective film on the metallic surface.[40]

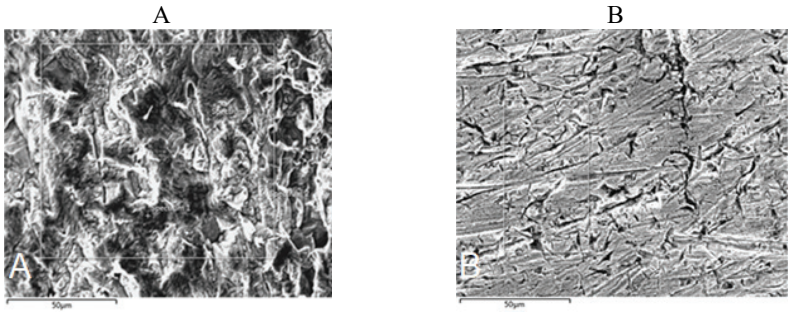

Fig. 5. SEM images of the MS sample without (A) and with inhibitor compound **3** at 1 mM (B).

EDS analysis of both MS samples (without and with the addition of compound **3**) was performed to record elemental compositions. EDS analysis of the MS samples without the inhibitor compound **3** showed the presence of high content of oxygen (9.67 %). On the other hand, EDS analysis of the sample immersed in the solution with the inhibitor compound **3** showed a significant influence of its presence on the corrosion of the sample, since the oxygen content was reduced to only 0.12 %, obviously due to the formation of thin protective layer of inhibitor molecules on the MS surface. This protective film was also responsible for the inhibition of corrosion.[41]

The 3D micrographs of MS surfaces acquired from AFM without and with the compound **3** are displayed in Fig. 6. Fig. 6A shows MS surface after immersion in 0.5 M HCl solution without the inhibitor with average roughness of 337 nm. It should be noted that the roughness parameters of the sample are much higher and that the peak heights of the roughness profile exceed the measuring range, so the sampling area where the heights are smaller and the surface is more uniform was selected for analysis. Fig. 6B shows MS surface immersed in the solution with the inhibitor compound **3** with the average roughness of 97.5 nm, suggesting good adsorption on the metal surface.

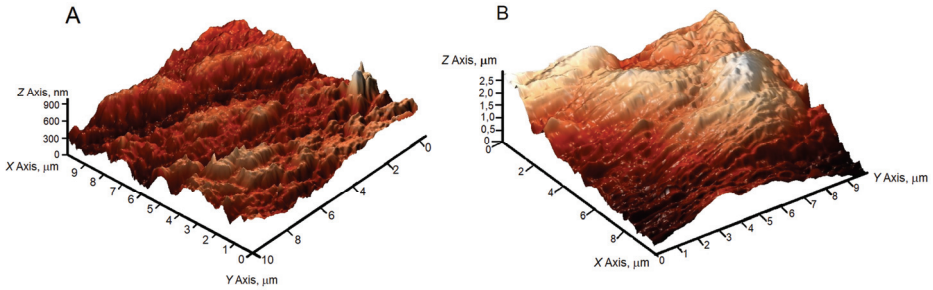

Fig. 6. AFM images of MS without (A) and with inhibitor compound **3** (B).

CONCLUSION

Four 2-thiohydantoin–Shiff base derivatives were synthesized as eco-friendly corrosion inhibitors and evaluated for their anti-corrosion performance for MS in 0.5 M HCl solution. The corrosion inhibition efficiency of all inhibitors increases with their concentration reaching a maximum value at 1.0 mM. The polarization curves reveal that the thiohydantoin derivatives act as mixed type inhibitors. The derivative with a heteroaryl furyl group, compound **3**, is the most effective inhibitor, exhibiting the inhibition efficiency in the range from 82–90 % depending on the method used. The changes in impedance parameters indicate the adsorption of inhibitors on the MS surface and thus formation of a protective film. SEM and AFM confirmed the presence of the inhibitor protective film on the MS surface. The present investigation has shown that these low cost and environment-

ally friendly inhibitors provide good protection for mild steel against corrosion in the acidic medium.

SUPPLEMENTARY MATERIAL

Additional data and information are available electronically at the pages of journal website: https://www.shd-pub.org.rs/index.php/JSCS/article/view/11776, or from the corresponding author on request.

Acknowledgement. The authors are grateful for financial support from The Ministry of Education, Science and Technological Development of Republic of Serbia (Agreement Nos: 451-03-68/2022-14/200378, 451-03-68/2022-14/200026 and 451-03-68/2022-14/200052).

ИЗВОД

АНТИКОРОЗИОНА АКТИВНОСТ ДЕРИВАТА ШИФОВИХ БАЗА 2-ТИОХИДАНТОИНА ЗА МЕКИ ЧЕЛИК У 0,5 M HCl

ПЕТАР Б. СТАНИЋ[1], НАТАША М. ВУКИЋЕВИЋ[2], ВЕСНА С. ЦВЕТКОВИЋ[2], МИРОСЛАВ М. ПАВЛОВИЋ[2], СИЛВАНА Б. ДИМИТРИЈЕВИЋ[3], БИЉАНА ШМИТ[1] и МАРИЈА Д. ЖИВКОВИЋ[4]

[1]Институт за информационе технологије Крагујевац, Универзитет у Крагујевцу, Јована Цвијића бб, 34000 Крагујвац, [2]Институт за хемију, технологију и металургију, Универзитет у Београду, Његошева 12, 11000 Београд, [3]Институт за рударство и металургију Бор, Зелени булевар 35, 19210 Бор и [4]Факултет медицинских наука, Универзитет у Крагујевцу, Светозара Марковића 69, 34000 Крагујевац

Неколико деривата Шифових база 2-тиохидантоина су направљени као еколошки прихватљиви инхибитори корозије меког челика у киселој средини. Њихова антикорозиона својства су испитана на меком челику у 0,5 M раствору HCl као корозионом електролиту, користећи уобичајене гравиметријске и различите електрохемијске технике (мерење губитка масе, потенциодинамичка поларизација, потенциостатска спектроскопија електрохемијске импеданције). Површина меког челика је окарактерисана двема аналитичким техникама, скенирајућом електронском микроскопијом за морфологију површине и елементарни састав и микроскопијом атомске силе. Студија је показала да се инхибиторно деловање ових еколошки бенигних инхибитора, синтетисаних из јефтиних комерцијално доступних полазних материјала, може приписати адсорпцији инхибитора на површини меког челика.

(Примљено 12. априла, ревидирано 12. јула, прихваћено 24. августа 2022)

REFERENCES

1. G. Koch, J. Varney, N. Thompson, O. Moghissi, M. Gould, J. Payer, *NACE Int.* (2016) (http://impact.nace.org/documents/Nace-International-Report.pdf)
2. D. Dwivedi, K. Lepková, T. Becker, *RSC Adv.* **7** (2017) 4580 (https://www.doi.org/10.1039/C6RA25094G)
3. T. J. Harvey, F. C. Walsh, A. H. Nahlé, *J. Mol. Liq.* **266** (2018) 160 (https://www.doi.org/10.1016/j.molliq.2018.06.014)
4. D. Douche, H. Elmsellem, E. H. Anouar, L. Guo, B. Hafez, B. Tüzün, A. El Louzi, K. Bougrin, K. Karrouchi, B. Himmi, *J. Mol. Liq.* **308** (2020) 113042 (https://www.doi.org/10.1016/j.molliq.2020.113042)
5. A. Y. Musa, A. A. H. Kadhum, M. S. Takriff, A. R. Daud, S. K. Kamarudin, N. Muhamad, *Corros. Eng. Sci. Technol.* **45** (2010) 163 (https://www.doi.org/10.1179/147842208X386359)

6. N. Errahmany, M. Rbaa, A. S. Abousalem, A. Tazouti, M. Galai, E. H. El Kafssaoui, M. E. Touhami, B. Lakhrissi, R. Touir, *J. Mol. Liq.* **312** (2020) 113413 (https://www.doi.org/10.1016/j.molliq.2020.113413)
7. E. Akbas, E. Yildiz, A. Erdogan, *J. Serb. Chem. Soc.* **85** (2020) 481 (https://www.doi.org/10.2298/JSC190326081A)
8. F. Bentiss, M. Lagrenée, *J. Mater. Environ. Sci.* **2** (2011) 13 (https://www.jmaterenvironsci.com/Document/vol2/3-JMES-62-2011-Bentiss2.pdf)
9. K. Tamalmani, H. Husin, *Appl. Sci.* **10** (2020) 3389 (https://www.doi.org/10.3390/APP10103389)
10. G. Gece, *Corros. Sci.* **53** (2011) 3873 (https://www.doi.org/10.1016/j.corsci.2011.08.006)
11. C. Verma, E. E. Ebenso, M. A. Quraishi, C. M. Hussain, *Mater. Adv.* **2** (2021) 3806 (https://www.doi.org/10.1039/d0ma00681e)
12. V. Saraswat, M. Yadav, I. B. Obot, *Colloids Surfaces, A* **599** (2020) 124881 (https://www.doi.org/10.1016/j.colsurfa.2020.124881)
13. Y. Abboud, O. Tanane, A. El Bouari, R. Salghi, B. Hammouti, A. Chetouani, S. Jodeh, *Corros. Eng. Sci. Technol.* **51** (2016) 557 (https://www.doi.org/10.1179/1743278215Y.0000000058)
14. M. Rbaa, F. Benhiba, P. Dohare, L. Lakhrissi, R. Touir, B. Lakhrissi, A. Zarrouk, Y. Lakhrissi, *Chem. Data Collect.* **27** (2020) 100394 (https://www.doi.org/10.1016/j.cdc.2020.100394)
15. N. Y. Silvère Diki, N. H. Coulibaly , K. F. Kassi, A. Trokourey, *J. Electrochem. Sci. Eng.* **11(2)** (2021) 97-106 (https://doi.org/10.5599/jese.952)
16. F. E. Abeng, V. Anadebe, P. Y. Nkom, K. J. Uwakwe, E. G. Kamalu, *J. Electrochem. Sci. Eng.* **11(1)** (2021) 11 (https://doi.org/10.5599/jese.887)
17. M. A. Metwally, E. Abdel-Latif, *J. Sulfur Chem.* **33** (2012) 229 (https://www.doi.org/10.1080/17415993.2011.643550)
18. S. H. Cho, S. H. Kim, D. Shin, *Eur. J. Med. Chem.* **164** (2019) 517 (https://www.doi.org/10.1016/j.ejmech.2018.12.066)
19. L. H. Madkour, A. M. Hassanein, M. M. Ghoneim, S. A. Eid, *Monatsh. Chem.* **132** (2001) 245 (https://doi.org/10.1007/s007060170134)
20. L. O. Olasunkanmi, B. P. Moloto, I. B. Obot, E. E. Ebenso, *J. Mol. Liq.* **252** (2018) 62 (https://www.doi.org/10.1016/j.molliq.2017.11.169)
21. A. O. Yüce, G. Kardaş, *Corros. Sci.* **58** (2012) 86 (https://www.doi.org/10.1016/j.corsci.2012.01.013)
22. A. O. Yüce, E. Telli, B. D. Mert, G. Kardaş, B. Yazici, *J. Mol. Liq.* **218** (2016) 384 (https://www.doi.org/10.1016/j.molliq.2016.02.087)
23. M. S. Kumar, S. L. A. Kumar, A. Sreekanth, *Ind. Eng. Chem. Res.* **51** (2012) 5408 (https://www.doi.org/10.1021/ie203022g)
24. M. Chafiq, A. Chaouiki, H. Lgaz, R. Salghi, S. L. Gaonkar, K. S. Bhat, R. Marzouki, I. H. Ali, M. I. Khan, H. Shimizu, I. M. Chung, *J. Adhes. Sci. Technol.* **34** (2020) 1283 (https://www.doi.org/10.1080/01694243.2019.1707561)
25. R. Kumar, H. Kim, G. Singh, *J. Mol. Liq.* **259** (2018) 199 (https://www.doi.org/10.1016/j.molliq.2018.02.123)
26. S. T. Arab, *Mater. Res. Bull.* **43** (2008) 510 (https://www.doi.org/10.1016/j.materresbull.2007.10.025)
27. B. Šmit, R. Z. Pavlović, A. Radosavljević-Mihailović, A. Došen, M. G. Ćurčić, D. S. Šeklić, M. N. Živanović, *J. Serb. Chem. Soc.* **78** (2013) 217 (https://www.doi.org/10.2298/JSC120725154S)

28. M. Elfaydy, H. Lgaz, R. Salghi, M. Larouj, S. Jodeh, M. Rbaa, H. Oudda, K. Toumiat, B. Lakhrissi, *J. Mater. Environ. Sci.* **7** (2016) 3193 (https://www.jmaterenvironsci.com/Document/vol7/vol7_N9/333-JMES-2379-ELfaydy.pdf)
29. S. Fatima, R. Sharma, F. Asghar, A. Kamal, A. Badshah, H. B. Kraatz, *J. Ind. Eng. Chem.* **76** (2019) 374 (https://www.doi.org/10.1016/j.jiec.2019.04.003)
30. M. El Faydy, B. Lakhrissi, A. Guenbour, S. Kaya, F. Bentiss, I. Warad, A. Zarrouk, *J. Mol. Liq.* **280** (2019) 341 (https://www.doi.org/10.1016/j.molliq.2019.01.105)
31. M. T. Alhaffar, S. A. Umoren, I. B. Obot, S. A. Ali, *RSC Adv.* **8** (2018) 1764 (https://doi.org/10.1039/C7RA11549K)
32. M. K. Pavithra, T. V. Venkatesha, K. Vathsala, K. O. Nayana, *Corros. Sci.* **52** (2010) 3811 (https://doi.org/10.1016/j.corsci.2010.07.034)
33. M. El Faydy, M. Rbaa, L. Lakhrissi, B. Lakhrissi, I. Warad, A. Zarrouk, I. B. Obot, *Surf. Interfaces* **14** (2019) 222 (https://www.doi.org/10.1016/j.surfin.2019.01.005)
34. A. Yousefi, S. Javadian, N. Dalir, J. Kakemam, J. Akbari, *RSC Adv.* **5** (2015) 11697 (https://www.doi.org/10.1039/c4ra10995c)
35. M. A. Hegazy, H. M. Ahmed, A. S. El-Tabei, *Corros. Sci.* **53** (2011) 671 (https://www.doi.org/10.1016/j.corsci.2010.10.004)
36. I. Ahamad, M. A. Quraishi, *Corros. Sci.* **51** (2009) 2006 (https://www.doi.org/10.1016/j.corsci.2009.05.026)
37. E. Mccafferty, N. Hackerman, *J. Electrochem. Soc.* **119** (1972) 146 (https://doi.org/10.1149/1.2404150)
38. M. Quraishi, J. Rawat, *Mater. Chem. Phys.* **70** (2001) 95 (https://www.doi.org/10.1016/S0254-0584(00)00459-4)
39. R. Hsissou, O. Dagdag, S. Abbout, F. Benhiba, M. Berradi, M. El Bouchti, A. Berisha, N. Hajjaji, A. Elharfi, *J. Mol. Liq.* **284** (2019) 182 (https://www.doi.org/10.1016/j.molliq.2019.03.180)
40. P. Muthukrishnan, B. Jeyaprabha, P. Prakash, *Arab. J. Chem.* **10** (2017) S2343 (https://www.doi.org/10.1016/j.arabjc.2013.08.011)
41. K. Kansal, R. Chopra, R. Kumar, A. Kumar, B. Yadav, R. Kishore Sharma, G. Singh, *Indian J. Chem. Technol.* **24** (2017) 169 (http://op.niscair.res.in/index.php/IJCT/article/view/13124).

Journal of the Serbian Chemical Society
JSCS@tmf.bg.ac.rs • www.shd.org.rs/JSCS
J. Serb. Chem. Soc. *87* (12) S480–S487 (2022) *Supplementary material*

SUPPLEMENTARY MATERIAL TO

Anticorrosion activity of 2-thiohydantoin–Shiff base derivatives for mild steel in 0.5 M HCl

PETAR B. STANIĆ[1], NATAŠA M. VUKIĆEVIĆ[2#], VESNA S. CVETKOVIĆ[2#], MIROSLAV M. PAVLOVIĆ[2#], SILVANA B. DIMITRIJEVIĆ[3], BILJANA ŠMIT[1*#] and MARIJA D. ŽIVKOVIĆ[4**#]

[1]Institute for Information Technologies Kragujevac, University of Kragujevac, Jovana Cvijića bb, 34000 Kragujevac, Serbia, [2]Institute of Chemistry, Technology and Metallurgy, University of Belgrade, Njegoševa 12, 11000 Belgrade, Serbia, [3]Mining and Metallurgy Institute Bor, Zeleni bulevar 35, 19210 Bor, Serbia and [4]Faculty of Medical Sciences, University of Kragujevac, Svetozara Markovića 69, 34000 Kragujevac, Serbia

J. Serb. Chem. Soc. *87* (12) (2022) 1409–1423

*3-[(phenylmethylene)amino]-2-thioxo-4-imidazolidinone (**1**)*

Yield 1.158 g (72 %). IR (KBr): 3419m, 3055m, 3032w, 2967m, 2768m, 1711s, 1645s, 1591s, 1490w, 1445w, 1409w, 1345m, 1327m, 1310m, 1249s, 1225m, 1213m, 1074w, 1039w, 969m, 877m, 854m, 835m, 788m, 756m, 734m, 713m 695m, 629w cm^{-1}. ^1H NMR (200 MHz, DMSO-d_6, δ): 8.40 (*s*, 1H), 7.75 (*m*, 2H), 7.45 (*m*, 3H), 3.89 (*s*, 2H). ^{13}C NMR (50 MHz, DMSO-d_6, δ): 174.33, 165.51, 156.31, 134.31, 130.76, 128.96, 127.76, 33.26.

*3-[(2-hydroxybenzylidene)amino]-2-thioxoimidazolidin-4-one (**2**)*

Yield 2.102 g (89 %). IR (KBr): 3441m, 3318m, 3031w, 2958m, 2776m, 1718s, 1640s, 1623s, 1568w, 1492w, 1469w, 1334m, 1317m, 1266m, 1254m, 1204m, 1149w, 890w, 838w, 757m, 735m, 710m, 637w cm^{-1}. ^1H NMR (200 MHz, DMSO-d_6, δ): 12.09 (*bs*, NH, exchangeable with D_2O), 10.88 (*s*, OH, exchangeable with D_2O), 8.64 (*s*, 1H), 7.58 (*dd*, 1H, J_1 = 8.0, J_2 = 1.9 Hz), 7.32 (*dt*, 1H, J_1 = 7.8, J_2 = 1.8 Hz), 6.95 (*m*, 2H), 3.97 (*s*, 2H). ^{13}C NMR (50 MHz, DMSO-d_6, δ): 173.77, 164.44, 158.01, 157.76, 132.17, 130.62, 119.54, 118.50, 116.38, 33.46.

*3-[(2-furanylmethylene)amino]-2-thioxo-4-imidazolidinone (**3**)*

Yield 1.186 g (57 %). IR (KBr): 3434m, 3153w, 3114m, 3023m, 2949m, 2752m, 1713s, 1642s, 1594s, 1476m, 1436m, 1390w, 1360m, 1320s, 1249s, 1206m, 1154m, 1074w, 1044w, 1018m, 964w, 939m, 895m, 884m, 852m, 824m, 787m, 771m, 732m, 677w, 599w, 514m cm^{-1}. ^1H NMR (200 MHz,

* Corresponding authors. E-mail: (*)biljana.smit@uni.kg.ac.rs; (**)mzivkovic@kg.ac.rs

DMSO-d_6, δ): 8.21 (*s*, 1H), 7.85 (*d*, 1H, J = 1.8 Hz), 6.95 (*d*, 1H, J = 3.4 Hz), 6.64 (*dd*, 1H, J_1 = 3.6, J_2 = 1.8 Hz), 3.87 (*s*, 2H). ^{13}C NMR (50 MHz, DMSO-d_6, δ): 174.32, 165.00, 149.48, 146.00, 145.77, 115.88, 112.59, 33.40.

*3-[[(4-hydroxy-3-methoxyphenyl)methylene]amino]-2-thioxo-4-imidazolidinone (**4**)*

Yield 2.540 g (96 %). IR (KBr): 3393m, 2938m, 2774m, 1696s, 1640s, 1613s, 1513m, 1472m, 1435m, 1398w, 1326m, 1271m, 1248s, 1210m, 1167m, 1123w, 1042w, 803w, 768w, 737w, 155w, 519w cm^{-1}. ^{1}H NMR (200 MHz, DMSO-d_6, δ): 11.83 (*bs*, NH, exchangeable with D_2O), 9.63 (*s*, OH, exchangeable with D_2O), 8.26 (*s*, 1H), 7.32 (*d*, 1H, J = 1.6 Hz), 7.19 (*dd*, 1H, J_1 = 8.2, J_2 = 1.6 Hz), 3.87 (*s*, 2H), 3.80 (*s*, 3H). ^{13}C NMR (50 MHz, DMSO-d_6, δ): 174.13, 163.50, 156.22, 149.50, 147.91, 125.75, 122.18, 115.69, 110.66, 55.70, 33.08.

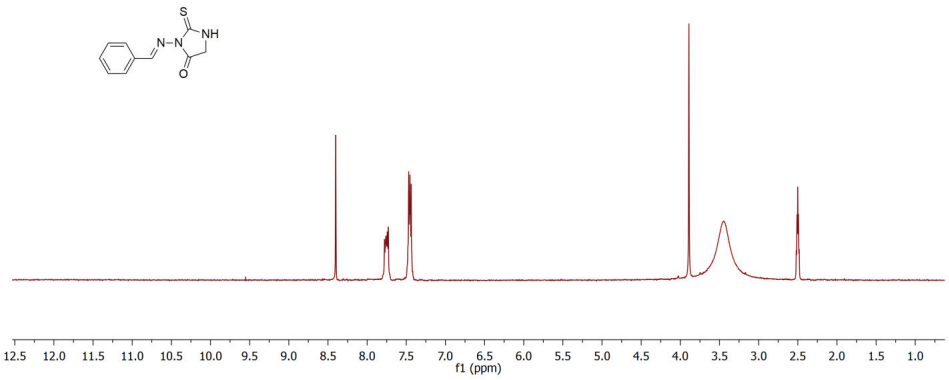

Fig. S-1. ^{1}H NMR spectra of 3-[(phenylmethylene)amino]-2-thioxo-4-imidazolidinone (**1**)

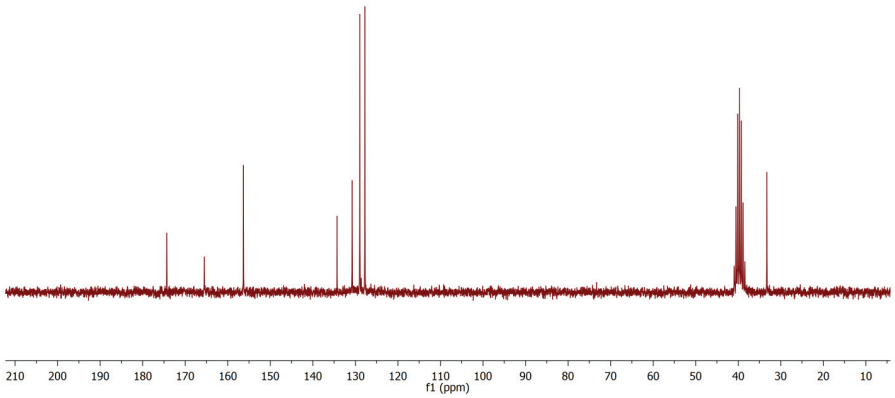

Fig. S-2. ^{13}C NMR spectra of 3-[(phenylmethylene)amino]-2-thioxo-4-imidazolidinone (**1**)

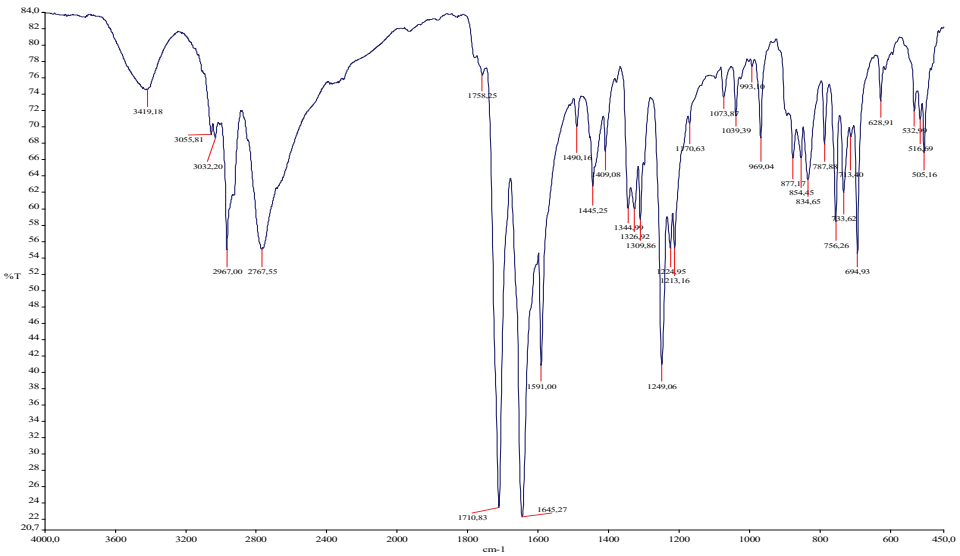

Fig. S-3. IR spectra of 3-[(phenylmethylene)amino]-2-thioxo-4-imidazolidinone (**1**)

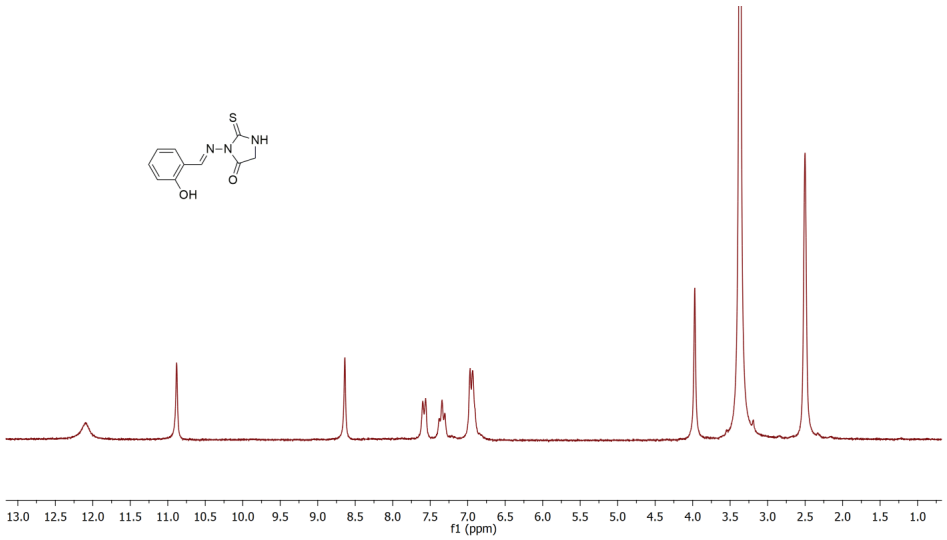

Fig. S-4. ^{1}H NMR spectra of 3-[(2-hydroxybenzylidene)amino]-2-thioxoimidazolidin-4-one (**2**)

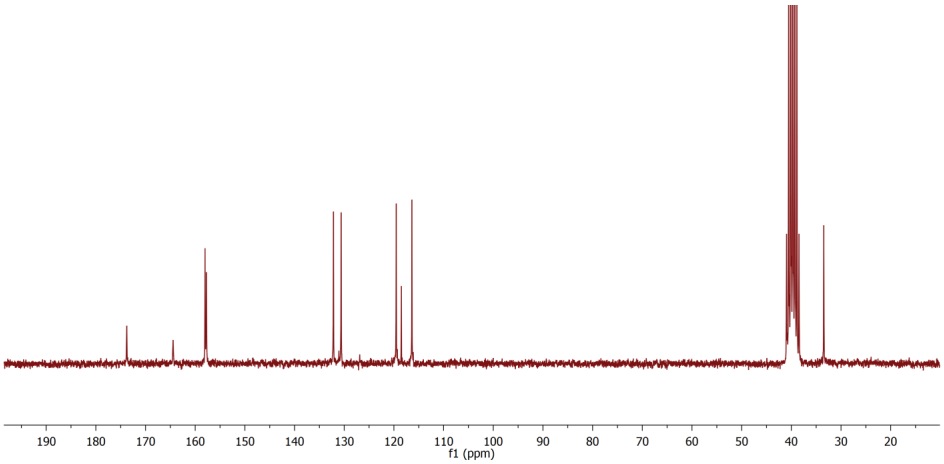

Fig. S-5. ^{13}C NMR spectra of 3-[(2-hydroxybenzylidene)amino]-2-thioxoimidazolidin-4-one (**2**)

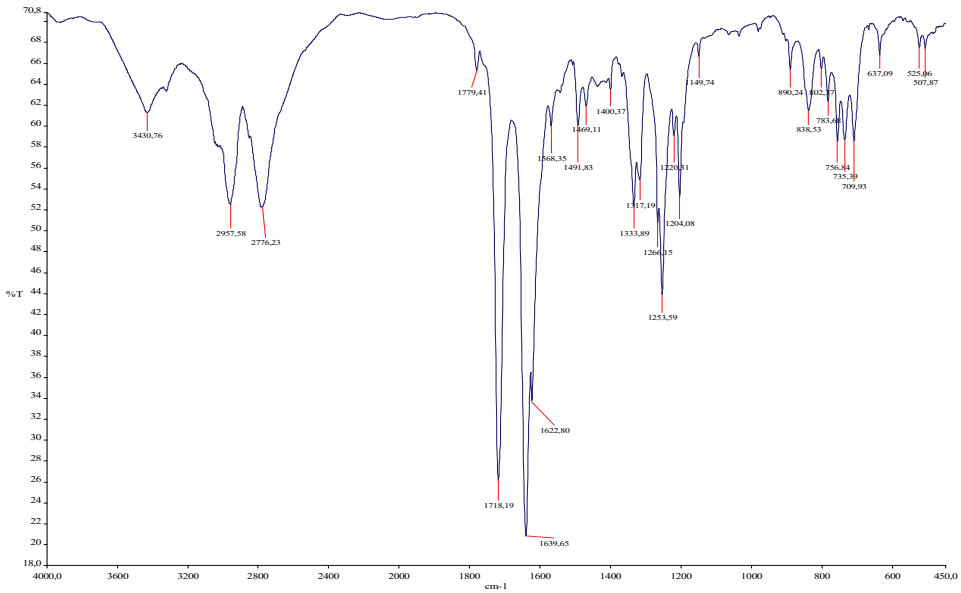

Fig. S-6. IR spectra of 3-[(2-hydroxybenzylidene)amino]-2-thioxoimidazolidin-4-one (**2**)

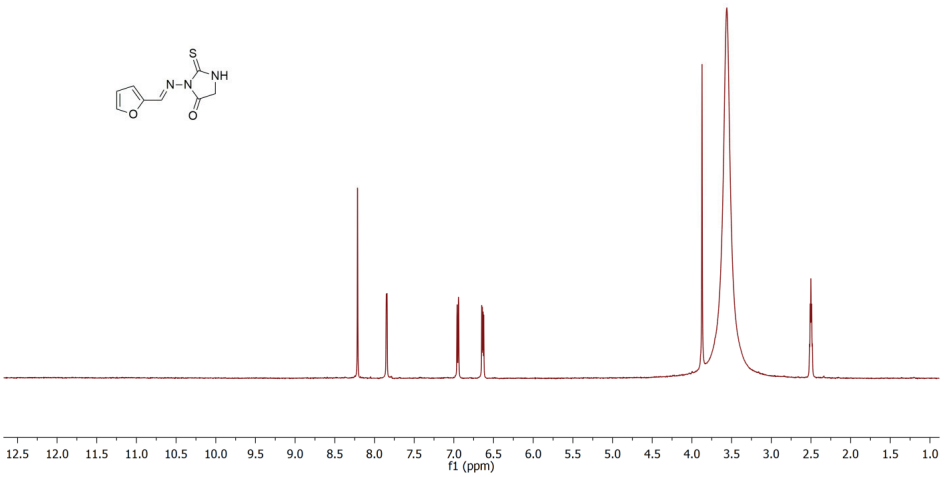

Fig. S-7. ^{1}H NMR spectra of 3-[(2-furanylmethylene)amino]-2-thioxo-4-imidazolidinone (**3**)

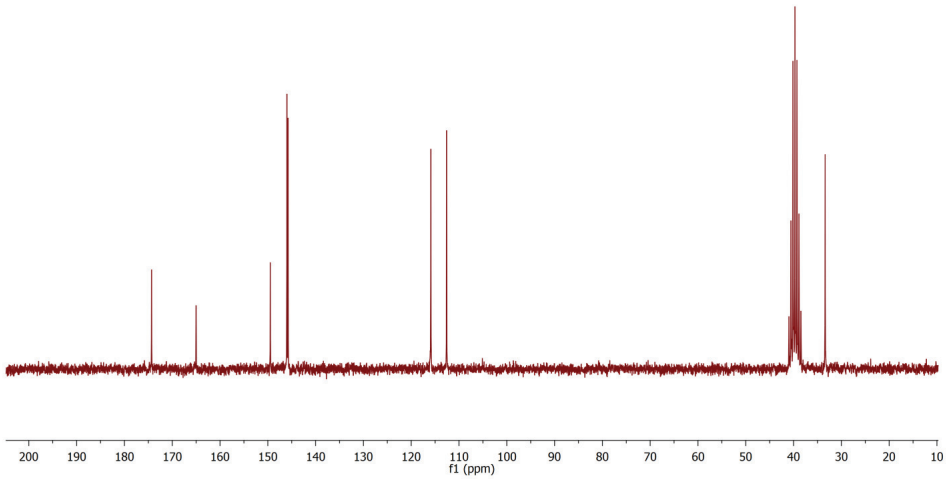

Fig. S-8. ^{13}C NMR spectra of 3-[(2-furanylmethylene)amino]-2-thioxo-4-imidazolidinone (**3**)

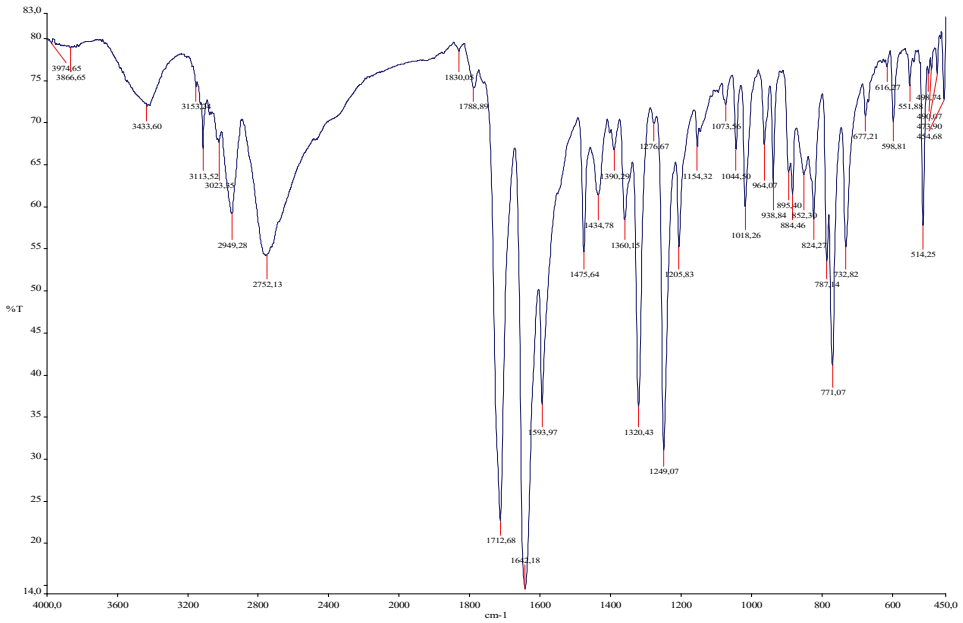

Fig. S-9. IR spectra of 3-[(2-furanylmethylene)amino]-2-thioxo-4-imidazolidinone (**3**)

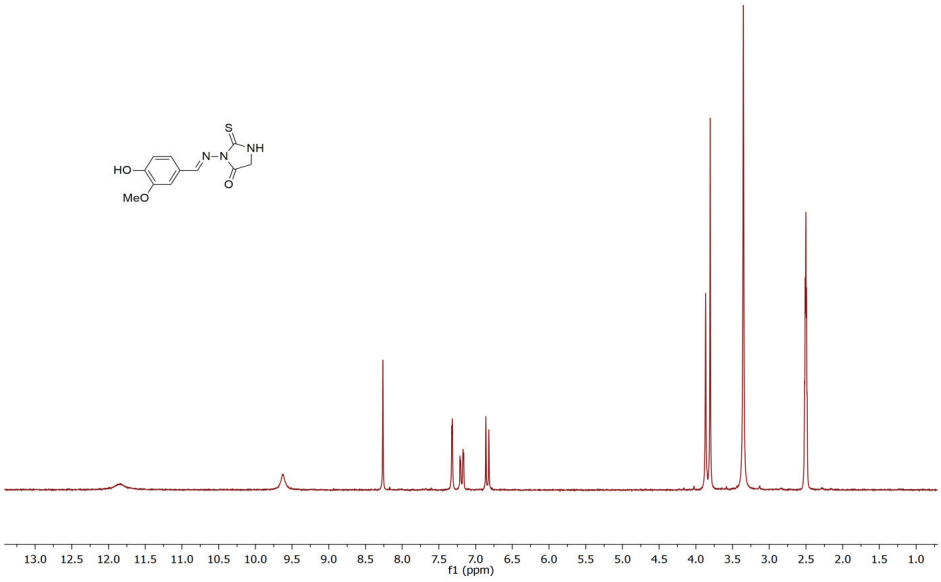

Fig. S-10. ^{1}H NMR spectra of 3-[[(4-hydroxy-3-methoxyphenyl)methylene]amino]-2-thioxo-4-imidazolidinone (**4**)

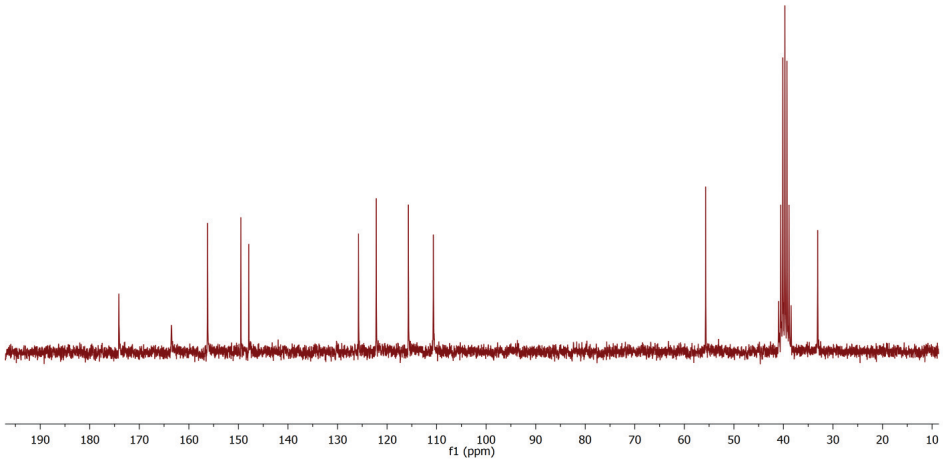

Fig. S-11. ^{13}C NMR spectra of 3-[[(4-hydroxy-3-methoxyphenyl)methylene]amino]-2-thioxo-4-imidazolidinone (**4**)

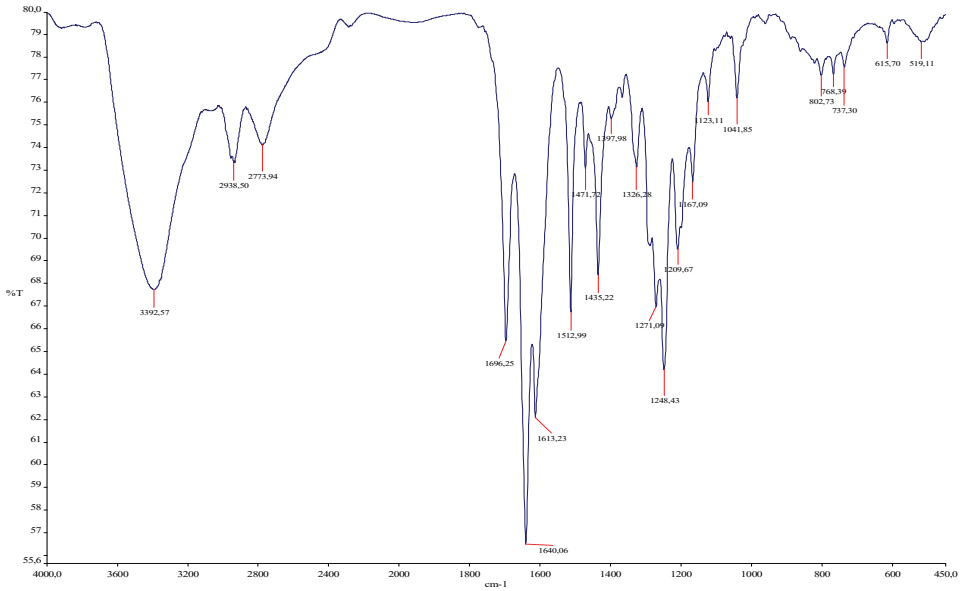

Fig. S-12. IR spectra of 3-[[(4-hydroxy-3-methoxyphenyl)methylene]amino]-2-thioxo-4-imidazolidinone (**4**)

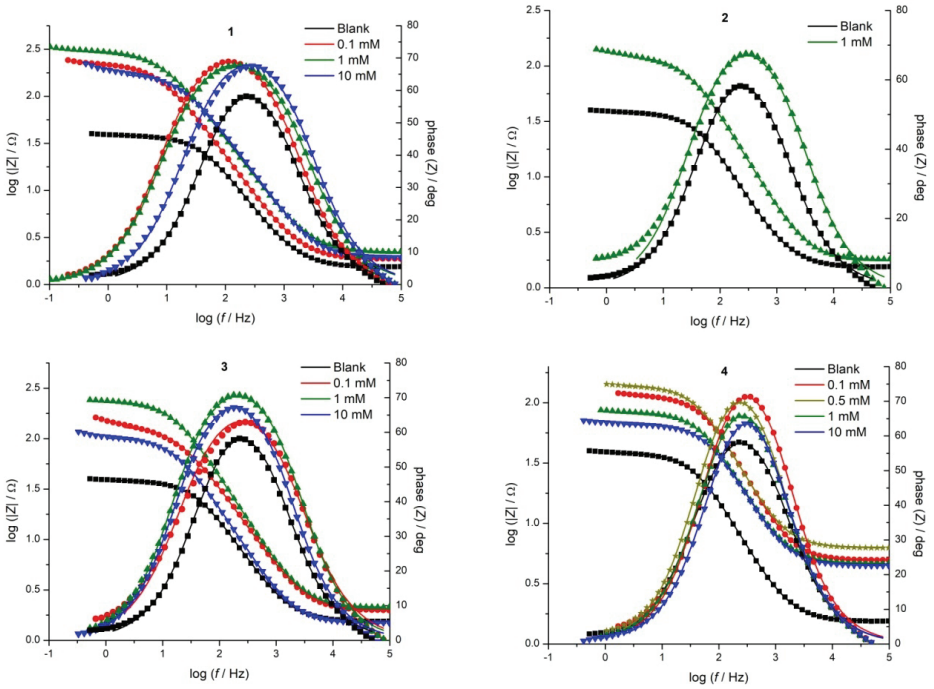

Fig. S-13. Bode plots for MS electrode and different inhibitors compounds **1**-**4** at various concentrations with respect to blank 0.5 M HCl. Scattered dots represent experimental data, while solid lines represent calculated and fitted results.

Journal of the Serbian Chemical Society
JSCS@tmf.bg.ac.rs • www.shd.org.rs/JSCS
J. Serb. Chem. Soc. *87* (12) 1425–1437 (2022)
JSCS–5604
Original scientific paper
Published 30 September 2022

Temporal trend of perfluorinated compounds in untreated wastewater and surface water in the middle part of the Danube River belonging to the northern part of Serbia

MAJA B. BULJOVČIĆ[1#], IGOR S. ANTIĆ[1#], KIWAO KADOKAMI[2] and BILJANA D. ŠKRBIĆ[1]*

[1]*University of Novi Sad, Faculty of Technology Novi Sad, Bulevar cara Lazara 1, 21000 Novi Sad, Serbia and* [2]*Institute of Environmental Science and Technology, University of Kitakyushu, Fukuoka, 808-0135Kitakyushu, Japan*

(Received 27 April, revised 24 June, accepted 18 July 2022)

Abstract: The occurrence and temporal variation of selected priority substances and contaminants of emerging concerns, *i.e.*, eleven perfluorinated compounds (PFCs, belonging to perfluorosulphonates, perfluorocarboxylic acids, and perfluorinated sulphonamides) have been investigated in composite surface water samples of the Danube River at the upstream and downstream locations from the discharge point of wastewater. Among the analyzed compounds, six PFCs (PFOA, PFOS, PFHxA, PFNA, PFDA and PFUnA) were quantified. Overall, the detection frequency for most quantified compounds was very high (>90 %), only PFDA and PFUnA were quantified with less frequency, 33 and 67 %, respectively. The highest quantified concentrations of PFOA and PFOS were 14.9 ng/L (average 12.1 ng/L) and 14.2 ng/L (average 6.11 ng/L), respectively. These ones together with PFHxA (average 10.0 ng/L) were quantified at the highest concentrations in comparison to the other investigated compounds. However, the determined levels of PFOS during investigated sampling period, for all samples analyzed, were always lower than the maximum allowable concentration set for inland river waters but always higher than the environmental quality standard threshold value-AA-EQS of 0.65 ng/L sets by the Directive of European Parliament. Moreover, the levels of PFOA were always several times lower than the set AA-EQS value.

Keywords: emerging contaminants; PFCs occurrence; PFOS; PFOA; environmental pollution.

* Corresponding author. E-mail: biljana@tf.uns.ac.rs
# Serbian Chemical Society member.
https://doi.org/10.2298/JSC220427061B

INTRODUCTION

It is well known that the contamination of fresh water with numerous toxic compounds is a global problem.[1,2] Unregulated chemicals gathering a wide range of so-called "emerging" or "new" contaminants have appeared as an environmental problem and become a priority topic in environmental analysis.[3] Among them, perfluorinated compounds (PFCs) attract considerable attention as they are globally distributed, environmentally persistent, bioaccumulative and potentially harmful.[2,4] A fully fluorinated hydrophobic alkyl chain attached to a hydrophilic end group is a common feature of these contaminants.[5] As a consequence, PFCs have been found ubiquitous in the environment and in biota.[6] However, despite being first synthesized back in 1940, PFCs have only recently been designated as contaminants of emerging concern.[7] PFCs include perfluorocarboxylic acids (PFCAs), perfluorosulphonates (PFSAs) and perfluoro sulfonamides (PFASA) and other polyfluorinated compounds, such as fluorotelomer sulphonates (FTSs), perfluoro phosphonic acids (PFPAs, *i.e.*, fluorotelomer).[5] The most important and widely-studied representatives of PFCAs and PFSAs are perfluorooctanoic acid (PFOA) and perfluorooctane sulfonic acid (PFOS), respectively. PFOS and PFOA were the first PFCs recognized as global pollutants because of their extended use during the past decades.[4] Surface water is considered to be the major environmental reservoir for PFCs,[5] because the surface water is a final sink for most PFCs. However, the presence of PFCs was determined also in groundwater,[8] sediment,[9,10] sludge samples,[11] agricultural plants,[12] food commodities,[13,14] and even in the human body.[5] Moreover, it is found that in every 20 children tested 19 had blood contaminated with PFOA which is extremely alarming.[15] Thus, among selected PFCs, PFOS and PFOA were of particular concern since they account for the major proportion of PFCs contamination worldwide, thanks to their high solubility in the aquatic environment.[15] Namely, PFOS and PFOA have high solubility of 570 and 9500 mg/L, respectively. The European Commission (EC) has declared PFCs as emerging organic contaminants, and PFOS and its derivatives as priority hazardous substances which must be monitored in the European Union (EU) water bodies. Namely, in the EU strong restrictions on the use and import of PFOS were introduced in 2006, while in 2012, through European Water Framework Directive, the EC established a threshold concentration in drinking water and fish for environmental quality assessment, and in 2013, it established Environmental Quality Standards[16] against which to measure PFOS concentrations in inland surface waters and biota. The maximum allowable concentration (*MAC*-EQS) for surface water and biota (EQS) is set at 36.0 and 9.1 ng/L, respectively; after a risk assessment study, the mean annual concentration (*AA*-EQS) limit is set to be 0.650 ng/L for inland surface water.[16] Moreover, PFOA, its salts and related substances are restricted with certain derogations within the EU with a transitional period until 2020. PFOA, its salts and

PFOA-related substances shall not be manufactured or placed on the market as substances on their own from 4 July 2020.[16] Accordingly, the mean annual concentration limit for PFOA is set to be 100 ng/L for inland surface water.[16] For perfluorononanoic acid (PFNA), perfluorododecanoic acid (PFDoA), perfluoroundecanoic acid (PFUnA), and perfluorodecanoic acid (PFDA) in the EU, regulatory restrictions similar to the ones in place for PFOS and PFOA are currently under discussion. As the carbon-fluorine bond in PFCs is one of the most stable in nature, removal of these contaminants in wastewater treatment plants (WWTPs) and also in the environment under aerobic and anaerobic conditions is limited. They are not significantly removed during secondary biological treatment, while their concentrations in treated wastewater are often higher compared to raw sewage.[4] Namely, it is observed that longer-related PFCs can biodegrade to short-chain PFCs which causes that WWTPs not only directly receive PFC loads from various inputs, but also enhance, *e.g.*, PFOS and PFOA concentration *via* degradation of their longer-related PFCs.[18] The threat posed by the release of these contaminants through wastewater treatment plant effluents is particularly worrisome in streams or small rivers, where the dilution capacity of the receiving freshwater ecosystem is small.[18]

Relating the present situation in Serbia only the small portion (around 10 %) of WW is treated by any standardized WW treatment procedures implying a common practice of discharging untreated municipal wastewater into surface water recipients.[19] Although the Danube River, the largest river in Serbia, has the greatest dilution capacity, even the worrisome problem is that 90 % of untreated wastewater is directly discharged into the rivers of Serbia. Since the surface water samples were collected upstream and downstream of the wastewater discharge point into the Danube River, the results obtained in this study were used to assess the impact of PFCs from discharged wastewater on surface water, as in the scientific literature, there is scarce information available on the occurrence of perfluorinated compounds in the Danube River and its tributaries. This is particularly important knowing that the Danube River is the second-largest river in Europe (2857 km long) that flows through 10 countries and receives a vast volume of untreated wastewater from domestic sources, industrial and agricultural activities, but, on the other hand, together with its tributaries, the Danube River provides a necessary resource for water supply, sustaining biodiversity, agriculture, industry, fishing, recreation, tourism, power generation and navigation.[20] Thus, in light of the present situation, the aims of this study were: *i*) to give a preliminary insight into the occurrence and levels of eleven perfluorinated compounds, which included two perfluorosulphonates; perfluorobutane sulfonic acid (PFBS) and perfluorooctane sulfonic acid (PFOS), eight perfluorocarboxylic acids; perfluorobutanoic acid (PFBA), perfluorohexanoic acid (PFHxA), perfluoroheptanoic acid (PFHpA), perfluorooctanoic acid (PFOA), perfluorononanoic

acid (PFNA), perfluorodecanoic acid (PFDA), perfluoroundecanoic acid (PFUnA), perfluorododecanoic acid (PFDoA) and one perfluorinated sulphonamides: perfluorooctane sulfonamide (PFOSA) in the surface water of the middle part of the Danube River belonging to Republic of Serbia by the method validated in this study, *ii*) to reveal hotspots in small-sized cities which might have a possible adverse effect on the environment as a consequence of the discharge of untreated wastewater, *iii*) to investigate the temporal variation in concentrations of studied PFCs and *iv*) to compare the determined levels with the ones found in the literature. To the best of our knowledge, there is no published data regarding the concentration of 11 PFCs in the surface water of the Danube in Balkan countries.

EXPERIMENTAL

Chemicals and standards

Eleven PFCs, *i.e*., PFBS, PFOS, PFBA, PFHxA, PFHpA, PFOA, PFNA, PFDA, PFUnA, PFDoA and PFOSA were obtained from Chiron AS (Trondheim, Norway). Purities of the standards were >98 %. More details about eight surrogate compounds (SSs) could be found in the Supplementary material. Waters Oasis HLB Plus LP (225 mg, 60 μm) solid-phase extraction (SPE) cartridges were purchased from Waters (Milford, MA, USA). Grade GF/C glass microfiber filters (0.47 μm) were purchased from Whatman International Ltd (Maidstone, Kent, UK). Ultra-pure water (resistivity 18.2 MΩ cm) was obtained from Milli-Q system (Millipore, Molsheim, France). Methanol and ammonium acetate (all LC–MS grade) were purchased from J.T. Baker (Deventer, Netherlands), and glacial acetic acid (trace analysis grade) was obtained from Fisher Chemicals (Fisher Chemicals, Loughborough, UK).

Sampling sites and sample collection

Details related to sampling are given in Supplementary material to this paper.

Twelve composite surface water samples were collected down-D ($n = 6$) and up-U ($n = 6$) stream of the discharge point of the local municipal collecting wastewater unit. Additionally, eight composite 24 h wastewater (WW) samples were collected from the discharged unit. The sampling frequency is given in Supplementary material, Table S-I. More about sample collection could be found in the Supplementary material.

Sample extraction

During the samples handling and analysis Teflon bottles, Teflon-lined caps and any suspect fluoropolymer materials were avoided in order to avert cross-contamination of the samples. Analytical methods for the determination of PFCs in wastewater and surface water samples were developed by Duong *et al.*[22] and re-validated by an "in-house" quality control procedure for purpose of the present study. More information could be found in the Supplementary material. The extract was then spiked with internal standards (ISs listed in Section *Chemicals and standards*) at the concentration of 2 ng/mL by transferring 20 μL of IS stock solution (50 μg/mL) into the 500 μL of the final extract.

Instrumental analysis

Concentrations of PFCs in SW and WW samples were determined by using Thermo ultra-high-performance liquid chromatography (UHPLC) coupled with a Thermo TSQ Vantage triple quadrupole mass spectrometer (MS/MS) equipped with heated-electrospray ioniz-

ation probe, HESI (Thermo Fisher Scientific, San Jose, CA, USA), more details could be found in Supplementary material, Table S-II.

Method validation parameters

The sample preparation method used for the analysis of polar compounds on UHPLC--MS/MS was published earlier.[22] Although the mentioned sample preparation methods were fully validated, an additional "in-house "quality control procedure was applied in order to check their applicability in the different laboratories and on different types of instruments. Parameters that were taken into account were: specificity, instrumental linearity, method limits of detection (*MDL*) and quantification (*MQL*), recovery, and precision (expressed as relative standard deviation). Criteria for PFCs identity confirmation by MS/MS were: *i*) the retention time, *ii*) the presence of two product ion transitions for each analyte and *iii*) the relative intensities of the detected products ions (ratio qualifier/quantifier transitions), which shall correspond to those of the calibration standards at comparable concentrations within tolerances ranging from 20 to 50 % depending on the relative intensity of the base peak.[23] To evaluate the linearity of the method mixed standard solutions were prepared in the expected concentration range of PFCs, *i.e.*, in accordance with available literature data. Acceptable linearity was achieved when the squared correlation coefficient (R^2) was higher than 0.99 for internal calibration curve. It's worth noting that the deuterium-labeled internal standards were provided for each studied PFCs. PFCs were quantified using an internal calibration procedure. In this way, preparation of matrix match calibration was avoided as the PFC residue-free matrix was really hard to obtain. Calibration solutions for internal calibration curves were prepared into previously analyzed ultra-pure water. The instrumental limit of detection (*IDL*) values were estimated as the concentration of each toxic compound that gives a signal that corresponds to three times the noise ($S/N = 3$). The instrumental limit of quantification (*IQL*) values was defined as the concentration of each toxic compound that gives a signal that corresponds to ten times the noise ($S/N = 10$). Then the method detection limits (*MDL*) and method quantification limits (*MQL*) were calculated taking into consideration the dilution factor and the volume of sample used (500 mL for surface water and 300 mL for wastewater).

Recovery tests were conducted by spiking a mixture of 11 PFCs (10 ng/L each) and a mixture of 8 surrogate compounds (10 ng/L each) into ultra-pure water. Spiked water was treated by the same procedures as real water samples. Before recovery experiments, unfortified water samples were previously analyzed in order to confirm that no PFCs were detected. Recovery of the method was determined for all compounds and defined as the ratio between the quantified and the spiked amount. The repeatability of the method was determined as relative standard deviation (*RSD* in %) of the PFCs in five fortified samples. Blank samples were included in every batch of samples to check for possible contamination. The accuracy of individual sample analysis was checked by examining the recoveries of the surrogate spiked into the samples before analysis. When reporting data, blank corrections were subtracted from sample concentration. The reporting values were corrected using recovery values. Whenever sample concentrations were below the *MQL*, a concentration equal to half of the limit of quantification was used for the calculations, according to Directive 2009/90/EC.[16] Also, when the total sum was reported results below the *MQL* of the individual substances were set to zero.[16]

Statistical treatment of the data

Microsoft Excel 2010 for Windows was used for basic statistical treatment (mean, maximum, minimum, kurtosis, skewness) of the obtained data. Statistically significant difference

between means of samples taken upstream and downstream during the monitoring period and statistically significant difference in quantified concentrations among each analyzed PFCs during the monitoring period of one month were checked by student's *t*-test.

RESULTS AND DISCUSSION

Quality assurance and quality control

In Table I are given the results obtained during the validation procedure carried out in order to prove that the applied sample preparation method and instrumental analysis fit the purpose for PFCs determination in surface and wastewater samples.

TABLE I. Validation parameters for PFCs determination; reproducibility (inter-day precision) was calculated as the relative standard deviation, %, of the analytes (ten replicates) of blank surface water fortified with 11 analytes at three concentrations (10, 20 and 50 ng/L) on three consecutive days

PFCs	Linearity	*MDL* / ng L^{-1}	*MQL* / ng L^{-1}	Recovery, %	*RSD* / %	Inter-day, %
PFBA	0.9985	0.430	1.43	89.4	12	9.2
PFBS	0.9975	0.0100	0.0402	86.6	13	12
PFHxA	0.9933	0.195	0.630	73.2	7.4	14
PFHpA	0.9914	0.124	0.398	79.0	8.2	8.8
PFOA	0.9933	0.0602	0.218	76.5	13	15
PFOS	0.9925	0.100	0.321	81.8	11	9.6
PFOSA	0.9982	0.281	0.932	120	9.4	12
PFNA	0.9925	0.393	1.32	84.3	14	12
PFDA	0.9964	0.172	0.584	80.4	13	9.4
PFUnA	0.9994	0.125	0.397	72.1	15	10
PFDoA	0.9935	0.104	0.332	73.8	14	11

Identification of PFCs after UHPLC–MS/MS analysis was carried out using the retention time of the targeted compounds, precursor ion and at least two selective product ions. The validation process showed that the reported transitions for PFCs were the same as was published in the previous study[22] although different UHPLC–MS/MS instruments were used. The linearity of the calibration curves was higher than 0.9900 for all studied compounds covering the range from 0.100 to 30 ng/L for surface water and from 0.170 to 50 ng/L for wastewater samples. Precision was lower than 15 % for all analyzed compounds. The efficiencies of extraction were in the range from 72 to 120 % obtained by analyzing five fortified replicates.

Relating the *MQL*, they were all lower than 1.43 ng/L. The obtained method validation parameters were comparable with the previously published data in which similar compounds were analyzed in surface and wastewater samples.[22] The obtained validation parameters are comparable, *e.g.*, with the results obtained during the analysis of PFCs in the Danube River where the range of *MQL* was

from 0.551 ng/L (PFBS) to 3.20 ng/L (PFHpA).[26] It is worth mentioning that there are no reports in which a significant number of PFCs (eleven) were analyzed.

PFCs in surface water in the middle part of the Danube River, belonging to Republic of Serbia

Out of eleven analysed PFCs four of them (PFNA, PFOS, PFOA and PFHxA) were detected in all surface water samples, whereas PFDA and PFUnA were detected sporadically (Table II). Namely, PFUnA and PFDA were detected with the frequency of detection of 33 and 67 %, respectively, while the other detected PFCs showed a high frequency of occurrence (100 %) with a uniform level of occurrence during the monitoring period. The quantified concentrations of PFOA and PFHxA were in all analysed samples higher than 5 ng/L. PFOA and PFHxA account between 27 and 46 % and 25 to 36 % of the total PFCs concentrations. PFOS accounts between 9.4 and 37 % of the total PFC concentrations. This distribution is similar to data reported for surface water in the Europe[24] and Sri Lanka[25] where PFOS and PFOA were dominant, but PFNA was a minor component, yet different to those in river from Japan and Vietnam where PFOA and PFNA were more abundant than PFOS. In particular, PFOA is used as adjuvant in the production of fluoropolymers such as Teflon® or similar products, and occurs in these applications as aqueous and gaseous process emission.[24] All the other quantified PFCs account for less than 10 % of the total PFC concentrations. There was no statistically significant difference in quantified concentrations among each analyzed PFCs during the monitoring period. The highest quantified concentrations of PFOS and PFOA were 14.9 ng/L (average 6.11 ng/L) and 14.2 ng/L (average 12.1 ng/L), respectively. These ones together with PFHxA (average 10.0 ng/L) were quantified at the highest concentrations in comparison to the other investigated compounds. The quantified concentrations of other detected compounds (PFUnA, PFDA and PFNA), were all lower than 5 ng/L. The concentration of PFOS exceeded the *AA*-EQS of 0.65 ng/L for each analyzed surface water sample during the whole sampling campaign. However, relating the maximum allowable concentration of PFOS in surface water sets for biota, the determined level was higher only for one sample analyzed upstream of the discharge point. Moreover, none of the analyzed samples showed a level that exceeds the *AA*-EQS of 100 ng/L set for PFOA in inland water. The Final Report of Joint Danube Survey 3[27] reports 8.10 ng/L as the average concentration of PFOA in the Danube River downstream Budapest and 7.20 ng/L as the average concentration of PFOS in the Danube River in Szob before Budapest.

Interestingly, PFHxA was detected in relatively high concentration (relative to other detected PFCs) in this study but not in the other mentioned papers, but still lower than the PFOA. Namely, besides some companies have switched to C6

PFCs such as perfluorohexanoic acid (PFHxA) to replace C8 PFCs as PFOA this trend is still not evidenced in the Danube River.

TABLE II. PFCs quantified in surface water samples

Sample	Concentration, ng/L					
	PFHxA	PFOA	PFOS	PFNA	PFDA	PFUnA
12.11.3-U	5.94	8.85	3.23	1.53	2.06	1.03
12.11.3-D	11.4	11.1	2.98	3.73	2.39	0.195[a]
20.11.5-U	8.37	13.9	3.82	1.54	1.97	0.96
20.11.5-D	11.8	13.8	3.53	4.95	0.292 [a]	0.195 [a]
21.11.6-U	11.1	12.9	4.08	4.17	2.03	0.195 [a]
21.11.6-D	10.3	10.9	14.9	3.66	0.290 [a]	0.195 [a]
25.11.8-U	11.0	11.9	5.27	1.42	4.42	0.195 [a]
25.11.8-D	8.38	14.2	6.27	1.69	1.89	0.94
27.11.10-U	9.49	11.8	4.64	1.62	1.71	0.195 [a]
27.11.10-D	8.89	11.6	3.4	1.99	2.10	0.195 [a]
29.11.12-U	12.0	11.4	9.53	2.36	0.290 [a]	0.195 [a]
29.11.12-D	11.8	13.0	11.7	4.6	0.290 [a]	4.60
Mean	10.0	12.1	6.11	2.77	1.64	0.758
Median	10.6	11.8	4.36	2.18	1.93	0.195
Min	5.94	8.85	2.98	1.42	0.290	0.195
Max	12.0	14.2	14.9	4.95	4.42	4.60
Frequency of occurrence, %	100	100	100	100	67.3	33.2

[a]Non-detected values were set to half the *MQL* for these calculations (in accordance with Directive 2009/EC)

Moreover, the obtained results were compared with the previously published data from the Joint Danube Survey 3[27] organized by the International Commission for the Protection of the Danube River (ICPDR) in 2013. JDS3 included in analysis six PFCs: PFBS, PFHxA, PFHpA, PFOA, PFOS and PFNA in the Danube River and its tributaries.[27] Of the mentioned ones, PFBS, PFHxA, PFOA and PFOS, were quantified with average and maximum value of 1.60 and 3.70, 4.00 and 8.50, 8.10 and 36.5 and 7.20 and 26.2, respectively. PFOS, PFOA and PFHxA were quantified with frequency over 90 %, which is in accordance with the results obtained in this study. The average concentrations of PFOS (7.2 ng/L), PFOA (8.1 ng/L) and PFHxA (4.0 ng/L) were of the same order as the results obtained in this study. PFOS exceeded the target value of 0.651 ng/L sets by EU Environmental Quality Standard at 94 % of the sampling sites during JDS3 survey and for all samples analysed in this study. The ICPDR had also organized, in 2007, a monitoring program[26] on the occurrence of some polar organic pollutants among them six PFCs (PFHpA, PFOA, PFNA, PFOS, PFDA, PFUnA) in the Danube River. Again, PFOS and PFOA were quantified with frequency over 90 % with the average concentrations of 8 and 20 ng/L, respectively. Additionally, the mean value of PFOA and PFOS obtained in this study was compared with the data of a few studies investigating the vulnerability of European river systems

such as Kampen IJssel (Netherland),[28] Ebro River (Spain),[29] Thames River (United Kingdom),[30] and Rhine River (Germany)[31] in order to assess PFCs pollution levels, Table III.

TABLE III. Comparison of PFOA and PFOS levels in European river systems; n.d. – not detected, n.e. – not estimated

System	Concentration, ng/L	
	PFOA	PFOS
This study	12.1	6.11
Wastewater canal in Pančevo (Serbia)[a10]	n.e.	24.09[b]
Joint Danube Survey 3[27]	8.50	7.20
Kampen IJssel (Netherland)	n.d.	9.90
Ebro River (Spain)[29]	125	27.0
Thames River (United Kingdom)[30]	11.7	18.9
Rhine River (Germany)[31]	3.66	8.56

[a]The analyzed soil and sediment samples are from within and around the Petrochemical Industry of Pančevo; [b]recalculated based on published concentration level in sediment sample[10]

It can be concluded that concentrations of PFOS in Kampen IJssel[28] and Rhine River[31] were of the same order, but a bit higher than the concentrations obtained in this study being 9.90 and 8.56 ng/L, respectively while concentrations in Ebro River[29] and Thames River[30] were 4.4 and 3.1 times higher than concentrations obtained in this study. In respect of PFOA concentrations in Rhiner River and Thames River were lower being 3.66 and 11.7 ng/L while concentrations in Ebro River were 10.3 times higher.[29–31] The study published by Beškoski *et al.* (2013) represents the first data on the presence of PFCs in sediment samples in Serbia.[10] The study deals with the determination of PFCs in sediment samples of wastewater canal draining wastewater from the industrial complex of Pančevo, Serbia. PFOS was quantified in a concentration up to 5.7 ng/g dry weight (dw), while the total PFCs content was up to 6.3 ng/g (dw). The recalculated PFOS concentration in water using the adsorption coefficient from the literature was 24.09 ng/L. The mean recalculated PFOS concentration (24.09 ng/L) was almost four times higher than the mean concentration of PFOS (6.11 ng/L) reported in the present study. Furthermore, it is interesting to note that the sum of identified PFCs determined in the Danube River surface samples during the sampling campaign was always a few times lower than the action limit for drinking water sets in Denmark, by the Environmental Protection Agency of 100 ng/L for the sum of 11 PFCs compounds including perfluorobutane sulfonate (PFBS), perfluorohexane sulfonate (PFHxS), PFOS, 6:2 fluorotelomer sulfonic acid (6:2 FTSA), PFBA, perfluoro-*n*-pentanoic acid (PFPeA), PFHxA, PFHpA, PFOA, PFNA and PFDA; as well as, the sum of PFCs in the Danube surface water samples were lower than the concentration limit sets in Sweden by National Food Agency of 90 ng/L for sum of seven PFCs including PFOA, PFOS,

PFBS, PFPeA, PFHxA, PFHpA and PFHxS. Besides, it is worth mentioning that the United Kingdom Drinking Water Institute sets the action limit only for PFOA and PFOS of 10.0 ng/L for each of them, in 2021, while in the Netherlands, the concentration limits of 390 ng/L for PFOA and 90 ng/L for PFOS are set, in 2020.

PFCs in wastewater

Among 11 analyzed PFCs, only PFOS and PFOSA were quantified in WW samples (Fig. 1). PFOS was quantified in the concentration range from 0.321 to 3.54 ng/L, while PFOSA was quantified in the concentration range from 0.140 to 7.38 ng/L. PFOS and PFOSA were quantified with the frequency of occurrence of 50 and 88 %, respectively. Since PFOSA was not detected in surface water samples it could be concluded that untreated wastewater does not have an influence on PFOSA content in the Danube River.

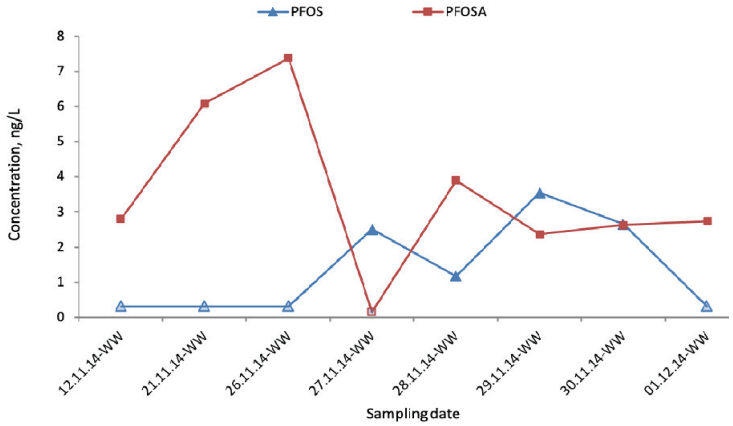

Fig. 1. Concentrations of PFOS and PFOSA in wastewater samples.

A similar conclusion can be drawn for PFOS, since its mean value (6.1 ng/L) for surface water samples upstream and downstream of the wastewater discharge into the Danube River is almost 2.5 times higher than in wastewater samples (2.50 ng/L).

CONCLUSIONS

The obtained results contributed to the previous two EU studies on the occurrence of perfluorinated compounds in Danube River water. The method, developed in this study, is capable to detecting perfluorobutane sulfonic acid (PFBS); perfluorooctane sulfonic acid (PFOS); perfluorooctane sulfonamide (PFOSA); perfluorobutyric acid (PFBA); perfluorohexanoic acid (PEHxA); perfluoroheptanoic acid (PFHpA); perfluorooctanoic acid (PFOA); perfluorononanoic acid (PFNA); perfluorodecanoic acid (PFDA); perfluoroundecanoic acid

(PFUnA); perfluorododecanoic acid (PFDoA). SPE technique was chosen for the clean-up step in the analytical procedures used for analysis of PFCs in water. The concentrations of PFOS were quite constant in the Danube River, while the concentrations of PFOA have been in decreasing trends probably as a consequence of strong restrictions on the use and import. Regarding the other investigated PFCs, although the data on their presence is still limited, the levels of occurrence were in stagnation or in slightly increase over time in the Danube River (*e.g.*, PFNA was quantified in average concentration of 1.00, 1.20 and 2.77 ng/L during JDS2,[26] JDS3[27] and in this study, respectively). There was no statistically significant difference between the mean values obtained for the PFCs in upstream and downstream water samples indicating that the discharge of wastewater from small-sized towns (Inđija, Stara Pazova and Nova Pazova, with total population of about 150.000) had not influenced the water quality.

SUPPLEMENTARY MATERIAL

Additional data and information are available electronically at the pages of journal website: https://www.shd-pub.org.rs/index.php/JSCS/article/view/11811, or from the corresponding author on request.

Acknowledgements. The parts of this investigation were obtained within the project no. 172050 supported by the Ministry of Education, Science and Technological Development of the Republic of Serbia. Biljana Škrbić would like to thank the Japanese Society for the Promotion of Science Fellow Program 2014 No. S-14034 for granting her fellowship to the University of Kitakyushu, Kitakyushu, Japan.

ИЗВОД

СЕЗОНСКЕ ПРОМЕНЕ У КОНЦЕНТРАЦИЈАМА ПЕРФЛУОРОВАНИХ ЈЕДИЊЕЊА У НЕПРЕЧИШЋЕНИМ ОТПАДНИМ И ПОВРШИНСКИМ ВОДАМА СРЕДЊЕГ ДЕЛА РЕКЕ ДУНАВ НА СЕВЕРУ СРБИЈЕ

МАЈА Б. БУЉОВЧИЋ[1], ИГОР С. АНТИЋ[1], KIWAO KADOKAMI[2] и БИЉАНА Д. ШКРБИЋ[1]

[1]Универзитет у Новом Саду, Технолошки факултет Нови Сад, Булевар цара Лазара 1, 21000 Нови Сад и [2]Institute of Environmental Science and Technology, University of Kitakyushu, Fukuoka, 808-0135, Kitakyushu, Japan

Сезонске промене у концентрацијама једанаест перфлуорованих једињења (PFCs) испитиване су у композитним узорцима површинске воде реке Дунав, узводно и низводно од места испуштања отпадних вода. Међу једанаест анализираних PFCs квантификовано је шест PFCs једињења (PFOA, PFOS, PFHxA, PFNA, PFDA и PFUnA) у дванаест испитиваних узорака. Највеће концентрације одређене су за PFOA и PFOS и то 14,9 ng/L (средња вредност 12,1 ng/L) и 14,2 ng/L (средња вредност 6,11 ng/L), редом, у поређењу са осталим испитиваним PFCs једињењима. Међутим, добијене концентрације PFOS током испитиваног периода узорковања биле су ниже од максимално дозвољених концентрација прописаних за реке, али су биле веће од граничних вредности концентрација (0,65 ng/L) за квалитет животне средине, прописаних Директивом европског парламента. Додатно, добијене концентрације за PFOA биле су неколико пута ниже од концентрација прописаних поменутом Директивом.

(Примљено 27. априла, ревидирано 24. јуна, прихваћено 18. јула 2022)

REFERENCES

1. J. C. G. Sousa, A. R. Ribeiro, M. O. Barbosa, M. F. R. Pereira, A. M. T. Silva, *J. Hazard. Mater.* **344** (2018) 146 (https://doi.org/10.1016/j.jhazmat.2017.09.058)
2. B. D. Škrbić, K. Kadokami, I. Antić, *Environ. Res.* **166** (2018) 130 (https://doi.org/10.1016/j.envres.2018.05.034)
3. M. Čelić, B. D. Škrbić, S. Insa, J. Živančev, M. Gros, M. Petrović, *Environ. Poll.* **262** (2020) 114244 (https://doi.org/10.1016/j.envpol.2020.114344)
4. S. Kurwadkar, J. Dane, S. R. Kanel, M. N. Nadagouda, R. W. Cawdrey, B. Ambade, G. C. Struckhoff, R. Wilkin, *Sci. Total Environ.* **809** (2022) 151003(https://doi.org/10.1016/j.scitotenv.2021.151003)
5. D. Negrete-Bolagay, C. Zamora-Ledezma, C. Chuya-Sumba, F. B. De Sousa, D. Whitehead, F. Alexis, V. H. Guerrero, J. *Environ. Manage.* **300** (2021) 113737 (https://doi.org/10.1016/j.jenvman.2021.113737)
6. F. Bacci, P. Campo, *Earth Syst. Environ.* **4** (2021) 247 (https://doi.org/10.1016/B978-0-12-819166-8.00038-4)
7. Y. Aminot, S. J. Sayfritz, K. V. Thomas, L. Godinho, E. Botteon, F. Ferrari, V. Boti, T. Albanis, M. Köck-Schulmeyer, M. S. Diaz-Cruz, M. Farré, D.Barceló, A. Marques, J. W. Readman, *Environ. Poll.* **252** (2019) 1301 (https://doi.org/10.1016/j.envpol.2019.05.133)
8. J. Bräunig, C. Baduel, A. Heffernan, A. Rotander, E. Donaldson, J. F. Mueller, *Sci.Total Environ*. **596**–**597** (2017) 360 (https://doi.org/10.1016/j.scitotenv.2017.04.095)
9. X. Bai, Y. Son, *Sci. Total Environ.* **751** (2021) 141622 (https://doi.org/10.1016/j.scitotenv.2020.141622)
10. V. P. Beškoski, S. Takemine, T. Nakano, L. Slavković Beškoski, G. Gojgić-Cvijović, M. Ilić, S. Miletić, M. Vrvić, *Chemosphere* **91** (2013) 1408 (https://doi.org/10.1016/j.chemosphere.2012.12.079)
11. J. Liang, L. Zhang, M. Ye, Z. Guan, J. Huang, J. Liu, L. Li, S. Huang, S. Sun, *J. Clean. Prod.* **265** (2020) 121839 (https://doi.org/10.1016/j.jclepro.2020.121839)
12. R. Ghisi, T. Vamerali, S. Manzetti, *Environ. Res.* **169** (2019) 326 (https://doi.org/10.1016/j.envres.2018.10.023)
13. M. Lorenzo, J. Campo, M. Farré, F. Pérez, Y. Picó, D. Barceló, *Sci. Total Environ.* **540** (2016) 191 (https://doi.org/10.1016/j.scitotenv.2015.07.045)
14. F. Pérez, M. Llorca, M. Köck-Schulmeyer, B. D. Škrbić, L. F. O. Silva, K. da Boit Martinello, N. A. Al-Dhabi, I. Antić, M. Farré, D. Barceló, *Environ. Res.* **135** (2014) 181 (http://dx.doi.org/10.1016/j.envres.2014.08.004)
15. *EWG*, https://www.ewg.org/research2014/pfcs-global-contaminants/pfoa-pervasive-pollutant-human-blood-are-other-pfcs (accessed 18 April 2022)
16. Directive 2013/39/EU of the European Parliament and of the Council of 12 August 2013 amending Directives 2000/60/EC and 2008/105/EC as regards priority substances in the field of water policy, *J. Eur. Union* 226 (**2013**) 1 (https://eur-lex.europa.eu/legal-content/EN/ALL/?uri=CELEX%3A32013L0039)
17. B. Göckener, A. Fliednerb, H. Rüdel, I. Fettig, J. Koschorreck, *Sci. Total Environ.* **782** (2021) 146825 (https://doi.org/10.1016/j.scitotenv.2021.146825)
18. B. Huerta, S. Rodriguez-Mozaz, C. Nannou, L. Nakis, A. Ruhi, V. Acuna, S. Sabater, D. Barcelo, *Sci. Total Environ.* **540** (2016) 241 (https://doi.org/10.1016/j.scitotenv.2015.05.049)
19. P. Schröder, B. Helmreich, B. D. Škrbić, M. Carballa, M. Papa, C. Pastore, Z. Emre, A. Oehmen, A. Langenhoff, M. Molinos, J. Dvarioniene, C. Huber, K. P. Tsagarakis, E.

Martinez-Lopez, S. Meric Pagano, C. Vogelsang, G. Mascolo, *Environ. Sci. Pollut. Res.* **23** (2018) 12835 (https://doi.org/10.1007/s11356-016-6503-x)
20. I. Natchkov, Case Study IX – (1997) WHO/UNEP ISBN 0 419 22910 8
21. M. Babić Mladenović, M. Radovanović, P. Radosavljević, *Water Resour. Manage.* **3** (2013) 3 (https://www.wrmjournal.com/index.php/wrm/article/download/47/47)
22. H. T. Duong, K. Kadokami, H. Shirasaka, R. Hidaka, H. T. C., L. Kong, T. Q. Nguyen, T. T. Nguyen, *Chemosphere* **122** (2015) 115 (https://doi.org/10.1016/j.chemosphere.2014.11.025)
23. M. Onghena, Y. Moliner-Martinez, Y. Picó, P. Campíns-Falcó, D. Barceló, *J. Chromatogr., A* **1244** (2012) 88 (https://doi.org/10.1016/j.chroma.2012.04.056)
24. J. S. McLachlan, J. J. Hellmann, M. W. Schwartz, *Conserv. Biol*. **2** (2007) 297 (https://doi: 10.1111/j.1523-1739.2007.00676.x. PMID: 17391179)
25. K. S. Guruge, S. Taniyasu, N. Yamashita, P. M. Manage, *Mar. Pollut. Bull.* **54** (2007) 1667 (https://doi.org/10.1016/j.marpolbul.2007.05.021)
26. JDS2, Joint Danube Survey 2, Final Scientific Report, ICPDR—International Commission for the Protection of the Danube River /Permanent Secretariat Vienna International Centre, D0412 P. O. Box 500, 1400 Vienna / Austria, 2008 (accessed 15 April 2022)
27. JDS3, Joint Danube Survey 3, A Comprehensive Analysis of Danube Water Quality, ICPDR—International Commission for the Protection of the Danube River / Permanent Secretariat Vienna International Centre, D0412 P. O. Box 500, 1400 Vienna / Austria, 2015 (accessed 15 April 2022)
28. H. Fiedler, T. Kennedy, B. J. Henry, *Integr. Environ. Assess. Manage.* **17** (2019) 331 (https://doi.org/10.1002/ieam.4352)
29. M. Lorenzo, J. Campo, M. Farré, F. Pérez, Y. Picó, D. Barceló, *Sci. Total Environ.* **540** (2016) 191 (https://doi.org/10.1016/j.scitotenv.2015.07.045)
30. T. G. Schwanz, M. Llorca, M. Farré, D. Barceló, *Sci. Total Environ.* **539** (2016) 143 (https://doi.org/10.1016/j.scitotenv.2015.08.034)
31. D. Skutlarek, M. Exner, H. Farber, *Environ. Sci. Pollut. Res. Int.* **13** (2006) 299 (https://doi.org/10.1065/espr2006.07.326).

Journal of the Serbian Chemical Society
JSCS@tmf.bg.ac.rs • www.shd.org.rs/JSCS
J. Serb. Chem. Soc. *87* (12) S488–S498 (2022) *Supplementary material*

SUPPLEMENTARY MATERIAL TO

Temporal trend of perfluorinated compounds in untreated wastewater and surface water in the middle part of the Danube River belonging to the northern part of Serbia

MAJA B. BULJOVČIĆ[1#], IGOR S. ANTIĆ[1#], KIWAO KADOKAMI[2] and BILJANA D. ŠKRBIĆ[1]*

[1]*University of Novi Sad, Faculty of Technology Novi Sad, Bulevar cara Lazara 1, 21000 Novi Sad, Serbia and* [2]*Institute of Environmental Science and Technology, University of Kitakyushu, Fukuoka, 808-0135Kitakyushu, Japan*

J. Serb. Chem. Soc. *87* (12) (2022) 1425–1437

SAMPLING SITES AND SAMPLE COLLECTION

Sampling was carried out during November and at the beginning of December 2014. A qualified and well-trained person, from the public water management company "Vode Vojvodine" Novi Sad, collected the wastewater samples and surface water samples from the Danube River.[21] The wastewater discharge point is located on the bank of the Danube flow between Novi Sad (the second largest town in Serbia) and Belgrade (the capital of Serbia). It has been used to discharge the municipality wastewater, collected from four towns (Inđija, Stara Pazova, Nova Pazova and Batajnica, with approximately 150000 inhabitants in total) and from small villages located in that area, without any pre-treatment directly into the Danube River (Fig. S-1).

Surface water was sampled from a boat with a 1 L polyethylene (PE) bottle previously washed with methanol¸ ultra-pure water and with the sample. The bottles containing water samples were kept in an ice-box, transported to a laboratory and analyzed immediately after receiving. Field blanks were collected by filling the laboratory water (Milli-Q) from the field blank bottle into the sampling device, letting it stand for 5 min, and then transferring this water back to the field blank bottle.

CHEMICALS AND STANDARDS

In the present study the following surrogate standards (SS): perfluoro-n--[1,2,3,4,5-$^{13}C_5$] pentanoic acid (M5PFPeA), perfluoro-n-[1,2,3,4,6-$^{13}C_5$] hexanoic acid (M5PFHxA), perfluoro-n-[1,2,3,4-$^{13}C_4$]-heptanoic acid (M4PFHpA),

* Corresponding author. E-mail: biljana@tf.uns.ac.rs

perfluoro-n-[$^{13}C_8$]-octanoic acid (M8PFOA), perfluoro-n-[$^{13}C_9$]-nonanoic acid (M9PFNA), perfluoro-n-[1,2,3,4,5,6-$^{13}C_6$]-decanoic acid (M6PFDA), perfluoro-n-[1,2,3,4,5,6,7-$^{13}C_7$]-undecanoic acid (M7PFUnA), sodium perfluoro-1 [1,2,3-$^{13}C_3$]-hexane sulfonate (M3PFHxS); and nine internal standards (IS): perfluoro-n-[1,2,3,4-$^{13}C_4$]-butanoic acid ([$^{13}C_4$]-PFBA), perfluoro-n-[1,2-$^{13}C_2$]-hexanoic acid ([$^{13}C_2$]-PFHxA), perfluoro-n-[1,2,3,4,-$^{13}C_4$]-octanoic acid ([$^{13}C_4$]-PFOA), perfluoro-n-[1,2,3,4,5-$^{13}C_5$]-nonanoic acid ([$^{13}C_5$]-PFNA), perfluoro-n-[1,2-$^{13}C_2$]-decanoic acid ([$^{13}C_2$]-PFDA), perfluoro-n-[1,2-$^{13}C_2$]-undecanoic acid ([$^{13}C_2$]-PFUnA), perfluoro-n-[1,2,$^{13}C_2$]-dodecanoic acid ([$^{13}C_2$]-PFDoA), sodium perfluoro-1-hexane-[$^{18}O_2$]-sulfonate ([$^{18}O_2$]-PFHxS), sodium perfluoro-1-[1,2,3,4-$^{13}C_4$]-octane sulfonate ([$^{13}C_4$]-PFOS) obtained from Wellington Laboratories (Guelph, Ontario, Canada) were used.

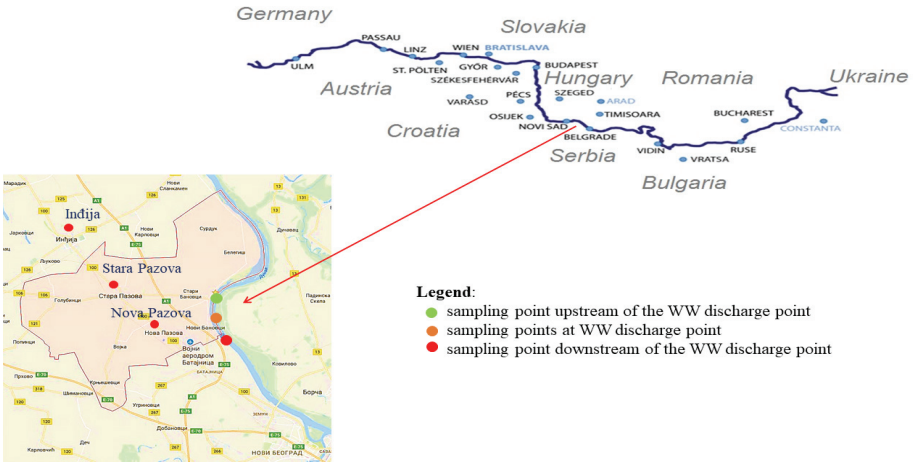

Fig. S-1. Map of sampling locations.

SAMPLE EXTRACTION

Briefly, water samples (500 mL of SW and 300 mL for WW) were filtered through 0.22 μm fiberglass filters (GF/F), previously pre-conditioned with 10 mL of methanol and 10 mL ultra-pure water. Before filtration, the samples were spiked at the 10 ng/L level with surrogate standards (SSs listed in Section S-1 Chemicals and standards). 20 μL of SSs working solutions of 250 ng/mL and 150 ng/mL were used for spiking the SW and WW samples, respectively for achieving a 10 ng/L concentration of SSs in SW and WW. All samples were extracted by SPE with Oasis HLB cartridges. The SPE cartridges were first preconditioned by passing 5 mL of methanol and 10 mL of ultra-pure water at a flow rate of 10 mL/min. The samples were loaded onto SPE cartridges at a flow rate of 10 mL/min. The cartridges were rinsed with 3 mL of ultra-pure water at a flow rate 10 mL/min, and the cartridges were dried for 30 min using nitrogen at

0.6 bar. Elution was performed with 5 mL of methanol at a flow rate 3 mL/min. Evaporation of the extracts to the final volume of 500 µL was performed at a temperature of 35 °C in a gentle nitrogen stream.

INSTRUMENTAL ANALYSIS

The concentrations of PFCs were obtained by Thermo ultra-high-performance liquid chromatography (UHPLC) coupled with a Thermo TSQ Vantage triple quadrupole mass spectrometer (MS/MS). Separation of analytes was achieved using an injection volume of 10 µL of a sample on a Hypersil GOLD^{TM} (50×2.1 mm i.d. 1.9 µm) column (Thermo Fisher Scietific) at 25 °C. A flow rate of 0.35 mL/min was used and the gradient was composed of eluent A containing water/acetic acid (99:1, v/v), and eluent B containing of methanol/acetic acid (99:1, v/v). Eluent A contained 10 mM ammonium acetate, while eluent B contained 5 mM ammonium acetate. The gradient program started with 2 % B for 1 min. Then, the linear gradient was programmed up to 20 % B for 4 min.; to 50 % B for 3 min, to 98 for 2 min and maintained for 2 min. Finally, the gradient was returned to initial conditions 2 % B (0.5 min) and maintained for 2.5 min. in order to re-equilibrate the column. The MS/MS system equipped with HESI was operated in negative ionization mode. The parameters of the ion source were as follows: spray voltage: 3.4 kV, vaporizer temperature: 350 °C, sheath gas pressure: 40 arbitrary units, auxiliary gas pressure: 10 arbitrary units, and capillary temperature: 270 °C. Conditions for target Selected Reaction Monitoring (SRM) analysis are given in Table S-II. Ionization and mass spectrometric conditions were optimized by direct continuous pump infusion of 5 µg/mL standard solution of each tested compound dissolved in the initial mobile phase (98% of A and 2 % of B phase) into the mass spectrometer using a syringe pump at a flow rate of 10-20 µL/min. Data acquisition was performed initially in full scan to determine an abundant precursor ion. Next, the MS/MS fragmentation conditions were investigated and collision energies and S-lens voltage were optimized for all studied compounds and their transitions. Fragmentation reactions were done in SRM by choosing the optimum voltage of collision energies for selected compounds. Ultra high-purity argon (Ar) was used as collision gas. Two product ions were measured for precursor ion: one was used as the quantifier ion (SRM1) and the other was used as the qualifier ion (SRM2). In SRM mode, a mass resolution of 0.7 Da full width at half maximum (FWHM) was set on the first (Q1) and the third (Q3) quadrupole and scan width of 0.5 m/z were used. Instrument control and data collection were handled by computer equipped with Xcalibur 2.1.0 (Thermo Fisher Scientific, USA). For determination of SRM1/SRM2 signal transition ratios were used TraceFinder 3.1 (Thermo Fisher Scientific, USA).

Table S-I. Sampling frequency

Day	Date	Number of samples	Sample label (date+ sampling day + U/D)
WED	12-nov	3	12.11.3.-U*, 12.11.3.-D*, 12.11.14.-WW
THU	20-nov	2	20.11.5-U, 20.11.5-D
FRI	21-nov	3	21.11.6-U, 21.11.6-D, 21.11.14-WW
TUE	25-nov	2	25.11.8-U, 25.11.8-D
WED	26-nov	1	26.11.14.-WW
THU	27-nov	3	27.11.10-U, 27.11.10-D, 27.11.14-WW
FRI	28-nov	1	28.11.14.-WW
TUE	29-nov	3	29.11.12-U, 29.11.12-D, 29.11.14-WW
SAT	30-nov	1	30.11.14.-WW
MON	1-dec	1	01.12.14.-WW

*U -upstream, D - downstream, WW - wastewater

Table S-II. Instrument parameters

TSQ Vantage Triple Quadrupole UHPLC-MS/MS									
Column	Hypersil GOLDTM (50 mm x 2.1 mm i.d., 1.9 μm)								
Column temperature, °C	25								
Mobile phase	A: 10 mM annmonium accetate								
	B: Methanol 5 mM ammonium acetate								
Gradient profile	Time, min	0	1	5	8	10	12	12.5	15
	B mobile phase composition (%)	2	2	20	50	98	98	2	2
Flow rate:	500 μL/min								
Injection volume;	10 μL								
Ion source parameters ionization $ESI^{(-)}$									
Spray voltage:	3.4 kV								
Vaporizer temperature:	350 °C								
Sheath gas pressure:	40 arbitrary units								
Auxiliary gas pressure:	10 arbitrary units								
Capillary temperature:	270 °C								

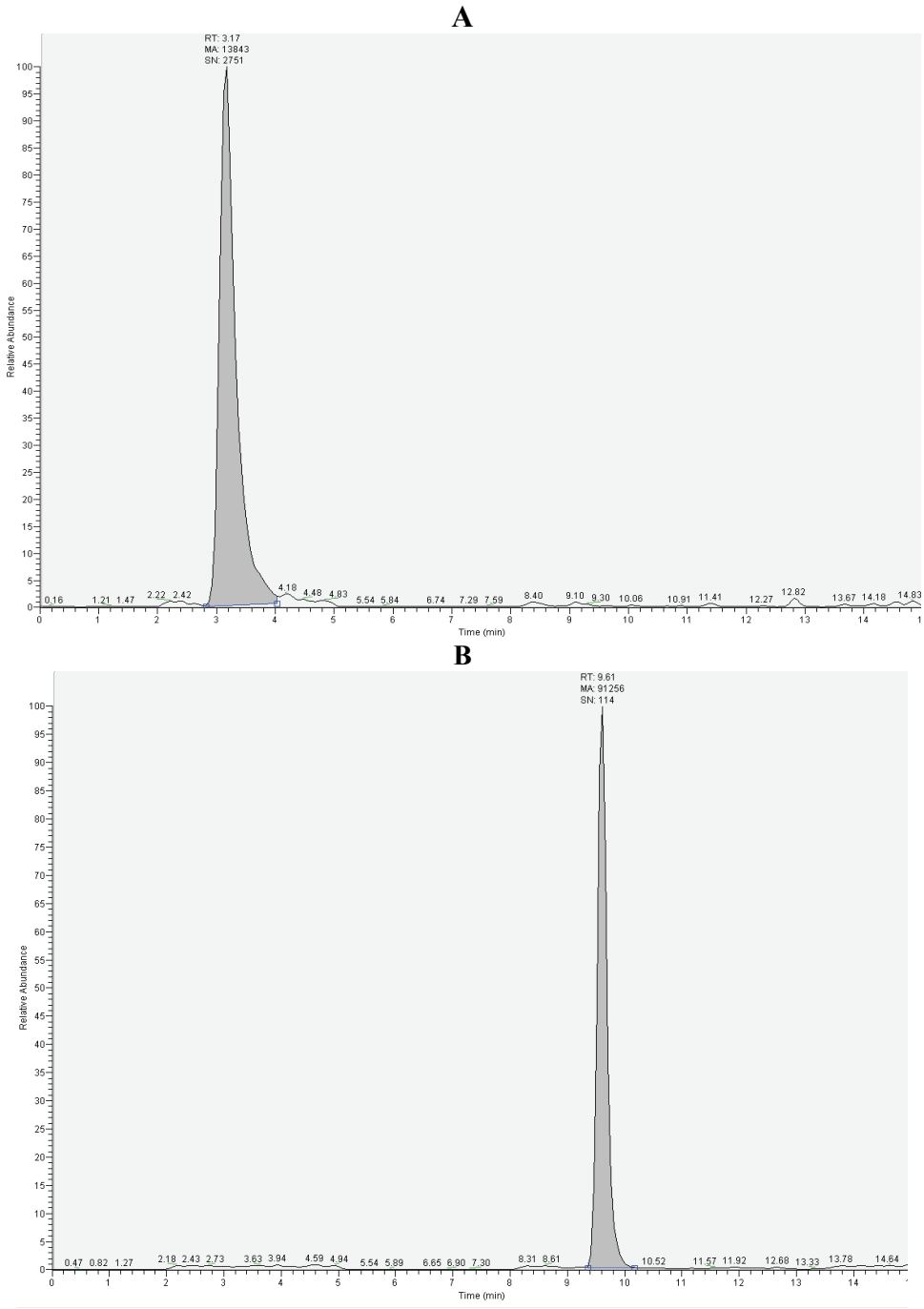

Fig. S-2. Chromatograms A: PFBA, B: PFHxA

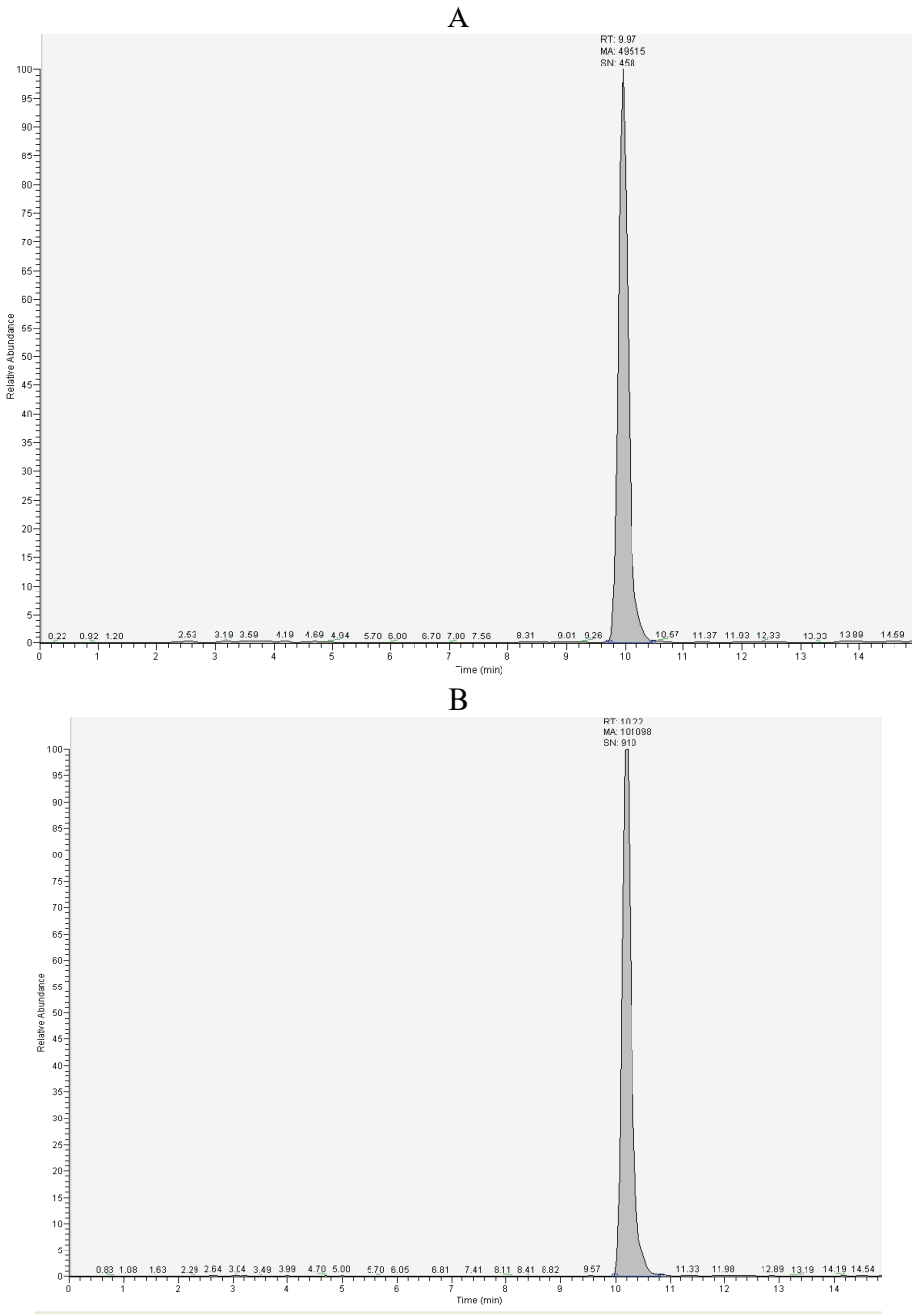

Fig. S-3. Chromatograms of A: PFHpA, B: PFOA

A

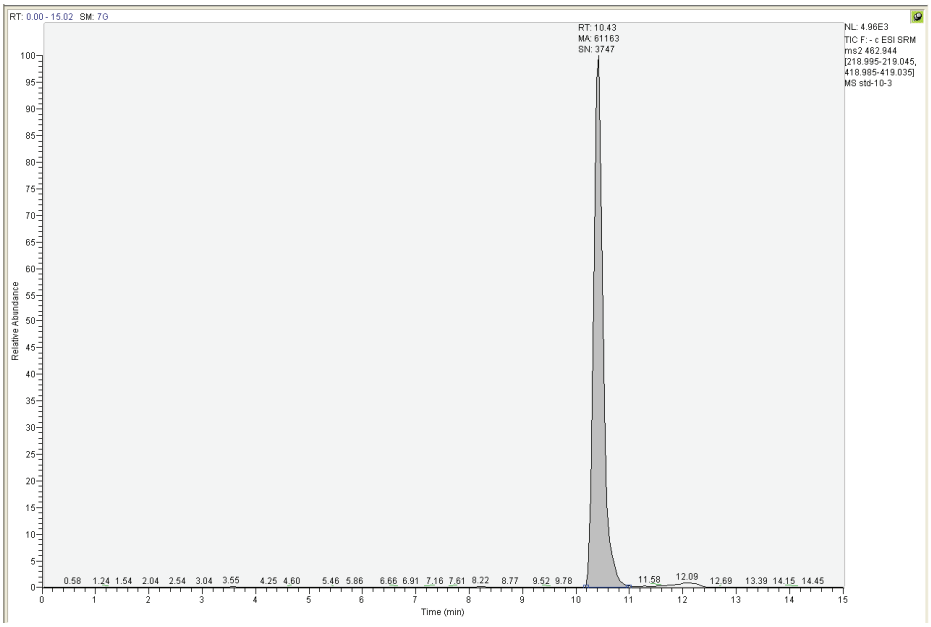

B

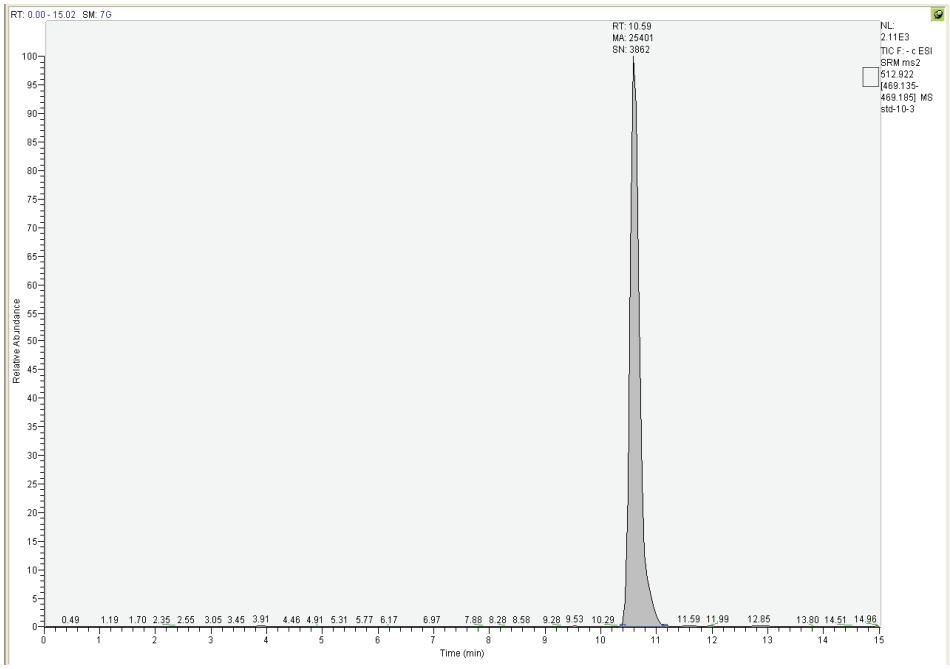

Fig. S-4. Chromatograms of A: PFNA, B: PFDA

A

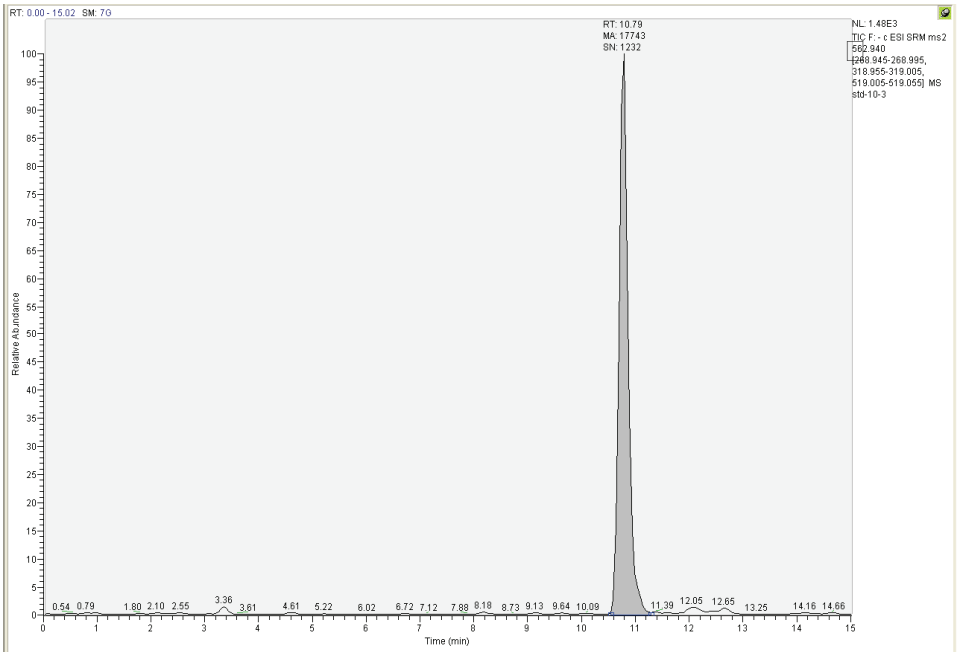

B

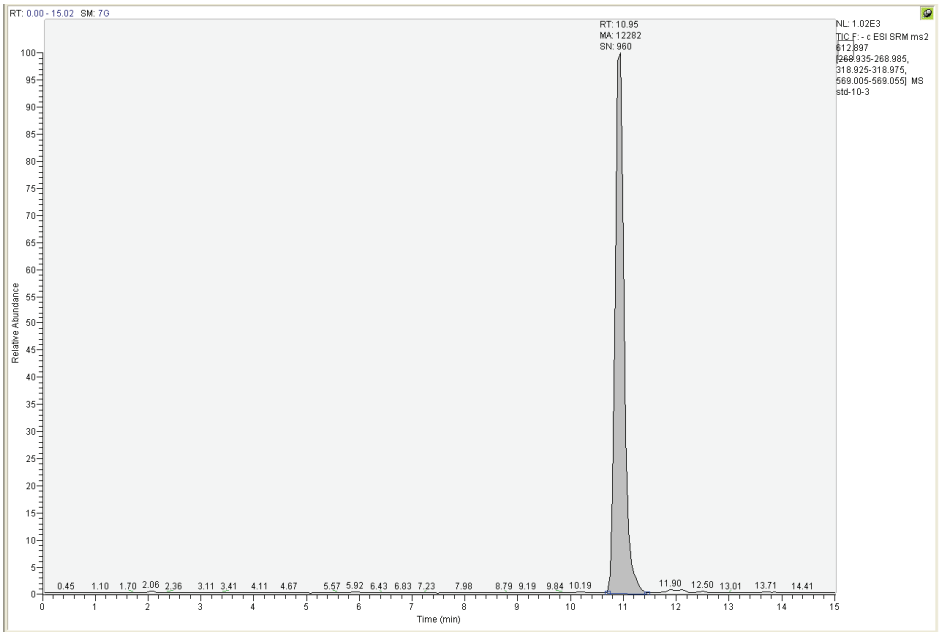

Fig. S-5. Chromatograms of A: PFUnA, B: PFDoA

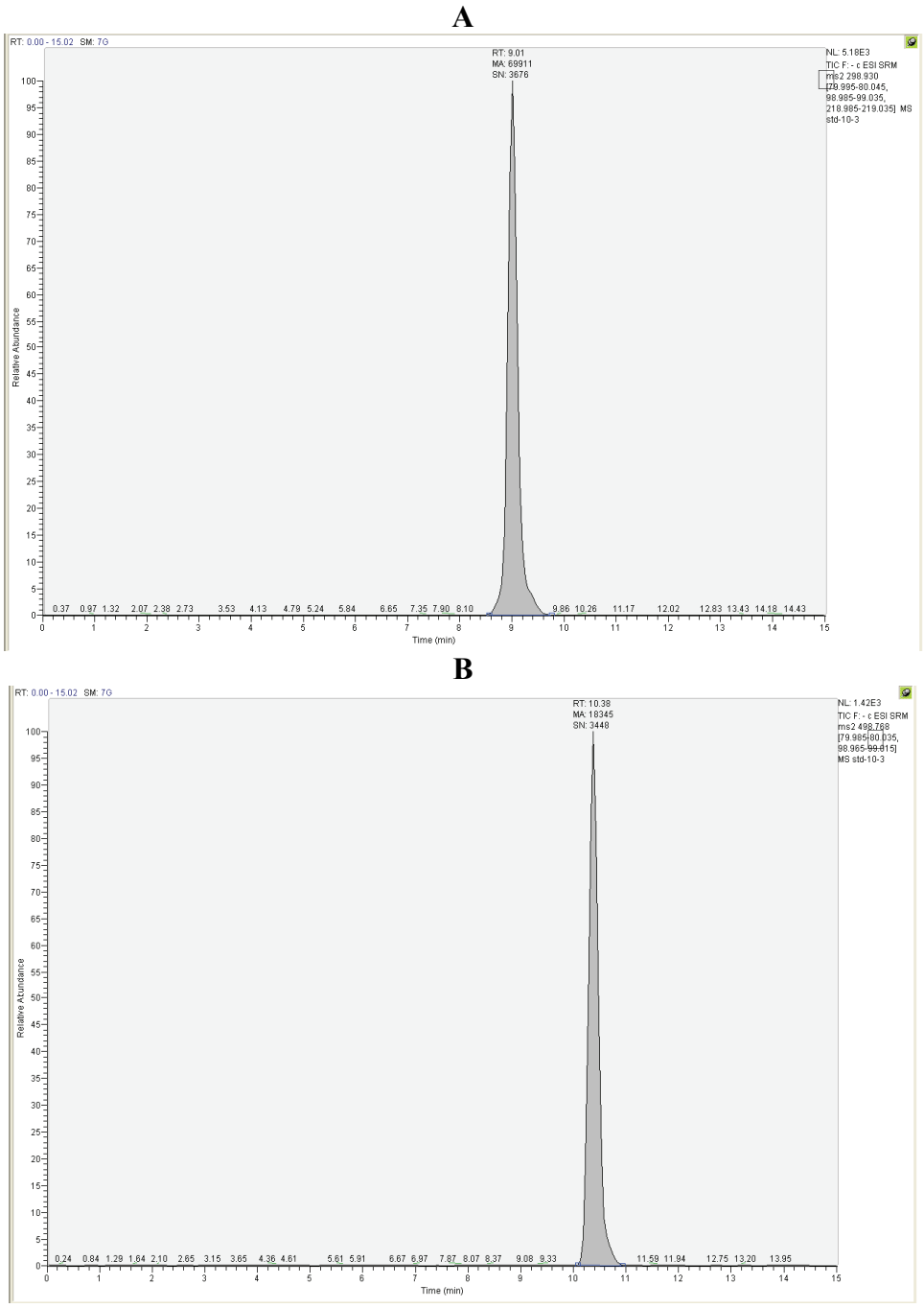

Fig. S-6. Chromatograms of A: PFBS B: PFOS

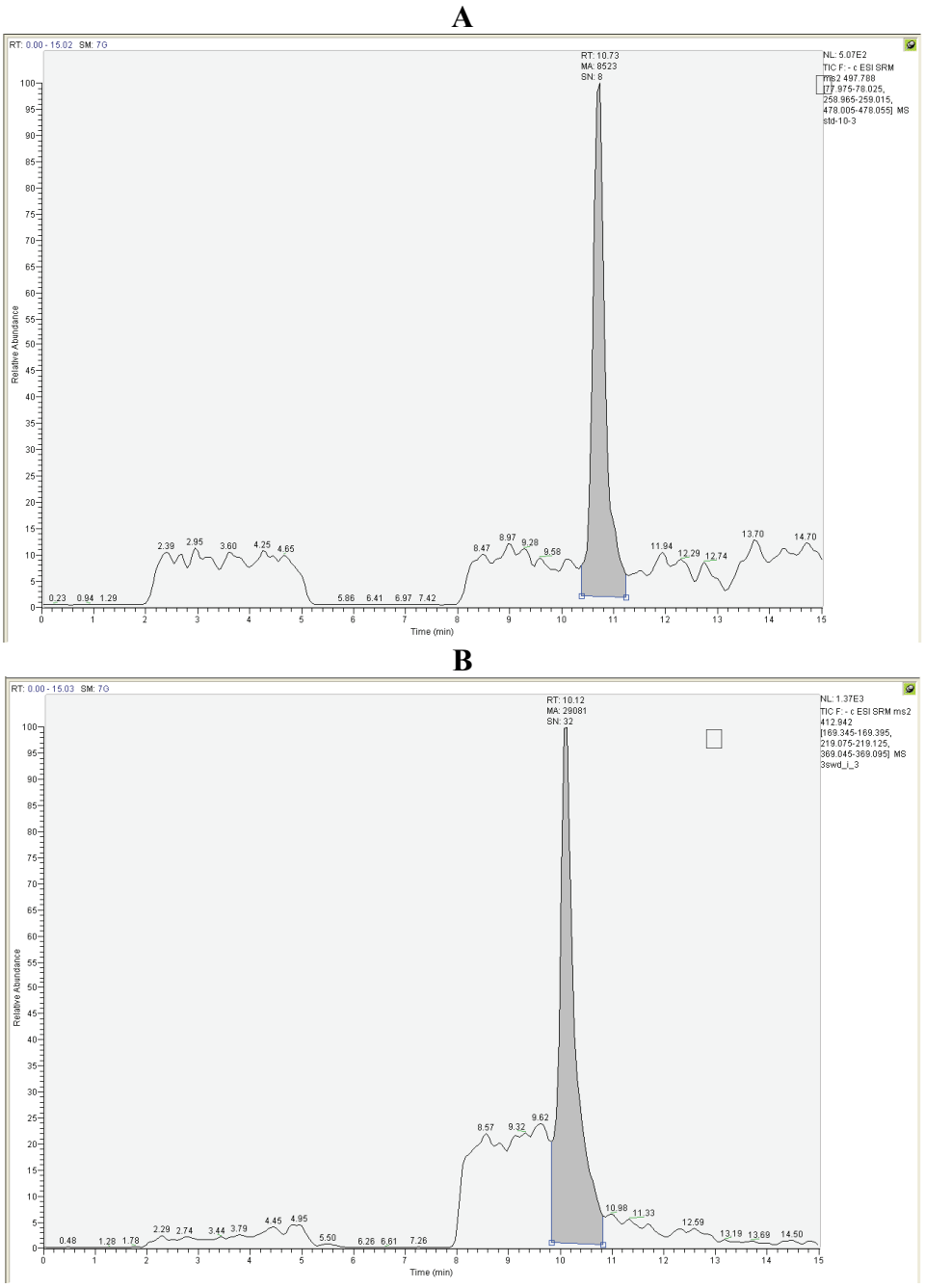

Fig. S-7. Chromatograms of A: PFOSA B: PFOA-12.11.3-D

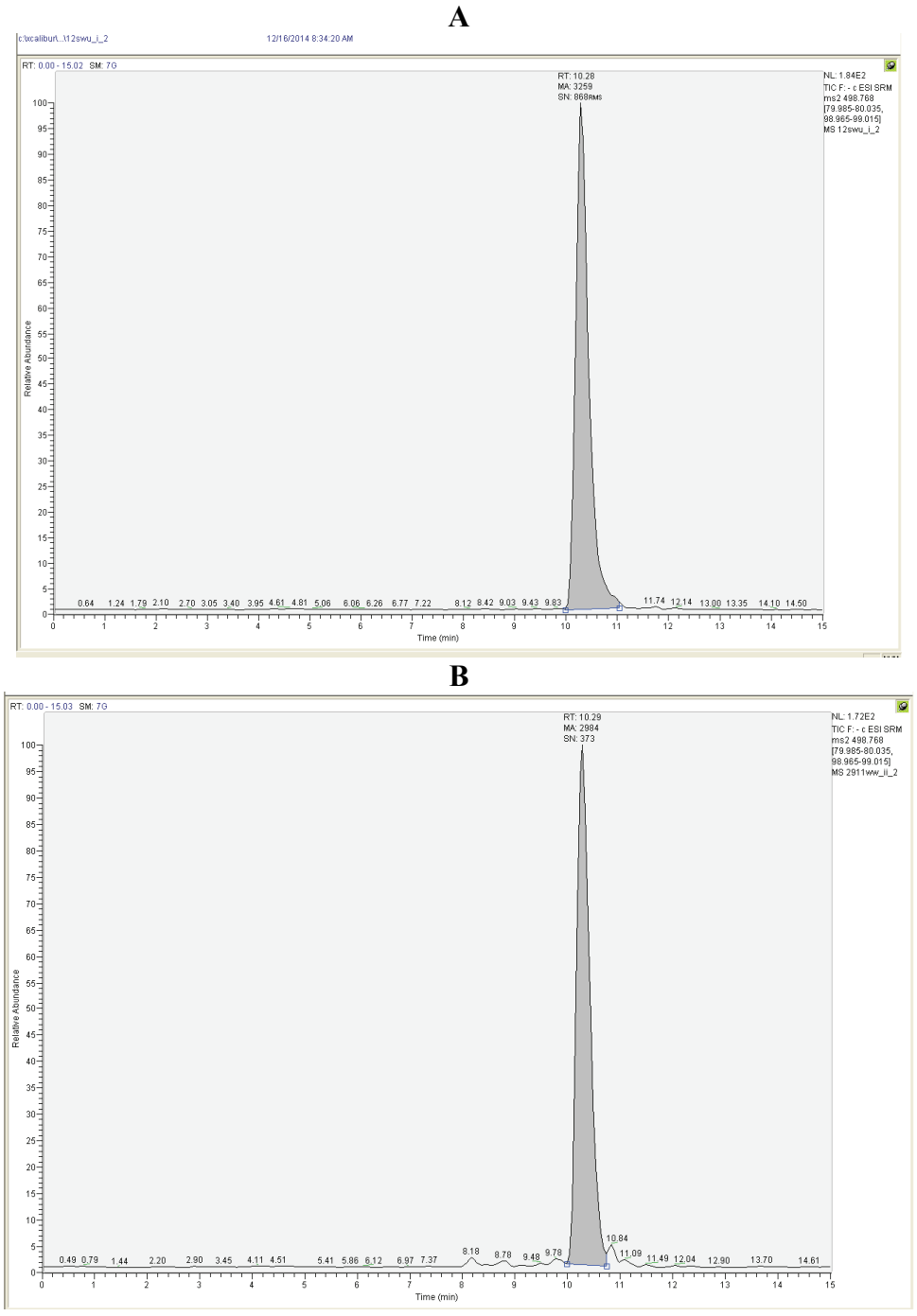

Fig. S-8. A: PFOS-29.11.12-U, B: PFOS-29.11.14.WW.

Journal of the Serbian Chemical Society
JSCS-info@shd.org.rs • www.shd.org.rs/JSCS
J. Serb. Chem. Soc. *87* (12) 1439–1446 (2022)
JSCS–5605
Letter to the Editor
Published 16 September 2022

LETTER TO THE EDITOR

25 years of NICS – much more than nothing![•]

RALPH PUCHTA[1-3]*, SLAĐANA ĐORĐEVIĆ[4#], SLAVKO RADENKOVIĆ[4**#], HAIJUN JIAO[5] and NICO J. R. VAN EIKEMA HOMMES[1]

[1]Computer Chemistry Center, Department of Chemistry and Pharmacy, University of Erlangen-Nuremberg, Nägelsbachstr. 25, 91052 Erlangen, Germany, [2]Inorganic Chemistry, Department of Chemistry and Pharmacy, University of Erlangen-Nuremberg, Egerlandstr. 1, 91058 Erlangen, Germany, [3]Central Institute for Scientific Computing (ZISC), University of Erlangen-Nuremberg, Martensstr. 5a, 91058 Erlangen, Germany, [4]University of Kragujevac, Faculty of Science, Radoja Domanovića 12, 34000 Kragujevac, Serbia and [5]Leibniz-Institut für Katalyse e.V., Albert-Einstein-Str. 29a, Rostock, 18059 Germany

(Received 3 December 2021, revised 21 June, accepted 6 July 2022)

Abstract: The famous aromaticity index NICS (nucleus independent chemical shift) was introduced 25 years ago. The authors use this anniversary for a short and to some degree personal retrospective.

Keywords: aromaticity; history; anniversary.

In 1996 Paul von Ragué Schleyer and his team published a new index for aromaticity based on gauge-independent atomic orbital (GIAO) NMR-calculations called nucleus independent chemical shift (NICS).[1] The abbreviation NICS is a pun with the colloquial German word for nothing – "Nix", as to obtain NICS values one can calculate chemical shift at any place, in the space around a molecule, using a ghost atom – more or less nothing.

NICS values had been the enhancement of earlier NMR-calculation to evaluate aromaticity based on Li^+ or He-atoms.[2–6] Both nuclei interact with the system that shall be investigated. A ghost atom is not interacting and the awareness that one can calculate chemical shifts independently from a nucleus anywhere around a molecule was a milestone in investigating aromaticity. That NICS is a scientific bonanza one can easily see in the number of current citations obtained from the Web of Science database.[7] The original NICS manuscript from 1996[1] was cited

*,** Corresponding authors. E-mail: (*)ralph.puchta@fau.de; (**)slavkoradenkovic@kg.ac.rs
Serbian Chemical Society member.
• Dedicated to the memory of Paul von Ragué Schleyer (1930–2014) and all scientists who profited from the application of NICS.
https://doi.org/10.2298/JSC211203057P

around 4500 times in November 2021 and in the review[8] published by Paul von Ragué Schleyer, around 10 years later, more than 2300 times. Of course, in 1996 there was only the "nativity" of NICS, before Schleyer and his team nurtured that idea. Already in summer 1995 Schleyer reported at the 8th International Symposium on Novel Aromatic Compounds (ISNA-8) in Braunschweig, Germany, about this new upcoming method. The first publication applying NICS[9] appeared in 1996, but already in February, around half a year before the well-known method paper was published.*

What makes NICS so precious and useful? Why are scientists all over the world attracted by NICS? Surely a very striking argument is the simplicity of application. A NMR-calculation based on a structure extended by one or more ghost atoms is simple to do and the results are easy to analyze, as the resulting shielding only has to be multiplied by –1, and with straightforward interpretation. No reference systems are necessary, one calculation can extend the knowledge of the investigated system significantly, independently if organic or inorganic. Adopting Schleyer's color scheme a red ball shows aromaticity and a green ball anti-aromaticity. If the ball is tiny (values between –5 and 5) than one has no aromatic influences at all (Fig. 1).

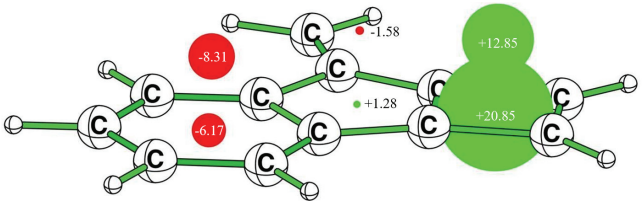

Fig. 1. 7-Methylene-7*H*-cyclobuta[*a*]indene. The NICS and geometry were calculated at the B3LYP/6-311+G** level of theory.

This simple concept allows to understand the nature of individual rings in polycyclic systems (see, *e.g.*, Fig. 1) and is therefore extremely useful in understanding fullerenes, nanotubes or graphenes. A striking example for a better understanding of graphenes, and an impressive support for Clar's picture of aromatic π-sextets in polycyclic aromatic hydrocarbons (PAHs), is the work of Schleyer and team, demonstrating that only rings were all carbon atoms are members of a single sextet show high NICS values, compared to rings having migrating π-sextets and showing intermediate values. This leads to clearly differentiable Clar sextet ring patterns and makes the concept of Clar more concrete.[10]

The possibilities of NICS inspired other teams to get new, unexpected but absolutely impressive ideas in their research. Perhaps the most striking was an idea of Klod and Kleinpeter,[11–13] they used NICS points around interesting

* The submission of the NICS-method paper was exactly 168 years after the famous letter from Friedrich Wöhler to Jens Jacob Berzelius reporting his unintentional preparation of urea.

molecules and structural motives to plot the "iso-chemical-shielding surfaces" (ICSS) investigating through space NMR shieldings and making them visible.[14] It is worth mentioning that an analogous one-dimensional approach, also known as the NICS-scan method, is widely addopted.[15]

More straightforward was the concept of separating π- and σ-influences of the NICS values in order to get dissected NICS values. The first idea was to apply the Pipek–Mezey localization procedure (LMO-NICS)[16] which was successfully applied and taught that NICS(0) shows great influences of the σ-system.[17,18] Unluckily the formalism of Pipek and Mezey has some shortcomings, *e.g.*, that the strict σ–π separation is only applicable for planar molecules.[16] Therefore, alternative methods were developed to separate the influences, like the concept of Corminboeuf *et al.*, to calculate dissected NICS of selected canonical molecular orbitals resulting in NICSπ.[19] An alternative dissection concept is based on individual canonical molecular orbital (CMO) contributions to the magnetic shielding of the atoms. These CMO-NICS contributions allow additional insights to the results of the localized MO based dissected NICS (LMO-NICS).[20] Another CMO-NICS concept utilizes natural bond orbitals (NBOs).[21]

An alternative concept to a more detailed understanding of NICS, beside σ- and π-influences, is to analyze the tensors of NICS. While by definition NICS*xx* and NICS*yy* are in the ring's plain NICS*zz* is perpendicular and can give values unhampered by the in-plain effects easily.

While these examples show nicely why NICS is interesting for theoretical considerations, but why is NICS so fascinating for practical chemistry? The convenience while applying NICS (*vide supra*) certainly is a very big advantage, especially in combination with a probe not altering the system. The other huge plus for NICS is the wide range of application in organic,[22–30] inorganic,[31–35] metal clusters,[36–38] carbon-materials,[39–41] supramolecular chemistry,[42–45] bio-related chemistry,[46–49] porphyrin chemistry,[50–53] chemistry of taylor-made properties,[54] polymer chemistry,[55,56] *etc.* and these topics can again be divided into sub topics, *e.g.*, in organic chemistry like reaction mechanism with aromatic transition states,[8,57,58] Möbius[59–61] and Craig–Möbius[62–65] aromatic systems, chelate systems[66] or to metalla aromatic systems,[65,67–69] only to list the most prominent examples. Along these lines, it is worth mentioning that some of the present authors have been part of Schleyer's research group when the very first papers were published on NICS, describing its definition and possibilities of its applications[1,2,9,17] Some of the authors contributed significantly to further NICS envelopment and to its promotion among the broader chemical community.[8,18,61] What authors of this paper have in common is that all of us actively use the NICS in our research, and the topics range from organic[26–30,70–73] and inorganic molecules,[33,34] metal clusters,[37,38] supramolecular chemistry,[44,45] mechanistic studies[8,58] and bio-related molecules.[46–49,74]

The simplicity of NICS-calculations can be a curse, too. Of course, NICS has also some clear shortcomings that should not be.[75] While NICS correlates very well with the other criteria for aromaticity like aromatic stabilization energy, other magnetic criteria[70] or structure,[76,77] it is not a method applicable without critical intelligence, as impressively pointed out by recent publications.[78–80] The reasons are manifold from conceptual shortcomings, via contribution of different effects or the tendency to overinterpretation of data, *e.g.*, to make quantitative statements about aromaticity. That NICS has restrains was obvious for Schleyer and his team and so they stated in the concluding remarks of their review from 2005[8] "the limitations of NICS must also be appreciated." After they had given a view sentence above some assisting hints how to handle NICS. But have all persons applying NICS read that part?

What can we expect in the next 25 years? NICS had turned out to be a Swiss army knife for investigating aromaticity. Beside its shortcomings and limitations, it will surely continue being a robust craftsman tool for exploring aromaticity abreast with structural criteria and the different ways to calculate aromatic stabilization energy. One can expect that NICS will also find additional applications, as recently demonstrated as a criterion for the design of new antifungal benzofuranones[81] and in the modelling of antioxidative capacity of phenolic compounds.[74] May be NICS will one day be a common tool included in QSAR studies or any other fascinating application.

Ad multos annos, NICS!

ИЗВОД

25 ГОДИНА NICS – МНОГО ВИШЕ ОД НИЧЕГА!

RALPH PUCHTA[1-3], СЛАЂАНА ЂОРЂЕВИЋ[4], СЛАВКО РАДЕНКОВИЋ[4], HAIJUN JIAO[5] и NICO J. R. VAN EIKEMA HOMMES[1]

[1]Computer Chemistry Center, Department of Chemistry and Pharmacy, University of Erlangen-Nuremberg, Nägelsbachstr. 25, 91052 Erlangen, Germany, [2]Inorganic Chemistry, Department of Chemistry and Pharmacy, University of Erlangen-Nuremberg, Egerlandstr. 1, 91058 Erlangen, Germany, [3]Central Institute for Scientific Computing (ZISC), University of Erlangen-Nuremberg, Martensstr. 5a, 91058 Erlangen, Germany, [4]Универзитет у Крагујевцу, Природно-математички факултет, 34000 Крагујевац и [5]Leibniz-Institut für Katalyse e.V., Albert-Einstein-Str. 29a, Rostock, 18059 Germany

Познати индекс ароматичности NICS је уведен пре 25 година. Аутори користе прилику да ову годишњицу искористе за кратку и делом личну ретроспективу.

(Примљено 3. децембра 2021, ревидирано 21. јуна, прихваћено 6. јула 2022)

REFERENCES

1. P. von R. Schleyer, C. Maerker, A. Dransfeld, H. Jiao, N. J. R. van Eikema Hommes, *J. Am. Chem. Soc.* **118** (1996) 6317 (https://doi.org/10.1021/ja960582d)
2. H. Jiao, P. von R. Schleyer, Y. Mo, M. A. McAllister, T. T. Tidwell, *J. Am. Chem. Soc.* **119** (1997) 7075 (https://doi.org/10.1021/ja970380x)

3. M. Saunders, H. A. Jiménez-Vázquez, R. J. Cross, S. Mroczkowski, D. I. Freedberg, F. A. L. Anet, *Nature* **367** (1994) 256 (https://doi.org/10.1038/367256a0)
4. M. Buehl, W. Thiel, H. Jiao, P. v. R. Schleyer, M. Saunders, F. A. L. Anet, *J. Am. Chem. Soc.* **116** (1994) 6005 (https://doi.org/10.1021/ja00092a076)
5. M. Bühl, A. Hirsch, *Chem. Rev.* **101** (2001) 1153 (https://doi.org/10.1021/cr990332q)
6. E. Shabtai, A. Weitz, R. C. Haddon, R. E. Hoffman, M. Rabinovitz, A. Khong, R. J. Cross, M. Saunders, P.-C. Cheng, L. T. Scott, *J. Am. Chem. Soc.* **120** (1998) 6389 (https://doi.org/10.1021/ja9805831)
7. *Web of Science online database*, https://www.webofscience.com
8. Z. Chen, C. S. Wannere, C. Corminboeuf, R. Puchta, P. von R. Schleyer, *Chem. Rev.* **105** (2005) 3842 (https://doi.org/10.1021/cr030088+)
9. P. v. R. Schleyer, H. Jiao, H. M. Sulzbach, H. F. Schaefer, *J. Am. Chem. Soc.* **118** (1996) 2093 (https://doi.org/10.1021/ja953126i)
10. D. Moran, F. Stahl, H. F. Bettinger, H. F. Schaefer, P. v. R. Schleyer, *J. Am. Chem. Soc.* **125** (2003) 6746 (https://doi.org/10.1021/ja034497z)
11. S. Klod, E. Kleinpeter, *J. Chem. Soc., Perkin Trans. 2* (2001) 1893 (https://doi.org/10.1039/B009809O)
12. S. Klod, A. Koch, E. Kleinpeter, *J. Chem. Soc., Perkin Trans. 2* (2002) 1506 (https://doi.org/10.1039/B204629F)
13. E. Kleinpeter, S. Klod, *J. Mol. Struct.* **704** (2004) 79 (https://doi.org/https://doi.org/10.1016/j.molstruc.2003.12.062)
14. E. F. Kleinpeter, A. Koch, *ARKIVOC* **2012** (2011) 94 (https://doi.org/10.3998/ark.5550190.0013.510)
15. A. Stanger, *J. Org. Chem.* **71** (2006) 883 (https://doi.org/10.1021/jo051746o)
16. J. Pipek, P. G. Mezey, *J. Chem. Phys.* **90** (1989) 4916 (https://doi.org/10.1063/1.456588)
17. P. von R. Schleyer, H. Jiao, N. J. R. van E. Hommes, V. G. Malkin, O. L. Malkina, *J. Am. Chem. Soc.* **119** (1997) 12669 (https://doi.org/10.1021/ja9719135)
18. P. von R. Schleyer, M. Manoharan, Z.-X. Wang, B. Kiran, H. Jiao, R. Puchta, N. J. R. van Eikema Hommes, *Org. Lett.* **3** (2001) 2465 (https://doi.org/10.1021/ol016217v)
19. C. Corminboeuf, T. Heine, J. Weber, *Phys. Chem. Chem. Phys.* **5** (2003) 246 (https://doi.org/10.1039/B209674A)
20. T. Heine, P. v. R. Schleyer, C. Corminboeuf, G. Seifert, R. Reviakine, J. Weber, *J. Phys. Chem., A* **107** (2003) 6470 (https://doi.org/10.1021/jp035163z)
21. J. A. Bohmann, F. Weinhold, T. C. Farrar, *J. Chem. Phys.* **107** (1997) 1173 (https://doi.org/10.1063/1.474464)
22. M. Baranac-Stojanović, *J. Org. Chem.* **85** (2020) 4289 (https://doi.org/10.1021/acs.joc.9b03472)
23. M. Mauksch, S. B. Tsogoeva, *Chem. – A Eur. J.* **27** (2021) 14660 (https://doi.org/https://doi.org/10.1002/chem.202102230)
24. M. Jirásek, H. L. Anderson, M. D. Peeks, *Acc. Chem. Res.* **54** (2021) 3241 (https://doi.org/10.1021/acs.accounts.1c00323)
25. G. J. Richards, J. P. Hill, *Acc. Chem. Res.* **54** (2021) 3228 (https://doi.org/10.1021/acs.accounts.1c00315)
26. J. I. Wu, F. G. Pühlhofer, P. von R. Schleyer, R. Puchta, B. Kiran, M. Mauksch, N. J. R. van E. Hommes, I. Alkorta, J. Elguero, *J. Phys. Chem., A* **113** (2009) 6789 (https://doi.org/10.1021/jp902983r)

27. S. Radenković, J. Đurđević, P. Bultinck, *Phys. Chem. Chem. Phys.* **14** (2012) 14067 (https://doi.org/10.1039/C2CP41472D)
28. S. Radenković, I. Gutman, P. Bultinck, *J. Phys. Chem., A* **116** (2012) 9421 (https://doi.org/10.1021/jp307281y)
29. S. Radenković, J. Kojić, J. Petronijević, M. Antić, *J. Phys. Chem., A* **118** (2014) 11591 (https://doi.org/10.1021/jp507309m)
30. M. Antić, B. Furtula, S. Radenković, *J. Phys. Chem., A* **121** (2017) 3616 (https://doi.org/10.1021/acs.jpca.7b02521)
31. C. Riesinger, G. Balázs, M. Seidl, M. Scheer, *Chem. Sci.* **12** (2021) 13037 (https://doi.org/10.1039/D1SC04296C)
32. J. T. Boronski, J. A. Seed, D. Hunger, A. W. Woodward, J. van Slageren, A. J. Wooles, L. S. Natrajan, N. Kaltsoyannis, S. T. Liddle, *Nature* **598** (2021) 72 (https://doi.org/10.1038/s41586-021-03888-3)
33. S. Radenković, M. Antić, N. D. Savić, B. Đ. Glišić, *New J. Chem.* **41** (2017) 12407 (https://doi.org/10.1039/C7NJ02634J)
34. M. Walther, R. Puchta, *RSC Adv.* **2** (2012) 5815 (https://doi.org/10.1039/C2RA20665J)
35. R. Puchta, B. Neumüller, K. Dehnicke, *Zeitschr. Anorg. Allg. Chem.* **635** (2009) 1196 (https://doi.org/https://doi.org/10.1002/zaac.200801360)
36. A. I. Boldyrev, L.-S. Wang, *Chem. Rev.* **105** (2005) 3716 (https://doi.org/10.1021/cr030091t)
37. S. Radenković, P. Bultinck, *J. Phys. Chem., A* **115** (2011) 12493 (https://doi.org/10.1021/jp2020947)
38. S. Đorđević, S. Radenković, *Phys. Chem. Chem. Phys.* **21** (2019) 7105 (https://doi.org/10.1039/c9cp00541b)
39. M. M. Hossain, M. S. Mirzaei, S. V Lindeman, S. Mirzaei, R. Rathore, *Org. Chem. Front.* **8** (2021) 2393 (https://doi.org/10.1039/D1QO00068C)
40. K. Amsharov, D. I. Sharapa, O. A. Vasilyev, M. Oliver, F. Hauke, A. Goerling, H. Soni, A. Hirsch, *Carbon N. Y.* **158** (2020) 435 (https://doi.org/https://doi.org/10.1016/j.carbon.2019.11.008)
41. Z. Chen, J. I. Wu, C. Corminboeuf, J. Bohmann, X. Lu, A. Hirsch, P. von R. Schleyer, *Phys. Chem. Chem. Phys.* **14** (2012) 14886 (https://doi.org/10.1039/C2CP42146A)
42. D. Tzeli, I. D. Petsalakis, G. Theodorakopoulos, F.-U. Rahman, Y. Yu, J. Rebek, *Phys. Chem. Chem. Phys.* **23** (2021) 19647 (https://doi.org/10.1039/D1CP02277F)
43. Y. Cohen, S. Slovak, L. Avram, *Chem. Commun.* **57** (2021) 8856 (https://doi.org/10.1039/D1CC02906A)
44. D. Ćoćić, R. Puchta, R. van Eldik, *J. Coord. Chem.* **73** (2020) 2602 (https://doi.org/10.1080/00958972.2020.1820494)
45. R. Puchta, R. van Eldik, *Eur. J. Inorg. Chem.* **2007** (2007) 1120 (https://doi.org/https://doi.org/10.1002/ejic.200600715)
46. T. V. Soldatović, E. Selimović, B. Šmit, D. Ašanin, N. S. Planojević, S. D. Marković, R. Puchta, B. M. Alzoubi, *J. Coord. Chem.* **72** (2019) 690 (https://doi.org/10.1080/00958972.2019.1569229)
47. S. Jovanović, R. Puchta, O. Klisurić, Ž. D. Bugarčić, *J. Coord. Chem.* **69** (2016) 735 (https://doi.org/10.1080/00958972.2016.1146257)

48. B. Petrović, Ž. D. Bugarčić, A. Dees, I. Ivanović-Burmazović, F. W. Heinemann, R. Puchta, S. N. Steinmann, C. Corminboeuf, R. van Eldik, *Inorg. Chem.* **51** (2012) 1516 (https://doi.org/10.1021/ic201807a)
49. M. D. Kostić, V. M. Divac, B. M. Alzoubi, R. Puchta, *Zeitschr. Naturforsch., B* **71** (2016) 883 (https://doi.org/doi:10.1515/znb-2016-0055)
50. I. Casademont-Reig, R. Guerrero-Avilés, E. Ramos-Cordoba, M. Torrent-Sucarrat, E. Matito, *Angew. Chemie Int. Ed.* **60** (2021) 24080 (https://doi.org/https://doi.org/10.1002/anie.202108997)
51. J. Y. M. Chan, Y. Okada, T. Kawata, N. Kobayashi, D. K. P. Ng, *Org. Lett.* **23** (2021) 5942 (https://doi.org/10.1021/acs.orglett.1c02039).
52. M. Rauhalahti, D. Sundholm, M. P. Johansson, *Phys. Chem. Chem. Phys.* **23** (2021) 16629 (https://doi.org/10.1039/D1CP02381K)
53. H. Kawashima, S. Ukai, R. Nozawa, N. Fukui, G. Fitzsimmons, T. Kowalczyk, H. Fliegl, H. Shinokubo, *J. Am. Chem. Soc.* **143** (2021) 10676 (https://doi.org/10.1021/jacs.1c04348)
54. F. Golpayegani, Z. Mirjafary, J. M. Aliabad, H. Saeidian, *Comput. Theor. Chem.* **1206** (2021) 113469 (https://doi.org/https://doi.org/10.1016/j.comptc.2021.113469)
55. M. Y. Borzehandani, E. Abdulmalek, M. B. Abdul Rahman, M. A. M. Latif, *Polymers (Basel).* **13** (2021) (https://doi.org/10.3390/polym13111861)
56. C. Zeng, W. Shen, X. Xie, M. Li, *Polym. Sci., A* **52** (2010) 1355 (https://doi.org/10.1134/S0965545X1012014X)
57. M. Mauksch, S. B. Tsogoeva, *ChemPhysChem* **17** (2016) 963 (https://doi.org/https://doi.org/10.1002/cphc.201600086)
58. H. Jiao, P. von Ragué Schleyer, *J. Chem. Soc., Perkin Trans. 2* (1994) 407 (https://doi.org/10.1039/P29940000407)
59. M. Mauksch, V. Gogonea, H. Jiao, P. von R. Schleyer, *Angew. Chemie Int. Ed.* **37** (1998) 2395 (https://doi.org/https://doi.org/10.1002/(SICI)1521-3773(19980918)37:17<2395::AID-ANIE2395>3.0.CO;2-W)
60. C. Castro, C. M. Isborn, W. L. Karney, M. Mauksch, P. von R. Schleyer, *Org. Lett.* **4** (2002) 3431 (https://doi.org/10.1021/ol026610g)
61. C. Castro, Z. Chen, C. S. Wannere, H. Jiao, W. L. Karney, M. Mauksch, R. Puchta, N. J. R. van E. Hommes, P. von R. Schleyer, *J. Am. Chem. Soc.* **127** (2005) 2425 (https://doi.org/10.1021/ja0458165)
62. Z. Huang, Y. Zhang, W.-X. Zhang, J. Wei, S. Ye, Z. Xi, *Nat. Commun.* **12** (2021) 1319 (https://doi.org/10.1038/s41467-021-21648-9)
63. K. An, T. Shen, J. Zhu, *Organometallics* **36** (2017) 3199 (https://doi.org/10.1021/acs.organomet.7b00341)
64. C. Zhu, S. Li, M. Luo, X. Zhou, Y. Niu, M. Lin, J. Zhu, Z. Cao, X. Lu, T. Wen, Z. Xie, P. v. R. Schleyer, H. Xia, *Nat. Chem.* **5** (2013) 698 (https://doi.org/10.1038/nchem.1690)
65. M. Mauksch, S. B. Tsogoeva, *Chem. – A Eur. J.* **16** (2010) 7843 (https://doi.org/https://doi.org/10.1002/chem.201000396)
66. M. K. Milčić, B. D. Ostojić, S. D. Zarić, *Inorg. Chem.* **46** (2007) 7109 (https://doi.org/10.1021/ic062292w)
67. M. Mauksch, S. B. Tsogoeva, *Chem. – A Eur. J.* **24** (2018) 10059 (https://doi.org/https://doi.org/10.1002/chem.201802270)

68. D. W. Szczepanik, M. Solà, *ChemistryOpen* **8** (2019) 219 (https://doi.org/https://doi.org/10.1002/open.201900014)
69. I. Fernández, G. Frenking, *Chem. – A Eur. J.* **13** (2007) 5873 (https://doi.org/https://doi.org/10.1002/chem.200601674)
70. S. Radenković, S. Đorđević, *Phys. Chem. Chem. Phys.* **23** (2021) 11240 (https://doi.org/10.1039/D1CP00784J)
71. J. Đ. Nikolić, S. Đorđević, S. Radenković, *J. Mol. Model.* **26** (2020) 275 (https://doi.org/10.1007/s00894-020-04543-w)
72. I. Gutman, S. Radenkovic, M. Antic, J. Djurdjevic, *J. Serb. Chem. Soc.* **78** (2013) 1539 (https://doi.org/10.2298/JSC130520057G)
73. S. Radenković, M. Antić, S. Đorđević, B. Braïda, *Comput. Theor. Chem.* **1116** (2017) (https://doi.org/10.1016/j.comptc.2017.01.028)
74. S. Jeremić, S. Radenković, M. Filipović, M. Antić, A. Amić, Z. Marković, *J. Mol. Graph. Model.* **72** (2017) 240 (https://doi.org/https://doi.org/10.1016/j.jmgm.2017.01.011)
75. P. Lazzeretti, *Phys. Chem. Chem. Phys.* **6** (2004) 217 (https://doi.org/10.1039/B311178D)
76. P. von Ragué Schleyer, H. Jiao, B. Goldfuss, P. K. Freeman, *Angew. Chemie Int. Ed. English* **34** (1995) 337 (https://doi.org/https://doi.org/10.1002/anie.199503371)
77. L. Nyulászi, P. von R. Schleyer, *J. Am. Chem. Soc.* **121** (1999) 6872 (https://doi.org/10.1021/ja983113f)
78. A. Stanger, *Eur. J. Org. Chem.* **2020** (2020) 3120 (https://doi.org/https://doi.org/10.1002/ejoc.201901829)
79. R. Gershoni-Poranne, A. Stanger, *Chem. Soc. Rev.* **44** (2015) 6597 (https://doi.org/10.1039/C5CS00114E)
80. M. Solà, F. Feixas, J. O. C. Jiménez-Halla, E. Matito, J. Poater, *Symmetry* **2** (2010) (https://doi.org/10.3390/sym2021156)
81. M. D. Zermeño-Macías, M. M. González-Chávez, F. Méndez, A. Richaud, R. González--Chávez, L. E. Ojeda-Fuentes, P. D. Niño-Moreno, R. Martínez, *Mol.* **26** (2021) (https://doi.org/10.3390/molecules26165078).

Journal of the Serbian Chemical Society
JSCS-info@shd.org.rs • www.shd.org.rs/JSCS
J. Serb. Chem. Soc. *87* (12) 1447–1449 (2022)

IN MEMORIAM

Miroslav J. Gašić (1932–2022)

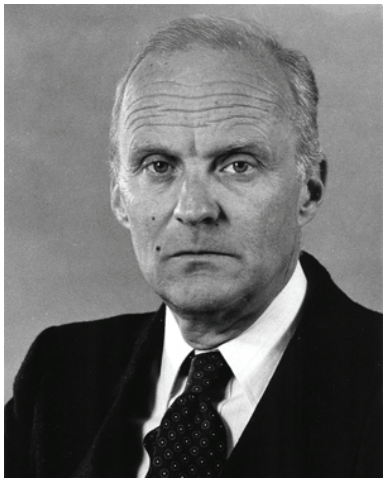

Miroslav Gašić, a longtime professor of Organic Chemistry at the Faculty of Chemistry, University of Belgrade, member of the Serbian Academy of Sciences and Arts, and former president of the Serbian Chemical Society passed away in March 2022.

Miroslav Gašić was born in Belgrade in December 1932. He graduated at the Chemistry Department, Faculty of Natural Sciences and Mathematics, University of Belgrade in 1959, and was appointed as an assistant at the same department in 1960. He defended his PhD Thesis „Acetoxylation of steroid hormones“, supervised by Milutin Stefanović and Mihailo Mihailović, at the Faculty of Natural Sciences and Mathematics, University of Belgrade, in 1964. Immediately after getting his PhD, he did his postdoctoral research on oxidation of steroid ketones with Eliahu Caspi at the Worcester Foundation for Experimental Biology, Shrewsbury, Massachusetts, and on non-classical homoallylic carbocations with Saul Winstein at the University of California, Los Angeles. In 1970 he was appointed as an assistant professor at the Chemistry Department, Faculty of Natural Sciences and Mathematics, University of Belgrade, in 1976 as an associate professor, and in 1983 as a full professor. He spent a year (1972/73) as a visiting professor at the University of Indiana, Bloomington. In 1985, Miroslav Gašić was elected as the corresponding member of the Serbian Academy of Sciences and Arts, and in 1994 as the full member.

Research activity of Miroslav Gašić is very varied, encompassing diverse areas of Organic Chemistry and Biochemistry. He published 120 papers, mostly in the most outstanding journals, and several monographs. He was an invited lecturer at many universities in USA and Europe, as well as at many scientific conferences. His principal research fields were: chemistry of steroids; physical organic chemistry, spectroscopy and organic electrochemistry; isolation, chemical and biological characterization of natural products. A large part of his res-

earch activities was dedicated to partial synthesis and synthetic transformations of steroids: synthesis and reactions of 5,10-secosteroids, oxidation of steroid 3-ketones, acetoxylation of steroid lactones using lead tetraacetate, and oxidation of estrogen-type steroids. Since the beginning of his scientific career, Miroslav Gašić was very interested in physical organic chemistry. At the University of California he investigated a hot topic at that time, non-classical carbocations. This work is intersting both from a mechanistic and a synthetic point of view. Very early he realized huge possibilities of ^{13}C-NMR spectroscopy and published many works in this area, including very useful review articles. His studies in organic electrochemistry were mainly focused on redox behaviour of biologically active quinones and hydroquinones as well as on electrochemical synthesis of drugs. During the late seventies Miroslav Gašić started research on isolation and characterization of natural products, both from terrestrial plants and marine organisms. He was the pioneer of marine natural product chemistry in Serbia, studying principally marine invertebrates (sponges, corals, ascidians), but also marine algae and seagrasses. His research was mostly focused on terpenes, steroids, fatty acids, halogen-containing lipids, but also on nucleosides and proteins (lectins, enzymes). Especially interesting are his publications on sponge sesquiterpene hydroquinone avarol and its derivatives, which show strong and selective antineoplastic activity. His papers on avarol and related compounds have been cited in more than 600 publications. He had a very intense collaboration with scientists from all over the world (USA, Germany, Italy, Montenegro, Greece, Bulgaria), and was a leader and participant at many international and national scientific projects.

Miroslav Gašić was an outstanding teacher. He drafted a very modern curriculum in organic chemistry for students of the new group of molecular biology and physiology, adapted for students of this group. His erudition and profound knowledge of various areas of chemistry and biology contributed to the high quality of his lectures. He supervised a great number of PhD theses. As a mentor, he was allowing a lot of freedom to his students, stimulating their creativity and supporting their ideas. Many of his PhD students pursued a successful scientific career.

Miroslav Gašić held several important positions: President of the Serbian Chemical Society, President of the Union of Chemical Societies of Yugoslavia, member of the Chemical Nomenclature Division of IUPAC, Secretary of the Department of Chemical and Biological Sciences of the Serbian Academy of Science, Head of the Department of Chemistry and Physical Chemistry of the Faculty of Science and Mathematics, University of Belgrade, Head of the Department of Organic Chemistry of the Faculty of Chemistry, University of Belgrade, member of the Crown Council of the Royal Family of Serbia, *etc*.

He was awarded the Order of Labour with the Red Flag (1988), the October Award of the City of Belgrade (1988), the Medal of the Serbian Chemical Society for lasting and outstanding contribution to science (1997) and was elected as honorary president of the Serbian Chemical Society in 2006.

Miroslav Gašić will be remembered and respected as an outstanding scientist and teacher, with broad interests, brilliant intelligence and problem-solving ability, but also for his erudition, tact, benevolence, sense of humour and other human qualities.

Prof. Dušan Sladić

Journal of the Serbian Chemical Society
JSCS@tmf.bg.ac.rs • www.shd.org.rs/JSCS
J. Serb. Chem. Soc. *87* (12) 1451–1459 (2022)

Contents of Volume 87

NUMBER 1: In Memoriam issue dedicated to Professor Peter Pfendt

NUMBER 2

NUMBER 3

NUMBER 6

NUMBER 7–8

NUMBER 12

Journal of the Serbian Chemical Society
JSCS-info@shd.org.rs • www.shd.org.rs/JSCS
J. Serb. Chem. Soc. *87* (12) 1461–1466 (2022)

Author Index

Subject Index of Vol. **87** and List of Referees in 2022 are given in the electronic form at the Internet address of the Journal of the Serbian Chemical Society: http://www.shd.org.rs/JSCS

End of Volume 87.

Journal of the Serbian Chemical Society
JSCS-info@shd.org.rs • www.shd.org.rs/JSCS
Volume *87* (2022)

Subject index